NASA Contractor Report 3827

Design Study of Test Models of Maneuvering Aircraft Configurations for the National Transonic Facility (NTF)

S. A. Griffin, A. P. Madsen,
A. A. McClain, et al.

CONTRACT NAS1-16848
AUGUST 1984

NASA

ERRATA

NASA Contractor Report 3827

Design Study of Test Models of Maneuvering Aircraft Configurations for the National Transonic Facility (NTF)

August 1984

S. A. Griffin, A. P. Madsen, A. A. McClain, et al.

The flexibility matrix shown on page B-21 should be changed from:

$$\begin{bmatrix} 10.05 & 1.90 & -.104 \\ 1.90 & .657 & .014 \\ -.104 & .014 & 1.47 \end{bmatrix} \times 10^{-6}$$

to

$$\begin{bmatrix} 10.05 & 3.164 & -.173 \\ 3.164 & 1.825 & .038 \\ -.173 & .038 & 3.937 \end{bmatrix} \times 10^{-6}$$

ISSUE DATE: February 1985

NASA Contractor Report 3827

Design Study of Test Models of Maneuvering Aircraft Configurations for the National Transonic Facility (NTF)

S. A. Griffin, A. P. Madsen,
A. A. McClain, et al.
General Dynamics Corporation
San Diego, California

Prepared for
Langley Research Center
under Contract NAS1-16848

National Aeronautics
and Space Administration

**Scientific and Technical
Information Branch**

1984

Page intentionally left blank

Page intentionally left blank

FOREWORD

This report describes the work performed on NASA Contract NAS 1-16848 by the Convair and Fort Worth Divisions of General Dynamics Corporation at San Diego and Fort Worth, respectively.

The work was administered by the Langley Research Center of NASA, Hampton, Virginia. Mr. Blair Gloss is the NASA Technical Monitor.

This program was conducted in the Research and Engineering Departments of the General Dynamics aerospace divisions, and was managed by S. A. Griffin. A. A. McClain coordinated the San Diego activity and A. P. Madsen the Fort Worth activity. The work was accomplished between September 1981 and May 1983.

Principal contributors to the study include:

Aerotest Design:	A.A. McClain, M.F. Nicodemus, E.A. Collinge
Aerodynamics:	B.D. Miller, W.W. Braymen
Thermodynamics:	G. Worcheck
Structural Test Laboratory:	M.A. Riley
Structural Analysis:	A.E. Brady
Materials Evaluation:	W.E. Witzell
Wind Tunnel Test Plan:	D.G. Hammond
Aerodynamic Consultant:	R.G. Bradley, Jr.
Dynamics:	W.A. Rogers, M.H. Love

Page intentionally left blank

Page intentionally left blank

TABLE OF CONTENTS

Section			Page
1	INTRODUCTION		1-1
2	PROGRAM ORGANIZATION		2-1
3	SELECTION OF AIRCRAFT CONFIGURATIONS		3-1
	3.1	SINGLE-ENGINE	3-1
	3.2	TWIN-ENGINE	3-1
4	MODEL SIZING		4-1
	4.1	CWC CONFIGURATION	4-1
	4.2	F-111 TACT CONFIGURATION	4-1
5	AERODYNAMIC CONSIDERATIONS AND TEST PLANS		5-1
	5.1	SINGLE ENGINE CONFIGURATION – 1/15-SCALE CWC	5-1
	5.1.1	Test Objectives and Proposed Test Plan	5-1
	5.1.2	Test Plan Rationale	5-1
	5.1.3	Model Loads Data	5-5
	5.1.4	Pressure Data Requirements	5-13
	5.2	TWIN-ENGINE CONFIGURATION F-111 TACT	5-13
	5.2.1	Test Objectives and Proposed Test Plan	5-13
	5.2.2	Test Plan Rationale	5-16
	5.2.3	Model Loads Data	5-22
	5.2.4	Pressure Date Requirements	5-22
	5.3	MODEL SURFACE REQUIREMENTS	5-27
	5.4	REGIONS OF REYNOLDS NUMBER SENSITIVITY	5-33
6	BASIC DESIGN PHILOSOPHY		6-1
7	FABRICATION AND MATERIALS REVIEW		7-1
	7.1	CANDIDATE HIGH STRENGTH STEELS	7-1
	7.1.1	Cryogenic Properties	7-2
	7.1.2	Fracture Toughness	7-2
	7.1.3	Fabrication Processes	7-4

TABLE OF CONTENTS, Contd

Section			Page
	7.1.4	Heat Treat/Aging	7-5
	7.2	COMPOSITES	7-6
	7.3	THERMAL EXPANSION, CONTRACTION, AND CONDUCTIVITY	7-8
	7.4	METHODS OF ATTACHMENT CONSIDERED IN DESIGN	7-8
	7.4.1	Adhesives	7-9
	7.4.2	Welding/Soldering	7-9
	7.4.3	Brazing	7-10
	7.4.4	Attachment Screws	7-11
	7.5	FILLER MATERIALS	7-11
	7.6	PROOF-OF-CONCEPT RATIONALE	7-12
	7.7	SPECIAL REIVEW OF MATERIALS FOR THE SUPPORT SYSTEM	7-13
8	FACILITY REQUIREMENTS IMPACTING MODEL DESIGN		8-1
	8.1	THE OPERATING ENVIRONMENT AND FACILITY DESCRIPTION	8-1
	8.2	SAFETY FACTORS AND DEVIATIONS	8-1
	8.3	ACCESSIBILITY AND EASE OF MODEL CHANGES	8-2
	8.4	REQUIRED DOCUMENTATION	8-2
	8.5	MODEL CHECK AT FACILITY	8-5
	8.6	DYNAMIC TESTING REQUIREMENTS	8-5
	8.7	QUALITY ASSURANCE	8-5
9	MODEL DESIGN REQUIREMENTS AND DESCRIPTIONS		9-1
	9.1	DESIGN APPROACH – CWC	9-1
	9.1.1	Forward Fuselage – Instrumentation Bay	9-1
	9.1.2	Midbody Section	9-2
	9.1.3	Aft Body and Tailcone	9-3
	9.1.4	Inlet and Internal Ducting	9-3
	9.1.5	Wings and Attachment	9-4
	9.1.6	Vertical Tail	9-5
	9.1.7	Balance Selection and Calibration Requirements	9-5
	9.1.8	Support System and Divergence	9-8
	9.2	DESIGN APPROACH – F-111 TACT	9-8
	9.2.1	Forward Fuselage – Instumentation Bay	9-8
	9.2.2	Midbody Section	9-10

TABLE OF CONTENTS, Contd

Section			Page
	9.2.3	Aft Body and Aft Fuselage Sting Fairing	9-10
	9.2.4	Inlet and Internal Ducting	9-11
	9.2.5	Wings and Attachment	9-12
	9.2.6	Vertical Tail/Horizontal Stabilizer	9-14
	9.2.7	Balance Selection and Calibration Requirements	9-14
	9.2.8	Support System and Divergence	9-15
	9.2.9	Remote Control of Horizontal Tail	9-16
	9.3	MODEL INSTRUMENTATION	9-16
	9.4	SURFACE FINISH AND TOLERANCES	9-17
	9.5	PRESSURE ROUTING AND INSTALLATION	9-18
	9.6	MODEL FLUTTER	9-18
	9.7	THERMAL CONTROL AND OVERLOAD SYSTEMS	9-18
	9.8	SUPPORT SYSTEMS	9-19
	9.9	MODEL DEFORMATION	9-20
	9.10	MODEL HANDLING	9-20
10	SUMMARY OF STRUCTURAL/THERMAL ANALYSES		10-1
	10.1	THERMAL ANALYSES	10-1
	10.1.1	Summary	10-2
	10.1.2	Chilldown Analysis	10-2
	10.1.3	Instrumentation Heater Requirements	10-7
	10.1.4	Model Temperature Distribution During a Test Run	10-20
	10.2	STRUCTURAL ANALYSIS – CWC	10-20
	10.3	STRUCTURAL ANALYSIS – F-111 TACT	10-41
	10.4	ACHIEVED SAFETY FACTORS	10-58
	10.5	PROOF TESTING AND DYNAMIC ANALYSIS	10-58
11	ESTIMATED MODEL COSTS AND SCHEDULES		11-1
12	CONCLUSIONS		12-1
13	RECOMMENDATIONS		13-1
14	REFERENCES AND BIBLIOGRAPHY		14-1

Appendix

A	RESULTS OF PROOF-OF-CONCEPT TESTS	A-1
B	FEASIBILITY STUDY OF A 1/20 SCALE STATIC AEROELASTICALLY SIMILAR, F-111 TACT WING	B-1

LIST OF FIGURES

Figure		Page
2-1	Program Operations Chart	2-2
5-1	One-fifteenth-Scale CWC Proposed Test Condition with NTF Envelope and Simulated Altitude Superimposed	5-3
5-2	NTF Operating Limits of Dynamic Pressure as a Function of Mach Number at RN = 5, 10, and 15 × 10^6	5-4
5-3	NTF Operating Limits of Dynamic Pressure as a Function of Mach Number at RN = 40, 50, and 65 × 10^6	5-5
5-4	Estimated NTF Performance Map for Free Stream Mach Number of 0.60	5-6
5-5	Estimated NTF Performance Map for Free Stream Mach Number of 0.90	5-7
5-6	Estimated NTF Performance Map for Free Stream Mach Number of 1.20	5-8
5-7	Drag Rise Characteristics for Several Highly Swept Cranked Wing Configurations (CWC)	5-9
5-8	One-fifteenth-Scale CWC Fuselage Loads Distribution	5-9
5-9	One-fifteenth-Scale CWC Vertical Tail Loads	5-10
5-10	One-fifteenth-Scale CWC Wing Control Surface Loads	5-11
5-11	One-fifteenth-Scale CWC Total Wing Loads	5-12
5-12	One-fifteenth-Scale CWC Wing/Fuselage Pressure Orifice Array	5-14
5-13	F-111 TACT Proposed Test Conditions with NTF Envelope and Simulated Altitude Superimposed	5-18
5-14	F-111 TACT Estimated NTF Performance Map for Free Stream Mach Number of 0.70	5-19
5-15	F-111 TACT Estimated NTF Performance Map for Free Stream Mach Number of 0.90	5-20

LIST OF FIGURES, Contd

Figure		Page
5-16	F-111 TACT Estimated NTF Performance Map for Free Stream Mach Number of 1.20	5-21
5-17	One-twentieth-Scale F-111 TACT Fuselage Loads Distribution	5-22
5-18	One-twentieth-Scale F-111 TACT Horizontal Tail Loads	5-23
5-19	One-twentieth-Scale F-111 TACT Wing Loads	5-24
5-20	One-twentieth-Scale F-111 TACT Wing/ Fuselage Pressure Orifice Array	5-25
5-21	Compressability Effects on Skin Friction Coefficient for Smooth and Rough Surface	5-29
5-22	F-111 TACT Predicted Cut-off Reynolds Numbers Superimposed on Proposed F-111 TACT Outline	5-32
7-1	Coefficient of Contraction Comparison of 18Ni-200 Steel, A286 Steel, and an Epoxy Laminate	7-9
7-2	"Ideal" Composite Support Sting	7-15
9-1	Typical Six-Component Strain-Gage Balance	9-7
9-2	NTF Balance Load Rhombus with 1/15-Scale CWC Model Loads Superimposed	9-7
9-3	Support Sting for the 1/15-Scale CWC Model and 1/20-Scale F-111 TACT Model	9-9
9-4	F-111 TACT Model Assembly Procedures	9-13
9-5	NTF Balance Load Rhombus with 1/20-Scale F-111 TACT Model Test Points Superimposed	9-15
9-6	Matched-point Flutter Analysis at M = 0.90	9-19
10-1	CWC Forward/Mid-Body Sections	10-3
10-2	Instrumentation Package (Section A-A in Figure 10-1)	10-4
10-3	Thermal Model, CWC Kevlar®/18Ni-200 Joint	10-4
10-4	F-111 TACT Wind Tunnel Thermal Model at Sta 19.00	10-5

LIST OF FIGURES, Contd

Figure		Page
10-5	F-111 TACT Wind Tunnel Thermal Model at Sta 24.38	10-5
10-6	F-111 TACT Wind Tunnel Thermal Mode at Sta 27.00	10-6
10-7	F-111 TACT Wind Tunnel Thermal Model at Sta 38.51	10-7
10-8	Predicted Temperature Versus Time after Chilldown Start at Representative Nodes for the CWC	10-8
10-9	Predicted Temperature Versus Time after Chilldown Start at Sta 19.00 for the F-111 TACT	10-9
10-10	Predicted Temperature Versus Time after Chilldown Start at Sta 24.38 for the F-111 TACT	10-9
10-11	Predicted Temperature Versus Time after Chilldown Start at Sta 27.00 for the F-111 TACT	10-10
10-12	Predicted Temperature Versus Time after Chilldown Start at Sta 38.51 for the F-111 TACT	10-10
10-13	Predicted Temperatures (F) 20 Seconds after Chilldown Start for the CWC	10-11
10-14	Predicted Temperatures (F) 40 Seconds after Chilldown Start for the CWC	10-11
10-15	Predicted Temperatures (F) 10 Seconds after Chilldown Start at F-111 TACT Sta 19.00	10-12
10-16	Predicted Temperatures (F) 20 Seconds after Chilldown Start at F-111 TACT Sta 19.00	10-12
10-17	Predicted Temperatures (F) 40 Seconds after Chilldown Start at F-111 TACT Sta 19.00	10-13
10-18	Predicted Temperatures (F) 600 Seconds after Chilldown Start at F-111 TACT Sta 19.00	10-13
10-19	Predicted Temperature (F) 10 Seconds after Chilldown Start at F-111 TACT Sta 24.38	10-14
10-20	Predicted Temperature (F) 20 Seconds after Chilldown Start at F-111 TACT Sta 24.38	10-14
10-21	Predicted Temperature (F) 40 Seconds after Chilldown Start at F-111 TACT Sta 24.38	10-15

Figure		Page
10-22	Predicted Temperature (F) 10 Seconds after Chilldown Start at F-111 TACT Sta 27.00	10-15
10-23	Predicted Temperature (F) 20 Seconds after Chilldown Start at F-111 TACT Sta 27.00	10-16
10-24	Predicted Temperature (F) 40 Seconds after Chilldown Start at F-111 TACT Sta 27.00	10-16
10-25	Predicted Temperature (F) 10 Seconds after Chilldown Start at F-111 TACT Sta 38.51	10-17
10-26	Predicted Temperature (F) 20 Seconds after Chilldown Start at F-111 TACT Sta 38.51	10-17
10-27	Predicted Temperature (F) 40 Seconds after Chilldown Start at F-111 TACT Sta 38.51	10-18
10-28	Forward Body Specimen Thermocouple Locations	10-19
10-29	Model Temperature Gradients	10-21
10-30	CWC Wing Panel	10-22
10-31	CWC Wing Tip Panel	10-29
12-1	Critical Areas of the Model Recommended for Monitoring Strain	12-2

Foldout

FO-3	One-fifteenth Scale CWC Model Assembly
FO-4	One-twentieth-Scale F-111 TACT Model Assembly
FO-5	One-fifteenth-Scale CWC Model Fuselage Assembly
FO-6	One-fifteenth-Scale CWC Model Wing Assembly and Instrumentation
FO-7	One-twentieth F-111 TACT Mode Inlet/Ducting Assembly
FO-8	One-twentieth F-111 TACT Model Assembly

LIST OF TABLES

Table		Page
5-1	One-fifteenth-Scale CWC Wing Pressure Orifice Locations	5-15
5-2	One-fifteenth-Scale CWC Fuselage Pressure Orifice Locations	5-16
5-3	One-twentieth-Scale F-111 TACT Wing Pressure Orifice Locations	5-26
5-4	One-twentieth-Scale F-111 TACT Fuselage/ Glove Pressure Orifice Locations	5-27
5-5	Summary of Prediction Methods for Compressibility Effects on Turbulent Skin Friction Coefficient for Smooth and Rough Surfaces	5-31
7-1	Mechanical Properties of Various Metals	7-3
7-2	Mechanical Properties of Various Composites	7-7
8-1	Summary of Achieved Safety Factors for the 1/15-Scale CWC Model	8-3
8-2	Summary of Achieved Factors for the 1/20-Scale F-111 TACT Model	8-4
9-1	Wing Fabrication Methods (Wing 18Ni-200)	9-6
10-1	Wing Analysis Results	10-23
10-2	Tension Load on Screws (78K)	10-28
11-1	Cost Comparison of Conventional Pressure Model and NTF Model	11-2

Foldout

FO-1	Proposed NTF Test Plan for 1/15-Scale CWC
FO-2	Proposed NTF Test Plan for 1/15-Scale F-111 TACT Model

ABBREVIATIONS AND SYMBOLS

Symbol	Nomenclature	Units
A	Area	in^2
A.F.	Axial force	lb.
B.L.	Buttock Line station	in.
BMC	Balance Moment Center	
C	Cord or dimension	in.
$\bar{c}$	Mean Aerodynamic Chord	in.
c	Distance	in.
C_D	Drag Coefficient	
C_f	Skin Friction Coefficient	
C_{fi}	Incompressible Skin Friction Coefficient	
C_L	Lift Coefficient	
C_N	Normal Force Coefficient	
C.P.	Center of Pressure	
CVN	Charpy V-Notch	
D	Diameter	in.
d	Distance, Reference Length	in.
D_{bf}	Deflection of Balance due to Applied Load	in.
D_{bm}	Deflection of Balance due to Applied Moment	in.
D_{Cna}	Derivative C_{NA} with respect to α where $C_{NA} = NF/q_\infty S$	
D_{Cnw}	Derivative C_{NW} with respect to α where $C_{NW} = N_W/q_\infty S$	
D_{Cma}	Derivative C_{MA} with respect to α where $C_{MA} = PM/q_\infty Sd$	
D_{Cmw}	Derivative C_{MW} with respect to α where $C_{MW} = M_W/q_\infty Sd$	

ABBREVIATIONS AND SYMBOLS (Continued)

Symbol	Nomenclature	Units
DS	Total Angular Deflection of Sting	Deg
DS_f	Portion of Total Angular Deflection of Sting due to Applied Load	Deg
DS_m	Portion of Total Angular Deflection of Sting due to Applied Moment	Deg
E	Modulus of elasticity	lb/in^2
E.A.	Elastic axis	
E_c	Modulus of elasticity in compression	lb/in^2
F	Fahrenheit	Deg
F_b	Allowable bending stress	lb/in^2
F_{bru}	Ultimate bearing stress	lb/in^2
F_{bry}	Bearing yield stress	lb/in^2
F_{cy}	Compressive yield stress	lb/in^2
F_n	Ultimate tension allowable	lb/in^2
F_{su}	Ultimate shear allowable	lb/in^2
F_{tu}	Ultimate tension allowable	lb/in^2
F_{ty}	Tensile yield stress	lb/in^2
F.S.	Fuselage station	in.
f_b	Calculated bending stress	lb/in^2
f_{br}	Calculated bearing stress	lb/in^2
f_c	Calculated compressive stress	lb/in^2
f_n	Calculated principal stress	lb/in^2
f_s	Calculated shear stress	lb/in^2
f_t	Calculated tension stress	lb/in^2
G	Modulus of rigidity	lb/in^2
I	Moment of inertia	in^4

ABBREVIATIONS AND SYMBOLS (Continued)

Symbol	Nomenclature	Units
J	Polar moment of inertia	in^4
k	Admissible surface roughness factor	
K	Thermal conductivity	BTU/hr ft^2°F
K	Polar section modulus	in^3
K_{1c}	Plane strain fracture toughness	ksi in.
K_n	Spring constant of sting-balance combination due to applied load	°/lb
K_m	Spring constant of sting-balance combination due to applied moment	°/in-lb
L	Load	lb
ℓ	Length	in.
ℓ_c	Characteristic length (MAC for wings)	in.
M	Moment	in-lb
M	Mach No.	
$M\ell$	Local Mach number	
M_∞	Free stream Mach number	
MAC	Mean Aerodynamic Chord	
M_W	Pitching moment due to the normal component of the weight; the sign is determined by the signs of N_W and X_W, and is positive for pitch up: $M_W = N_W X_W$	in-lb
n	Designates a number	
N.F.	Aerodynamic force normal to the balance axis, acting on the complete model; positive for tendency to increase angle of attack	lb
N_W	Component of model weight normal to the balance axis; negative for tendency to reduce the normal positive angle of attack or to increase to a more negative nominal angle of attack	lb

ABBREVIATIONS AND SYMBOLS (Continued)

Symbol	Nomenclature	Units
P	Load	lb
P_t	Total pressure	PSI
P_s	Static pressure	PSI
PM	Pitching moment due to airloads about the load-reference point, positive for pitch up	in-lb
P_S	Shear load	lb
P_{SA}	Allowable shear load	lb
P_T	Tensile load	lb
P_{TA}	Allowable tensile load	lb
Q	Static moment of a cross-section	in-lb
q	Dynamic pressure	lb/ft^2
q_∞	Freestream dynamic pressure	lb/ft^2
RM	Rolling moment; positive for tendency of right wing down	in-lb
S	Reference area used in forming the force and moment coefficients	in^2
S.F.	Safety factor	
SF	Side force; positive is right when looking upstream	lb
S.S.	Span station, sting station	in.
T	Torsion	in-lb
T.E.	Trailing edge	
T.S.	Tail panel station	in.
t	Thickness	in.
V	Shear load	lb
W	Total weight of the model which is transmitted through the balance	lb
W.S.	Wing station	in.

ABBREVIATIONS AND SYMBOLS (Continued)

Symbol	Nomenclature	Units
x_{cp}	Axial center of pressure location	in.
X_W	Distance from the load-reference point to the center of gravity of the model, measured parallel to the longitudinal axis of the balance; X_W is positive for a center of gravity upstream of the load-reference point	in.
y_L	Distance to lower fibers	in.
y_T	Distance to upper fibers	in.
YM	Yawing moment; positive in nose right	in-lb
α^t	Coefficient of thermal expansion	
α	Angle of attack	Deg
α_o	Nominal angle of attack of the model, i.e., the angle of attack setting for zero airloads with dead weight acting positive for pitch up	Deg
β	Side slip angle	Deg
δ_{LEF}	Leading Edge flap deflection	Deg
δ_e	Elevon deflection	Deg
δ_a	Aileron deflection	Deg
δ_H	Horizontal tail deflection	Deg
Δ	Incremental or differential	
Λ	Leading edge sweep angle	Deg
θ	Angle	Deg
μ-in.	Microinch	in.x 10^{-6}
ν	Poissons Ratio	
χ	Rotational deflection	Deg
ρ	Density	slug/ft^3

ABBREVIATIONS AND SYMBOLS (Continued)

Symbol	Nomenclature	Units
K	Degrees Kelvin	Deg
$\perp$	Perpendicular	
$\overrightarrow{+}$	Vectorial addition symbol	
C_{N_w}	Normal Force Coefficient, Wing Contribution	
SIC	Structural Influence Coefficient	
FS	Full Scale	
F.S.	Front Spar	
R.S.	Rear Spar	
M.S.	Mid Spar	
RN	Reynolds Number	
δ_{SP}	Spoiler deflection	Deg
ALT	Altitude	ft
ng	Load Factor expressed as gravitational force equivalents	g
%C	Increment of Chord Length	
σ	Stress component	lb/in^2
ε	Strain component	in/in
τ	Shear stress	lb/in^2
γ	Shear strain	in/in
η	Nondimensional Spur Station	
ξ	Nondimensional Chord Station	
KEAS	Knots Equivalent Air Speed	Knots
ω	Shear flow	lb/in
ϕ	Angle of roll	Deg
u	Ultimate	

SUMMARY

The need for a National High Reynolds Number Transonic Wind Tunnel has been recognized for many years. The National Transonic Facility (NTF), located at NASA Langley Research Center, is well able to fill that need. NTF will provide an effective tool for the study of phenomena sensitive to Reynolds number, while also offering the potential of making wind tunnel-to-full scale data correlations for a wide range of flight vehicles.

The usefulness of the NTF will be largely influenced by the ability of industry to design and build model systems, capable of withstanding the severe operating environment of the facility, at a reasonable cost, and within an acceptable schedule. The objective of this program is to study the feasibility of designing advanced technology, highly maneuverable, fighter aircraft models to achieve full-scale Reynolds number in the NTF, and to identify problem areas that jeopardize achievement of that objective.

Each of the configurations selected, (Cranked Wing Configuration (CWC) and F-111 TACT) meets the requirements of advanced aerodynamic technology. Each configuration has a wind tunnel data base sufficient for accurate loads predictions, and each has the potential for full-scale flight data correlations. Test plans that encompass the complete flight envelope of the vehicle are developed for both configurations. Model loads are defined from available force/pressure data. Aeroelastic effects on bending and twist are determined from pressure data.

A review of materials and material processes is presented. This is a key area, since the NTF operating environment precludes the use of many currently used high strength steels. In addition, the needs and methods for the protection of instrumentation are investigated. Certain "proof-of-concept" tests were conducted under simulated tunnel conditions to verify design acceptance.

The study concludes that advanced technology fighter-type aircraft models can be designed and built that will meet the severe operating criteria of the facility, and that the NTF can provide the test conditions for full-scale flight data correlation. *It should be emphasized that the design must be completed in such depth that the facility drive system is not endangered by the model; however, the model design should not be so conservative that the full capability of the facility is unusable.*

SECTION 1

INTRODUCTION

The international concern over the inability of existing wind tunnel facilities to approach or match full-scale Reynolds numbers has led to the development of the National Transonic Facility (NTF), which will provide the United States with a long needed significant advance in transonic aerodynamic test capability. The selected concept, derived from a series of study programs, is a continuous flow, fan driven, high pressure facility, capable of operating at cryogenic temperatures. NTF is located at NASA Langley Research Center. NTF will be available for both research and development testing.

The objective of this program is to study the feasibility of designing and building wind tunnel models (of advanced technology, highly maneuverable, fighter aircraft) that are capable of meeting the requirements needed to achieve full-scale Reynolds number in the NTF, and to identify any problem areas that jeopardize achievement of that objective. In each case the models are specified as development models and include flow-through engine simulation, movable control surfaces, and the necessary instrumentation associated with a combined force and pressure model.

Reynolds number performance is achieved in a wind tunnel through a balance of tunnel/model size, dynamic pressure, and temperature. As the test section size is decreased (with corresponding reduction in model size based upon model blockage criteria), the dynamic pressure must be increased and/or the operating temperature decreased to maintain the desired Reynolds number. The combination of high pressure and low temperature creates extremely adverse operating conditions for the model system. The high pressure causes the stresses and deflections of the model, balance, and support system to increase. The low temperature creates the need for environmental control for instrumentation, special materials and material processes, and strict quality control. In addition to pressure and temperature effects, the allowable model surface finish and tolerance are decreased in order to achieve a scaled roughness Reynolds number.

NASA handbook LHB 1710.15, Reference 1, describes "Wind Tunnel Model Systems Criteria." It contains criteria for the design, fabrication, inspection and documentation of wind tunnel models and support systems to be tested in the NTF. Design allowables are also included in the handbook. It should be noted, however, that under certain conditions, reduced safety factors can be accepted. The need for such a deviation becomes apparent in the design of the 1/15 scale CWC and the 1/20 F-111 TACT. Full-scale Reynolds number is achieved in the NTF, but only at the expense of reduced safety factors in certain areas of the

model. Reference 1 describes the policy that must be followed in such cases. It must be emphasized that the relaxation of safety factors to achieve the desired Reynolds number, while necessary in certain cases, is done with extreme caution. A too conservative design approach for these configurations, however. would not make full use of the tunnel capability, and full-scale Reynolds number could not be achieved.

The selected configurations were chosen because they met the requirements of advanced technology aircraft. The CWC is a single-engine aircraft, and the F-111 TACT is a twin-engine aircraft. Sections 3, 4, and 5, respectively, cover the selection of these aircraft, the sizing of the models for use in the 2-1/2 meter NTF, and the aerodynamic considerations and test plans associated with those aircraft configurations.

The basic design philosophy applied to this study is discussed in Section 6. A review of materials and processes and fabrication techniques is found in Section 7. The impact of the NTF requirements upon the design of the models is presented in Section 8, including:

- The operating environment
- Safety factors and deviations
- Accessibility and ease of model changes
- Documentation
- Balance check calibrations in tunnel
- Dynamic testing requirements
- Quality assurance

The design of each configuration is more fully discussed in Section 9, which includes not only the basic structural design of the models, but a description of:

- Model instrumentation and the need and method of environmental control.
- Required surface finish and tolerance for full scale Reynolds number simulation.
- Methods of pressure routing and installation with minimum degradation of surface finish.
- A review of potential flutter as a result of high model loads and model/support system stiffness.

- Thermal control and overload systems.
- The model support system, and a review of potential divergence.
- Model deformation and a means of measuring it.
- Model handling.

Structural/thermal analyses are performed on each of the model configurations. While the majority of the test plan calls for testing at cryogenic temperatures, the potential of testing at room temperature is also considered since for a given dynamic pressure, room temperature testing is more critical. Those analyses and critical areas of the models that do not meet the desired safety factors are identified and presented in Section 10.

Section 11 is devoted to a review of model costs and schedules, and includes a discussion of the escalation of costs for an NTF model as compared with a current, conventional model.

Conclusions and recommendations are discussed in Sections 12 and 13 respectively.

Full-scale Reynolds number in NTF is an established goal, and in this study, we show that the goal can be achieved. It must be clearly understood, however, that such an achievement is very configuration sensitive. Each case should be treated separately and no assumption made that full-scale Reynolds is always achieveable.

SECTION 2

PROGRAM ORGANIZATION

General Dynamics, through its Convair and Fort Worth Divisions, established a team within its Research and Development Departments to conduct the design study of test models for the National Transonic Facility. The technical information (with respect to the two configurations) and the test plan were generated at the Fort Worth Division. The design, stress/thermal/material analysis, and proof-of-concept testing were performed at the Convair Division. The teams organized to conduct the study were led by Mr. S. A. Griffin, who reports to Mr. T. Sammon, Director of Test and Evaluation. The entire organization is under the senior management of Mr. D. E. DaPra, Vice President of Research and Engineering.

The program operations chart (Figure 2-1) illustrates the flow of information from the various technical groups through design to the final report.

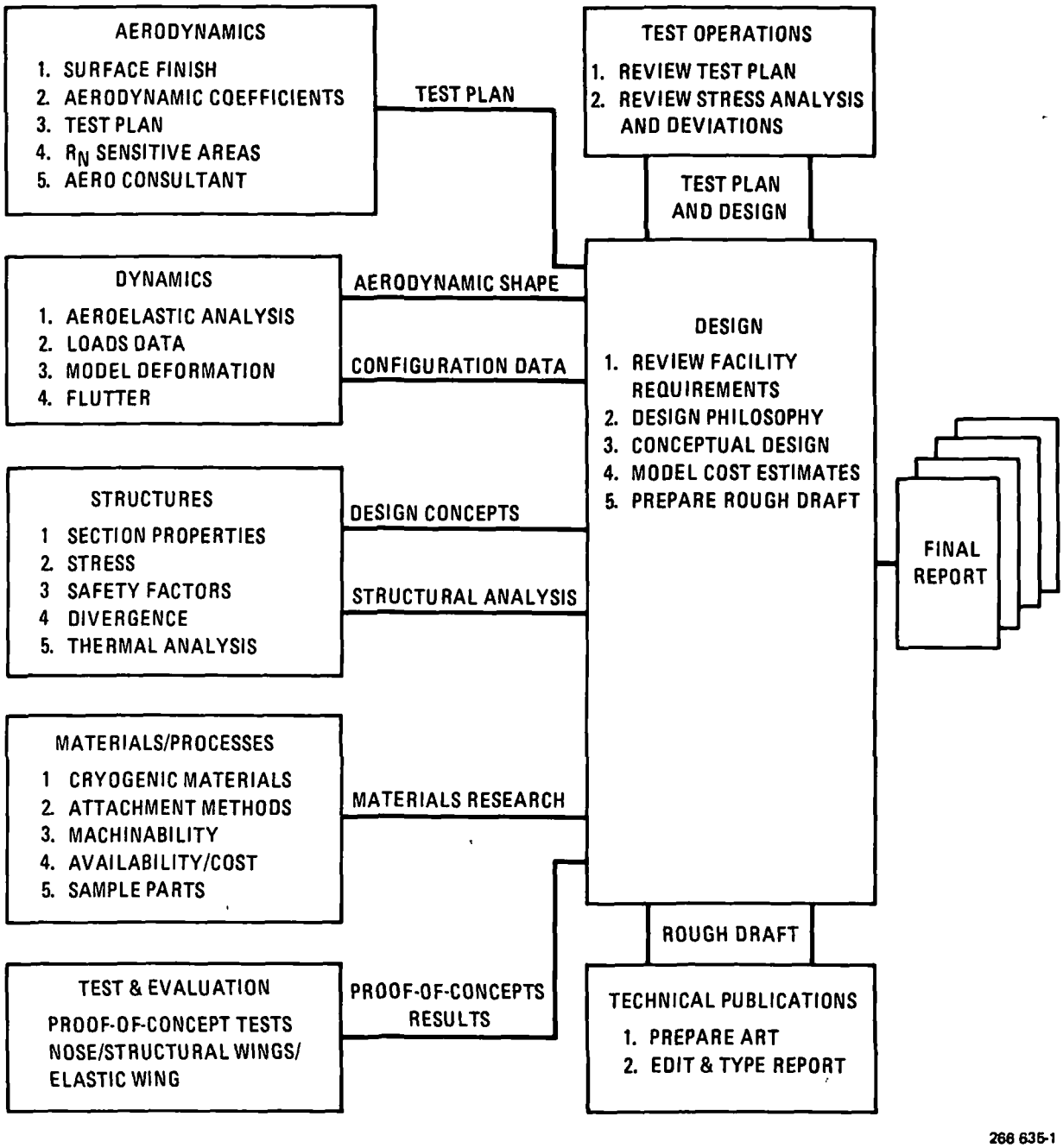

Figure 2-1. Program Operations Chart

SECTION 3

SELECTION OF AIRCRAFT CONFIGURATIONS

The configurations considered in this model design study program were selected after careful consideration of the program objectives. On this basis, the selection criteria used put special emphasis on having each configuration meet the following basic requirements:

- Be representative of current or advanced aerodynamic technology
- Be non-proprietary and unclassified
- Have a wind tunnel data base sufficient to enable making accurate force, moment, and loads predictions
- Offer the potential for making tunnel (NTF) to full-scale data correlations

3.1 SINGLE-ENGINE

The single-engine configuration selected is the CWC. This configuration evolved during an extensive NASA/General Dynamics cooperative effort and is similar to the two F-16XL prototype aircraft now undergoing flight testing. In-house studies by General Dynamics, aimed at improving the supersonic performance of the F-16 while retaining its outstanding transonic maneuverability and performance characteristics, were supported by a NASA/General Dynamics experimental research program to develop a refined wing design. Wind tunnel test results indicated that these performance goals could be met by incorporating a cranked-leading-edge wing in the design. The CWC is therefore an outstanding selection for the current NTF model design study since it embodies advanced aerodynamic technology and has the potential of providing high Reynolds number data to guide efforts to improve the aerodynamic design of the F-16XL. Also, a substantial wind tunnel data base exists for the CWC including both force and pressure data.

3.2 TWIN-ENGINE

The F-111 TACT configuration will make an excellent twin-engine model for NTF comparison and correlation. Besides having a broad data base available, both from flight and in conventional wind tunnels, the configuration is a good case for investigating Reynolds number effect on attached flow.

The airfoil is supercritical and moderately thick (8.5%), and tests will provide insight into shock-induced separation and leading-edge separation. Pressure data and buffet data will also provide information for load correlations, and new information for structural design will be obtained.

A comprehensive wind tunnel and flight test data base is available on this configuration from the work performed under the joint NASA/Air Force/General Dynamics Transonic Aircraft Technology Program (TACT). Approximately 1500 hours of wind tunnel testing was performed to document the aerodynamic characteristics of this variable sweep, advanced supercritical wing configuration. Included in the number of models tested was a "high-strength" model, which was used to obtain high Reynolds number data at transonic speeds to the limits available in the NASA ARC 11-foot Unitary Tunnel.

F-111A aircraft No. 13 was converted to the TACT configuration and flight tested at the NASA Dryden Flight Test Center. Flight test pressure data have been obtained, and together with the operating conditions of the NTF, provide an excellent opportunity for wind-tunnel-to-flight correlation of supercritical wing data at full-scale Reynolds numbers.

SECTION 4

MODEL SIZING

The model scales of the single- and twin-engine configurations have been selected to be of a maximum size to accomplish the test objectives while maintaining compatibility with the size of the NTF test section. A maximum model size is desirable to obtain the highest possible Reynolds number, to simulate internal flow, to provide for control surface deflection, to provide adequate pressure tube and other instrumentation routing, and to permit the installation of "on-board" instrumentation systems.

4.1 CWC CONFIGURATION

A 1/15-scale model has been selected for the single-engine CWC configuration. The model span-to-tunnel-width ratio is 0.26. This is comparable to the model-to-tunnel-size tested under the CWC program to obtain aerodynamic design data. This model can take full advantage of the NTF facility capability and exceeds the coverage of the full-scale flight Reynolds number/Mach number envelope for all points except at Mach 1.2 below 5400 feet of altitude.

4.2 F-111 TACT CONFIGURATION

A 1/20-scale model has been selected for the twin-engine F-111 TACT configuration. The variable sweep feature of the configuration gives a model span-to-tunnel-width ratio of 0.36 with the wings forward (Λ = 26 degrees) and 0.24 with an aft sweep (Λ = 58 degrees). Since the forward sweep configuration requires only subsonic testing, the larger ratio is acceptable. One-fifteenth and 1/24 scale models of this configuration have been successfully tested in conventional tunnels of comparable size to the NTF.

The 1/20-scale model permits installation of a balance large enough to take advantage of the NTF capability and provide complete coverage of the full-scale flight envelope of Reynolds number/Mach number except below 15,000 feet of altitude at Mach 1.2.

SECTION 5

AERODYNAMIC CONSIDERATIONS AND TEST PLANS

5.1 SINGLE-ENGINE CONFIGURATION – 1/15-SCALE CWC

5.1.1 TEST OBJECTIVES AND PROPOSED TEST PLAN. The proposed test plan for the highly swept cranked wing configuration is shown in Table FO-1. (Foldouts are placed at the back of the book.) The philosophy taken in its development was to exploit the capability of the NTF. The research nature of this program suggests that a comprehensive set of data be obtained. The test plan addresses several important objectives, as discussed below.

A parametric variation in the major variables is provided in the test plan. These include:

a.	Mach number	(M)
b.	Angle of attack	(α)
c.	Reynolds number	(RN)
d.	Dynamic pressure	(q)
e.	Leading-edge flap deflection	(δ_{LEF})
f.	Elevon deflection	(δ_e)
g.	Aileron deflection	(δ_a)

The test plan provides test Mach numbers and configurations that can be used in tunnel-to-tunnel correlations to establish NTF tunnel and model confidence. However, the lowest Reynolds numbers available in the NTF (Reference 2) are higher than the values corresponding to currently available test data for the cranked wing configuration. Therefore, it is recommended that the NTF model be tested in other facilities to duplicate all conditions including Reynolds number. These data will provide an excellent source for tunnel-to-tunnel correlations. It is noted, however, that the scope of the test plan in Table FO-1 is limited to testing in the NTF.

5.1.2 TEST PLAN RATIONALE. An interesting phenomenon to be investigated for the highly swept cranked wing configuration is the effect of Reynolds number on leading-edge vortex development, shedding, and bursting. The parametric variations in Mach number, angle of attack, and Reynolds number will provide the data to determine if the effect is significant.

The test plan was developed so that the high Reynolds number data can be obtained at the lowest dynamic pressure available. This approach provides the desired data without placing unnecessary demands on the model design. The test plan covers conditions representative of flight test points over as much of the flight envelope as possible. Determination of scale effects due to Reynolds number changes is the primary capability unique to the NTF. Some of the full-scale Reynolds numbers were selected to simulate specific altitude conditions where flight data would be more available (e.g., 30,000 feet). Figure 5-1 shows the planned test points (Reynolds number/Mach number) with the operating range of the NTF and simulated altitude superimposed.

The capability for separation of Reynolds number and dynamic pressure effects is one of the unique features of the NTF. This allows the separation of Reynolds number effects from aeroelastic effects. Though these models are "rigid" models, they will undoubtedly show some flexibility at the high values of q; therefore, the test plan was designed to separate the effects of these parameters as much as possible. However, study of the estimated NTF performance maps provided in Reference 2 reveals that it will not be possible to test at the lowest and highest Reynolds numbers at constant dynamic pressure. The tunnel operating limits shown in Reference 2 were used to develop the upper and lower bounds of dynamic pressure available at given Reynolds numbers as a function of Mach number. Figure 5-2 presents the results for Reynolds numbers of 5 and 10×10^6, and Figure 5-3 shows similar results for Reynolds numbers of 40, 50, and 65×10^6. The Reynolds numbers are based on a reference length ($\bar{c}$) of 0.25 meter, which is consistent with Reference 2. Figures 5-2 and 5-3 show that the maximum q available at $RN_{\bar{c}} = 5 \times 10^6$ is below the minimum q available at $RN_{\bar{c}} = 40 \times 10^6$. To address this problem in the test plan, the variation from wind tunnel Reynolds numbers to full-scale Reynolds numbers was accomplished by alternately varying Reynolds numbers at constant q and then varying q at constant Reynolds number. This results in a stairstep path as illustrated in Figures 5-4, 5-5, and 5-6 for Mach numbers of 0.6, 0.9, and 1.2. The solid symbols in these figures indicate conditions where force and pressure data will be obtained, and the open symbols indicate where only force data will be acquired.

One of the objectives of the proposed test plan will be to obtain Reynolds number effects on Mach critical and drag rise. Figure 5-7 shows wind tunnel drag rise data for various highly swept cranked wing configurations. This supports the need for obtaining data at closely spaced intervals above Mach 0.9 to define the drag rise characteristics. The proposed test plan provides for such data at Reynolds numbers of 5, 10, 15, and 50×10^6. In each case the value of q will be 880 lb/sq ft, except at 50×10^6, where tunnel limits exclude a value across the Mach range below approximately 2640 lb/sq ft (pt = 3 at Mach = 1.2). Schedule H in Table FO-1 shows the variation in total pressure as a function of Mach number to keep q_∞ constant. The constant value of q, for each Reynolds

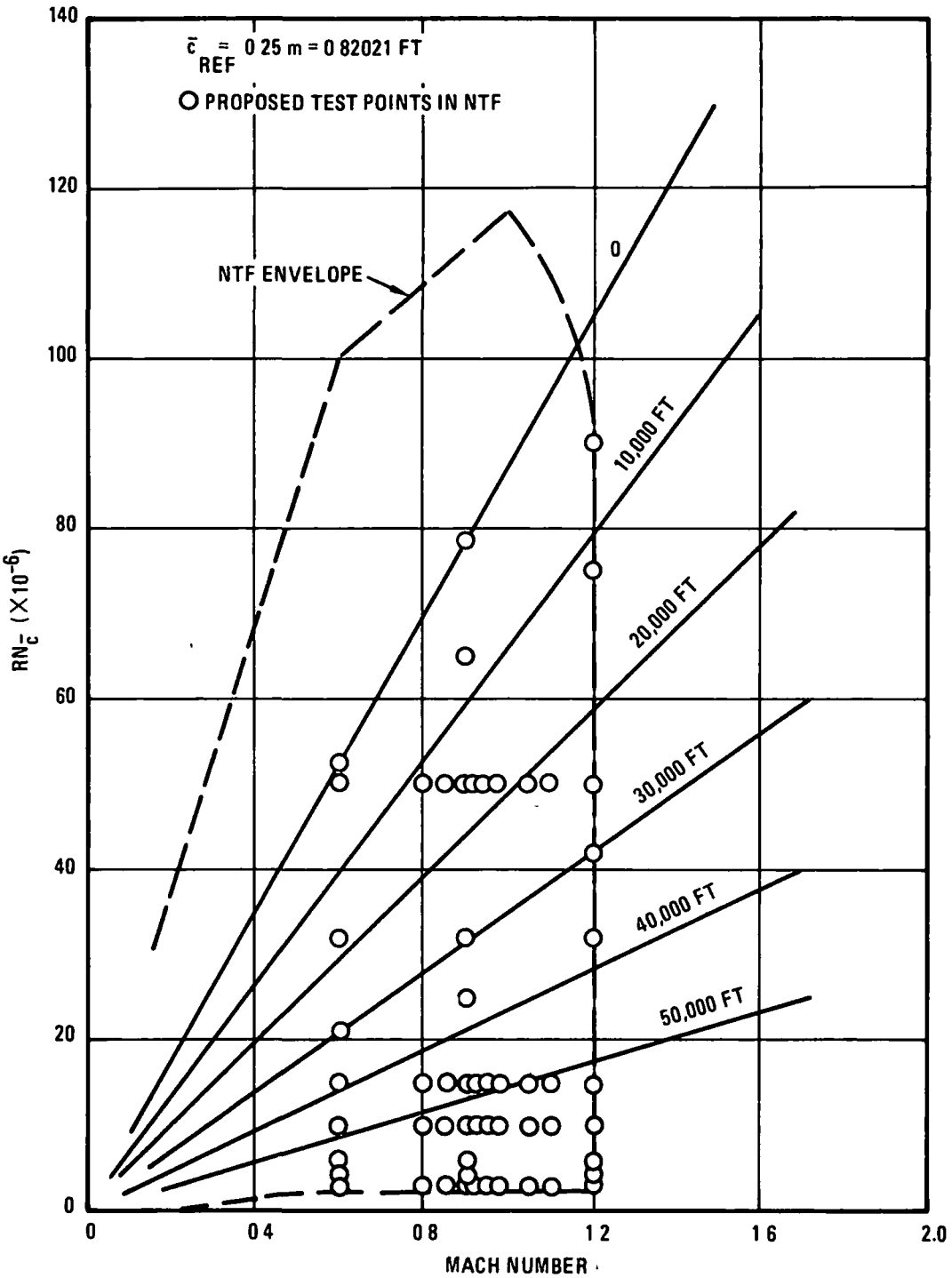

Figure 5-1. One-fifteenth-Scale CWC Proposed Test Condition with NTF Envelope and Simulated Altitude Superimposed

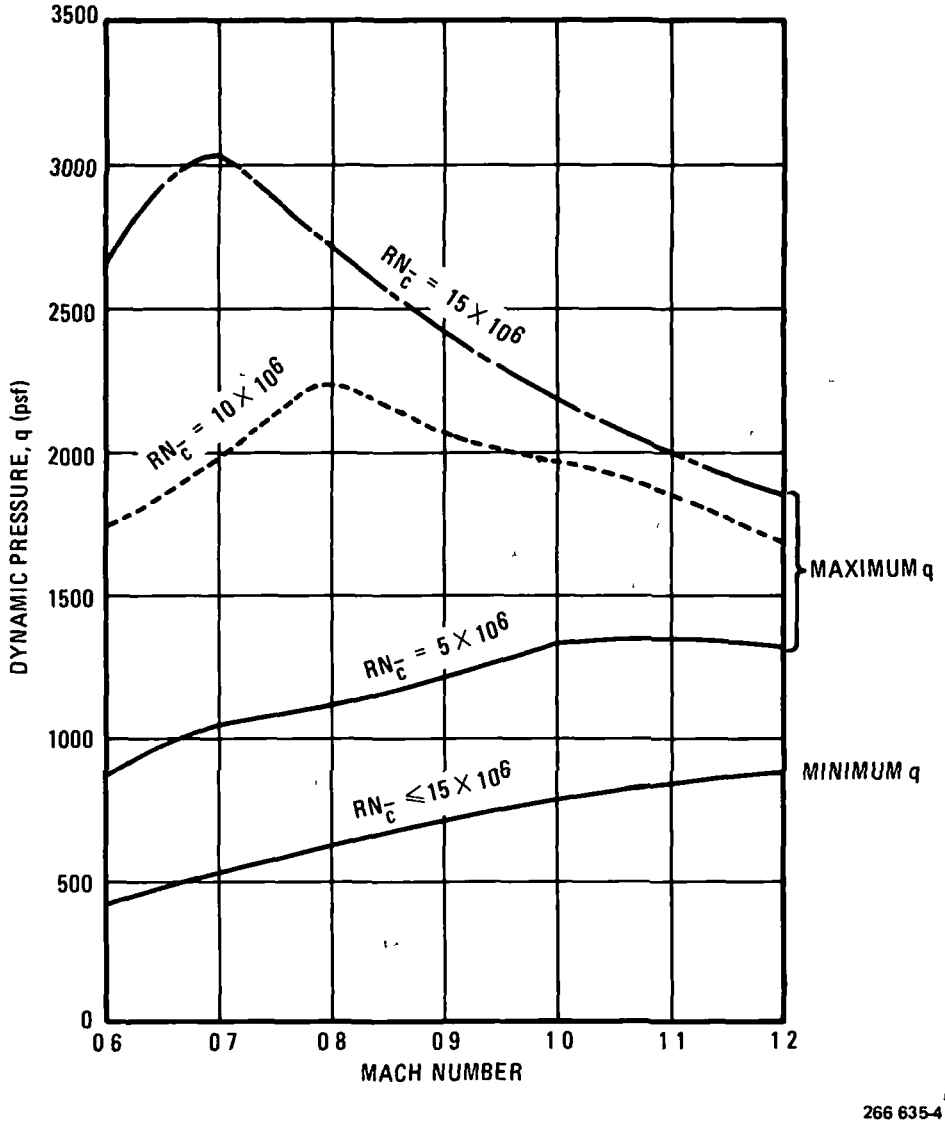

Figure 5-2. NTF Operating Limits of Dynamic Pressure as a Function of Mach Number at RN = 5, 10, and 15 × 10^6

number condition, is used to avoid aeroelastic effects from being superimposed on the Mach number effect. It is also noted that the lowest Reynolds number shown for the Mach sweeps is 5 × 10^6 instead of the generally used value of 3 × 10^6. The value of 5 × 10^6 is the lowest Reynolds number for which a constant value of q_∞ could be obtained across the Mach range from 0.6 to 1.2.

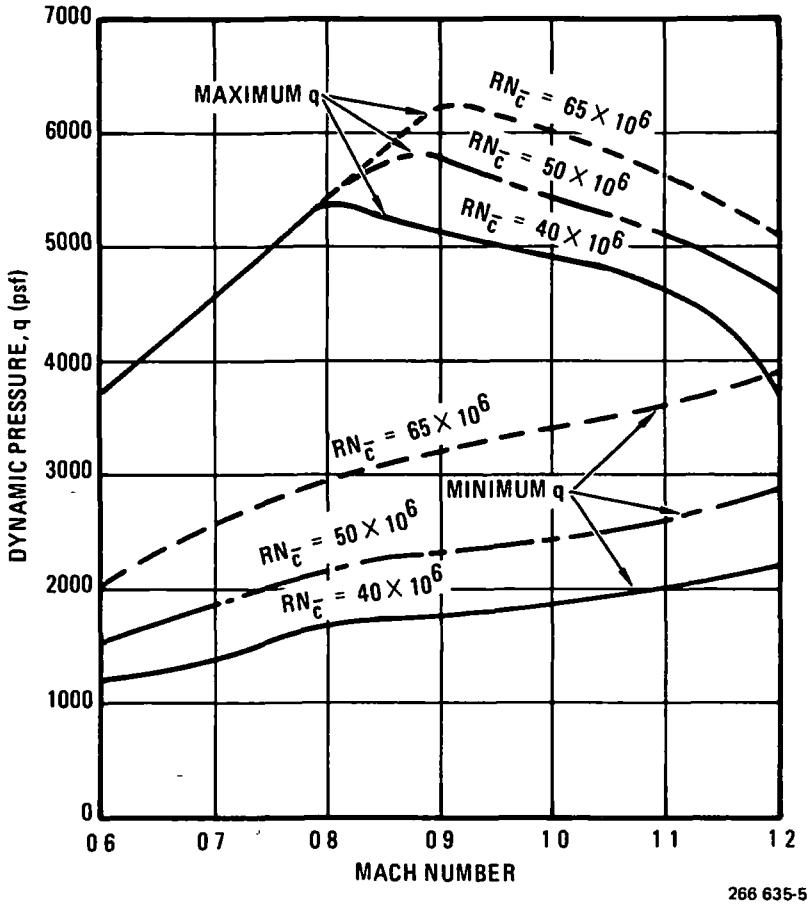

Figure 5-3. NTF Operating Limits of Dynamic Pressure as a Function of Mach Number at RN = 40, 50, and 65 × 10^6

Acquisition of wind tunnel test data at several Reynolds numbers at Mach 0.6, 0.9, and 1.2 will serve two purposes. It will allow the cut-off Reynolds number (the Reynolds number beyond which there is no longer a decrease in friction drag) to be determined. The cut-off value is dependent on the degree of model roughness due to surface finish, mismatches, etc. Determination of this value is an important factor in correlation of wind tunnel-to-flight scale effects. (This subject is discussed in depth in Section 5.3.)

5.1.3 MODEL LOADS DATA. The loads data presented in Figures 5-8 through 5-11 were acquired from the integration of pressure data from a fully instrumented 1/9-scale model of the CWC. These data represent the maximum loads that will be experienced by each component of the configuration as dictated by the test plan shown in Table FO-1 for each Mach/alpha/Reynolds number combination.

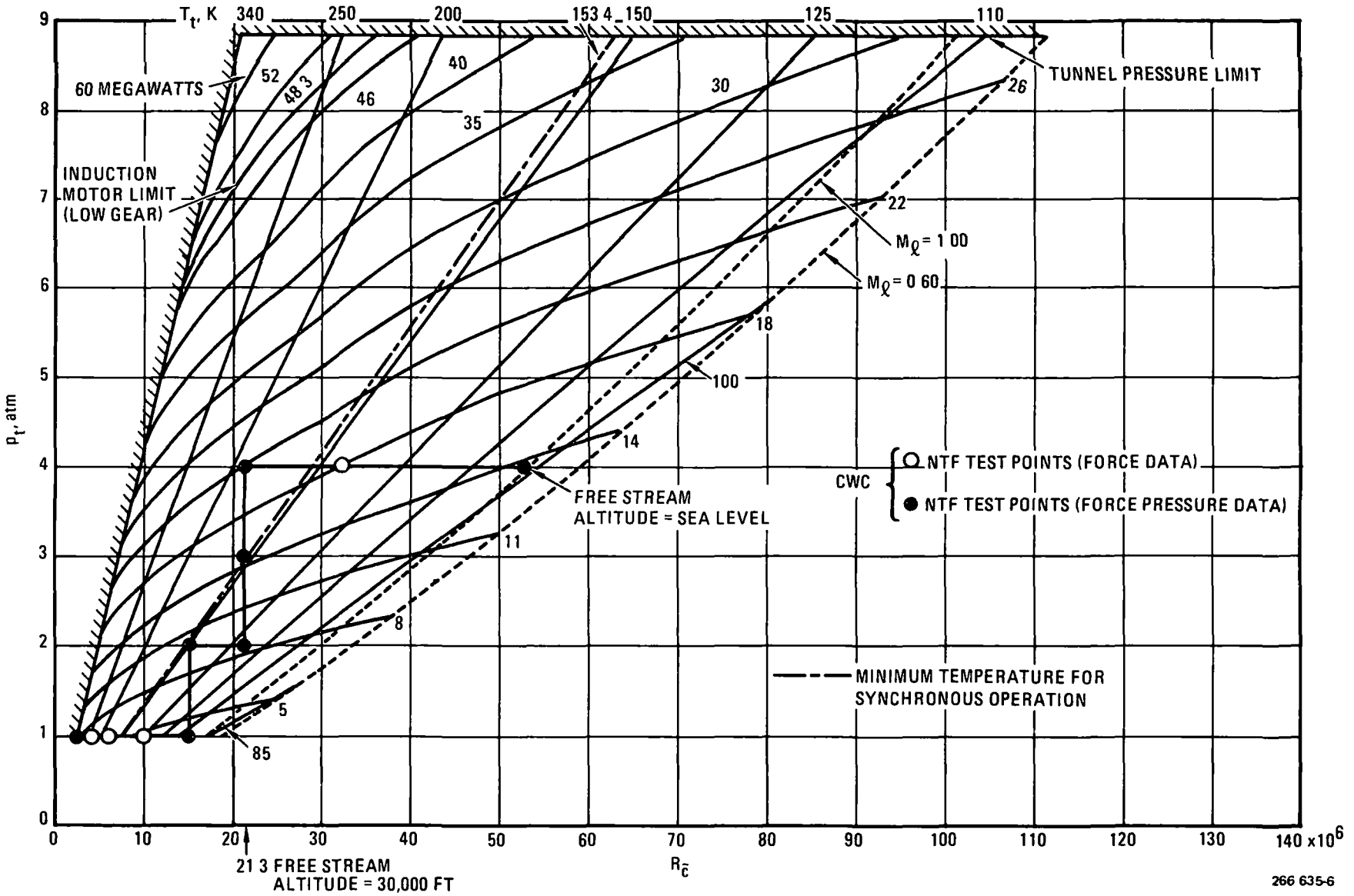

Figure 5-4. Estimated NTF Performance Map for Free Stream Mach Number of 0.60

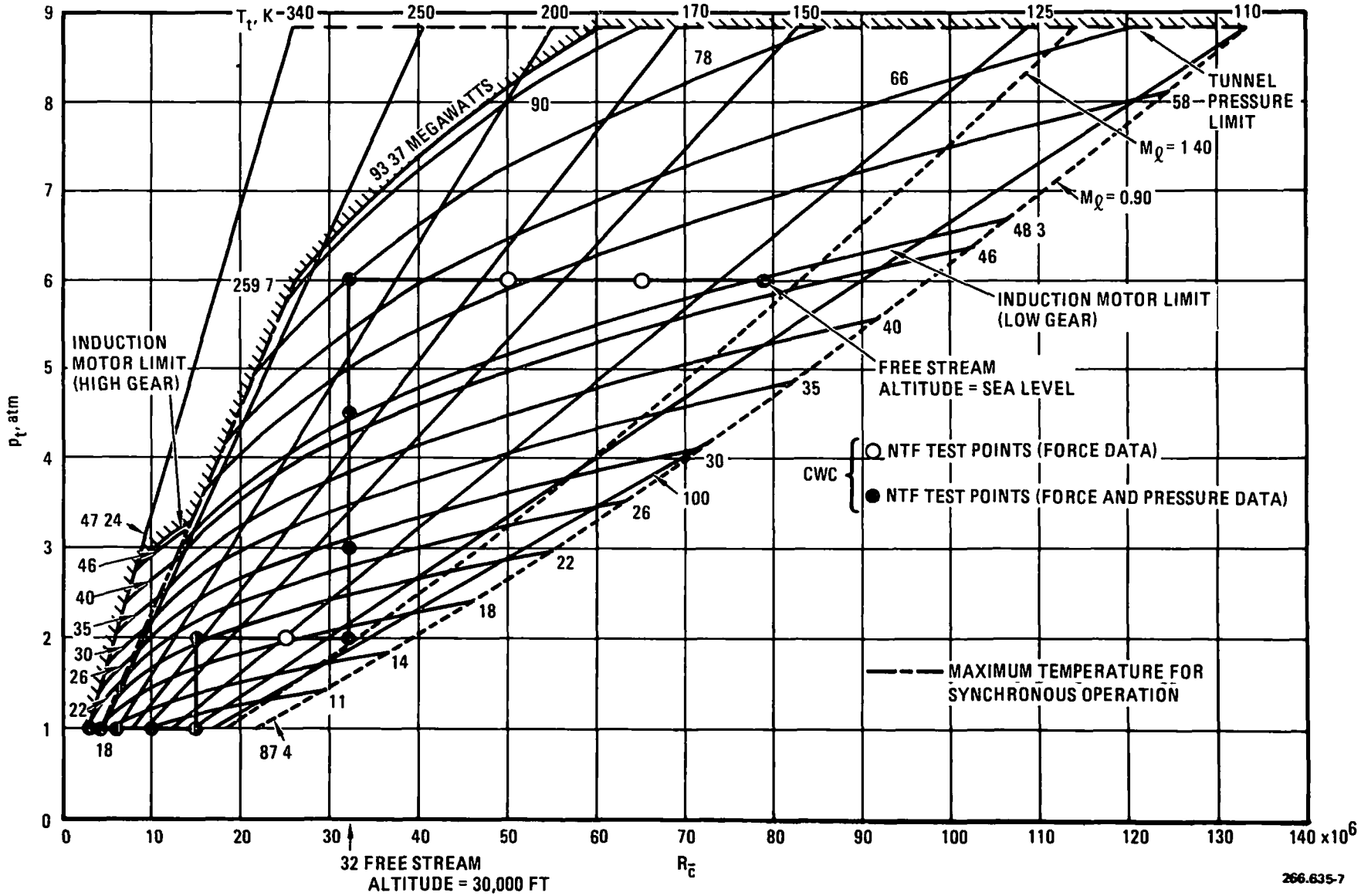

Figure 5-5. Estimated NTF Performance Map for Free Stream Mach Number of 0.90

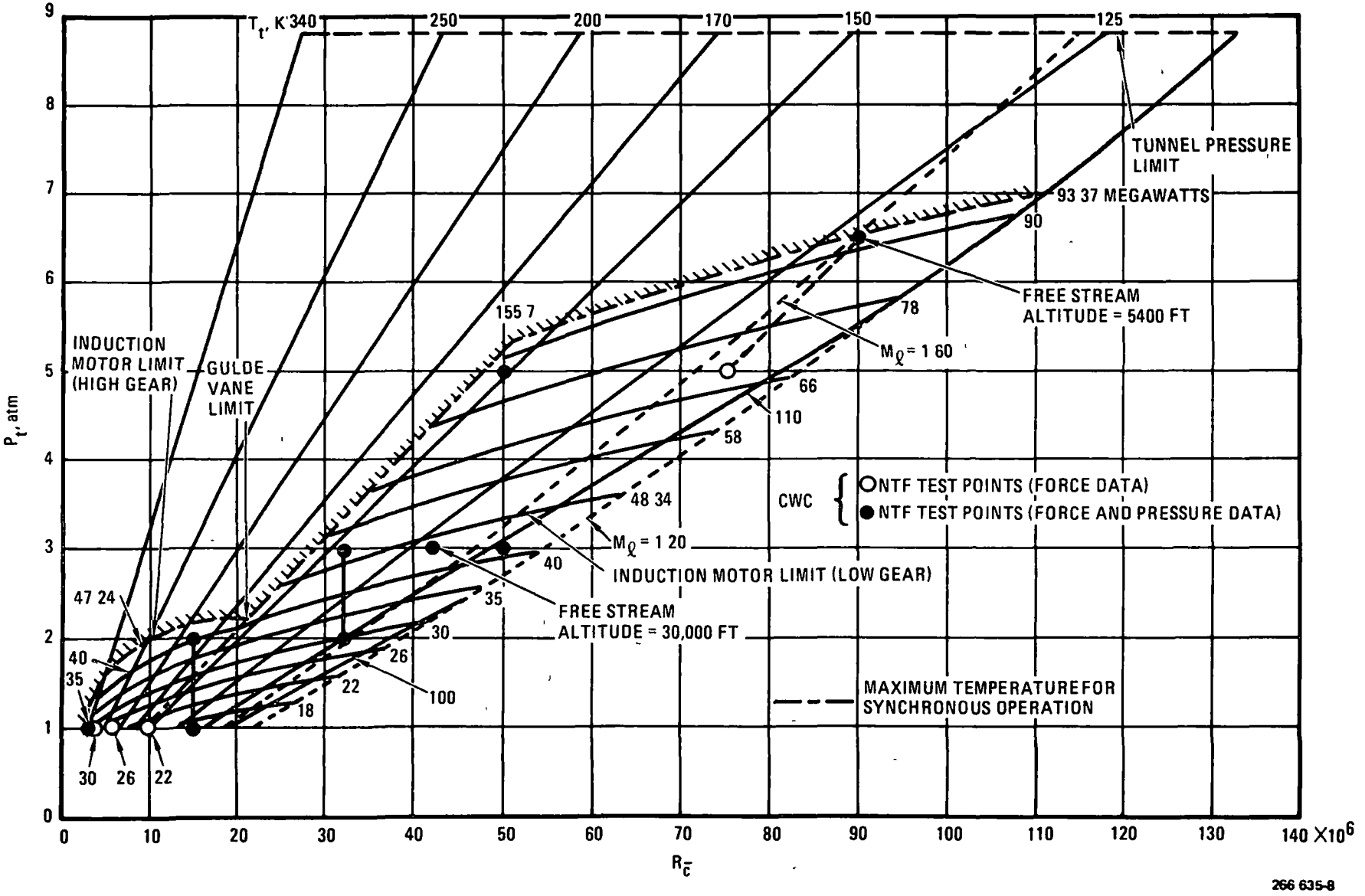

Figure 5-6. Estimated NTF Performance Map for Free Stream Mach Number of 1.20

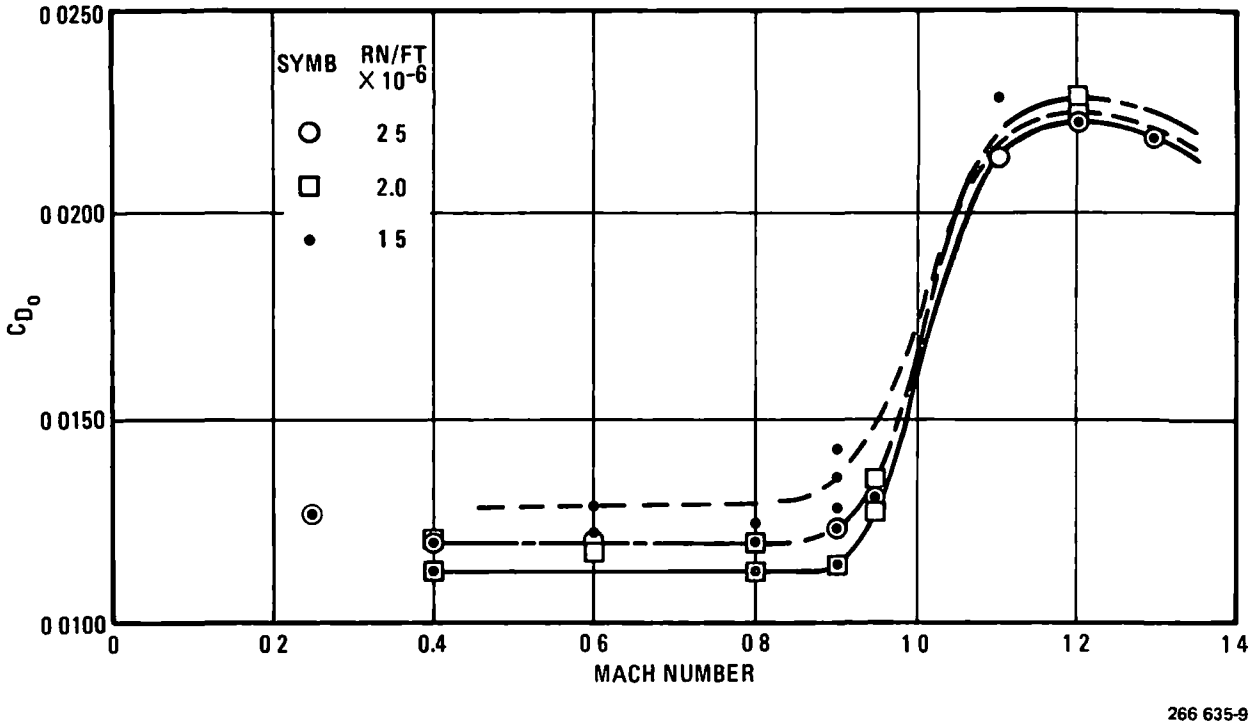

Figure 5-7. Drag Rise Characteristics for Several Highly Swept Cranked Wing Configurations (CWC)

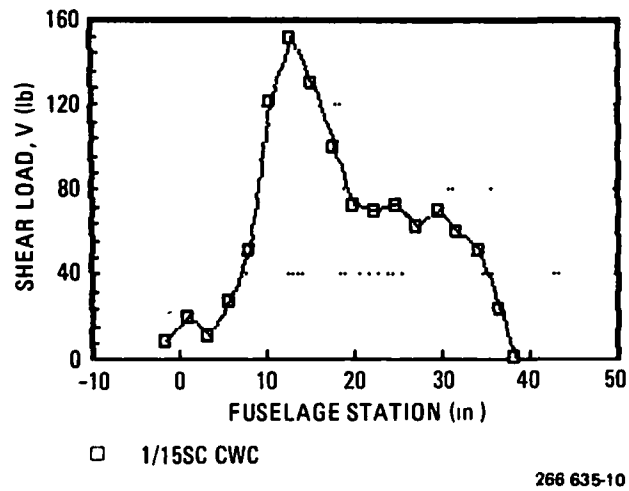

Figure 5-8. One-fifteenth-Scale CWC Fuselage Loads Distribution

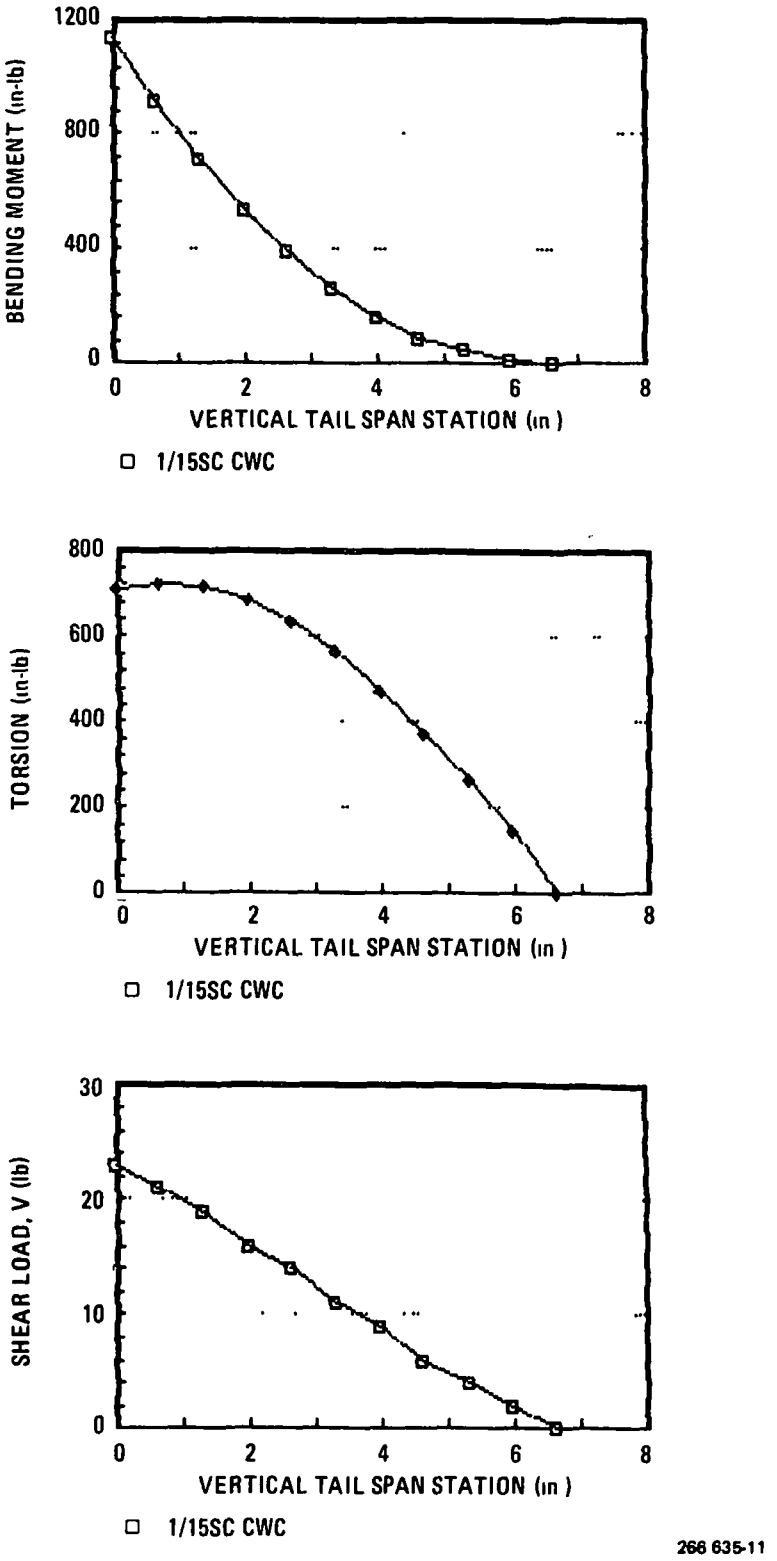

Figure 5-9. One-fifteenth-Scale CWC Vertical Tail Loads

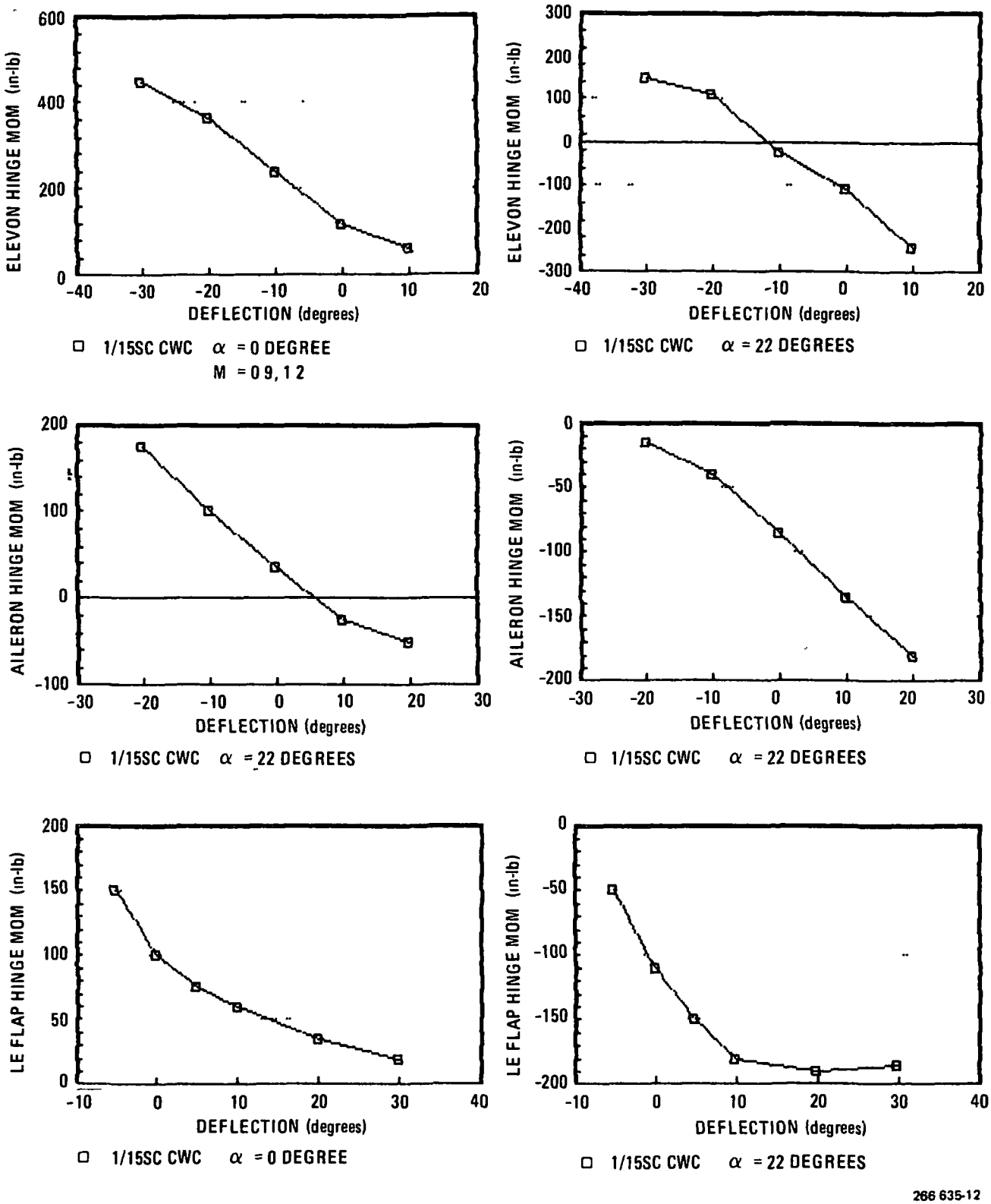

Figure 5-10. One-fifteenth-Scale CWC Wing Control Surface Loads

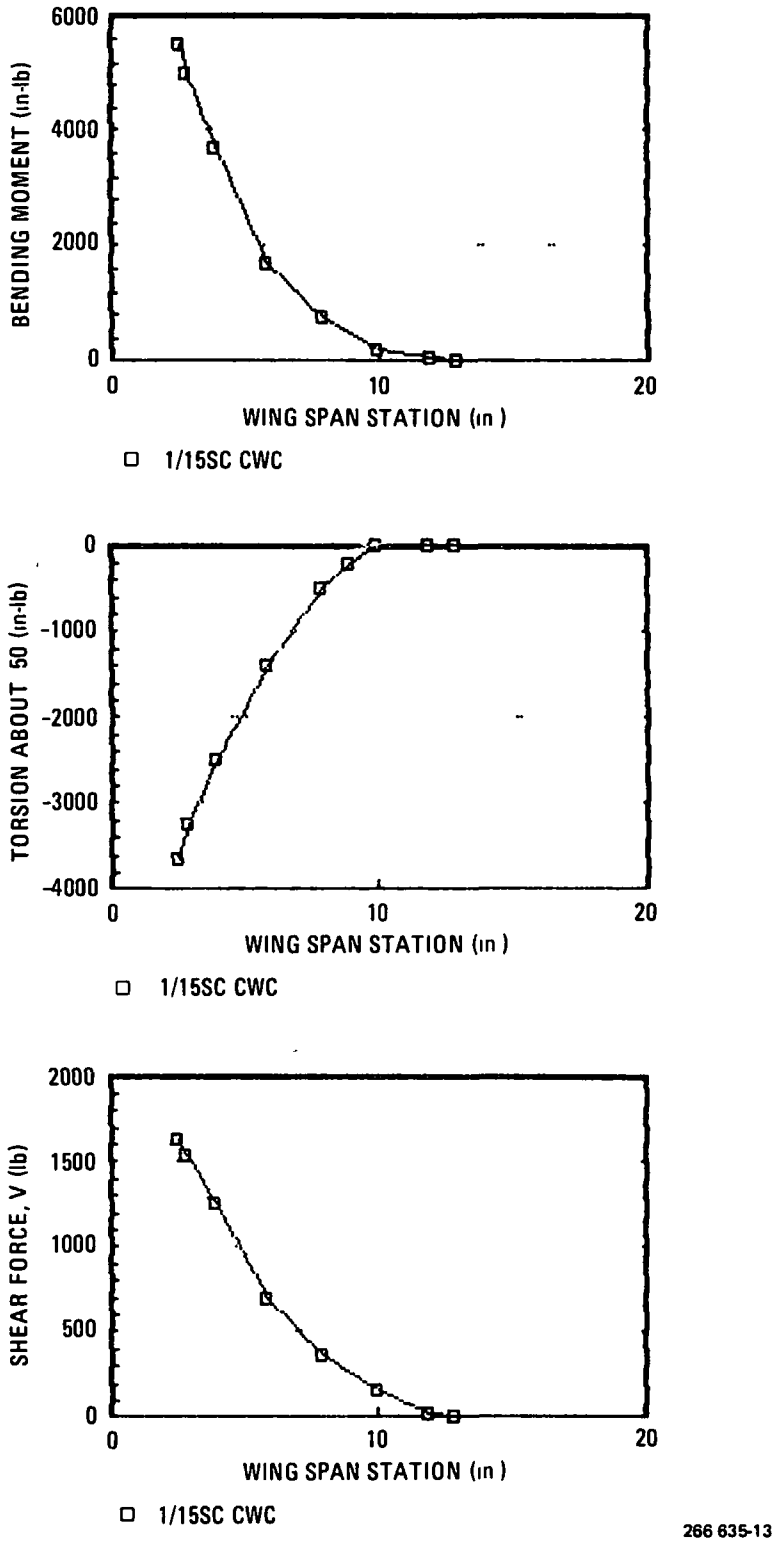

Figure 5-11. One-fifteenth-Scale CWC Total Wing Loads

5.1.4 PRESSURE DATA REQUIREMENTS. The CWC configuration will be instrumented with a total of 120 wing pressure orifices. These orifices will be divided, with all of the upper surface orifices located in the left hand wing and all of the lower surface orifices in the right hand wing. In addition, the fuselage will be instrumented with 46 pressure orifices. It is anticipated that during select runs, these fuselage pressure orifices will be substituted on the pressure scanners in place of an equal number of wing pressures. The fuselage pressures are of interest to correlate with existing pressure data, for diagnostic purposes, and to permit integration of pressure load to compare with total model forces.

The wing pressure orifice locations are depicted in Figure 5-12 with the locations detailed in Table 5-1 by span station and percent local chord. The fuselage pressure locations are presented in Table 5-2. (The wing and fuselage pressure taps will be located the same as on an existing 1/9-scale model of CWC.)

5.2 TWIN-ENGINE CONFIGURATION F-111 TACT

5.2.1 TEST OBJECTIVES AND PROPOSED TEST PLAN. The F-111 TACT configuration will make an excellent model for investigation in the NTF wind tunnel for several reasons. Approximately 1500 hours of wind tunnel testing was performed to document the aerodynamic characteristics of this variable sweep, supercritical wing configuration. Models of 1/24, 1/15, 1/12, and 1/6 scale have been tested. The 1/12-scale model was a "high-strength" model to obtain high Reynolds number data at transonic speeds to the limits available in the NASA ARC 11-foot Unitary Tunnel. Furthermore, flight test data are available from the F-111 TACT Program that was conducted jointly by NASA, the Air Force, and General Dynamics. F-111A aircraft No. 13 was converted to the F-111 TACT configuration and flight tested at the NASA Dryden Flight Test Center, where it is still operated by NASA. Flight test pressure data have been obtained and, together with the operating conditions of the NTF, provide an excellent opportunity for wind-tunnel-to-flight correlation of supercritical wing data at full-scale Reynolds numbers.

The proposed test plan for the F-111 TACT configuration is shown in Table FO-2. In many respects, the objectives sought with this configuration are similar to those described earlier for the highly swept cranked-wing configuration. Namely, a comprehensive set of data will be obtained by exploiting the high Reynolds number capability of the NTF wind tunnel. Parametric variations in the major variables are provided. These include:

a. Mach number

b. Angle of attack

c. Reynolds number

d. Dynamic pressure

e. Wing sweep

f. Horizontal tail deflection

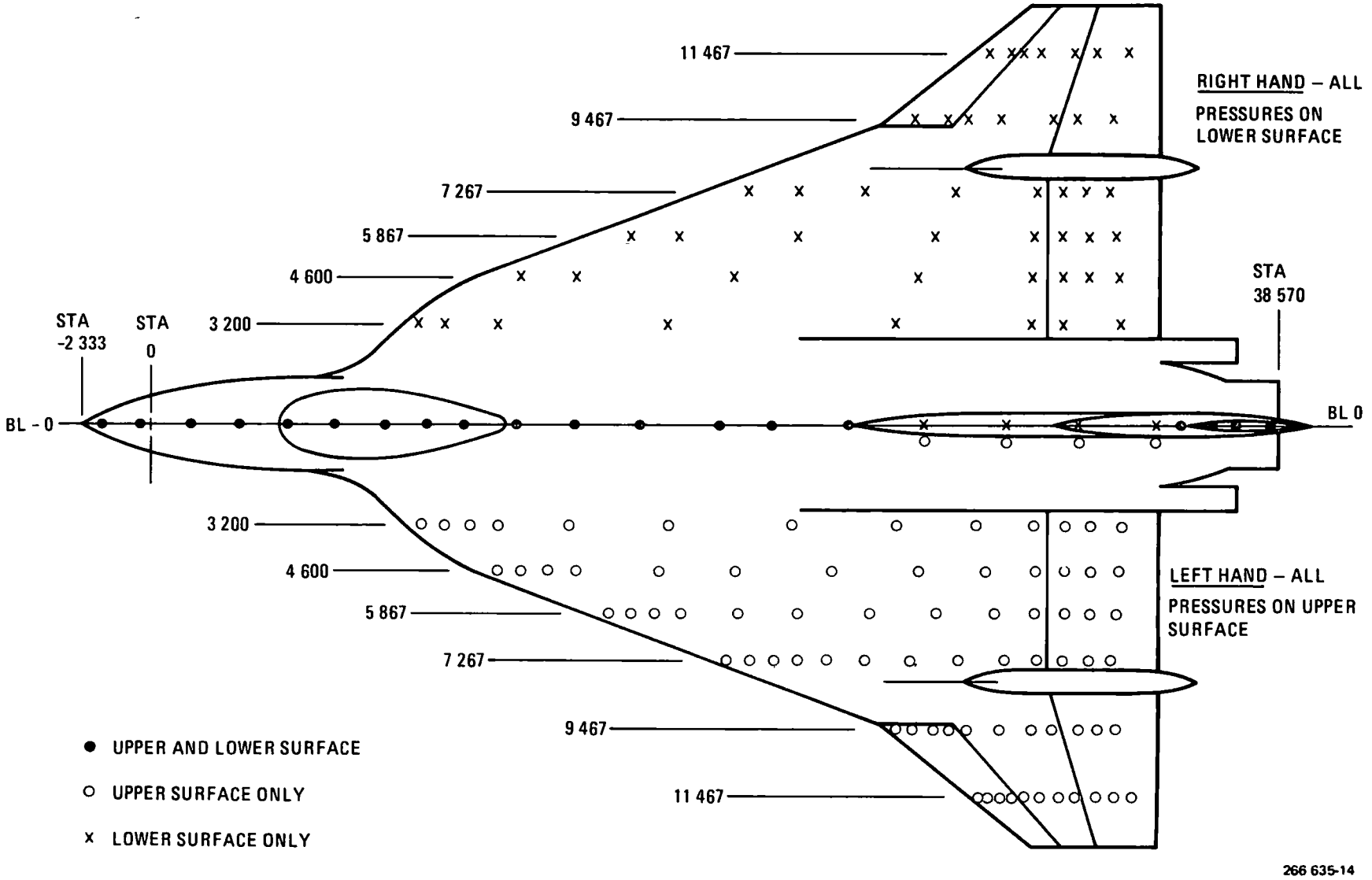

Figure 5-12. One-fifteenth-Scale CWC Wing/Fuselage Pressure Orifice Array

Table 5-1. One-fifteenth-Scale CWC Wing Pressure Orifice Locations

SS 3.200		SS 4.600		SS 5.867		SS 7.267		SS 9.467		SS 11.467	
%c		%c		%c		%c		%c		%c	
7.4	●	2.0	o	2.0	o	2.0	o	4.2	o	3.5	o
9.8	●	4.9	●	4.9	●	4.8	●	8.3	●	7.0	●
12.8	o	9.8	o	9.8	o	9.7	o	16.7	o	14.2	o
16.7	●	16.7	●	16.6	●	16.4	●	23.6	●	20.1	●
25.6	o	25.5	o	25.4	o	25.2	o	32.0	●	27.2	●
36.4	●	36.2	●	36.1	●	35.8	●	43.2	●	37.9	●
49.1	o	49.0	o	48.8	o	48.4	o	54.4	o	48.7	o
60.9	●	60.7	●	60.5	●	60.0	●	65.6	●	59.4	●
73.2	o	72.0	o	70.7	o	68.2	o	73.2	●	68.1	●
85.4*	●	83.5	●	80.9	●	76.4	●	79.4	o	75.4	o
88.7*	●	87.3	●	85.2	●	81.7	●	88.2	●	85.5	●
91.6*	o	90.4	●	88.8	●	86.2	●				
95.5*	●	94.8	●	93.9	●	92.3	●				

● Upper and lower surface orifice

o Upper surface orifice only

* Orifices at SS 3.233 on upper surface, SS 3.167 on lower surface

Note: All upper surface orifices are on the left hand wing panel and all lower surface orifices are on the right hand wing panel.

Table 5-2. One-fifteenth-Scale CWC Fuselage Pressure Orifice Locations

Fuselage Station	Buttock Line		Fuselage Station	Buttock Line	
-1.733	0	●	24.167	0	●
-0.333	0	●	26.733	0.187	o
1.333	0	●		0	x
3.000	0	●	29.333	0.393	o
4.667	0	●		0	x
6.333	0	●	31.933	0.513	o
8.000	0	●		0	x
9.400	0	●	34.487	0.540	o
10.833	0	●		0	x
12.460	0	●	35.267	0	●
14.633	0	●	36.267	0	●
16.833	0	●	37.467	0	●
19.333	0	●	38.400	0	●
21.213	0	●			

● Upper and lower surface

o Upper surface orifice only

x Lower surface orifice only

The first four are the same as included in the cranked-wing test plan. In the present case, wing sweep will be investigated in place of leading-edge flap deflection, and horizontal tail deflections have replaced elevon and aileron deflections as test variables.

5.2.2 TEST PLAN RATIONALE. The F-111 TACT configuration will be a better configuration than the CWC for examining Reynolds number effects. The nature of the F-111 TACT (airfoil, leading-edge radius, thickness-to-chord ratio, and airfoil type) suggests that Reynolds number effects would be greater than those expected on the CWC. The most significant effects should be observed in the Mach range between 0.80 and 0.90 (Reference 3).

The test plan in Table FO-2 was developed so that high Reynolds number data can be obtained at the lowest dynamic pressure available. As discussed earlier for the cranked-wing configuration, this approach provides the desired data without placing unnecessary demands on the model design. The test plan covers conditions representative of the flight test points over much of the flight envelope. Figure 5-13 presents the planned test points (Reynolds number/Mach number) with the operating range of the NTF and simulated altitude superimposed.

To separate the effects of Reynolds number and dynamic pressure (aeroelastic effects), the variation from wind tunnel Reynolds numbers to full-scale Reynolds numbers was accomplished by alternately varying Reynolds number at constant q and then varying q at constant Reynolds number. This stairstep path is illustrated in Figures 5-14, 5-15, and 5-16 for Mach numbers of 0.7, 0.9, and 1.2. This approach is identical to that planned for the cranked-wing configuration. The F-111 TACT test plan includes other similarities with the cranked-wing plan, such as the acquisition of sufficient data to define the cut-off Reynolds number and to determine Reynolds number effects on critical Mach number and drag rise characteristics. As explained for the CWC case, the Mach sweeps at constant Reynolds number are to be obtained at constant q by varying the total pressure as shown in Schedule J of Table FO-2.

Testing of the F-111 TACT configuration in the NTF will provide valuable insight into Reynolds number effects on attached flow, shock-induced separation, and leading-edge separation. These effects can be quite significant due to the unusual shape of the supercritical airfoil. In fact, testing of supercritical wings requires that special consideration be given to location of transition grit strips. There has always been some degree of uncertainty surrounding the question of the ability to simulate full-scale shock strength/location characteristics by locating boundary layer transition considerably aft of the airfoil leading edge (often near 40% chord). It is recognized that a turbulent boundary layer should exist ahead of a shock. If transition occurs aft of the shock, the thin laminar boundary layer can cause the shock to be located too far aft. In addition to affecting pitching moment, the thin boundary layer could provide optimistic results by retarding the onset of trailing-edge separation. On the other hand, if transition is located too far ahead of the shock, the thick, turbulent boundary layer may cause the shock to be located forward of the full-scale value and result in premature trailing-edge separation. Ideally, the grit location would need to be varied with Mach number and angle of attack to achieve simulation of full-scale results. Correlation of F-111 TACT NTF data across the Reynolds number spectrum should be extremely beneficial in establishing guidelines for grit location when testing at low Reynolds numbers in other facilities.

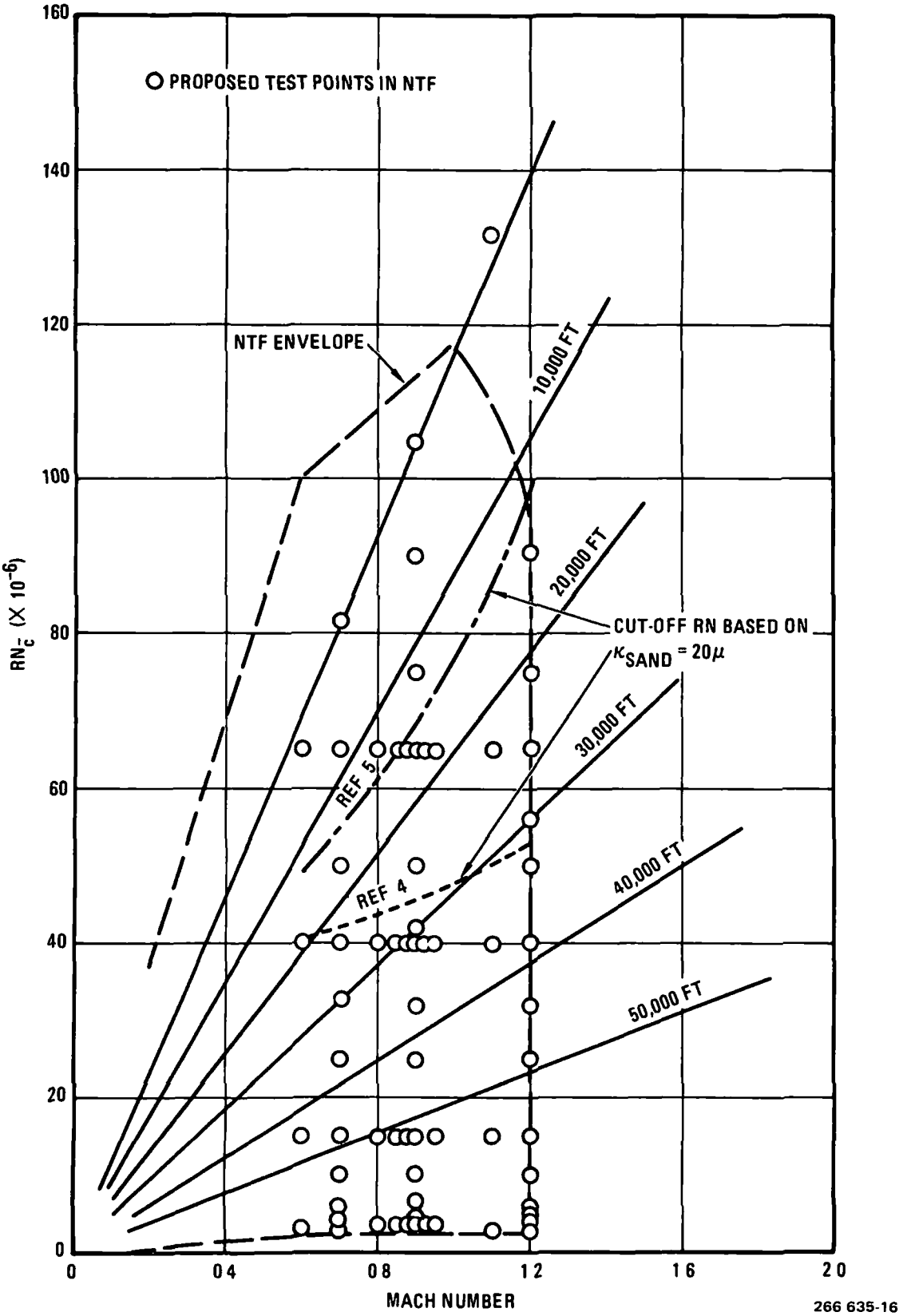

Figure 5-13. F-111 TACT Proposed Test Conditions with NTF Envelope and Simulated Altitude Superimposed

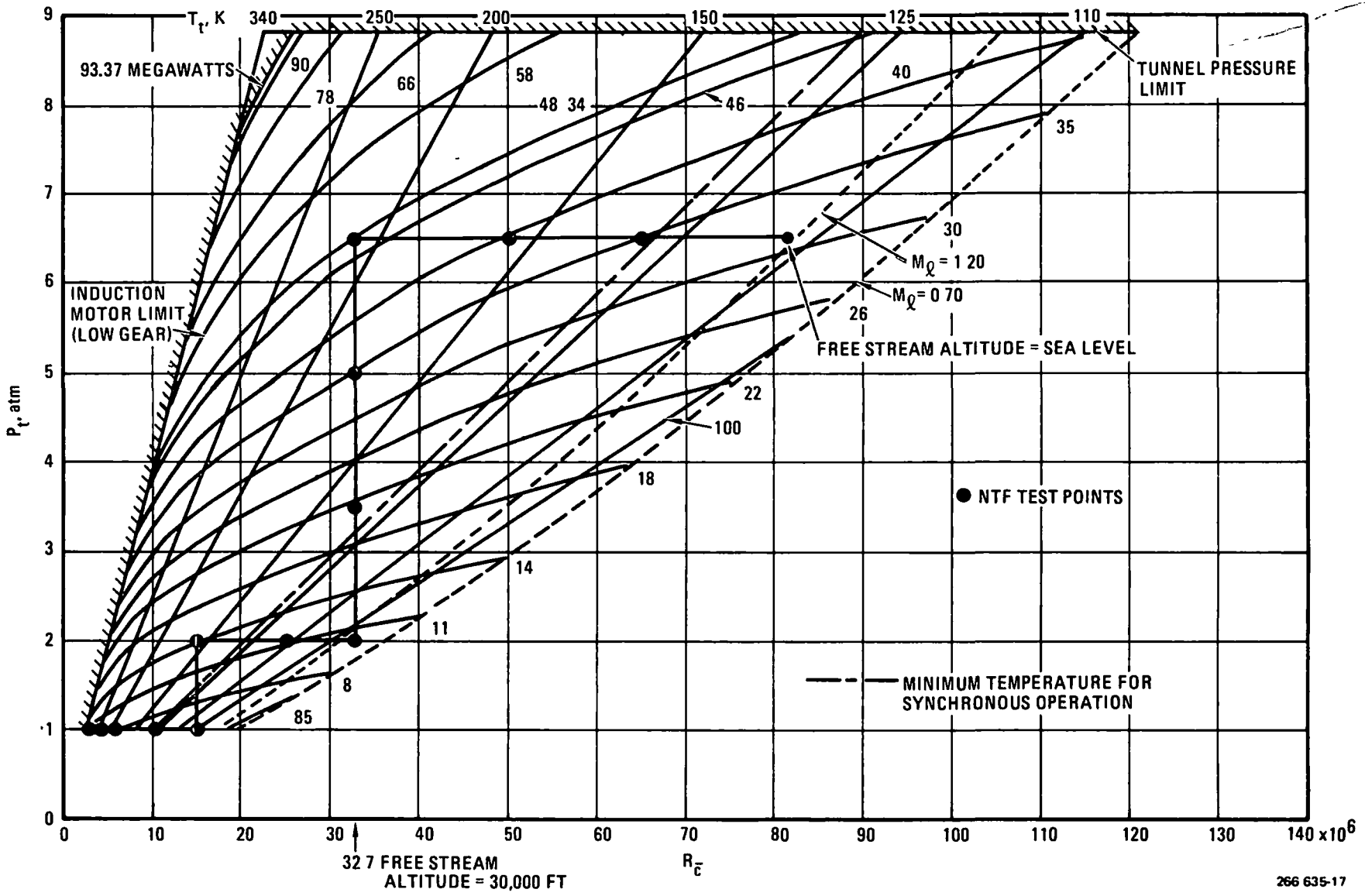

Figure 5-14. F-111 TACT Estimated NTF Performance Map for Free Stream Mach Number of 0.70

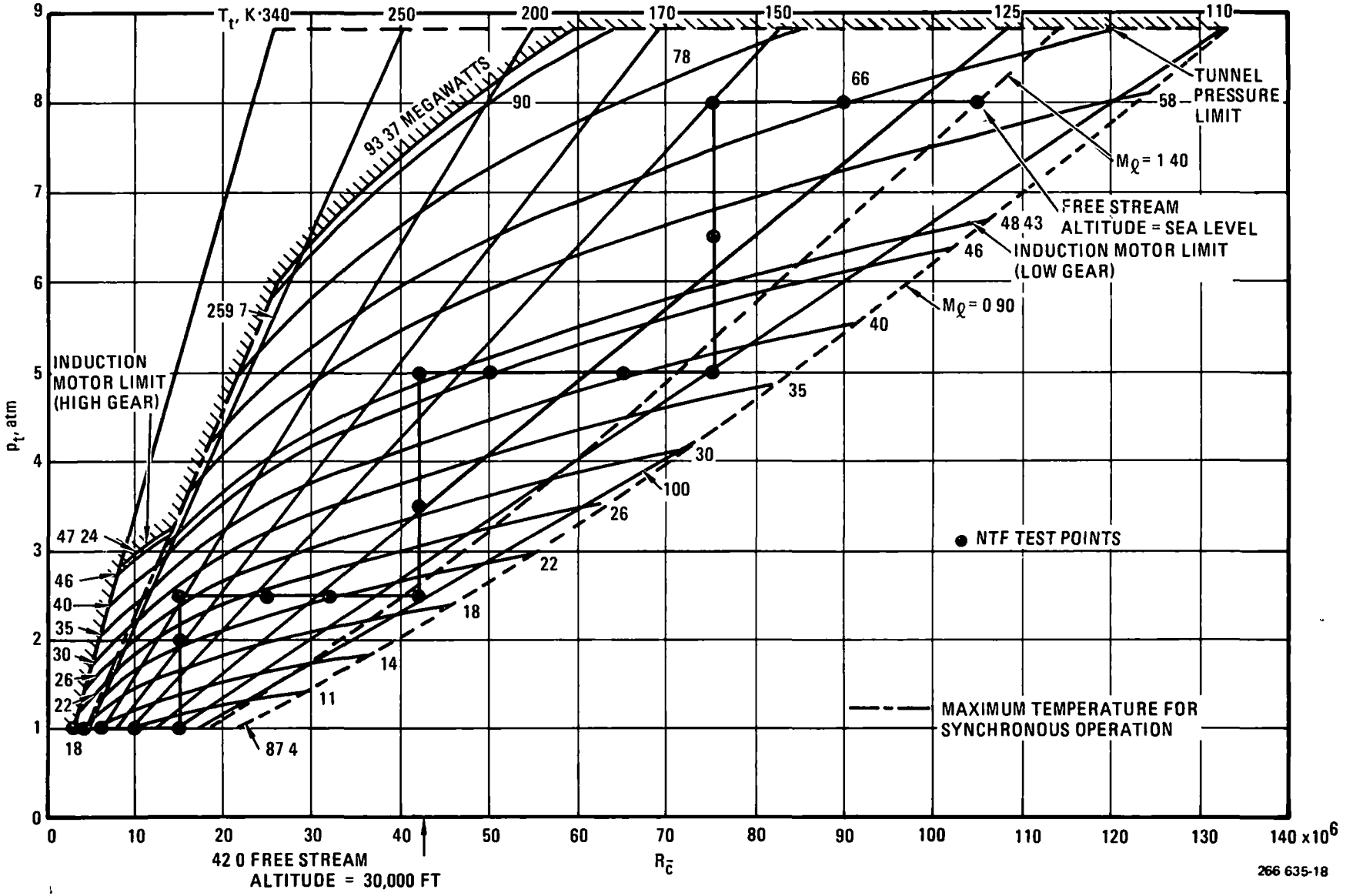

Figure 5-15. F-111 TACT Estimated NTF Performance Map for Free Stream Mach Number of 0.90

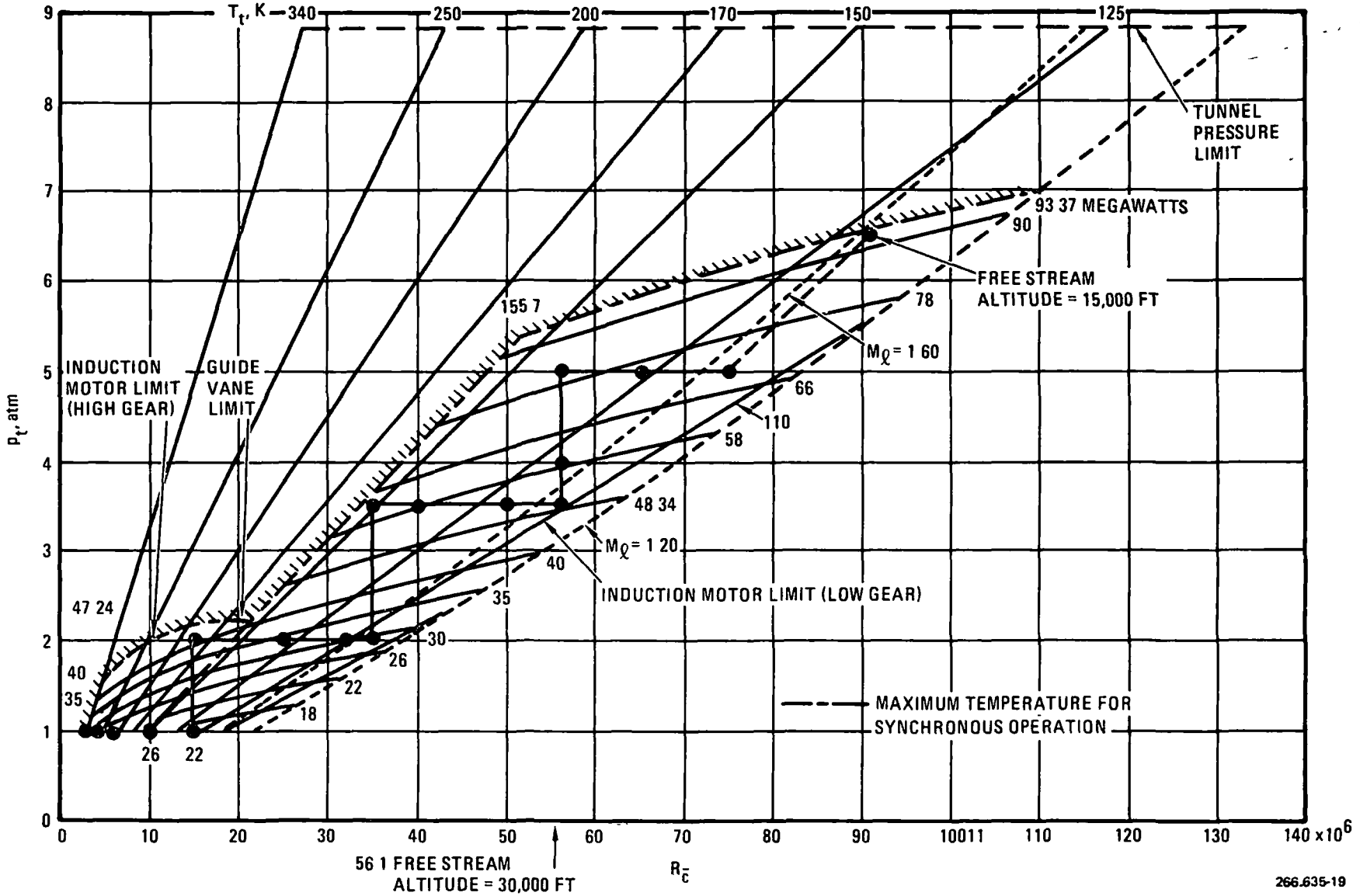

Figure 5-16. F-111 TACT Estimated NTF Performance Map for Free Stream Mach Number of 1.20

5.2.3 MODEL LOADS DATA. The loads data presented in Figures 5-17, 5-18, and 5-19 were acquired from the integration of pressure data from instrumented F-111 models. Fuselage and horizontal tail loads were derived from 1/12-scale model data while the TACT wing loads were obtained from 1/15-scale flexible wing pressure data. These data represent the maximum loads that will be experienced as dictated by the test plan of Section 5.2.2.

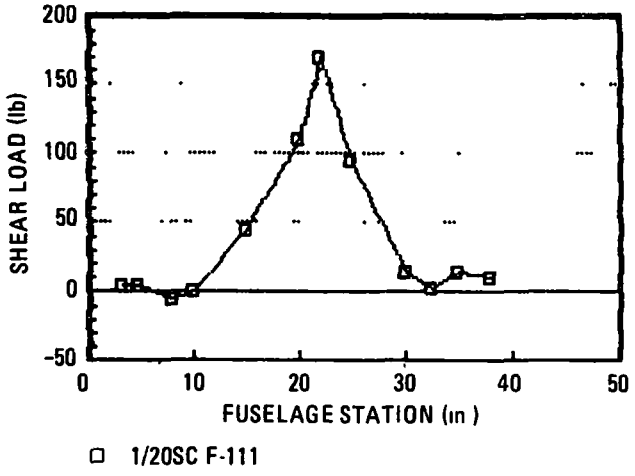

Figure 5-17. One-twentieth-Scale F-111 TACT Fuselage Loads Distribution

5.2.4 PRESSURE DATA REQUIREMENTS. The F-111 TACT configuration will be instrumented with 119 wing pressure orifices. These orifices will be divided with all of the upper surface orifices located in the left hand wing and the lower surface orifices in the right hand wing. In addition, the fuselage will be instrumented with 23 taps on the over-wing glove surfaces. During select runs, these fuselage orifices will be substituted on the pressure scanners in place of an equal number of wing pressures. The fuselage pressures are of interest to correlate with existing pressure data and for diagnostic purposes.

The wing pressure orifice locations are depicted in Figure 5-20, and the locations are defined by span station and percent local chord in Table 5-3. The fuselage pressure locations are presented in Table 5-4. The wing and fuselage pressure taps will be located the same as on an existing 1/12-scale model of F-111 TACT and the full-scale aircraft.

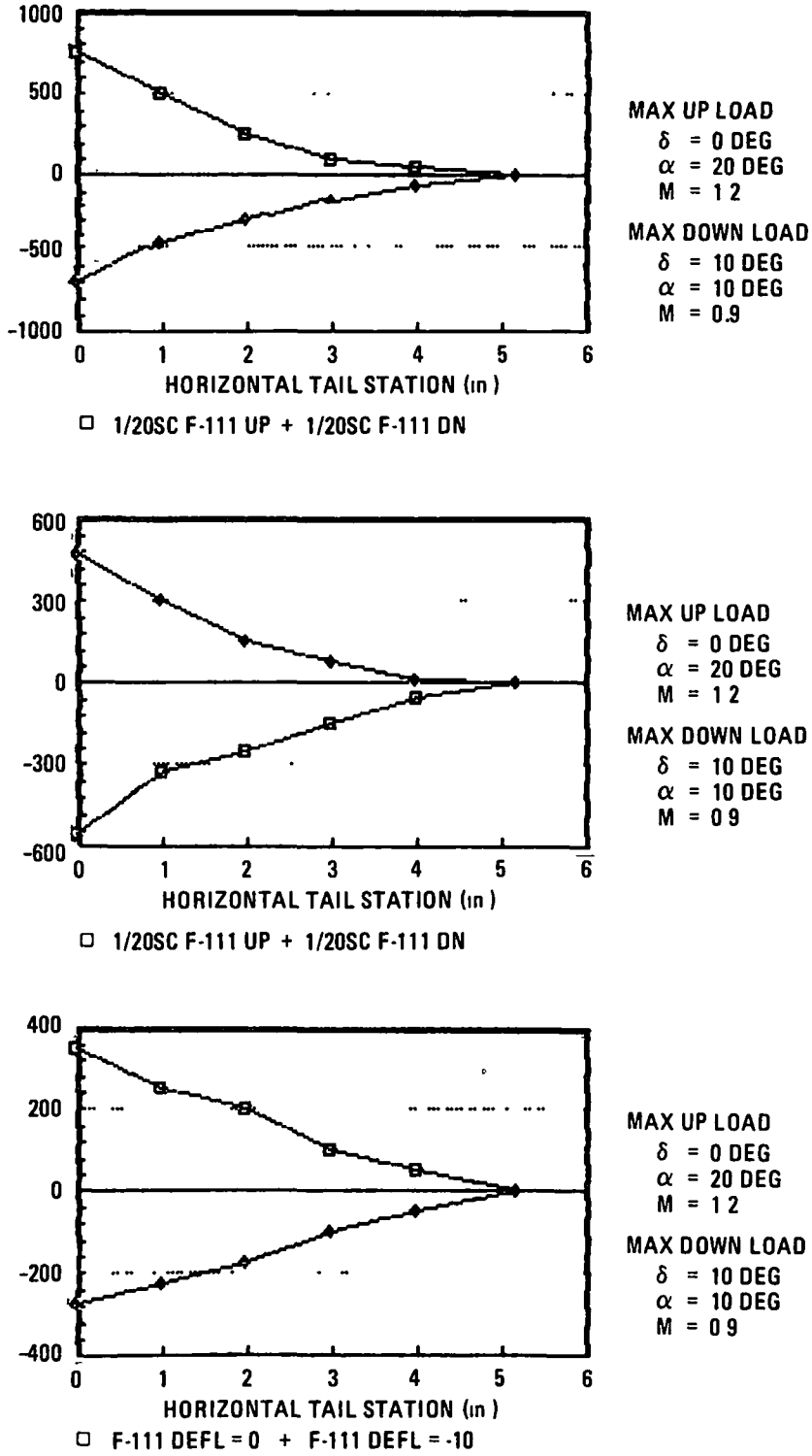

Figure 5-18. One-twentieth-Scale F-111 TACT Horizontal Tail Loads

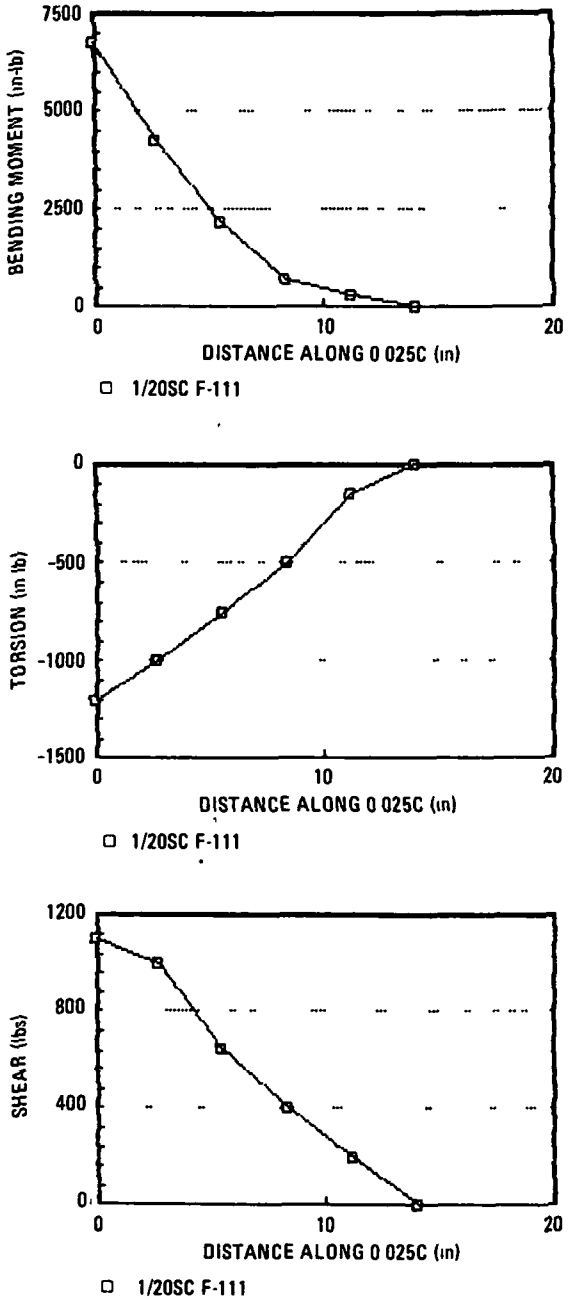

Figure 5-19. One-twentieth-Scale F-111 TACT Wing Loads

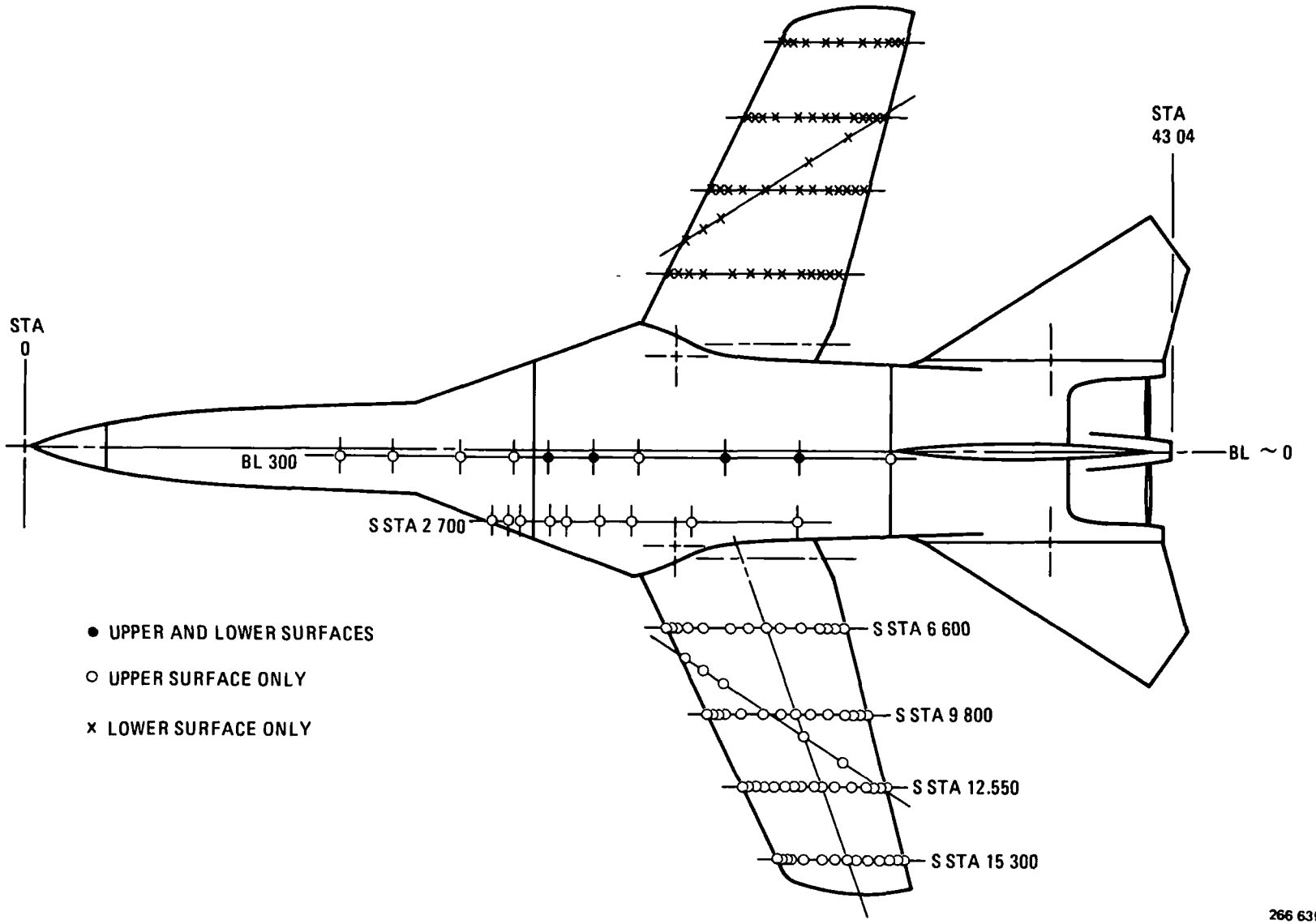

Figure 5-20. One-twentieth-Scale F-111 TACT Wing/Fuselage Pressure Orifice Array

Table 5-3. One-twentieth-Scale F-111 TACT Wing Pressure Orifice Locations

Span Station	%c		Span Station	%c		Span Station	%c		Span Station	%c		Span* Station	%c	
6.600	LE	o	9.800	LE	o	12.550	LE	o	15.300	LE	o	7.760	2	●
	2	●		2	●		2	●		2	●	8.277	11	●
	5.75	x		6	●		6	●		6	●	8.776	20	x
	6	o		11	●		11	●		11	●	8.798	19.13	o
	10.24	o		20	●		20	●	15.316	18.97	o	10.733	55	●
	11	x		35.85	●		30	o	15.220	19.11	x	11.485	75	●
	19.96	●		45.68	●		35	●	15.300	35	●			
	35	●		55	●		40	o		45	●			
	45	●		63	o		45	●		56.16	o			
	55	●	9.807	63.39	x		50	o		63	●			
	63	●	9.800	75	●		55	●		75	●			
	75	●		79.16	x		63	●		85	●			
	79.33	x		85	●		75	●		90	●			
	85	●	9.764	89.96	●		79.08	x		95	●			
	90	●	9.800	95	●		85.01	●		99.77	o			
	95	●		99.82	o		89.90	●						
	99.85	o					95	●						
							99.80	o						

● Upper and lower surface orifice

o Upper surface orifice only

x Lower surface orifice only

* Λ = 58-degree ray at SS 6.925

Note: All upper surface pressure orifices are on the left hand wing and all lower surface pressure orifices are on the right hand wing.

Table 5-4. One-twentieth-Scale F-111 TACT Fuselage/Glove Pressure Orifice Locations

Fuselage Station	Buttock Line		Glove Span Station	%c	
11.800	0.300	o	2.700	2	o
13.800		o		6	o
16.300		o		11	o
18.300		o		20	o
19.600		●		25	o
21.300		●		35	o
23.000		o		45	o
26.250		●		63	o
29.050		●		95	o
32.500		o			

● Upper and lower surface

o Upper surface orifice only

5.3 MODEL SURFACE REQUIREMENTS

To match full-scale Reynolds numbers in the NTF, the unit Reynolds number (per foot) will need to be larger than the corresponding full-scale value by the inverse of the model scale. Consequently, allowable surface roughness must be scaled down accordingly, so that it does not contribute unrealistically to the drag. Below a predetermined Reynolds number (referred to as the "cut-off" Reynolds number), roughness has no effect on the drag if all protuberances are contained within the laminar sublayer of the turbulent boundary layer. Since the laminar sublayer becomes larger with increasing distance from the leading edge, the admissable roughness can be larger at the trailing edge than at the leading edge. In addition to requiring a good surface finish, the model component buildup will require extreme care to minimize additional roughness due to gaps, mismatches, screw protuberances, and bumps around orifices. Otherwise, the builtup model roughness and surface finish will be inconsistent.

A variety of methods are available for predicting the friction drag of smooth as well as rough surfaces. The combination of methods used for smooth and rough surfaces will determine the value of cut-off Reynolds number, above which no further decrease in friction drag is assumed to occur. The determination of a realistic cut-off Reynolds number is a primary factor in establishing the surface finish requirements for an NTF model. Available methods for the prediction of *compressibility* effects as a function of surface roughness yield surprisingly different results. Reference 6 (dated 1981) states "the effects of compressibility and heat transfer on roughness effects have not been thoroughly investigated and reliable generalized relations are not yet available."

Two representative approaches for determining the cut-off Reynolds number are described in References 7 and 8. The method of Reference 7 utilizes the White-Christoph (Reference 9) relations for determining the smooth flat-plate skin-friction coefficient (C_f) as a function of Mach number and Reynolds number. The method of Reference 7 assumes that the variation of $C_f/C_{f\ \text{incompressible}}$ for a roughened surface varies with Mach number in the same manner as for a smooth plate, as shown in Figure 5-21. This approach is supported by test data found in References 10 and 11. The cut-off Reynolds number is given by the relation:

$$RN_{c.o.} = K_{1\bar{c}} \left(\frac{\ell_{\bar{c}}}{k} \right)^{1.0489}$$

where

$$K_{1\bar{c}} = 37.587 + 4.615M + 2.949M^2 + 4.132M^3$$

M = Mach number

$RN_{c.o.}$ = cut-off Reynolds number based on $\ell_{\bar{c}}$

$\ell_{\bar{c}}$ = the characteristic length (M.A.C. for wings)

k = admissible surface roughness factor

This relation is in close agreement with the analysis provided by Ekstein in Reference 12.

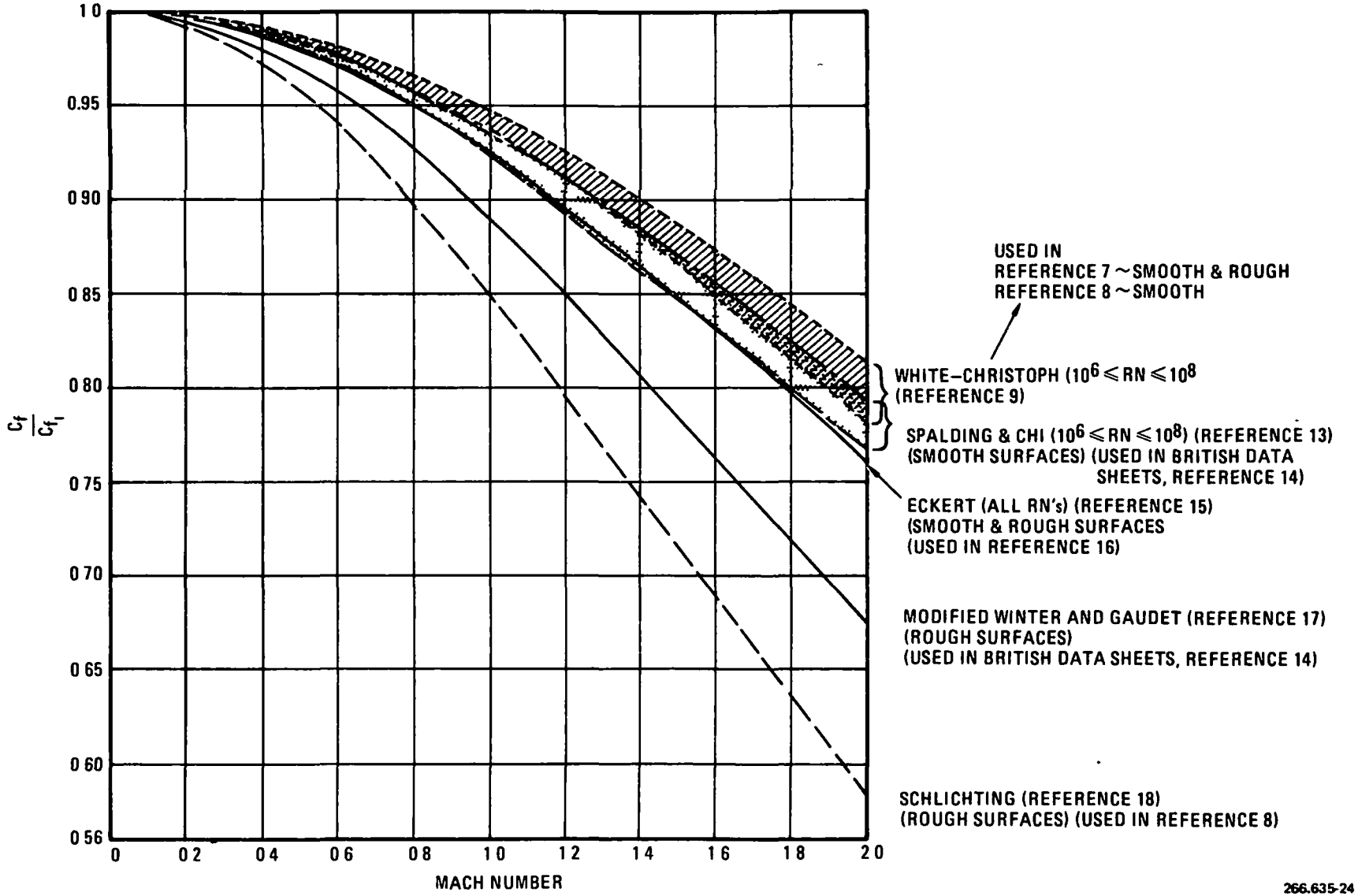

Figure 5-21. Compressibility Effects on Skin Friction Coefficient for Smooth and Rough Surface

The method of Reference 8 retains the use of the White-Christoph formulation for smooth flat-plate friction drag, but employs a more optimistic compressibility effect for rough surfaces. The method is recommended by Schlichting (Reference 18) and is based on test data from Reference 19. The variation of C_f/C_{f_i} is shown in Figure 5-21. The value of C_f for rough plates is given by:

$$C_f = (1 + 0.178M^2)^{-1} \quad (1.89 + 1.62 \log_{10} \frac{\ell}{k})^{-2.5}$$

The cut-off Reynolds number is determined as the value at which the smooth flat-plate variation with Reynolds number intersects the rough flat-plate value.

Figure 5-21 also shows the smooth and rough plate compressibility variations used in Reference 14 (British Data Sheets). The method of Reference 14 provides slightly less conservative compressibility effects for smooth surfaces (based on Spalding and Chi, Reference 13) than given by Reference 8 (White-Christoph), but it is more conservative for rough surfaces (modified Winter and Gaudet, Reference 17) than Reference 18 (Schlichting). Reference 14 states that for rough surfaces, the method is in better agreement with test data from Reference 20 (Defense Research Laboratory, University of Texas) than with the data of Reference 19 (Goddard). Reference 14 concludes that the data of Reference 20 are likely to be the more reliable of the two sets owing to the problems inherent in the test technique of Reference 19.

Finally, for completeness, Figure 5-21 shows the compressibility effect for the method of Reference 16, which employs the Eckert reference temperature method (Reference 15). Reference 16 assumes the same compressibility effects apply for smooth and rough surfaces as was the case for Reference 7.

A summary of the methods discussed above is provided in Table 5-5. Figure 5-21 shows that the primary difference in the methods lies in the compressibility effects for rough surfaces. Yet each method is supported by test data from references shown in Table 5-5. This disagreement among the methods is evidently why Young and Paterson (Reference 6) concluded that the effects of compressibility on roughness effects have not been thoroughly investigated.

The methods presented in References 7 and 8 were selected to calculate the cut-off Reynolds numbers as a function of Mach number for the 1/20-scale TACT model. A surface roughness of k = 20 micro-inches was assumed, which corresponds to k = 0.0004 inch full-scale. The value used in Reference 21 for predicting the full-scale TACT drag characteristics was k = 0.0008 inch, but it represented an overall roughness that incorporated the effects of gaps, mismatches, etc. in addition to surface finish roughness. The predicted cut-off Reynolds numbers are plotted in Figure 5-22. If the Reference 7 prediction is representative of the model, the proposed test plan will provide data that will allow determination of the cut-off Reynolds number. If Reference 8 is representative of the model characteristics, additional test runs would be required at the higher Reynolds numbers to allow an accurate determination of the cut-off Reynolds numbers.

Table 5-5. Summary of Prediction Methods for Compressibility Effects on Turbulent Skin Friction Coefficient for Smooth and Rough Surfaces

Prediction Method	Smooth Surface	Rough Surface	Supporting Test Data for Rough Surfaces
Schemensky (Reference 7)	White-Christoph (Reference 9)	White-Christoph (Reference 9)	Sevier and Czarnecki, et al (References 10 and 11)
Schemensky and Howell (Reference 8)	White-Christoph (Reference 9)	Schlichting (Reference 18)	Goddard (Reference 19)
British Data Sheets (Reference 14)	Spalding and Chi (Reference 13)	Modified Winter and Gaudet (Reference 17)	Shutts and Fenter (Reference 20)
Braymen and Webb (Reference 16)	Eckert (Reference 15)	Eckert (Reference 15)	Sevier and Czarnecki, et al (References 10 and 11)

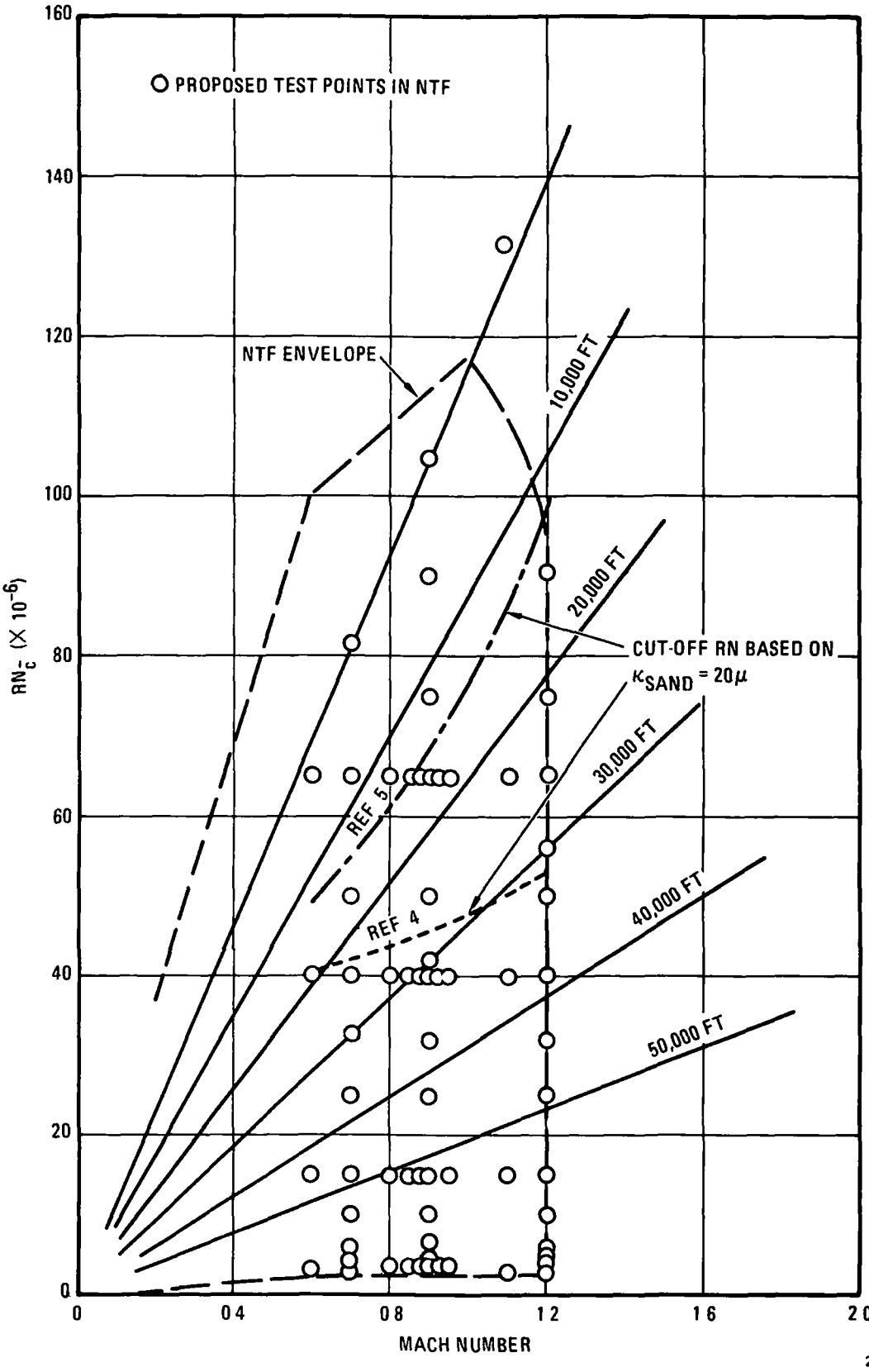

Figure 5-22. F-111 TACT Predicted Cut-off Reynolds Numbers Superimposed on Proposed F-111 TACT Outline

It is believed that the more conservative prediction (Reference 7) should be considered when establishing the surface finish requirements for the NTF model. A machined surface finish of at least 20 micro-inches (equivalent sand-grain roughness) is recommended for the NTF models. Reference 22 suggests that this is a realistic value for a "finished and polished surface."

As mentioned earlier, extreme care will need to be taken in model buildup as model changes are made to minimize the effect on cut-off Reynolds number. Though the proposed test plans do not indicate such, it may be necessary to obtain adequate data after each model change to allow determination of the cut-off Reynolds number. This point should receive careful consideration when the test plan is finalized.

5.4 REGIONS OF REYNOLDS NUMBER SENSITIVITY

Regions of Reynolds number sensitivity for the CWC and the F-111 TACT configurations were discussed as part of the overall test plan rationale in Sections 5.1.2 and 5.2.2. An interesting phenomenon to be investigated for the CWC is the effect of Reynolds number on leading-edge vortex development, shedding, and bursting. Since these effects are not expected to be largely Reynolds number dependent, a significant Reynolds number effect would be surprising. The parametric variations in Mach number, angle of attack, and Reynolds number will provide data to determine if the Reynolds number effect is significant.

The F-111 TACT configuration should be a better configuration for examining Reynolds number effects than the CWC configuration. The nature of the F-111 TACT configuration (airfoil leading-edge radius, thickness-to-chord ratio, and airfoil type) suggests that Reynolds number effects will be greater than those expected on the CWC. Testing of the F-111 TACT configuration in the NTF will provide insight into Reynolds number effects on attached flow, shock location, shock-induced separation, and leading-edge separation. Reference 3 presents past F-111 TACT wind tunnel data that indicate rather significant Reynolds number effects, especially in the Mach range from 0.80 to 0.90.

The determination of Reynolds number effects on Mach critical and drag rise characteristics is planned for both models. The complex flow phenomena present near and in drag rise justify a close examination of Reynolds number dependency. Runs at closely spaced Mach increments are planned in order to obtain the necessary data. Dynamic pressure will be held constant to avoid unwanted variations due to aeroelastic effects.

It will be important to establish an accurate value of cut-off Reynolds number (a function of overall model roughness) for each model. Cut-off Reynolds number is extremely important for any model to be tested in the NTF. This subject is discussed in Section 5.3.

SECTION 6

BASIC DESIGN PHILOSOPHY

To achieve the objective of matching full-scale Reynolds number on a wind tunnel model, full advantage must be taken of the capability of the NTF by prudent reduction of model safety factors where necessary, coupled with sound engineering reasons for doing so. *The facility drive system should not be endangered by the model, but neither should the model design be so conservative that the full capability of the facility be unusable.*

To achieve the design goals, known methods, materials, and procedures will be used consistent with use in a cryogenic environment. New design/manufacturing procedures that are "beyond the state of the art" will be avoided until all known and proven methods are eliminated. If the design reflects a new approach, the new concept will be evaluated by proof loading and/or fatigue testing of actual or simulated hardware under NTF environmental conditions. These tests should take place during the design phase, and in this study they are described as proof-of-concept tests (Section 7.6).

Section 5 describes the configurations, the aerodynamic requirements, and outlines regions of Reynolds number sensitivity. Test plans and loads data are included for use by the design engineers with the specific objective of matching the full-scale Reynolds number test envelopes in the NTF.

The selected configurations are representative of advanced technology fighter aircraft. Models of the two selected configurations can be designed to match full-scale Reynolds number for most operating conditions. For other configurations, an in-depth analysis is required to verify that similar goals can be achieved.

In this design study, specific areas of the model system are identified as potential problem areas in either design, manufacture, or instrumentation. These types of problems can be anticipated with this general type of aircraft configuration model, when designed for use in the NTF, and need special attention. They are:

- Model Size – as large as possible, but within the blockage constraints of the NTF.

- Surface Finish – Spanwise joints, attachment screws, and filler materials should be eliminated, or at least minimized. A surface roughness of 8μ inches at the leading edge, to 16μ inches at the trailing edge may be required for simulation of full-scale surface roughness Reynolds number. Surface finish is directly related to cost.

- Balance Size – For the load conditions, the designer seeks a large diameter, yet sensitive balance. In fighter type models with internal flow, the model center fuselage is critical in terms of space, as it contains the balance, duct area, wing splice, and cable routing for auxiliary systems. Compromises must be made.

- Environmental Control of Instrumentation – The balance developed by NASA Langley Research Center is unheated, but does require a thin convection shield over the gage areas. The model design should attempt to minimize temperature variations across the balance. All other instrumentation requires heating, and will be housed in an environmentally controlled Kevlar® nose section.

- Advanced fighter configurations have long, sharp, nose configurations that offer limited space for instrumentation forward of the balance. Packages must be miniaturized, with special consideration for pressure tube routing, and easy access.

- The instrumentation cable is routed from the nose to the sting through the cold section of the model. The low temperature increases cable stiffness, adversely affecting the balance.

- Installation of pressure tubes in a thin wing is difficult in terms of assembly, and degrades the surface finish. The loss of key pressure taps during the assembly process is also of concern. Assembly and checkout of pressures in a finished wing with cover plate removed is highly desirable.

- Internal ducting is a complex shape, and the preferred material would be Kevlar® or an equivalent easily worked material. Adjacent dissimilar materials, however, may well result in unacceptable thermal stresses and joint mismatches.

- Sting – The support system is a key element in the design. The standard problems of model clearance/sting size/divergence needs special attention.

- Stress and Safety Factors – The safety of the facility is paramount. A detailed analysis is mandatory (Reference 1, Chapter 7).

NASA Handbook LHB 1710.15 (Reference 1) sets forth criteria for the design, fabrication, inspection, and documentation of wind tunnel model systems to be tested at the Langley Research Center, including the NTF. The handbook is a key element in the design of models for the NTF, and the importance of its guidelines and requirements are acknowledged in this design study.

SECTION 7

FABRICATION AND MATERIALS REVIEW

Development of new fabrication techniques and materials and the extension of the uses of existing materials is essential in meeting the demands of constructing models for testing in the NTF at the maximum capability of the facility.

In recent years, a significant level of research has gone into the review and compilation of data, and the development and improvement of materials for use at cryogenic temperatures.

Research indicates that the high nickel content steels (i.e., maraging steels) exhibit great potential for structural applications in models and support systems. Additional research is necessary, however, to further develop these and other metals for cryogenic applications.

Composite materials are also of significant interest and merit additional research. Composites offer very favorable alternatives to metals in a number of applications.

In general, the development of new and better materials, and confidence in using them at lower safety factors, is the key to improving and extending the uses of the NTF.

7.1 CANDIDATE HIGH STRENGTH STEELS

Several types of steels suitable for cryogenic temperature applications have been identified through research by various groups. Reference 3, "Materials for Cryogenic Wind Tunnel Testing," is an excellent source of information.

In selecting candidate steels, availability (standard forms), machinability, weldability, bonding qualities, and other processes pertinent to model design and fabrication were considered along with strength, fracture toughness, impact resistance, and thermal properties.

Some candidate types of steels that have been termed acceptable for use are:

- Austenitic Fe-Ni alloys (Fe-36 Ni, Ni-Span C)
- Ferritic 9Ni (ASTM A353)
- 18Ni Maraging (Grades 200/250)
- Austenitic Stainless (AISI 304, Fe-21, Cr-6 Ni-9 MN-0.3N)

These materials vary widely in the properties (of strength, fracture toughness, charpy impact, etc.) that govern their selection, but each may be useful in appropriate applications. Thermal expansion/contraction is another key factor in the selection process, particularly when the use of dissimilar materials is contemplated. This is addressed in Section 7.2.

7.1.1 CRYOGENIC PROPERTIES. Candidate materials proposed for use at cryogenic temperatures generally exhibit an increase in strength (yield and ultimate) and stiffness (Young's Modulus) at cryogenic temperatures. This is a positive characteristic, but negative ones appear in other properties such as charpy V-notch, (CVN), fracture toughness (K_{Ic}), and Poisson's Ratio (μ). K_{Ic} and CVN are perhaps the two most critical properties when considering structural applications at cryogenic temperatures, for there is often a significant decrease in both properties.

Thermal properties, expansion/contraction (α), and conductivity are also important in selecting a material. Applications utilizing different materials interfacing each other and subjected to temperature gradients must be analyzed for thermal stresses.

Materials data indicates that 18Ni-200 steel offers excellent overall properties for wind tunnel model construction where structural strength and toughness are essential.

7.1.2 FRACTURE TOUGHNESS. Design procedures using fracture mechanics are very important in the selection of high strength materials. The design of structures operating at high stress levels must give special attention to fracture resistance to ensure reasonable safety from catastrophic failure. This is particularly true for high strength steels, where toughness generally decreases with increasing yield strength and decreasing temperature.

Flaws are inherent in all materials, and these defects can propagate under an applied stress, depending upon a number of factors including size, shape, location, and orientation. Components that typically have mounting holes, cutouts, or routing grooves and are highly loaded are high risk candidates for crack initiation and propagation. The capability of a material to absorb the energy imparted upon it is directly and proportionately related to its yield stress and fracture toughness at low temperatures. Materials should be selected that maintain a high ratio of fracture toughness to yield stress ($K_{Ic}/\delta y$), avoiding embrittlement at low temperatures. Table 7-1 lists various steels and their properties at cryogenic and room temperatures.

Materials may be loosely classified into high, medium, and low strength types. The significance of this grading does not intend to serve as a selection parameter, but to relate the general failure modes that may be tantamount with each type as a function of fracture toughness.

Table 7-1. Mechanical Properties of Various Metals

Material	Temperature (deg K)	Yield Stress (ksi)	Ultimate Stress (ksi)	E (10^3 ksi)	ν	α^t in/in/deg F	C_{VN} ft-lb	K_{IC} ksi-in$^{\frac{1}{2}}$
18Ni-200	300	205	210	28.1	0.311	---	35	170
	78	270	280	29.4	0.306	3.4×10^{-6}	25	80
18Ni-250	300	250	260	28.1	0.308	---	20	100
	78	320	330	29.4	0.304	3.4×10^{-6}	10	40
A286	300	100	160	28.4	0.330	---	55	120
	78	120	215	29.4	--	6.8×10^{-6}	50	110
Ti-6Al-4V	300	130	135	16.0	0.330	---	20	90
	78	190	205	17.6	--	---	10	55
Fe-36 Ni	300	41	80	22.0	0.284	---	--	159
	78	90	125	20.0	0.308	---	46	163
Ni-SPAN (c)	300	18	--	--	--	---	--	--
	78	225	--	--	--	---	46	--
Fe-9 Ni	300	100	115	26.9	0.286	---	77	--
	78	145	170	30.0	0.279	---	34	--
AISI 304	300	35	90	27.4	--	---	155	118
	78	60	230	29.6	--	6.0×10^{-6}	116	--

High strength materials generally fail in a low energy mode at all temperatures by shear rupture or cleavage. Fracture toughness analyses are duly required for these materials to provide fail-safe designs. It is crucial to maintain the operating stress below the fracture stress as determined by nondestructive testing.

Medium strength materials usually exhibit adequate fracture toughness at room temperature. Its failure mode is in shear, which absorbs a reasonable level of energy. However, some of the materials in this category show a gain in yield stress while losing fracture toughness at low temperatures, changing them into a low-energy-absorbing mode causing shear failures. Fracture analyses should be applied here to ensure that low temperature applications do not render the material useless.

Low strength materials generally are not subject to failures due to embrittlement. However, ferritic steels (i.e., 9Ni) undergo a shear to cleavage failure mode transition at low temperatures. Perhaps of greater concern and requiring attention is the treatment of processing of these materials. Welding, for example, greatly affects the fracture toughness at any temperature.

Materials used at cryogenic temperatures, regardless of type (high, medium, or low strength), should be analyzed sufficiently to insure fail-safe capability for its application.

7.1.3 FABRICATION PROCESSES. The quality control requirements of models designed for fabrication and testing in the NTF will necessitate the exploration and utilization of innovative approaches to solving engineering and manufacturing problems.

Requirements such as surface finish, joint fixity, and dimensional accuracy dictate that increased capabilities in all areas of manufacturing technology (as applied to wind tunnel models) must be developed. The assurance of fail-safe designs and high quality models and support systems is essential to obtaining data to meet the objectives of NTF.

Surface finish requirements for the models reviewed in this study will be 16 to 20 micro-inches (16√ to 20√) similar to the better present-day models (see Section 5.3). Surface discontinuities such as gaps or steps may, however, occur as a result of poor joint fixity, and degrade the finish. Simple tests conducted at General Dynamics with existing steel models indicated that a typical control surface attached to a wing with a lap joint displaced 0.001 to 0.002 inch under load, creating a step. This type of step does not show up during static inspection, and may not be revealed by a deformation measuring system, and yet can critically affect flow over the model. Special attention must therefore be given to the design and checkout of such joints, and for permanent joints, laser welding should be considered to seal the separation line.

Dimensional accuracy and stability is also critical for NTF models. Material stability during the fabrication process, such as the movement due to internal stresses and heat treatment/aging must be accounted for. Of particular interest to models designed for the NTF cryogenic environment is the impact of the low temperatures on material stability. There are indications that physical changes occur within materials subjected to cryogenic temperatures, and we recommend that critical model materials be stabilized by thermal cycling in the annealed state, prior to final machining. Computer Numerical Control (CNC) machining has become more prevalent in the fabrication of wind tunnel models and offers a significant improvement in efficiency, particularly in the manufacture of airfoils. Profiling using patterns, while an old method, is still an acceptable one, particularly in the fabrication of fuselage components. The choice between the two is directly related to how well defined the vehicle shape is, the engineering programming task defining the shape, as compared with making a pattern, and the related schedule. In either case, the key factor in achieving the desired accuracy efficiently, is good tooling and inspection. To avoid warpage, a wing, for example, must be rotated. Good tooling allows this to be done accurately, and provides the confidence to minimize hand finishing. Profile inspection should be done each time the wing is rotated. At the same time, the tooling pads and leveling holes are checked, and if necessary rebored/remachined if warpage has occurred. The inspection should be done independently of the CNC/profile milling machine, using accurate profile measuring equipment.

The use of composites is addressed in Section 7.2, and various attachment methods in Section 7.4.

In this design study, proven methods of fabrication were used where possible. The high loads and cryogenic environment did, in some cases, necessitate an investigation of new techniques and processes. When this occurs it is highly recommended that test specimens be made and tested to validate the vendors published values and suggested procedures.

7.1.4 HEAT TREAT/AGING. Materials used in models designed for the NTF will normally be heat treated/aged to provide maximum tensile strength. Table 7-1 lists the mechanical properties of candidate materials, and it can be seen that their strength increases as temperature decreases. In this study the primary steel selected is a maraging steel, 18Ni-200. One of its characteristics is excellent stability during the aging cycle, which allows for the majority of machining to be done in the annealed (soft) condition, prior to aging. Rockwell C-scale of 43 to 48 is achieved by aging for 6 hours at 900F to 925F. This steel has excellent heat treatment characteristics:

- Low furnace temperatures required.
- Precipitation hardening, aging heat treatment.
- Uniform, predictable shrinkage during heat treatment.

- Minimal distortion during heat treatment.
- Thorough hardening without quenching.
- No protective atmosphere required.
- Freedom from carburization or decarburization.

7.2 COMPOSITES

The development of advanced composites offer a viable alternative to metal components in many applications. Their high specific strength (strength-to-weight ratio) typically saves up to 25% of weight in aerospace structures.

The mechanical and thermal properties may be "tailored" through laminate stacking sequences. Strength properties are less than those of steels; however, their levels (Table 7-2) are adequate for selected design applications. A high modulus-to-density ratio is obtainable that provides vibration modes and frequencies not possible with metals. A negative coefficient of thermal expansion/contraction is inherent, which provides a high degree of dimensional stability. It is also possible to alter or tailor this factor in one direction to match different interfacing materials. Unlike metals, corrosion and related stress cracking are not problems.

Composites also exhibit a low thermal conductivity, which may be used to advantage in housing instrument packages requiring thermal insulation.

Several types of composite materials have been researched that provide a reasonable data-bank of information for alternate design/fabrication concepts to metals. Graphite/epoxy, glass/epoxy, Kevlar® /epoxy, boron/aluminum, graphite/aluminum, and others have been used at General Dynamics with great success.

During this study, a Kevlar® /epoxy forward body was designed, fabricated, and tested under cryogenic conditions to ascertain the viability of this concept both structurally and thermally as an alternative to 18Ni-200 steel.

The forward body shell was split along the vertical centerline for ease of access to the heated instrument packages designed to maintain and operate at or above a minimum temperature of approximately 32F. The shells were additionally insulated with a high density foam capable also of low thermal conductivity. The design of the structure is described in Sections 9.1.1 and 9.2.1, and the test results are given in Appendix A.

Minor cracking of the exterior polyurethane paint occurred in areas that were in the direct path of the injected LN2. Subsequent tests with sections of Kevlar epoxy chilled down indirectly, showed no cracking or peeling of the paint.

Table 7-2. Mechanical Properties of Various Composites

Material	Temperature	Tensile Stress		Modulus		α^t	C_{VN}	K_{IC}
		(with fiber)	(across fiber)	(with fiber)	(across fiber)			
	(deg K)	ksi	ksi	(10^3 ksi)	(10^3 ksi)	in/in/deg F	ft-lb/in^2	ksi-in^2
Kevlar 49	300	200	4.3	11	0.8	---	150	---
	78	---	---	--	---	5×10^{-6}	---	---
Epoxy-Fiber-glass Laminate	300	280	140	4.5	2.5	---	---	---
	78	320	190	3.5	3.2	---	---	---

It is believed that the above tests, although not conclusive, served to prove the acceptance of Kevlar® /epoxy at low temperatures.

Further research and refinement are needed in the application of Kevlar /epoxy and other fiber materials. Higher strength fibers, tougher resins, and improved manufacturing methods suggest potential for improved properties in these materials. Additional progress is needed in design concepts, analyses, and evaluation of failure modes to expand the use of composites in future applications.

7.3 THERMAL EXPANSION, CONTRACTION, AND CONDUCTIVITY

Models designed and fabricated for use in a cryogenic environment require a thermal analysis for the prediction of thermal properties required to ensure the use of compatible materials.

Thermal expansion, contraction, and/or conductivity each may offer severe consequences regarding the structural integrity of the model.

In this model study, the material proposed for use in fabricating the forward body section must have a low thermal conductivity coefficient to minimize the transmission of external surface temperatures into the internal area of the model.

After reviewing several materials to meet the conductivity requirement, Kevlar 49 was selected. A thermal analysis (Reference 6) was conducted. The analysis shows that in addition to the conductivity concerns, the expansion/contraction problems are also significant to the design (see Figure 7-1). The primary problem is the joint design at the Kevlar 49® and 18Ni-200 steel mid-body interface.

Some work in the area of composites has been conducted that analyzed the aforementioned concerns. Further studies are being conducted to find a means of "matching" the thermal properties of Kevlar 49® to 18Ni-200 steel.

7.4 METHODS OF ATTACHMENT CONSIDERED IN DESIGN

Standard methods of attaching one part to another usually involve fasteners such as screws, rivets, or pins. These methods all require drilling holes (countersinks, etc.), which sometimes causes discontinuities or disruptions in the adjoining surfaces.

To eliminate or minimize the potential surface problems caused by holes, investigations were made into various methods of attaching and joining model components.

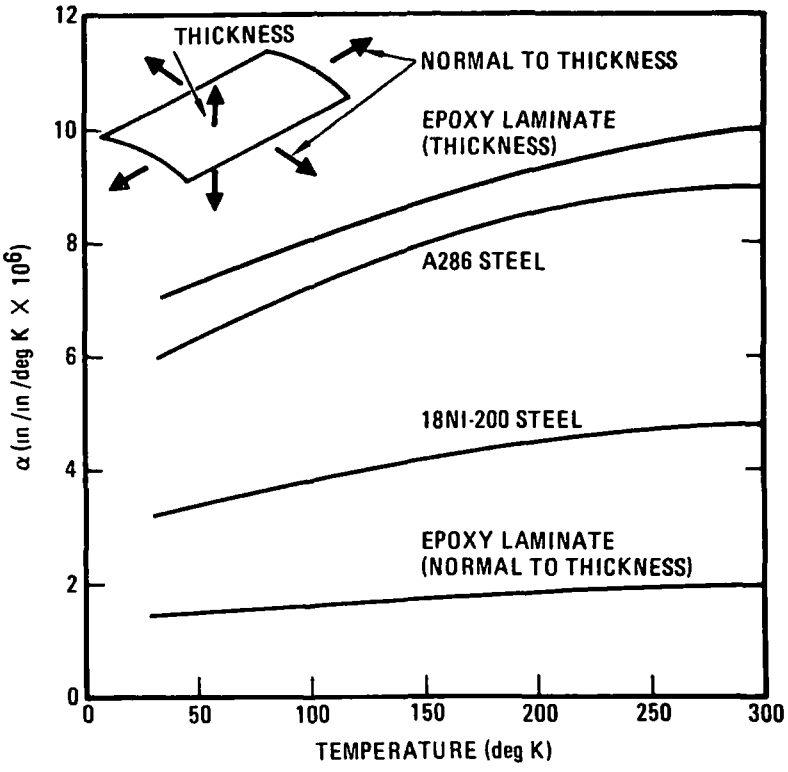

266 635-39

Figure 7-1. Coefficient of Contraction Comparison of 18Ni-200 Steel, A286 Steel, and an Epoxy Laminate

7.4.1 ADHESIVES. The use of an adhesive as a joining method was initially considered as a means of fastening the upper and lower wing panels of the CWC model wings. The wing design required an adhesive with a minimum ultimate shear strength of 4200 psi. This shear allowable provides a safety factor of approximately 2.7. Several adhesives were reviewed as possible candidates, but most did not meet the overall requirements. American Cyanamid Adhesive FM 1000 (which is recommended for use at cryogenic temperatures) was selected for further study. Single overlap shear coupons were tested at both room and cryogenic temperatures to determine ultimate load levels.

The projected tensile shear levels by the manufacturer and GDC were approximately 5000 psi at -320F and 4000 psi at -423F respectively. The maximum level achieved (2840 psi at -320F) did not meet the minimum factor of safety.

Further investigations produced another candidate process; namely diffusion brazing. A study of diffusion brazing was initiated and no further study of the FM 1000 adhesive was done (see Section 7.4.3).

7.4.2 WELDING/SOLDERING. Welding and soldering are well known and commonly used processes where joining or fastening without mechanical means is required; however, most of the standard procedures (i.e., TIG, heli-arc, soft

solder) are not suitable for the type of construction proposed under this study. The two processes studied were electron-beam (EB) and laser welding. Both of these processes have the advantage of applying a welding beam of high intensity while affecting the parent material only in a localized area. The EB weld is a type of fusion weld that fuses the joint parts with an additive material. Strength properties of this type are reported to be approximately 85% - 100% of the parent metal after heat treatment. The surface condition after welding leaves a concavity at the weld area that is an unacceptable surface finish for a model. This problem can be overcome by "puddling" (creating a mound) the weld for hand-finish later. This weld is applied by machine and may be computer numerically controlled (CNC), providing smooth and intricate applications.

Laser welding is a relatively new process in the area of industrial welding applications. It involves the application of a high intensity, narrow energy beam that fuses the surfaces of mating parts without the introduction of additive materials. Generally, the weld area is limited in width and penetration depth (0.025 by 0.020 to 0.050 inch). Strength properties are reported to be 100% of the parent material after heat treatment. It is also reported that post heat treat welding may approach full strength (dependent upon application). The laser beam imparts highly concentrated energy to a very localized area as it welds (fuses), thereby minimizing heat dissipation into the mass of the parts and minimizing distortion. A very minute concavity occurs (beam width by 0.003 to 0.005 inch deep). This cavity is difficult to fill, but is being addressed under filler materials in Appendix A, Sections 2, 3, and 5 (Proof-of-Concept Testing).

Several test specimens were fabricated using the laser welding technique. These specimens provided some data regarding the strength properties and surface effects.

Proof-of-concept testing is continuing in this area to further verify and/or justify the use of this technique as a practical means of joining parts.

7.4.3 BRAZING. Silver brazing and diffusion brazing were investigated as a part of this study.

Silver brazing is a widely used and highly documented process. It has been utilized with many different materials, and the availability of a large number of different alloys provides great flexibility in selecting the proper system. Many components of the model are constructed of 18Ni-200 steel, which readily accepts the application of silver brazing. There are, however, three major problems associated with model construction and silver brazing: 1) high temperature levels that cause dimensional distortions, 2) machining after brazing is required, and 3) heat treatment processing.

As a potential solution to these problems, a feasibility study was conducted on the use of diffusion brazing. This process involved the use of lap shear coupons tested at both room temperature and -320F. Aluminum foil materials were sandwiched between 18Ni-200 steel plates and subjected to elevated temperatures (less than the 900F heat treat level) and pressure (up to 4000 psi) acting as the fusion catalysts. The study was inconclusive but shows that diffusion brazing is a potential candidate method for joining parts without mechanical fasteners. The results of the study will be shown in the Proof-Of-Concepts, Appendix A, Section 2. Further study is required and recommended to ascertain the practicality of this approach.

7.4.4 ATTACHMENT SCREWS. The standard A286 steel attachment screw is used in this design study. In the majority of cases it is used with 18Ni-200 steel. Comparing the thermal coefficient of expansion (α^t) for the two steels at temperatures of 78K (-320F), A286 is 6.8×10^{-6} in/in/deg F, and 18Ni-200 is 3.4×10^{-6} in/in/deg F, see Figure 7-1. The screw therefore contracts considerably more than the surrounding material, resulting in potential loosening, and loss of strength. Provision of some form of locking device, suitable for cryogenic operation, becomes mandatory, and it must be positive. Consideration was also given to the use of 18Ni-200 steel custom made screws; they would of course be very expensive, and A286 is preferred providing that positive locking is achieved.

Appendix A6 describes the ongoing "proof-of-concept" tests that will determine the locking method to be used. It was found that the torque increased with reduced temperature, indicating that the reduction in length of the screw, causing a binding of the threads, was having more impact than the reduction in diameter. Loosening of the screw did not appear to be a problem.

7.5 FILLER MATERIALS

The use of filler materials is a very critical part of this study. It affects the fabrication, preparation, and servicing of the model.

Filler materials were investigated with the requirements of permanency, ease of application and removal, surface finish, and temperature effects.

Several filler materials are well documented in their use with conventional models and conditions; however, most do not have data reflecting their capability at cryogenic conditions.

A study was conducted (Appendix A5) on some suggested materials and others reflecting potential for use at cryogenic temperatures. The fillers were applied to flat plates that contained simulated pressure tubing slots, countersinks, and counterbores for screw heads. The plates were designed to have a similar

stiffness factor as the wing section of F-111 TACT. The test plates were loaded and deflected to simulate model wing conditions. The plates were tested at room temperature and at approximately -320F. The loads and deflections were run at a frequency of approximately 60 cycles per minute.

Preliminary results from these tests are very promising on the basis of the ability of the materials tested to respond favorably to the flexing and temperature exposure.

Surface finish is another important factor considered in this study. At this point in the investigation, all of the materials have proven to be reasonably satisfactory. Hysol Epoxy-Patch® appears to provide the best surface finish in terms of conformity and smoothness after being subjected to cryogenic temperatures.

7.6 PROOF-OF-CONCEPT RATIONALE

The design of model systems to achieve full scale Reynolds number in the NTF is a challenging task. The higher loads combined with a cryogenic environment necessitates an in-depth review of materials and processes. Space limitations in the models require additional research and development of miniaturized instrumentation packages. This problem is further compounded in certain cases by the need for environmental control in that portion of the model containing instrumentation. Thermal control systems are required that take up minimum space and do not adversely affect the accuracy of the unit they are heating.

Areas of the design that are new in concept must be identified early in the design process, and the need for a proof-of-concept test evaluated. These tests will lengthen the schedule and may result in design concept changes. Timely proof-of-concept tests will, however, help to validate the design, discover problems at an early stage in the model development, and save the high costs associated with model rework during assembly. In some cases, actual components of the model will be fabricated and proof-tested prior to start of model manufacture. In other instances, simulated structures and/or tensile specimens will be used to determine design allowables.

Proof-of-concept testing will provide a level of confidence in a new design concept, particularly where minimum safety factors are achieved.

In this design study, General Dynamics identified a need for proof-of-concept tests. All tests are applicable to both the CWC and F-111 TACT configurations. The proof-of-concept tests are described in detail in Appendix A, and include:

a. Simulated Wing Fatigue Test

b. Filler Materials

c. Locking Devices for Screws

d. Tensile Coupons

e. Installation of Pressure Tubes

f. Instrumentation Bay – Environmental Test

g. Cable Crossing the Balance

h. Wing Joint Analysis

   1. Fatigue

   2. Tongue and Groove, Pinned

   3. Lap Joint, Pinned

   4. Existing Model Wing – Joint Evaluation

7.7 SPECIAL REVIEW OF MATERIALS FOR THE SUPPORT SYSTEM

It has been recognized for some time that the sting is one of the most critical parts of the model system. The designer is constantly faced with the problem of minimizing the size of the sting without compromising the safety of the facility and model. An overly conservative approach, however, results in unacceptable distortion of the aft fuselage geometry, and in the case of the NTF will severely limit the capability of the facility to provide full-scale Reynolds number.

Present day technology dictates the use of a high grade steel sting. General Dynamics, in this study, reviewed the possibility of using other materials, including composites, in the design of the sting.

The primary objective of this section of the study is to identify advanced materials, or combinations of materials, that will provide increased strength and stiffness properties at cryogenic temperatures. Weight is also a key factor; the steel sting is approximately 500 pounds, creating obvious handling problems. From this point of view, composites would appear to be very attractive.

During the materials research, it was quickly discovered that very little information is available on material properties at the cryogenic operating temperatures of the NTF. Furthermore, much of the available information is for small billets, and for composite materials for thin sections. For example, considerable research has been done in the aerospace industry on the use of composite materials for space applications at low temperature. High strength boron/aluminum tubes and various graphite epoxies have been developed; in space applications, however, the thrust has been to develop high strength/weight ratios, and therefore the materials are relatively thinwalled. In sting applications, the material thickness is much greater, resulting in questionable material properties, and much higher manufacturing costs.

One material possessing interesting properties is Kennemetal K9®, a tungsten alloy with a stiffness three times that of steel. Again, very little information is available for this material at cryogenic temperatures. Kennemetal, Inc., conducted a study of the feasibility of using Kennemetal K9® as a sting material. The study revealed that the strength and stiffness of K9 was considerably less than the published values when applied to the physical size of material required to manufacture the sting. The properties had been developed from relatively small test samples, and the manufacturer, while initially optimistic, later determined that the desired characteristics of K9 would be degraded to an unacceptable level for an item with the physical size of an NTF sting. Our research also showed that there would be manufacturing problems associated with producing a K9 sting suitable for the NTF. Degradation of material properties due to size was, however, the key factor in determining the unsuitability of Kennemetal K9®.

As an alternative to a sting manufactured completely of Kennemetal K9® , our study turned to the use of Kennemetal K9® with its desirable stiffness properties combined with other high strength materials. A K9 outer shell and an A286 inner core was investigated, but again the K9 shell was found to be so large that properties were questionable and manufacture a problem. Using the K9 as an inner core rather than an outer shell was also considered.

General Dynamics then investigated the use of a high grade steel such as 18Ni-200, or Kennemetal K9® , with advanced composites such as boron/aluminum, or graphite epoxies. Finally, a combination of Kennemetal K9® , boron/aluminum, and 18Ni-200 steel was considered. A common problem (for all these sting designs using dissimilar materials) is that of coefficient of expansion, and the resulting thermal stresses. Figure 7-2 provides a comparison of properties and coefficients and shows a schematic of an "ideal" sting, combining the best available materials. In this design, however, it was found that the stiff Kennemetal K9 (modulus of elasticity = 90×10^6) became too highly stressed, due to picking up too high a proportion of the total load applied to the sting. The very stiff materials tend to have lower ultimate stress values and cannot achieve an acceptable safety factor. For this reason, the stiffness of K9 is unacceptably high when used in a composite sting with other materials of lesser stiffness. As shown in Figure 7-2, a material with an $E = 45 \times 10^6$ is required.

In a practical sense, the higher strength maraging steels may offer the best candidate for an advanced sting. While it is recognized that 18Ni-250, -300, -350 are unacceptable at the present time because of fracture toughness properties at low temperatures, the steel companies have indicated that with significant need, these steels can be improved. Young's Modulus (E), however, would remain critical.

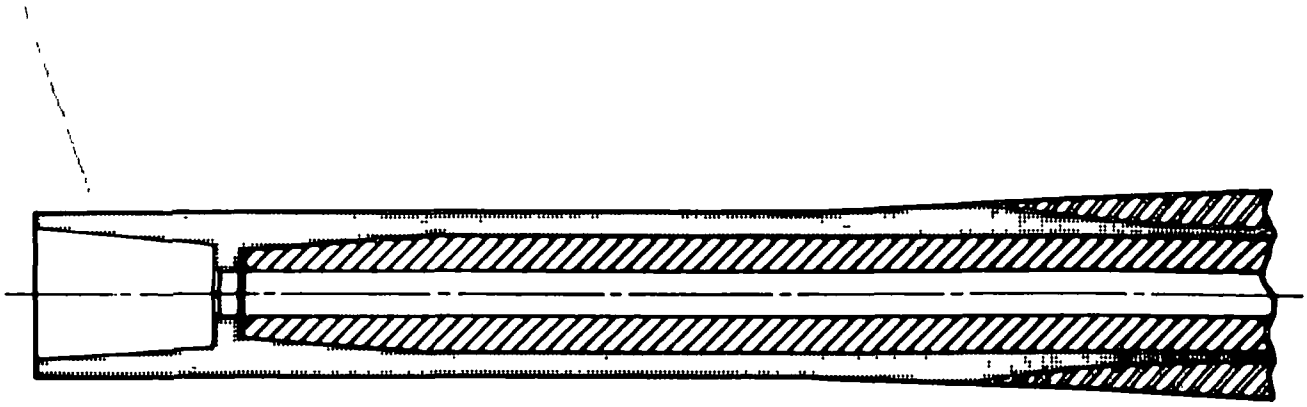

MATERIAL	Fty (ksi)		E (msi)		α = (IN./IN /F) (10^6)	
	RT	140 DEG R	RT	140 DEG R	RT	140 DEG R
18Ni-200	208	270	26.2		5.6	
KENNAMETAL K9 Ⓡ	100		94		2.0	
BORON/ALUMINUM	208*	(DIFFICULT TO OBTAIN)	32.2*		1.2 L 5 0 T	
"IDEAL"	160		45		5.0	

*BASED UPON MATERIAL THICKNESS OF 0 080 INCH MAXIMUM.

266 635-40

Figure 7-2. "Ideal" Composite Support Sting

SECTION 8

FACILITY REQUIREMENTS IMPACTING MODEL DESIGN

NASA Langley handbook LHB 1710.15 (Reference 1) sets forth criteria for the design, fabrication, inspection, and documentation of wind tunnel models and model support systems to be tested at the Langley Research Center (including the NTF). It is well recognized that testing in a cryogenic, high pressure transonic test facility such as the NTF is an advancement into a new and challenging era. Both the facility and model requirements must be fully understood and each safeguarded by in-depth engineering. Facility requirements impacting model design are described in the following sections.

8.1 THE OPERATING ENVIRONMENT AND FACILITY DESCRIPTION

The National Transonic Facility is a fan-driven, closed-circuit, continuous-flow, pressurized wind tunnel. The test section is 2.5 by 2.5 meters and 7.62 meters long with a slotted-wall configuration. The NTF will have a Mach number range from 0.2 to 1.2, with Reynolds numbers up to 120×10^6 at Mach 1 (based on a reference length of 0.25 meter). The pressure range for the facility will be from 1 to approximately 9 bars and the temperature can be varied from 340 to 78K.

The test gas may be dry air or nitrogen. Air is used in the 340K mode and gaseous nitrogen in the cryogenic mode.

8.2 SAFETY FACTORS AND DEVIATIONS

Allowable stresses used are the smaller of the values of one-quarter of the ultimate tensile (compressive) strength, or one-third of the tensile (compressive) yield strength of the material after processing (including heat treating, brazing, and so forth) at test conditions. Thermal stresses are to be algebraically added to mechanical stresses. Material properties are to be taken at the critical temperature levels.

Static tests can be conducted instead of a stress analysis if the loading rigs, devices, and weights are supplied and a deviation is obtained from the Facility Safety Head. The load must be directly and continuously monitored, and the stress tests must be carried to twice the predicted operating load at tunnel test temperatures. Measured deflections shall not indicate a permanent set. Plots of load versus deflection for a complete loading cycle will be included in the stress report.

If the required factors cannot be achieved, a deviation request can be submitted to the NTF Facility Safety Head. The procedure is explained in Chapter VIII of Reference 1. Generally speaking, approval of waivers is likely where model part failure, while not anticipated, will in the worst case cause only minor damage to the facility.

The achieved safety factors in this study are tabulated in Section 10.4. The models achieve acceptable safety factors under cryogenic operating conditions. At room temperature, however, a deviation will be required for some test conditions (see Tables 8-1 and 8-2).

8.3 ACCESSIBILITY AND EASE OF MODEL CHANGES

The design of both model configurations reflects good access to instrumentation, while at the same time ensuring structural integrity. Primary areas where access is needed are the instrumentation bay, the routing channel for the instrumentation cable, and the balance. They are shown in Figures FO-3 and FO-4.

The variation of wing sweep is the one major model change for the F-111 TACT model. For this change, the upper glove must be removed to expose the pivot pin and retaining screw. The pin and screw are retained with locking wire. There is a separate glove for each wing sweep. A suitable screw retaining method will be used for all screws (see Appendix A). The material used for filling the screw head recesses has not yet been determined, and development work is in progress. This material, by definition, should have a good finish and yet be easy to remove. Candidate materials tend to fit one requirement but not the other. This problem area is reviewed in Appendix A-5.

Longer model changes should be anticipated in the NTF. Experience with new materials and retaining methods will, however, ultimately result in acceptable model change times.

8.4 REQUIRED DOCUMENTATION

Chapter 4 of Reference 1 describes the documentation requirements for all models planned for use in the NTF. Compared with requirements for conventional tunnels, the documentation needs are increased. The additional documentation will increase the cost of the wind tunnel model system and schedule; however, a more reliable end product can be anticipated.

Minimum requirements include a set of as-build drawings of the test configuration, design loads, and stress report, a stability report, and an inspection report.

Table 8-1. Summary of Achieved Safety Factors for the 1/15-Scale CWC Model

Part/Joint	Material	Safety Factor: Yield 300K	Safety Factor: Yield 78K	Safety Factor: Ultimate 300K	Safety Factor: Ultimate 78K	Comments
Wing Tang	18Ni-200	4.3	5.7	--	--	
Wing Panel - tip	18Ni-200	4.0	5.5	--	--	
Wing Panel - pins	18Ni-200	3.0	--	--	--	Pins in shear - 1.2 inch spacing.
Elevon Attachment Screws	A286	2.0	1.3	3.2	2.4	Increase size/number of screws
Aileron Attachment Screws	A286	2.0	1.3	3.2	2.4	Limit RN and/or α
Leading Edge Flap Attachment Screws	A286	2.0	1.3	3.2	2.4	Limit RN and/or α
One Piece Wing Tip (Screws)	A286	4.5	2.0	7.2	3.5	
Forward Fuselage Attachment	A286	4.1	5.3	5.4	6.5	
Section Sta 12.75	Kevlar 49®	--	--	2.5	--	Proof-of-concept test required
Balance/Sting Socket	18Ni-200	4.7	6.7	--	--	Socket Shear
Sting*	18Ni-200	2.7	3.5	--	--	Proof test required

*Deviation required.

Table 8-2. Summary of Achieved Factors for the 1/20-Scale F-111 TACT Model

Part/Joint	Material	Safety Factor Yield 300K	78K	Comments
Wing Panel	18Ni-200	8.6	11.3	
Wing/Fuselage Attachment	18Ni-200	3.4	4.4	
Pivot Screw (3/8-24)*	A286	3.0	--	See load restriction. (Consider special 18Ni-200 screw.)
Wing Plate	18Ni-200	2.9	3.8	
Vertical Tail	18Ni-200	8.4	9.3	
Attachment Screws	A286	10.7	12.9	
Horizontal Tail	18Ni-200	6.3	8.3	At -20 degree incidence
Attachment Screws*	18Ni-200	3.7	4.9	Special Screws
Sting*	18Ni-200	2.3	3.2	Proof Test
Balance/Sting Socket	18Ni-200	4.7	6.2	Socket Shear

*Deviation required.

8.5 MODEL CHECK AT FACILITY

The model must be delivered to the facility prior to the test date. A checkout of the complete model system will be performed in a cryogenic chamber under full predicted model loads. Load points on the model will be used to apply maximum forces and moments. This is the final system check prior to entry into the wind tunnel facility. Clearances, deflections, operational integrity of heating systems, the balance, and all other instrumentation will be checked.

8.6 DYNAMIC TESTING REQUIREMENTS

The facility requirement is for a safety factor of 2 against flutter at the test dynamic pressure. An in-depth analysis is required and a vibration test is recommended where structural safety factors are marginal. For the configurations in this study, the candidate subassemblies for a vibration test are the wings for each configuration, and the horizontal tail for the F-111 TACT.

8.7 QUALITY ASSURANCE

Correct simulation of full-scale Reynolds numbers in the NTF will require an exceedingly high quality model in terms of surface finish and dimensional tolerances (Section 5.3). In addition, the structural quality of the model must be proven and well documented. Good documentation is particularly important in areas where safety factors are marginal and deviations are sought. Chapter 3 (Reference 1) outlines inspection requirements. For example, mechanical strength properties must be verified at test temperatures in the "as-built" condition, including laser welding. Nondestructive testing must be to ASME codes, inspection standards and methods defined, personnel certified, and last but not least, an Inspection Plan must be established and adhered to.

SECTION 9

MODEL DESIGN REQUIREMENTS AND DESCRIPTIONS

The model design concepts proposed herein were established to meet the criteria of testing in the National Transonic Facility (NTF) and to establish test conditions for matching full-scale flight Reynolds number in the facility.

The model configurations selected were the single-engine CWC and twin-engine F-111 TACT aircraft. These configurations provide a significant challenge in developing model systems for use at high load and in a cryogenic environment.

The CWC is a single-engine, modified delta wing configuration, with interchangeable wing control surfaces, and a vertical tail.

The F-111 TACT is a twin-engine, variable wing sweep configuration, utilizing a supercritical airfoil. The wings are to be tested in two sweep positions.

Both model configurations are complex force/pressure designs with internal flow simulation.

9.1 DESIGN APPROACH – CWC

9.1.1 FORWARD FUSELAGE – INSTRUMENTATION BAY. The forward fuselage section consists of the nose and canopy portions of the aircraft fuselage. In wind tunnel models requiring various types of instrumentation for data collection purposes, the forward fuselage section serves well as an area suitable for housing instrumentation packages. The upper portion of the forward fuselage is removable, which allows easy access to instrumentation (Figure FO-3).

A review of previous studies conducted on models tested in cryogenic wind tunnel environments revealed the necessity to maintain instrumentation at constant temperatures at all operating levels. In view of the potential thermal problems associated with the use of dissimilar materials in a cryogenic environment, initial consideration had been given to producing a fuselage fabricated of a homogeneous material (i.e., all steel). It was recognized, however, that such a design would require significantly greater insulation and/or heating requirements to maintain acceptable temperature level internally in the instrumentation bay.

To resolve these concerns, our design approach utilized the techniques employed in composite materials design and fabrication. Kevlar 49®, a nylon derivative laminating cloth exhibiting both low thermal conductivity and thermal expansion/contraction, was selected as the material for the forward fuselage section. The use of Kevlar 49® in the design provides several advantages: 1) tailoring the design to meet strength, stiffness, and volume requirements; 2) use of current techniques applied to laminating fabrics; and 3) cost effectiveness.

There are also several disadvantages to using Kevlar 49®: 1) difference in thermal expansion/contraction to midbody section material, 2) special machining techniques for joints and drilling of holes, and 3) surface porosity due to lamination imperfections.

Solutions considered for these problems are: 1) incorporating laminated nickel steel shim strips to obtain thermal expansion/contraction properties similar to steel sections at attachment joints and other desired locations, 2) utilizing special tooling designed to machine Kevlar 49®, and 3) development of processes and materials sufficient to minimize or eliminate surface porosity.

Proof-of-concept tests were conducted to evaluate the proposed composite nose/canopy section. The results are favorable toward utilizing laminated Kevlar 49® composites as a method and material for these purposes. Detailed results are reported in Appendix A1.

9.1.2 MIDBODY SECTION. The midbody section of the model is the principal structural member, which also serves to house the six-component balance support assembly. The midbody is designed as a multi-component assembly composed of backbone, inlet, and ducting sections. Included in the midbody section is an access cover that provides a means of routing and servicing instrumentation cables, tubing, and other required accessories (see Figures FO-3 and FO-5).

A machined mounting area for the vertical tail is provided in the aft region of the backbone. All components of the midbody are designed to be fabricated of 18Ni-200 steel.

Analyses (stress, thermal, and deformation) of the design has shown it to be structurally sound and within acceptable design criteria.

Since the design is a multicomponent assembly, the use of fasteners is necessary at most joint attachments. Use of "standard" (A286 steel) fasteners has been considered wherever possible.

In using fasteners, consideration was also given to methods of locking the fasteners and filling the cavities around the fastener heads in order to prevent premature disengagement of fasteners and maintaining desired surface finish.

Selection of filler materials must be based upon the type of fastener used, location and frequency of installation or removal, and the parent material of the model component. Self-locking fasteners of the Ny-Lok® or coated type are recommended. (See Appendix A.6.)

The split lines of joints have been designed with longitudinal direction whenever possible, avoiding or minimizing step profiles or discontinuities in mating surfaces that cause air flow separations. Joints have been designed as close fitting, overlapping, or tongue-and-groove surfaces that also provide labyrinth type sealing.

Whenever joints perpendicular to the flow are required, design tolerances are set to minimize discontinuities and allow aft-facing steps only, thus again minimizing air flow separation.

The multicomponent concept employed in the midbody design provides flexibility in varying configurations and facilitates making model changes while retaining structural integrity.

9.1.3 AFT BODY AND TAILCONE. The aft body section of the model is designed as a separate part constructed of 18Ni-200 steel. A windshield, which directs the internal ducting airflow aft and around the balance and sting through the model, is incorporated in the tailcone assembly.

The combination of the aft body and windshield affects the exit nozzle at the base of the model. Flat head screws are used to attach the exit nozzle to the backbone and the ducting sections through a machined surface ring. The windshield is a thin walled, tapered frustum, designed to provide (in combination with the aft body section) the desired exit plane area at the base of the model. It is attached to the backbone with flat head screws. The forward end of the windshield has an internal diameter that snugly fits the balance adapter. The assembly may be sealed with a suitable compound.

9.1.4 INLET AND INTERNAL DUCTING. The inlet and internal ducting are critical model components. It is very important for the internal flow areas to be held to close tolerances and to have surfaces that are smooth and free of undesirable protuberances. Discontinuities and surface mismatches that cause flow problems must be avoided.

In attempting to design the inlet and ducting of the CWC model to meet those exacting requirements, several design approaches were considered. Serious consideration was given to using composite materials (Kevlar 49®, graphite-epoxy, etc.), similar to that of the forward fuselage. A thermal analysis, however, indicated problems with relative displacement (translation of the ducting relative to the backbone structure) due to thermal gradients diametrically, and differential temperatures longitudinally, on the model. The use of floating fasteners and/or slotted attachment positions were briefly considered; however, they proved to be too complex in this configuration.

The proposed design utilizes an all 18Ni-200 steel assembly, which encompasses the full inlet and diverter in the forward region and the lower internal/external contour of the aft duct. In the forward region of the inlet, the part is designed with an upper section that is split along a horizontal plane and at a

fuselage station coincident with the end of the diverter. This concept allows for the separate machining of the parts and the joining into a permanent final assembly through the use of laser or electron-beam welding. The proposed design is also well suited for the use of computer aided design and manufacturing (CAD/CAM) techniques. Accessibility for installing pressure orifices, thermocouples, and other instrumentation is excellent – providing increased reliability and quality assurance.

The installation and final assembly of the inlet/ducting are achieved by fasteners that are attached lengthwise of the ducting along the sidewalls. Suitable compound sealants will be used along the joint and at fastener locations. The sealant will be identified during proof-of-concept tests (see Appendix A5).

9.1.5 WINGS AND ATTACHMENT. The design and fabrication of a thin wing ($t/c \approx 0.04$), such as the CWC model wing (Figure FO-6), is a significant challenge. Consideration must be given to such problems as: instrumentation installation, variations in control surfaces, attachments, deformation, and manufacturing techniques, surface finishes, and costs.

During the preliminary design phase, a great deal of emphasis was placed upon the desirability of completing the manufacture of the wing, including profiling, pressure tube installations, heat treating, and cryogenic cycling (reference Section 7.1.4), with one portion of the skin removed. This procedure would facilitate the installation, routing, and checkout of pressure tubes. The final operation would be attachment of the cover plate (skin) without the use of mechanical fasteners, thereby providing a superior surface finish. 18Ni-200 steel (used to fabricate the wing) is recognized as a very stable material and little warpage is expected during the aging cycle. Until further experience is obtained, however, the wing will be aged while the contour is approximately +0.030 inch full. This fabrication process requires that the cover plate be attached at a temperature less than the aging cycle to avoid the necessity of annealing and re-aging. This method of manufacture has distinct advantages with thin pressure wings such as the CWC. The most significant advantage is that the pressure tube routing and leak checking can be accomplished while the inside of the wing is still exposed.

The final design is to build a wing with the lower skin panel removed. The lower skin panel will be attached around the perimeter, and to spars oriented along element lines.

An adhesive (FM-1000®), recommended for cryogenic application, was selected as a proposed bonding agent due to its reported high strength (5000-7000 psi shear ultimate) at cryogenic temperatures. Preliminary tests, however, revealed much lower strengths than reported (2500 psi). This led to further searching for an improved bonding agent or other process.

A cursory stress analysis of the wing panel indicated the necessity to achieve a shear ultimate strength of 5000 psi or better, in order to meet minimum safety factor requirements. Vendor/product research revealed no adhesives capable of developing the shear strength and toughness required.

Discussions with materials and processes organizations (in the area of bonding and other related processes) led to research of diffusion bonding and brazing (see Sections 7.4 and 7.6) as potential processes for joining the upper and lower wing panels without the need for mechanical fasteners.

Early investigation eliminated diffusion bonding as a near term process due to complex tooling requirements (Table 9-1). However, favorable results were achieved with diffusion brazing during initial lap shear coupon tests. Extensive coupon testing followed as the wing design continued.

During the on-going diffusion brazing coupon testing and wing design efforts, laser and electron-beam welding were investigated as alternative methods of attachment.

All three joining processes (diffusion brazing, laser welding, and electron-beam welding) are applicable to the proposed wing design concept. The final decision is withheld pending the results of the proof-of-concept tests described in Appendix A2.

9.1.6 VERTICAL TAIL. The proposed design for the vertical tail is conventional with the exception that its support bracket (-15 in Figure FO-5) is integral with a portion of the tail at the root chord and forms a significant segment of the upper aft fuselage external contour.

The vertical tail has no control surfaces. It is attached to its bracket with flat head screws and locating pins. Screw heads and pins will be filled as required with the materials described in Section 7.5.

9.1.7 BALANCE SELECTION AND CALIBRATION REQUIREMENTS. The selected balance is one of a family of balances being developed for the NTF by NASA Langley Research Center. It is a 2.0-inch-diameter, one-piece balance dimensionally similar to Figure 9-1, but with the following forces and moments.

Normal 4000 pounds	Pitching Moment 12000 in-lb
Axial 400 pounds	Rolling Moment 6000 in-lb
Side 1500 pounds	Yawing Moment 6000 in-lb

This 2.0-inch-diameter balance is the largest that can be used in the 1/15-scale CWC when the model includes internal flow. Full-scale Reynolds number can be achieved with this balance (Figure 9-2). The balance is non-heated and requires a thin convection shield over its length.

Table 9-1. Wing Fabrication Methods (Wing 18Ni-200)

FABRICATION METHOD	ADHESIVE FOIL	FABRICATION PROCESS			INSPECTION METHOD	TOOLING	ESTIMATED STRENGTH (PSI)
		TEMPERATURE (DEG F)	PRESSURE (PSI)	TIME (HR)			
ADHESIVE BONDING	AMERICAN CYANAMID FM 1000	300	50	1 TO 2	UNDER DEVELOPMENT GDFW	MINIMUM	4000 TO 5000
DIFFUSION BRAZING		<900	TO BE DETERMINED APPROXIMATELY 1000	1 TO 3	ULTRASONIC OR C-SCAN	CERAMIC PROFILED	10,000
BRAZING	GOLD ALLOY	1800	MINIMUM		ULTRASONIC OR C-SCAN	STEEL FLAT	50,000
DIFFUSION BONDING	NONE	1800	5000 (EXAMPLE)	3	ULTRASONIC OR C-SCAN	STEEL PROFILED	70,000
ELECTRON BEAM/LASER WELDING/SPOT WELDING							

KEY PARAMETERS

- MAINTAIN SURFACE FINISH
- FABRICATION COST
- COMPLETE WING PROFILE BEFORE JOINING
- TOOLING FROM WING PROFILE
- REWORK INCOMPLETE BOND WITHOUT SCRAPPAGE/WARPAGE
- STRENGTH 6000 TO 10,000 PSI
- CURING TEMPERATURE LESS THAN 900F
- FATIGUE RESISTANT

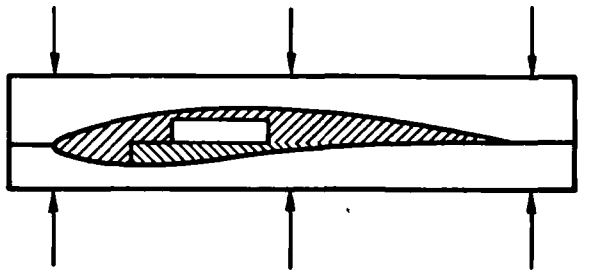

266 635-29

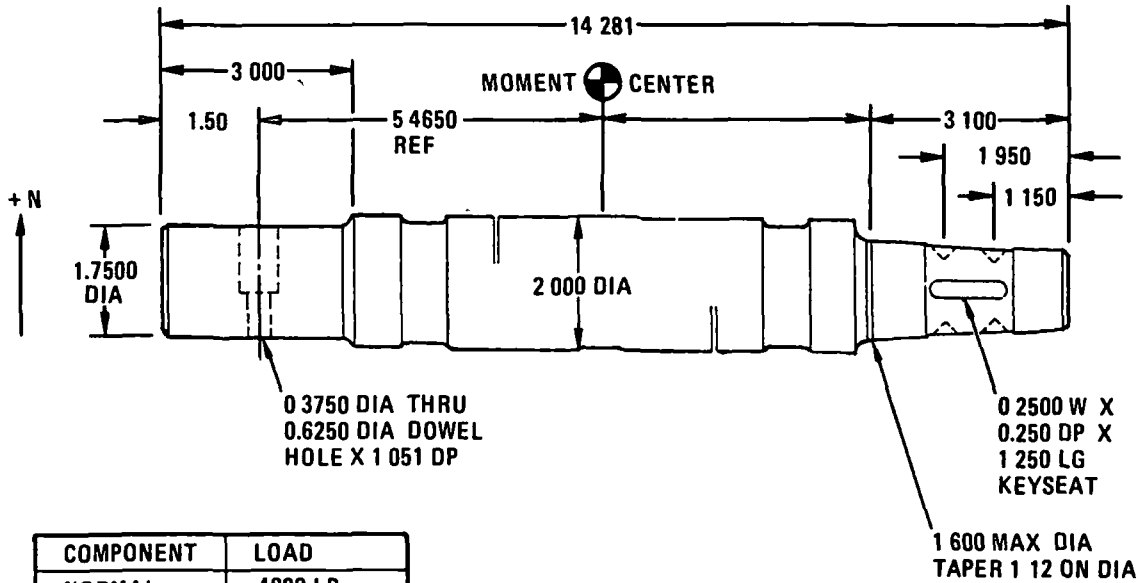

COMPONENT	LOAD
NORMAL	4000 LB
AXIAL	400 LB
PITCH	12000 IN LB
ROLL	6000 IN LB
YAW	6000 IN LB
SIDE	1500 LB

266 635 30

Figure 9-1. Typical Six-Component Strain-Gage Balance

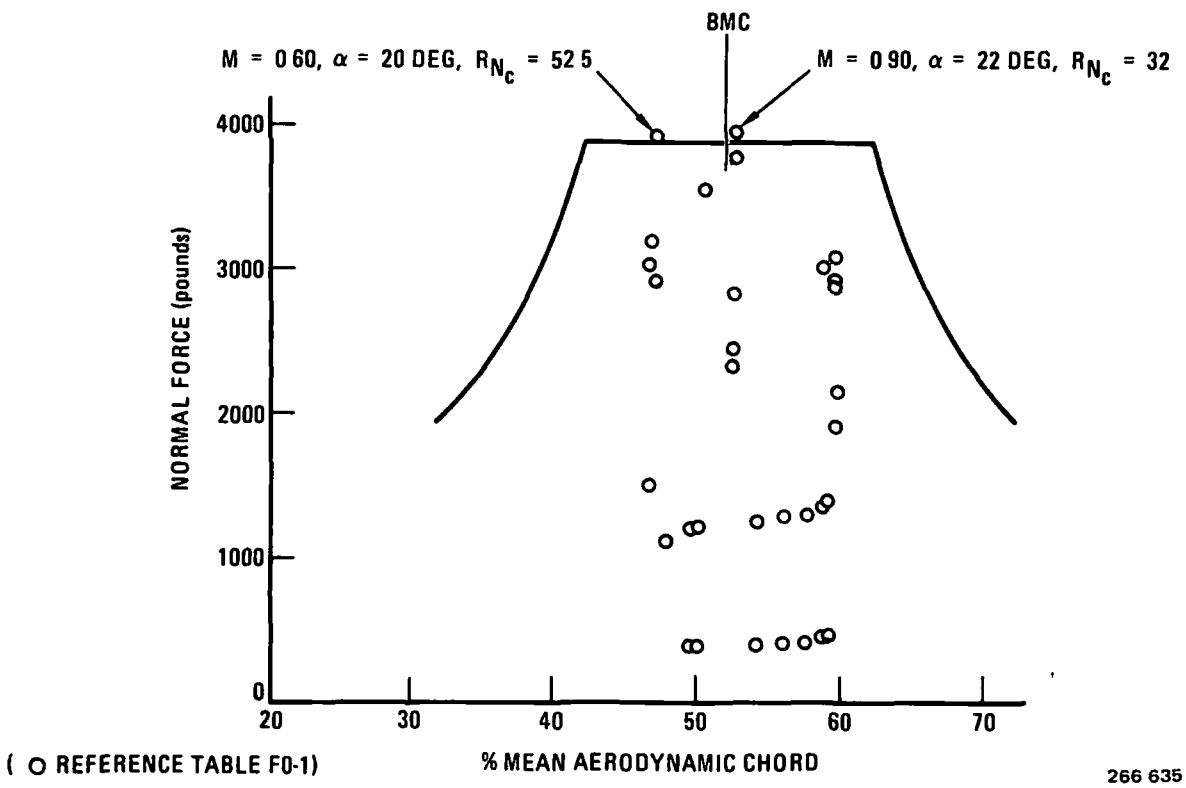

266 635 31

Figure 9-2. NTF Balance Load Rhombus with 1/15-Scale CWC Model Loads Superimposed

Calibration will be accomplished in a cryogenic chamber at NASA Langley Research Center.

9.1.8 SUPPORT SYSTEM AND DIVERGENCE. The support system used for the CWC model is analyzed in detail in Section 10.2. The 18Ni-200 steel sting is approximately 96 inches long, double tapered, and has a hole through its entire length to accommodate model system instrumentation cables. It is 2.00 inches in diameter at the upstream end and 7.8 inches in diameter at the downstream end (Figure 9-3).

The structural integrity of the sting is analyzed using the following combined balance loads.

Normal 4000 pounds	Pitching Moment 8000 in-lb
Axial 400 pounds	Rolling Moment 5500 in-lb

It was also analyzed in the side force plane using the same combination of loads.

Sting deflections and slope changes were calculated using these loads and, in conjunction with the balance deflection data provided by NASA, model-to-sting clearances were determined. The same loads information and stiffness data were used in the divergence analysis. Both 78K and 300K temperature conditions were analyzed. The results are reported in Section 10.3.

9.2 DESIGN APPROACH – F-111 TACT

9.2.1 FORWARD FUSELAGE – INSTRUMENTATION BAY. The forward fuselage of the F-111 TACT is an environmentally controlled instrumentation bay. It consists of the nose and canopy region, extending aft to include a portion of the wing leading edge intersection at the fuselage. This section of the fuselage is designed (Figure FO-4) as a laminated Kevlar 49® shell. The shell is split along the vertical centerline at buttock line zero (B.L. 0). One-half of the shell can be removed to allow easy access to instrumentation, tube routing, etc. Fasteners are used to assemble the half shells. The difference in the thermal properties of Kevlar 49® and 18Ni-200 steel (Table 7.1, 2) dictates the necessity to incorporate laminated strips of high-content nickel (which closely matches the expansion/contraction properties of 18Ni-200 steel) into the Kevlar® shell.

This design concept results in compatible and acceptable tolerances at the joint attachment of the forward fuselage to the midbody section.

Instrumentation packages are housed within the fuselage shells. The shells are insulated with high density foam. The insulation is capable of maintaining temperature gradients to a level where electric resistance heaters can provide enough heat to keep the instrumentation packages within acceptable limits.

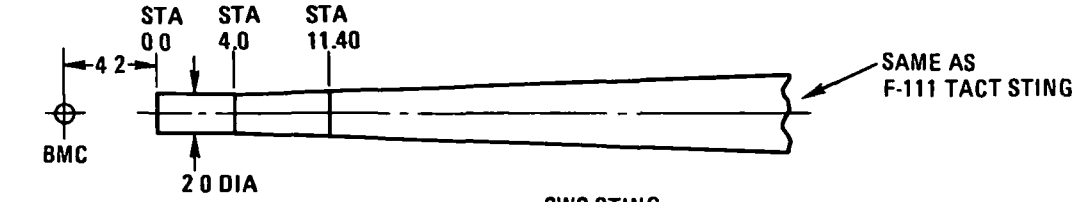

CWC STING

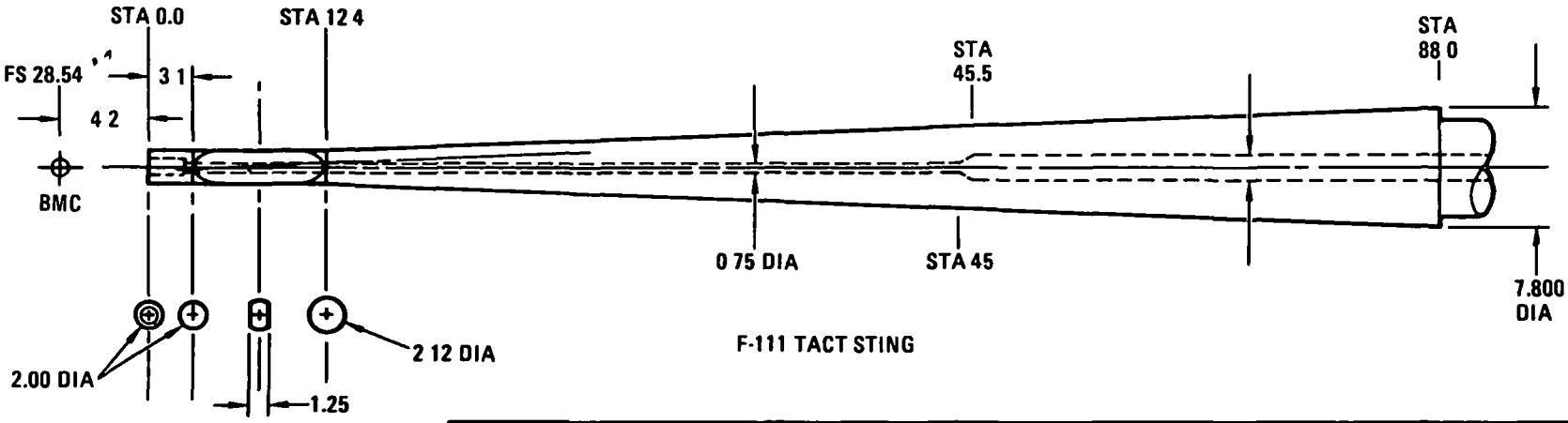

F-111 TACT STING

STA	O D. (IN.)	I D (IN.)	CWC STING					F-111 TACT STING				
			f_b (PSI)	300K		78K		f_b (PSI)	300K		78K	
				SFy	°DEFL	SFy	°DEFL		SFy	°DEFL	SFy	°DEFL
0.0	2 0	—	*26,770	4.7	3 6	6 2	3.4	*26,770	4.7	4 0	6.2	3 8
3.1	2.0	1.31	58,880	3.4	3.3	4.5	3.2	58,800	3.4	3.7	4.5	3.5
4.0	2.0	0.75	52,990	3.8	3.2	5.0	3.1	—	—	—	—	—
5.1	2.022	0.75	—	—	—	—	—	66,120	3.1	3.5	4 0	3.3
10.4	2.096	0.75	—	—	—	—	—	89,190	2.3	2.5	3.2	2.4
11 4	2 125	0.75	75,910	2 7	2 3	3 5	2.1	—	—	—	—	—
45 5	4.65	2.00	21,670	9.4	0.4	12.4	0.4	21,670	9.4	0.4	12.4	0.4
85.8	7 64	2.00	8,450	24 2	0	31.9	0	—	—	—	—	—
86.9	7 72	2.00	—	—	—	—	—	8,300	24 7	0	32 5	0

266 671-11
266 635-32

Figure 9-3. Support Sting for the 1/15-Scale CWC Model and 1/20-Scale F-111 TACT Model

Tests of a similar forward fuselage (CWC configuration) were conducted in a cryogenic environment with random vibrations to ascertain the capability of maintaining a normalized temperature suitable for operation of the various systems. Results are reported in Appendix A.

The design approach taken for the forward fuselage offers flexibility in the application of manufacturing techniques, is cost effective, provides ease of access, and generally meets all requirements for producing a quality part.

9.2.2 MIDBODY SECTION. The F-111 TACT is a variable sweep wing configuration of many components. In designing the midbody section, the complexity of the structure was recognized, and considerable thought was given to simplifying the assembly and structural attachment of adjacent components.

The midbody section includes the center core, balance support hardware, and instrumentation insulation block (Figure FO-4). The core and other support hardware are to be constructed of 18Ni-200 steel. They are the primary fuselage components transferring model forces and moments to the balance. Wing loads are carried through a saddle fitting arrangement to this structure.

The instrumentation insulation block is designed as a laminated fiberglass structure that is attached to the forward end of the core and serves as an insulated mounting for the instrumentation packages.

The upper mid glove fairing, aft support fairing, and inlet/duct subassembly also attach to the core section at final assembly – thus becoming the model's major structural component.

Separate glove fairings are required for each of the two wing sweeps.

9.2.3 AFT BODY AND AFT FUSELAGE STING FAIRING. The aft body and aft fuselage sting fairing sections combine to form the major components for supporting and attaching the horizontal stabilizers and vertical tail (Figure FO-4). Modifications to the upper and lower external contours were required to provide sufficient material thicknesses for mounting the vertical tail and horizontal stabilizers and to provide clearance for the support sting.

The aft body section attaches to both the core section and inlet/duct subassembly – forming a box construction with access for the sting support at the model centerline.

The aft fuselage sting fairing is a thin shell rectangular configuration (modified external contours) at the base of the model. It attaches to both the aft body section and inlet/duct subassembly at its forward end, where it blends into the external contours of both parts. The fairing is also split along its vertical centerline to facilitate assembly. Flat head fasteners are used to join the half shells.

9.2.4 INLET AND INTERNAL DUCTING. The inlet and forward duct sections are one of the most challenging areas of the model in terms of fabrication, due to the complexity of the internal/external contours (Figure FO-7). The design incorporates separate left and right hand subassemblies.

The inlet is designed as a subassembly comprising a "D-shaped" cowl lip (an approximately 90-degree segment), a top plate with lateral plow, a side plate closure to the cowl lip, a vertical plane diverter, airstream splitter plate, and several vane type supports. An inlet spike (located in the upper inboard corner of the assembly) is also a part of the configuration.

The complexity of this subassembly requires a design that must take advantage of various manufacturing techniques and processes. The cowl lip is radially contoured internally and externally (a shape that lends itself very well to CAD/CAM techniques). The top plate is wedge shaped but thin and well suited to normal machining practices. The side plate is also somewhat wedge shaped and suited to the same fabrication methods as the top plate.

The splitter plate is a very thin (0.015 inch) member, rectangular in shape, but also slightly contoured in its vertical plane. Vane supports are used to provide lateral stability. These supports are attached between the splitter plate and fuselage.

An air-flow diverter provides vertical plane shedding of the airstream between the fuselage and splitter plate. It is attached to the splitter plate and fuselage.

An inlet spike, radially contoured and tapered fore and aft, is installed internally to the cowl inlet and attaches to the top plate.

As stated above, most, if not all of the detail parts included in the cowl inlet subassembly are thin shapes that require special attention during the fabrication phase to maintain acceptable quality levels.

The proposed design views these detail parts as becoming a permanent subassembly, which is then assembled to the aft ducting and fuselage. This then becomes a sound structurally unitized subassembly.

General Dynamics proposes the use of laser welding as the assembly process for the inlet/cowl detail parts. Standard type A286 steel fasteners and 18Ni-200 steel pins are to be used for assembly to the aft ducting and fuselage. All components of the assembly will be 18Ni-200 steel.

During the early stages of this design study, consideration was given to making the forward duct of either Kevlar® or a combination of a nickel plated inside duct (made from a mandrel) together with an outer surface of Kevlar®. This is typically done in conventional models because the method provides a good inside surface finish at reasonable cost. It was determined, however, that the difference in coefficient of expansion between the Kevlar® and surrounding steel

was such that unacceptable thermal stresses and joint mismatches would occur at cryogenic temperatures.

The aft ducting is a 18Ni-200 steel assembly, split along the waterline plane. The complex internal/external contours again lend themselves toward the application of CAD/CAM techniques. Laser beam welding is applied to unitize the assembly. Both left and right hand units are similarly affected.

Completing the ducting assemblies are the exit nozzles (LH/RH), which attach to the aft ends of the ducting. The exit nozzles consist of a machined body (with an expanding internal exit) and a plug (designed to provide the desired exit area). Pressure instrumentation consisting of both static and total taps will be included (see details in Section 9.3).

Standard A286 steel fasteners are proposed for securing the exit nozzles to the ducting assemblies. Removable exit nozzles allow some measure of flexibility in installing, calibrating, and checking instrumentation prior to testing.

The general design approach provides a cost effective method of fabricating and assembling the inlet/ducting units while also providing more than adequate structural properties. The subassembly approach also facilitates the overall model assembly.

9.2.5 WINGS AND ATTACHMENT. The wing configuration is a supercritical, moderately thick (t/c = 0.085) airfoil. It has a leading edge sweep angle of 16 degrees and a reference area of 0.536 sq ft. The contour of the wing is established by airfoil shapes at two control stations (SS 6.20, SS 16.25) and applying the straight-line-element rule in between. The wing also has a wash-out (droop) of 6.587 degrees at the outboard span station (SS 16.25) and a differential twist angle of 3.103 degrees at the inboard span station (SS 6.20).

Each wing (Figure FO-8) is designed as a three-piece construction consisting of a leading edge, main spar section, and a trailing edge section (separated along the 60% chord line). Tongue-and-groove joints are used to assemble the sections. Shear pins (installed span-wise) are laser welded in place and surface ground to effect a permanent attachment.

The leading edge and main spar sections are designed using 18Ni-200 steel. They are solid except for instrumentation access slots. The access slots are electro-discharge machined (EDM) at four span-wise stations to facilitate installation of pressure taps.

The trailing edge section (which has an attachment tang at the 60% chord line) is machined internally to provide a routing cavity for instrumentation. The cavity expands from outboard to inboard to accommodate the increasing numbers of tubes and cable leads.

The proposed manufacturing process requires that the wing sections be: 1) profiled to within 0.030 inch, 2) cycled at cryogenic temperatures (see Section 7.1.3), and 3) aged, all operations are to be completed prior to final contouring.

The three wing pieces will then be assembled, using tooling pins, and the airfoil contouring will be completed (except in the area along each split line). The area around the split lines (including the surface around each pin hole) will be left 0.010 inch above contour (Figure 9-4). Pressure tubes will then be installed (including 0.910-inch orifices in the wing surfaces). Pressure continuity checks will be completed while the wing is in three pieces.

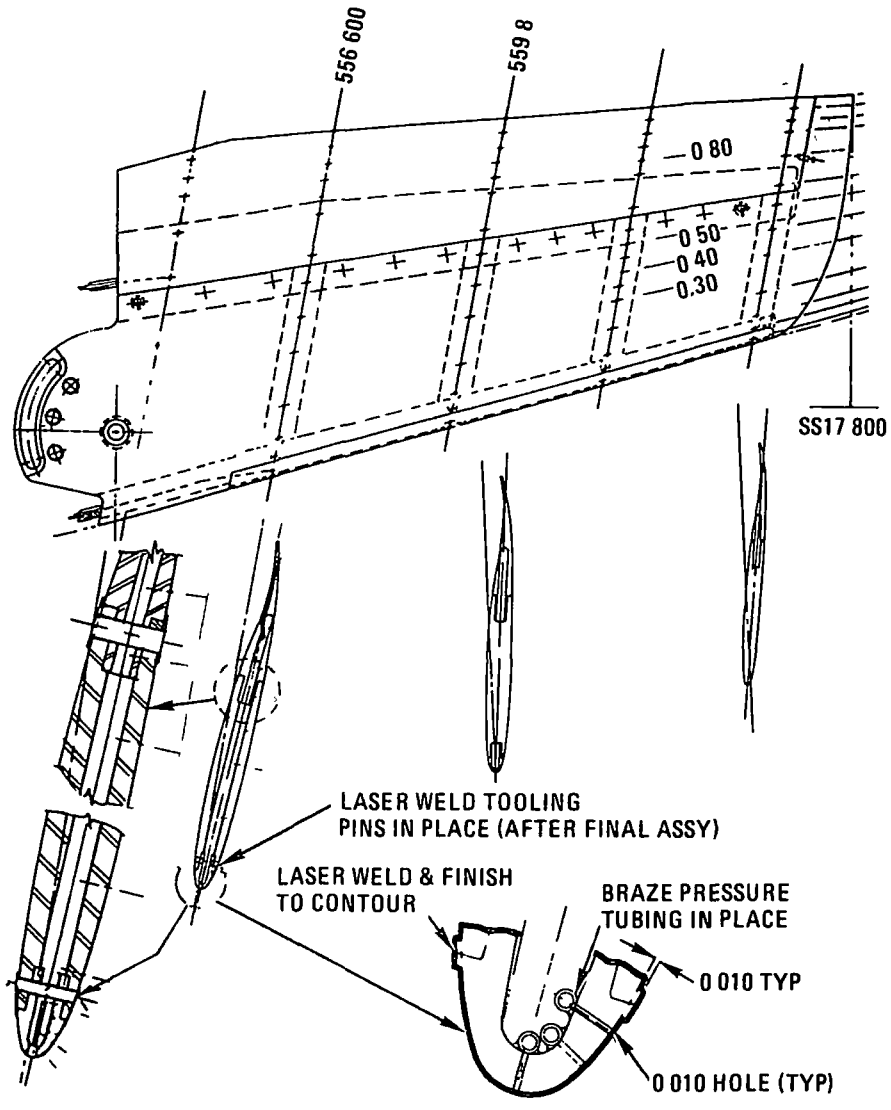

Figure 9-4. F-111 TACT Model Assembly Procedures

The next operation will be to replace the tooling pins with 18Ni-200 steel pins and to laser weld the three pieces of wing together.

The final operation will be to remove all of the material that was 0.010 inch above contour and polish the surface to the required surface finish.

Proof-of-concept testing is currently underway to study the joint characteristics under load at both room and cryogenic temperatures. The primary concern is unporting of the joint, and loss of the desired surface finish. See Appendix A for a detailed discussion of this subject.

The attachment of the wings to the fuselage is critical to the performance of the wing. The proposed concept has the left and right hand wing panel assemblies individually mounted to a wing mounting plate (Figure FO-4). This approach provides greater ease for installing the pressure wing at the two required sweepback angles (Λ = 26 and 58 degrees).

The wing glove fairings described in Section 9.2.2 do not carry wing loads. It is necessary, however, to change fairings with each wing sweep angle.

Inspection and quality assurance procedures are to be conducted to document dimensional tolerances and the structural integrity of the wing.

9.2.6 VERTICAL TAIL/HORIZONTAL STABILIZER. The vertical tail is designed with the mounting bracket as an integral part. There are no rudder deflections considered; therefore, the vertical tail is a conventional design.

It should be pointed out that the aft body upper external contour was modified to provide adequate thicknesses for structural integrity and proper seating of fasteners.

The requirement for trimming a variable sweep wing results in a large horizontal tail, and aerodynamic loads that are quite high. Previous models (for conventional wind tunnels) have had problems in the design of the attachment brackets.

The stabilizer is a modified delta planform with a symmetrical airfoil. It is mounted to the aft body and tailcone by 18Ni-200 steel brackets. The brackets are designed with an overlap joint at the root of the stabilizer, and they require the full thickness of the airfoil for strength. Separate brackets are required for each angle of incidence. The stabilizers and brackets are designed to provide flexibility in testing symmetrical or differential deflection angles (see Figure FO-4).

9.2.7 BALANCE SELECTION AND CALIBRATION REQUIREMENTS. The balance selected for the 1/20-scale F-111 TACT is the same as the one described in Section 9.1.7. Full-scale RN can be achieved, and the size can be accommodated, in conjunction with internal model flow. See Figure 9-5 for an example of a

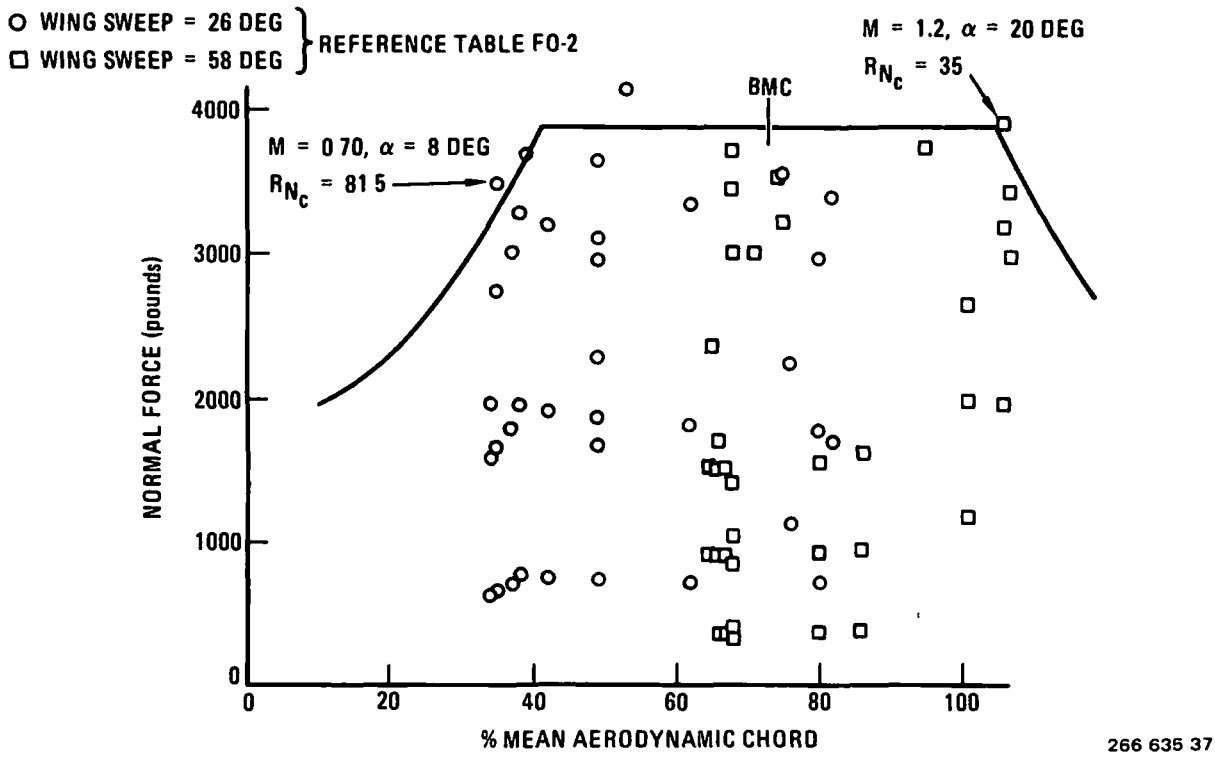

Figure 9-5. NTF Balance Load Rhombus with 1/20-Scale F-111 TACT Model Test Points Superimposed

typical NTF balance rhombus with proposed test points (Table FO-2) superimposed.

9.2.8 SUPPORT SYSTEM AND DIVERGENCE. The support system used for the F-111 TACT model is analyzed in detail in Section 10.3. It is similar to the CWC support system except that the section near the aft end of the model is reduced in width to provide clearance with the two model tailcones, in addition, there is a 2-degree offset. Otherwise the two stings have basically the same dimensions (see Figure 9-3).

The same combined balance loads were used to analyze the sting except for side force (-2000 pounds) and yawing moment (4000 in-lb). This restriction, a result of the reduced sting width, does not impact the test plan.

An analysis of sting deflections and slope changes provided model clearance data. The sting was also checked for divergence. Temperature conditions of 78K and 300K were analyzed. The results are reported in Section 10.2.

9.2.9 REMOTE CONTROL OF HORIZONTAL TAIL. A preliminary design study was made to ascertain the feasibility of utilizing remotely controlled horizontal stabilizers. Two concepts were studied with limited results.

System 1. The most promising approach was a drive shaft integral with the stabilizer brackets. The shaft crossed over the internal ducting to the aircraft centerline, and connected with a common drive bellcrank. A custom designed pneumatic cylinder provided the power for angular positioning and load control.

Several design problems have been identified and must be resolved to develop a viable remote control system for this configuration. The primary problems are:

a. Air loads at high Reynolds number test conditions are greater than system capacity.

b. The common drive does not allow differential deflections.

c. A blade type sting support is required, eliminating the vertical tail.

d. Efficient pneumatic seals must be developed to operate at cryogenic temperatures.

Although these problems present quite a challenge, the benefits derived from remote control warrant a continued design effort in this area. Model changes in the NTF will be time consuming and expensive, and the capability of remote control of the horizontal tail would be very cost effective. It would be potentially very useful even if full-scale RN could not be achieved.

A structural analysis was performed based upon horizontal tail loads encountered with tails at maximum deflection. The analysis revealed a number of critical areas with safety factors of less than 2 on yield. These areas include the shaft, bellcrank, and crank arm. Since space limitations prohibit larger components, remote control can be achieved only by reducing RN and/or the tail incidence angle.

System 2. An electro-mechanical system was considered. Limited available power and space indicated that a different approach was required for this purpose.

9.3 MODEL INSTRUMENTATION

The model instrumentation includes pressure taps (on the wings and fuselage), thermocouples (on the wings), a bending moment strain gage (at the wing root), and an accelerometer for measuring buffet-onset (near the wing tip).

All wing instrumentation leads are routed inboard through the wings then forward into the fuselage. Some of the leads are then routed to environmentally controlled instrumentation packages. These packages include electronic

pressure sensors (ESP), a thermocouple multiplexer, and model attitude accelerometers. The wing tip accelerometer and bending moment gage leads are routed aft through the model and support sting to instrumentation readout systems located outside the model. The pressure orifice locations are shown in Figures 5-12 and 5-20. A total of 120 pressure taps is the maximum number for any test condition. Wing pressure taps are distributed equally in number on the left and right hand wings with the left hand wing having only upper surface taps and the right hand wing having only lower surface taps. The fuselage pressure taps may be interchanged (for purposes of data collection) with either the left or right hand wing pressure taps input to the pressure scanner package.

The model has provisions for a total of 40 thermocouples. Three thermocouples are used for heater systems controls and the remaining 37 are available for use in the wings and fuselage. The thermocouple distribution is similar to the pressure orifice array.

9.4 SURFACE FINISH AND TOLERANCES

An important aspect of the Reynolds number selection at NTF is the model surface smoothness required to maintain similitude between model and flight aerodynamics. Since the unit Reynolds numbers at NTF are greater than those in flight (by the inverse of the model scale), the model surface roughness must be decreased in relation to the full-scale flight vehicle.

Various methods for determining the surface finish requirements for the NTF models are described in Section 5.3. This study shows that whereas in the early stages a machined surface finish of 8 to 16 micro-inches was felt to be needed, a finished and polished surface of 20 micro-inches is now acceptable. The required quality of surface finish is directly related to model cost, and an increase in allowable surface roughness from 8 to 20 micro-inches would be a significant cost savings.

Model tolerances are also directly related to cost. Close tolerances must be held for selected areas of the model based upon sound aerodynamic justification. Other areas of the model without justification for close tolerance should be treated accordingly. For the NTF models in this study, aerodynamic requirements are:

±0.002 in.	From 0 to 25% chord
±0.004 in.	From 20% to 100% chord
±0.005 in.	Fuselage

Requirements for very close tolerance rigging will probably be unjustified because the wing and tail deform under load in the tunnel and must be measured accurately by a deformation measuring system.

Model surface finish and tolerance requirements should be based upon sound aerodynamic analysis. Too conservative an approach will result in higher model costs.

9.5 PRESSURE ROUTING AND INSTALLATION

Where possible route all wing pressure tubes internally. External routing in grooves in the wing surface will be minimized in order to preserve the surface finish.

A standard pressure tube installation consists of:

a. An adapter brazed to one end of each steel pressure tube.

b. The adapter end of the tube is then inserted into a counterbored hole on the inside of the skin and brazed to the skin.

c. An 0.010-inch diameter hole is then drilled through the outside skin into the adapter.

In situations that require externally routed grooves, tubes will be laid in the grooves and their ends will be sealed. The grooves will then be filled with an appropriate filler material and the wing contour and finish restored. A pressure orifice (0.010-inch diameter) will then be drilled into the side of the tube.

An alternate method that shows promise for a better surface finish is: mill a slot in the surface, fill with Cera-True, nickel plate, finish the surface, and remove Cera-True® by melting.

9.6 MODEL FLUTTER

A matched-point flutter analysis was performed for the 1/20-scale F-111 TACT static aeroelastic model at a flight condition of M = 0.9 (see Figure 9-6). Although the analysis did not converge at that condition, the results indicate that the flutter dynamic pressure is at least five times higher than the capability of the tunnel at Mach = 0.90. Based on these findings and the relative stiffness of the rigid models to the flexible TACT model (i.e., almost 3:1 (deflection) for the TACT models), it is believed that a detailed flutter analysis would also show a large sufficient flutter margin for the rigid models. See Appendix B.

9.7 THERMAL CONTROL AND OVERLOAD SYSTEMS

Appendix A1 describes the proof-of-concept test conducted for instrumentation bay heating. Three distinct zones are heated separately, and in each case a single thermocouple identified as a primary control point. A Barber Colman 580 series microprocessor controller or similar thermal control unit is required to control and provide the heat input to the zones. Experience has shown that the zones can be controlled within ±3F.

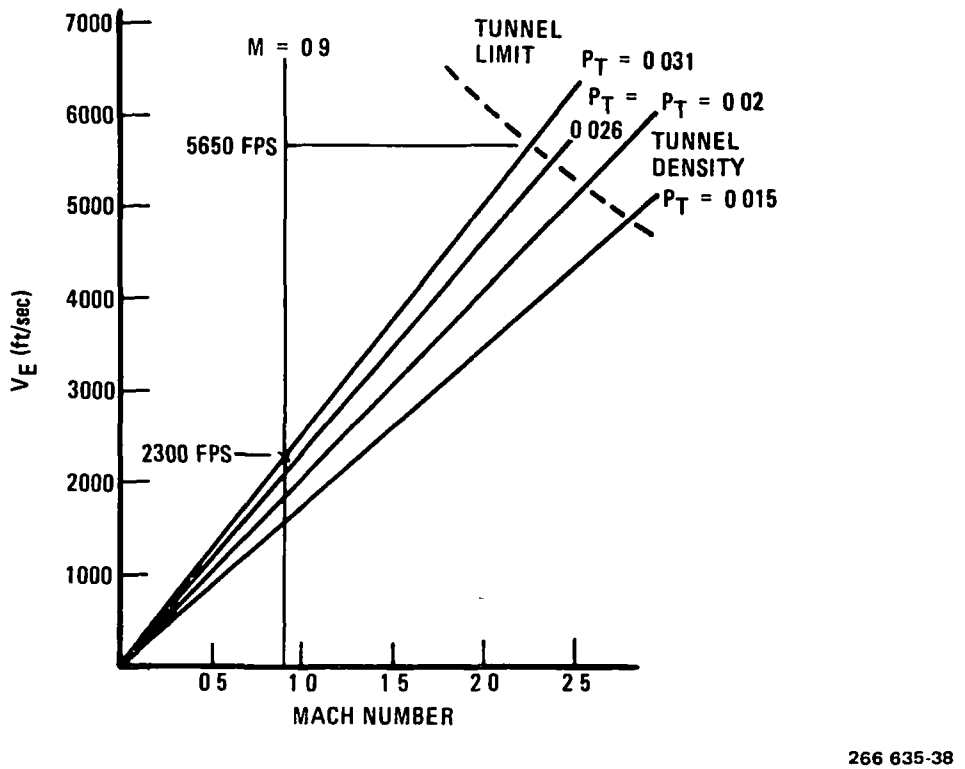

Figure 9-6. Matched-point Flutter Analysis at M = 0.90

The use of overload systems was considered for areas of the model that were marginal in safety factor, and where the loads increased with angle of attack or incidence changes. In this study, the critical areas are the F-111 TACT wing attachment, horizontal tail attachment, the sting near the base of the model, and the CWC control surface attachment screws (all at a test condition of 300K). A detailed analysis of the static and dynamic load conditions will verify the need for additional strain gages in the critical areas. If a deviation is sought, consideration will also be given and presented to the Facility Head, wherein output from the strain gages will be directly monitored, and based upon prior calibration, excess strain will activate a system for limiting pitch.

9.8 SUPPORT SYSTEMS

The sting analyses are shown in Sections 10.2 and 10.3. In each case the sting material is 18Ni-200 steel and is double tapered. The stings are very similar, with the F-111 TACT sting reduced in size at the fuselage tailcone because of the exit geometry. In the worst case, a safety factor of 2.3 on yield stress was achieved at room temperature.

Sting divergence was analyzed using full balance loads and is documented. The analysis indicated that a static divergence parameter (SDP) of 3 or greater would result in non-divergence, 6 was achieved.

During the detail design stage, a finite element model will be developed to assess and refine the structural details of the entire model, including the sting and balance. Fatigue, flutter, and divergence characteristics will be assessed. General Dynamics also recommends that strain be monitored at the critical sting section.

General Dynamics investigated the feasibility of designing/fabricating a composite sting; this effort is described in Section 7.7.

9.9 MODEL DEFORMATION

The methods of measuring model deformation have not been a part of this study. It is recognized, however, that there will be significant deformation, particularly of the wing, and that to get meaningful data the deformation must be measured. The most likely measuring method is at present a real-time photogrammetry system. Light emitting diodes (LED) will be required in the wings and fuselage in sufficient quantity to determine static aeroelastic deformations.

The present size of the LED is 0.040-inch diameter. The method of retaining them in the model is critical in terms of surface finish. A vibration test at cryogenic temperatures is highly recommended. For this purpose, a simulated wing would be satisfactory.

9.10 MODEL HANDLING

Models for the NTF will require special consideration and care when being handled. High quality surface finishes obtained at considerable expense must be protected by using fitted soft gloves over the airfoil surfaces. They should remain in place at all times when the model is not in work or in the tunnel. Extreme care should be taken in lifting the model. Where possible, fabric straps should be used around the fuselage. For the CWC, with its large delta wing, tapped holes in the balance block would be used together with a special harness. It is assumed that the model would not be lifted as a unit in the cold condition.

Shipping crates should have a plastic molded interior, allowing no relative movement between the crate and the model.

SECTION 10

SUMMARY OF STRUCTURAL/THERMAL ANALYSES

A basic structural analysis was performed on both the F-111 TACT and the CWC wind tunnel modes. The analysis included:

- Basic wing stresses
- Wing-to-fuselage attachment
- Empennage stresses
- Empennage attachment
- Backbone stresses
- Fuselage stresses and attachment
- Sting stresses and deflection
- Sting divergence

Each model was analyzed to determine the working stress levels under room temperature (300K) and cryogenic conditions (78K) (see Reference 23).

Although not shown in illustrations of the joints, all joints analyzed have pins for structural strength and for locating purposes.

The primary material used for most of the model and support sting components is 18Ni-200 steel. The mechanical properties of this and other materials are shown in Table 7-1 (see References 24, 25).

The model loads used were covered in detail in Sections 5.1.3 and 5.2.3. These analyses were based on the most stringent requirements to run the test plans as shown in Tables FO-1 and FO-2.

A summary of the results of these analyses are presented in Table 8-1 and 8-2.

10.1 THERMAL ANALYSES

The thermal analyses conducted under this study covers both the CWC and F-111 TACT models. Both are fighter type aircraft, with low profiles, minimum cross-section, and internal ducting. The design and analytical practices employed are therefore similar, and applicable to both models.

The thermal analyses conducted utilized the General Dynamics Convair Division's Thermal Analyzer Program to cover:

- The model chilldown period (temperature versus time)
- Temperature distributions
- Instrumentation packages – heater requirements

The analyses are only cursory in depth and do not include complete detailed temperature gradients and distributions. However, sufficient data is presented to establish basic trends and criteria necessary to support the design and structural analysis of both aircraft configurations.

10.1.1 SUMMARY. Scaled models of the CWC and F-111 TACT fighter aircraft (Figure 10-1) proposed for testing in the NTF have been analyzed for thermal characteristics in this study.

Thermal analyses were accomplished to determine model temperature gradients during chilling to a temperature of 78K, to determine instrumentation package heater (Figure 10-2) requirements for maintaining instruments at an acceptable operating level, and to determine temperature gradients during a test run.

10.1.2 CHILLDOWN ANALYSIS. The models will be subjected to temperatures as low as 78K during chilldown and testing. Areas of the model using dissimilar materials at joining sections are most critical in analyzing thermal gradients and distribution. The forward fuselage section of each model (CWC or F-111 TACT), is proposed as a Kevlar® composite with laminated nickel strips to provide both attachment strength and simulated thermal properties of (18Ni-200 at the joint (see Figure 10-1).

Nodalized thermal models of the joints (Sta 13.75 for CWC and Sta 19 for F-111 TACT) for both aircraft models are shown in Figures 10-3 and 10-4, respectively, and for F-111 TACT at Sta 24.38, 27.00, and 38.51 in Figures 10-5, 10-6, and 10-7, respectively. The NTF has the capability of rapidly changing its operating temperature. For the purposes of model design analysis, it was assumed that in the worst case an instantaneous temperature change of 48K would be realized. This condition is not considered to be as severe to the models as the initial chilldown shown in Figures 10-8 through 10-12.

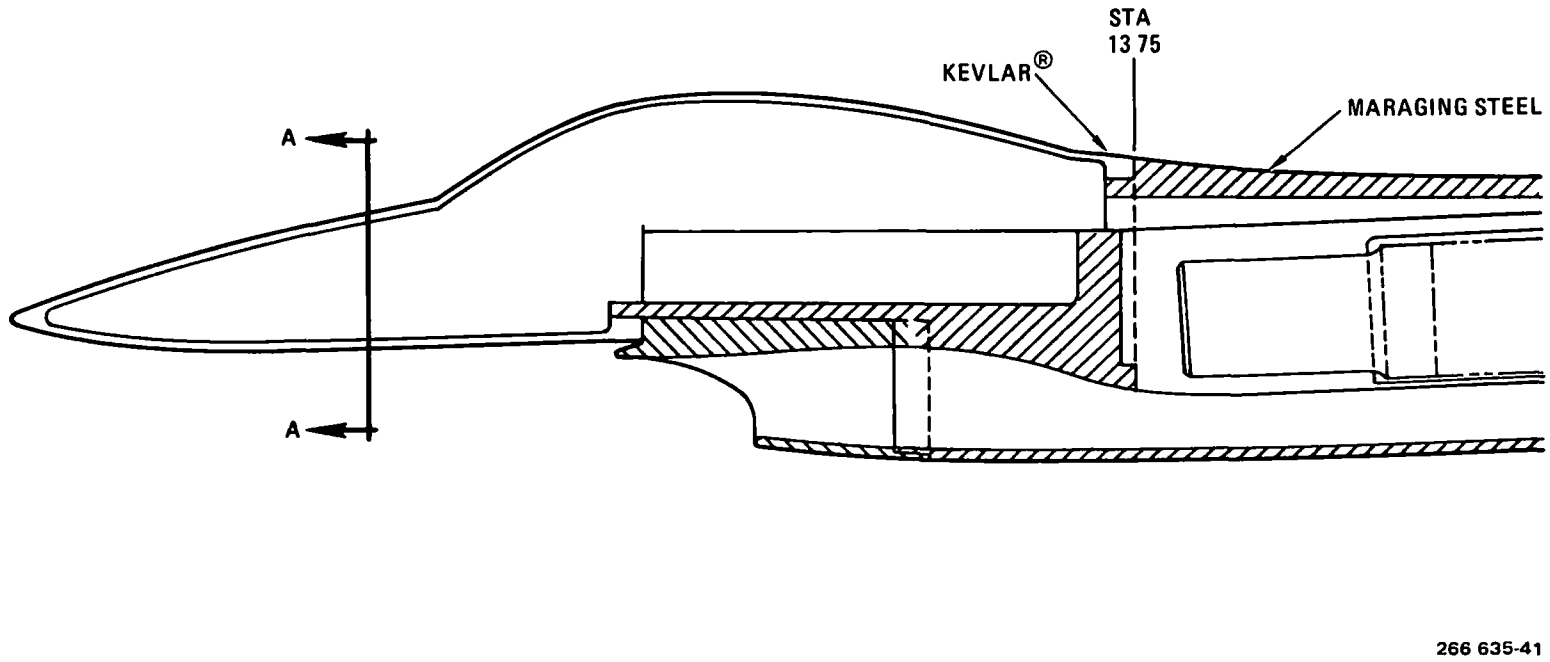

Figure 10-1. CWC Forward/Mid-Body Sections

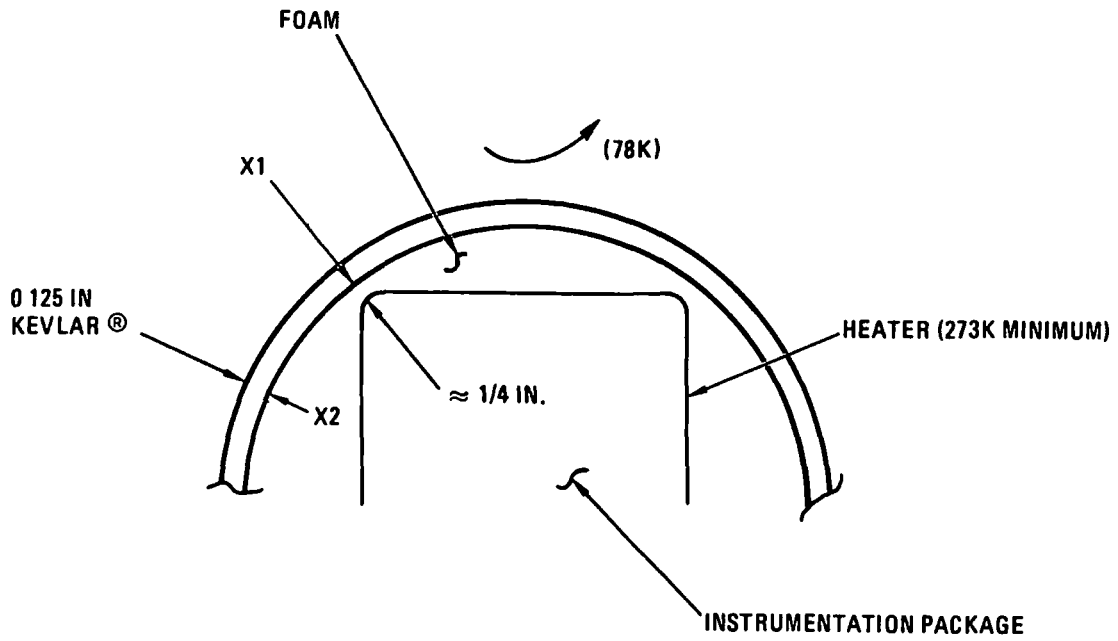

Figure 10-2. Instrumentation Package (Section A-A in Figure 10-1)

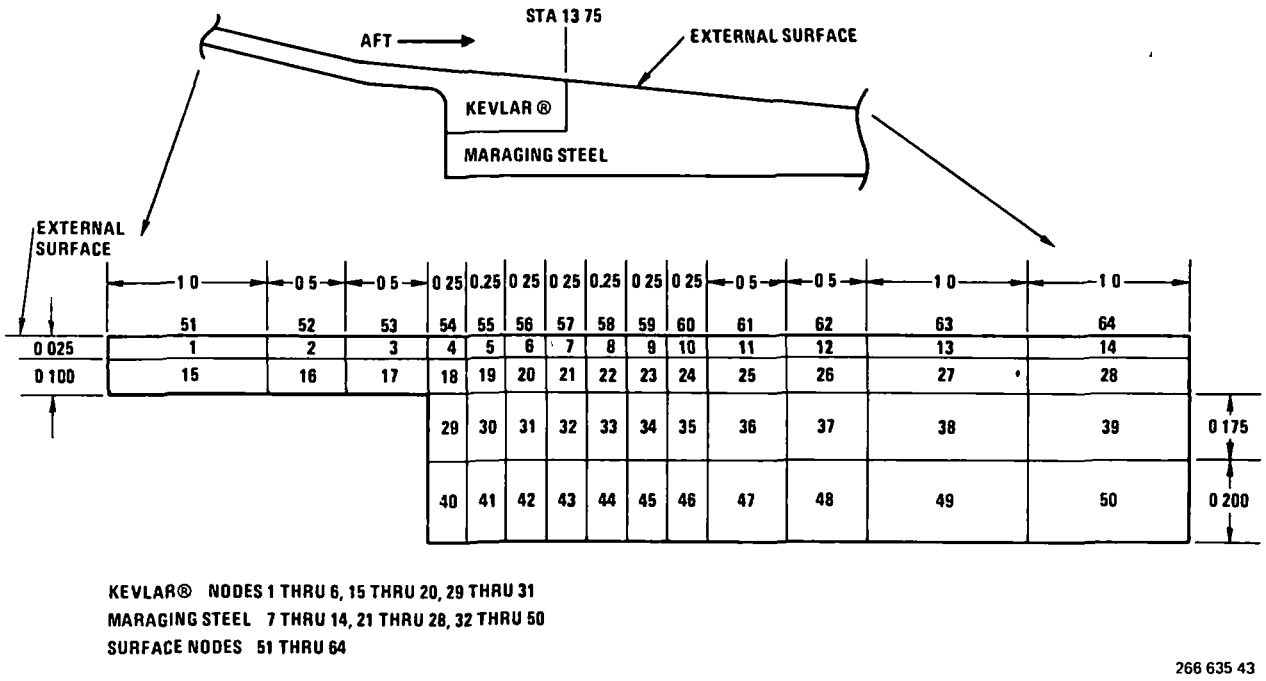

Figure 10-3. Thermal Model, CWC Kevlar® /18Ni-200 Joint

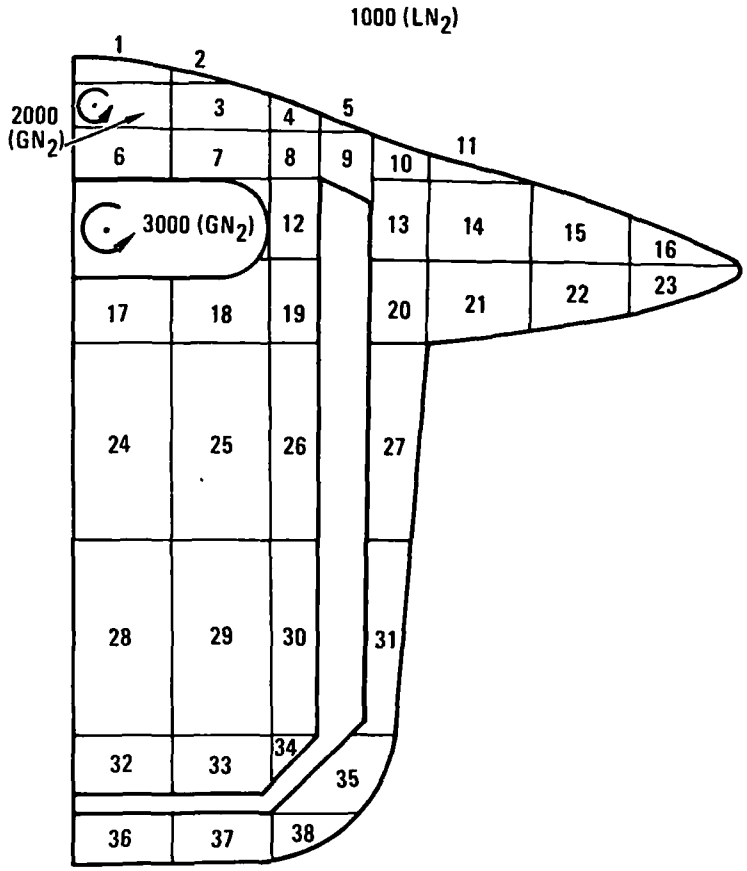

Figure 10-4. F-111 TACT Wind Tunnel Thermal Model at Sta 19.00

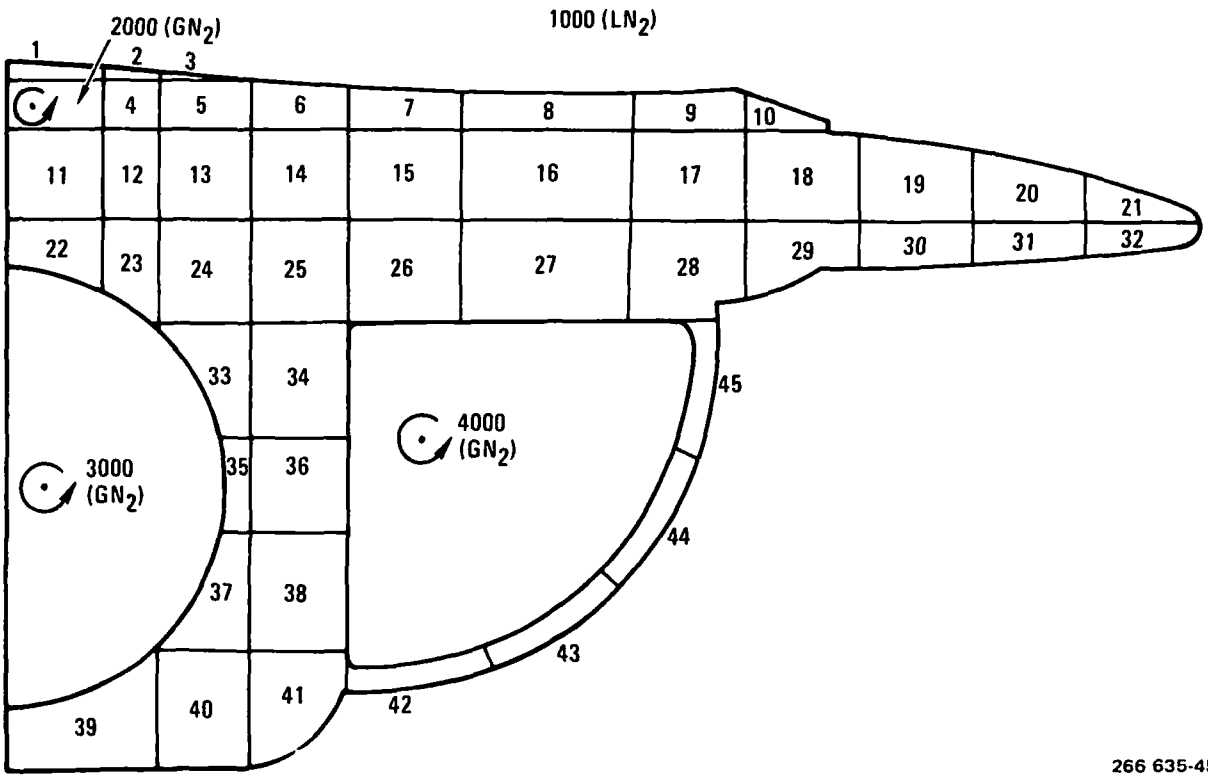

Figure 10-5. F-111 TACT Wind Tunnel Thermal Model at Sta 24.38

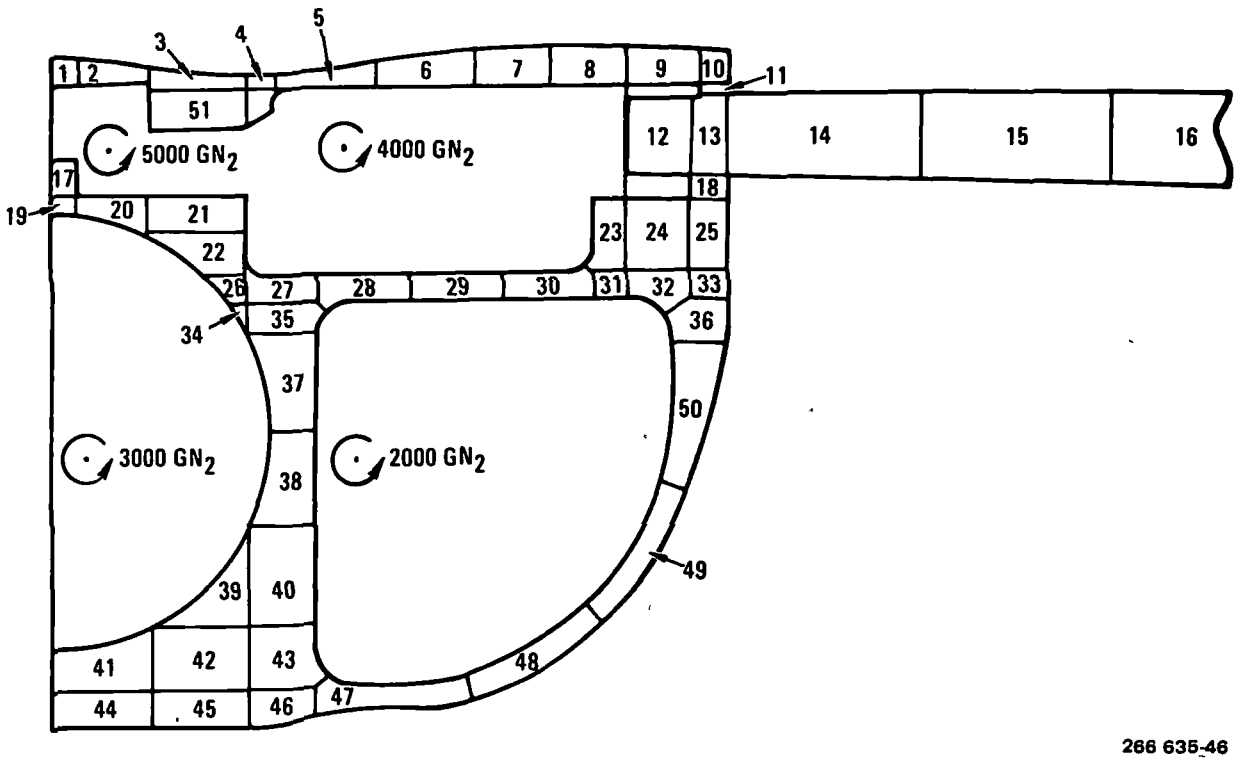

Figure 10-6. F-111 TACT Wind Tunnel Thermal Model at Sta 27.00

Representative predicted node temperatures are plotted versus time as shown in Figure 10-8 for the CWC and in Figures 10-9 through 10-12 for the F-111 TACT at Sta 19.00, 24.38, 27.00, and 38.51 respectively. Predicted temperatures for each node are shown in Figures 10-13 and 10-14 and 20 and 40 seconds after start of chilldown, respectively, for the CWC. Predicted temperatures at F-111 TACT Sta 19.00 at 10, 20, 40, and 600 seconds after start of chilldown, respectively, are shown in Figures 10-15 through 10-18. Figures 10-19 through 10-21 show predicted F-111 TACT temperatures at Sta 24.38 at 10, 20, and 40 seconds after start of chilldown, respectively. Figures 10-22 through 10-24 and Figures 10-25 through 10-27 show these conditions at F-111 TACT Sta 27.00 and 38.51, respectively.

Steady-state conditions were achieved about 30 minutes (1800 seconds) from the start of chilldown for 19.00 of the F-111 TACT model. Sta 24.38, 27.00, and 38.51 achieved steady-state conditions at approximately 300, 600, and 100 seconds after start of chilldown, respectively.

The outer surfaces of the models chill down more rapidly than the internal surfaces, thereby creating the greatest temperature gradients in the early stages of chilldown. Thin members or sections, e.g., ducting walls, tend to chill down throughout the cross section rapdily, with little or no differential.

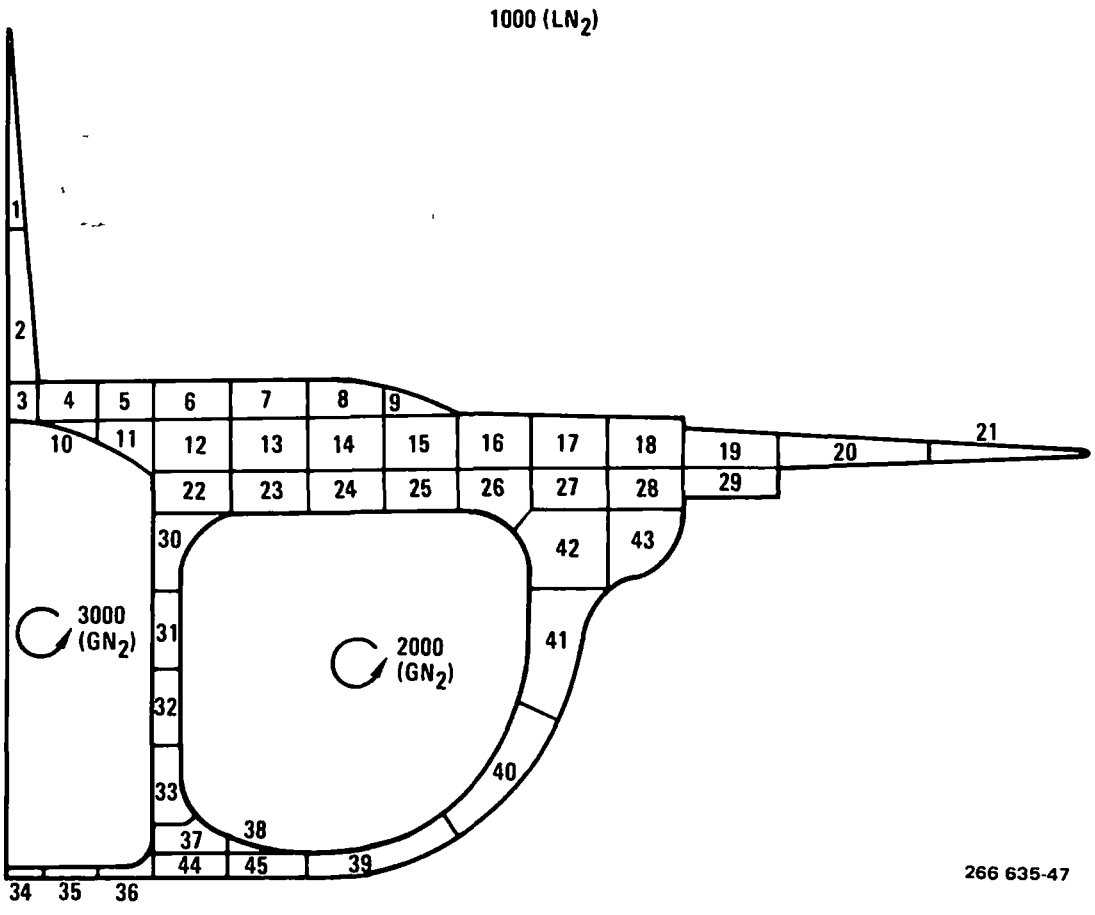

Figure 10-7. F-111 TACT Wind Tunnel Thermal Model at Sta 38.51

The general trend indicates that the models will reach steady-state conditions in approximately 30 minutes to 1 hour.

It is intended that the data provided herein serve as the basis for the stress analysis as relates to thermal conditions.

10.1.3 INSTRUMENTATION HEATER REQUIREMENTS. The CWC model was used to analyze the heater requirements for maintaining the specific minimum operating temperature of onboard instrumentation packages. Instrumentation packages installed in the interior of the model (Figures 10-2 and 10-28) are to be maintained at a temperature of 273K (minimum). Resistance heaters bonded to mounting housings/brackets and controlled by electric servo-controllers are used to maintain the required operating temperature.

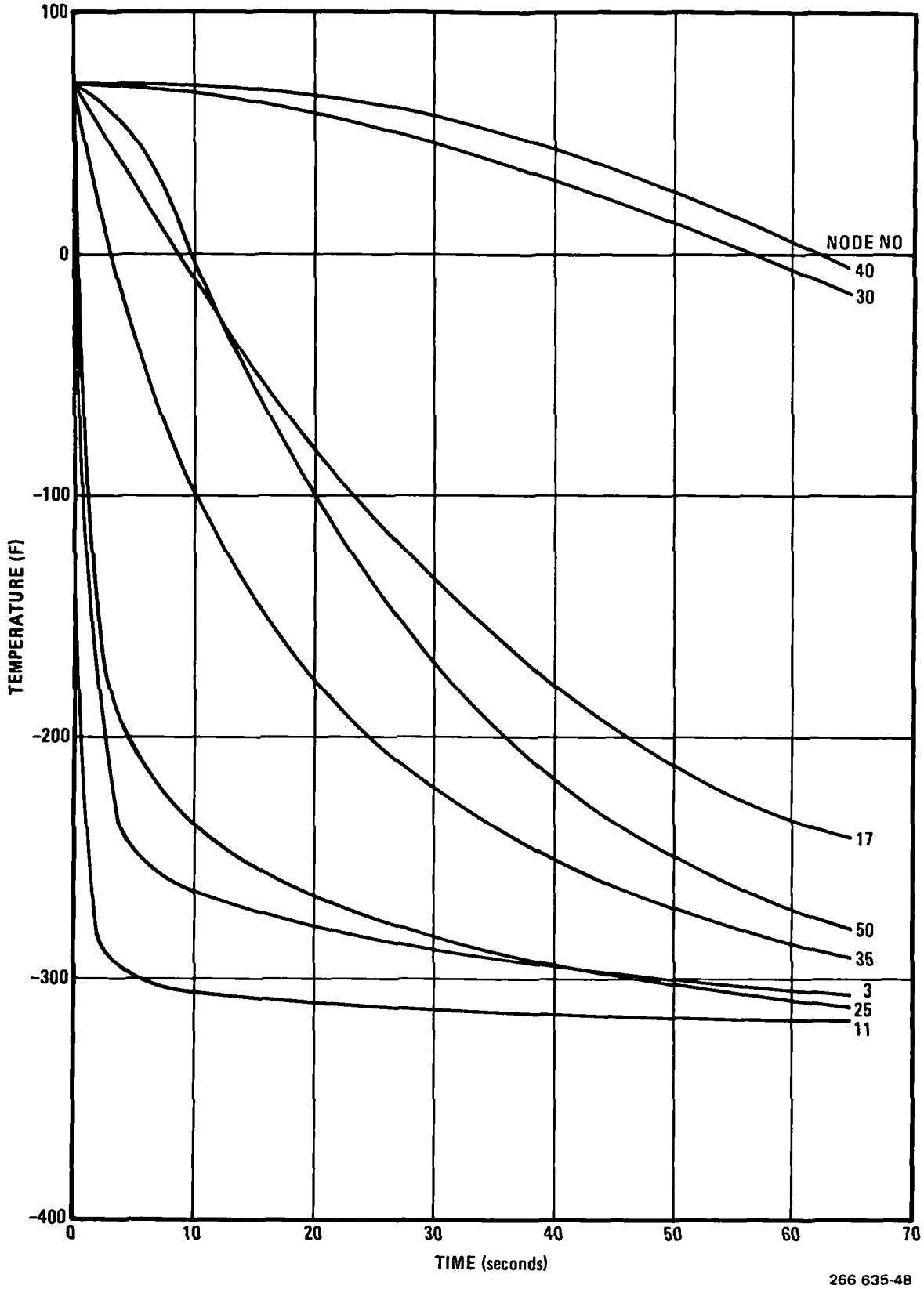

Figure 10-8. Predicted Temperature Versus Time after Chilldown Start at Representative Nodes for the CWC

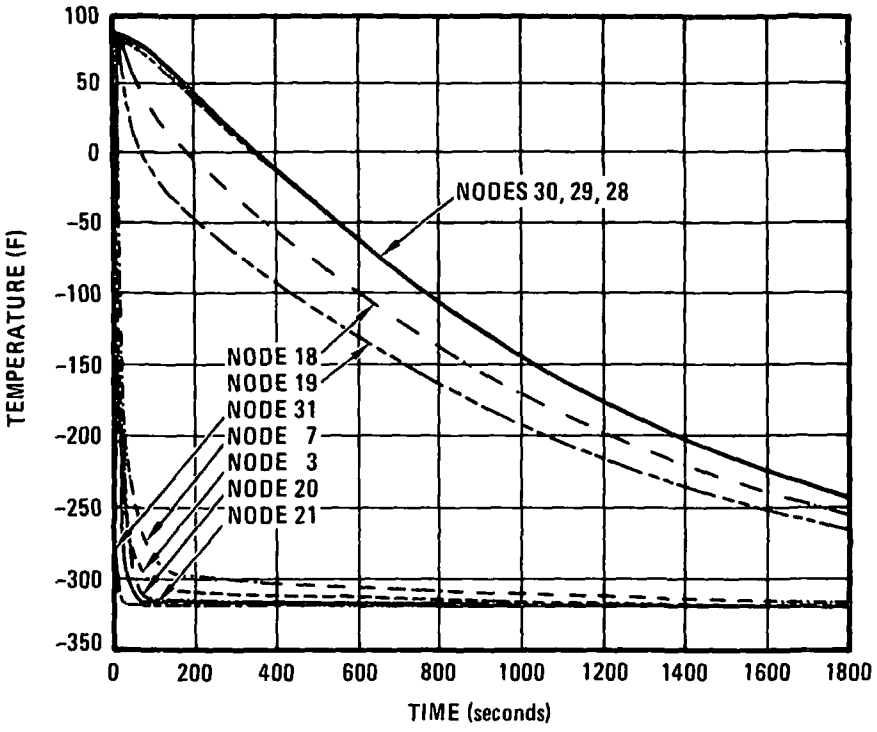

Figure 10-9. Predicted Temperature Versus Time after Chilldown Start at Sta 19.00 for the F-111 TACT

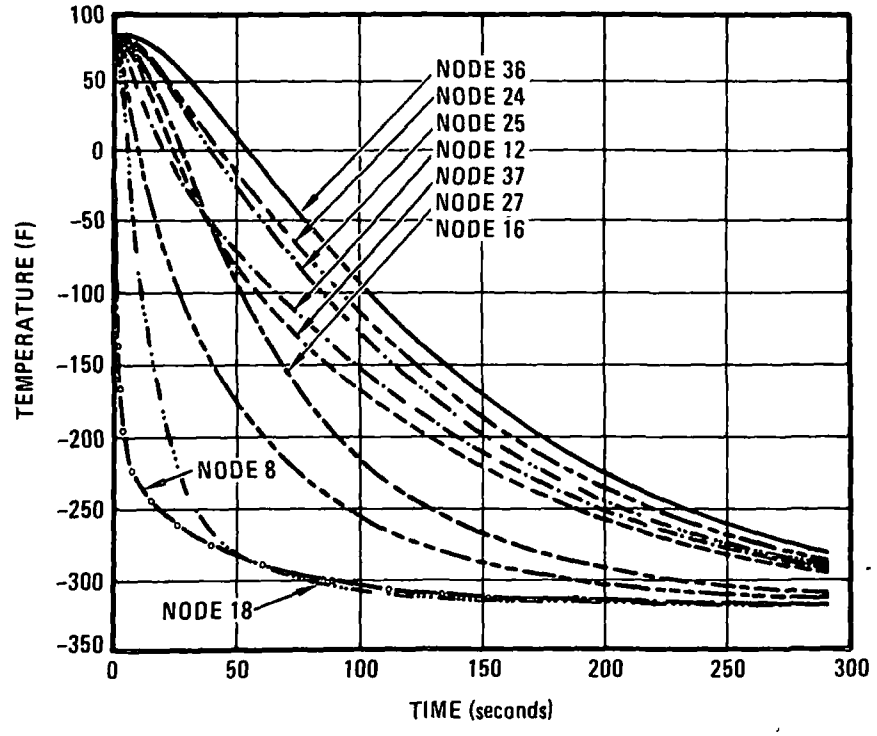

Figure 10-10. Predicted Temperature Versus Time after Chilldown Start at Sta 24.38 for the F-111 TACT

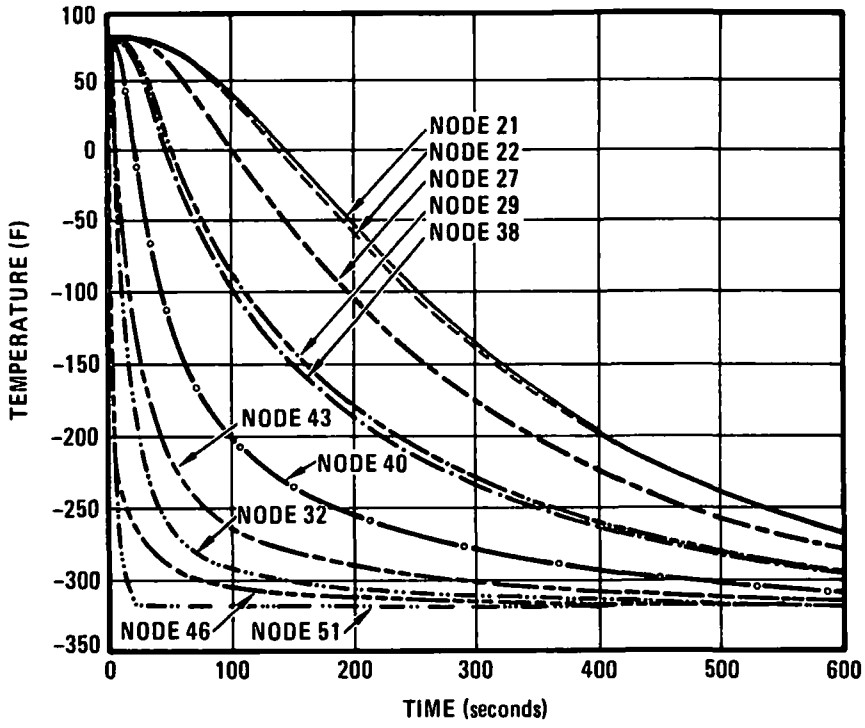

Figure 10-11. Predicted Temperature Versus Time after Chilldown Start at Sta 27.00 for the F-111 TACT

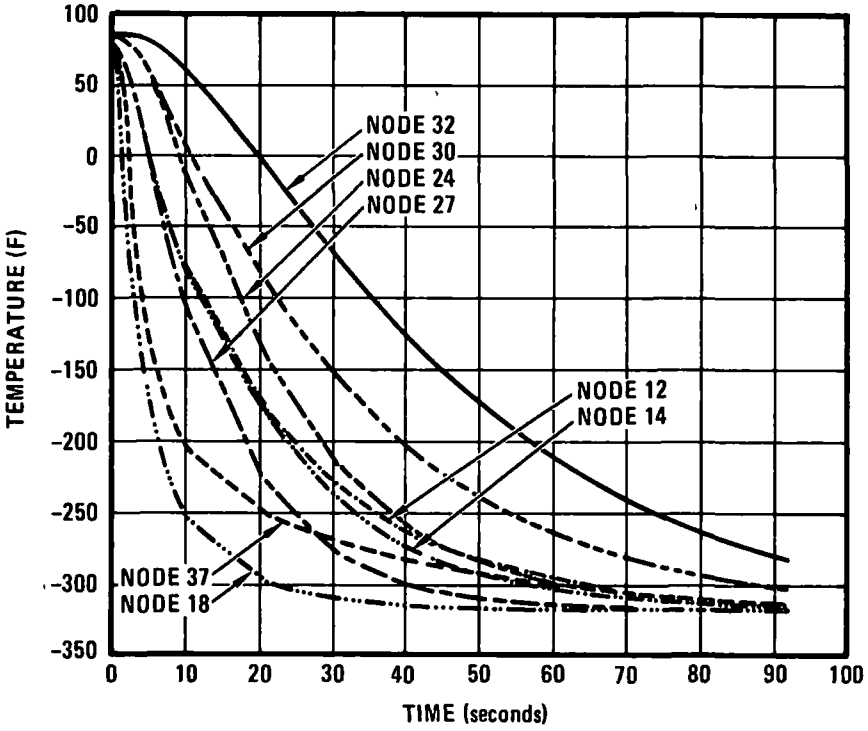

Figure 10-12. Predicted Temperature Versus Time after Chilldown Start at Sta 38.51 for the F-111 TACT

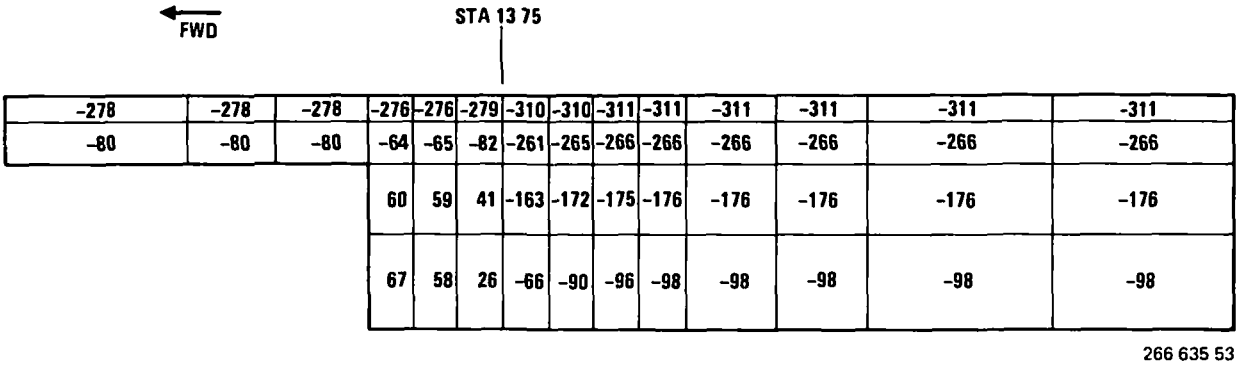

Figure 10-13. Predicted Temperatures (F) 20 Seconds after Chilldown Start for the CWC

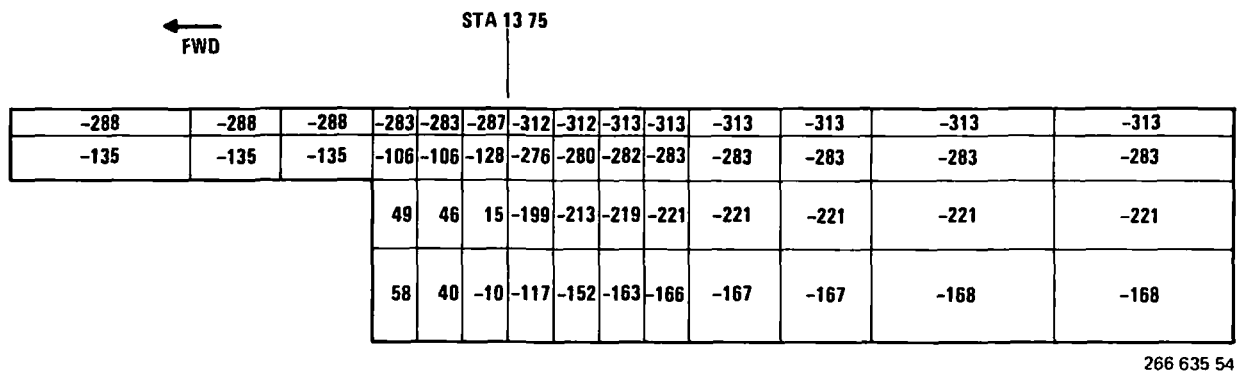

Figure 10-14. Predicted Temperatures (F) 40 Seconds after Chilldown Start for the CWC

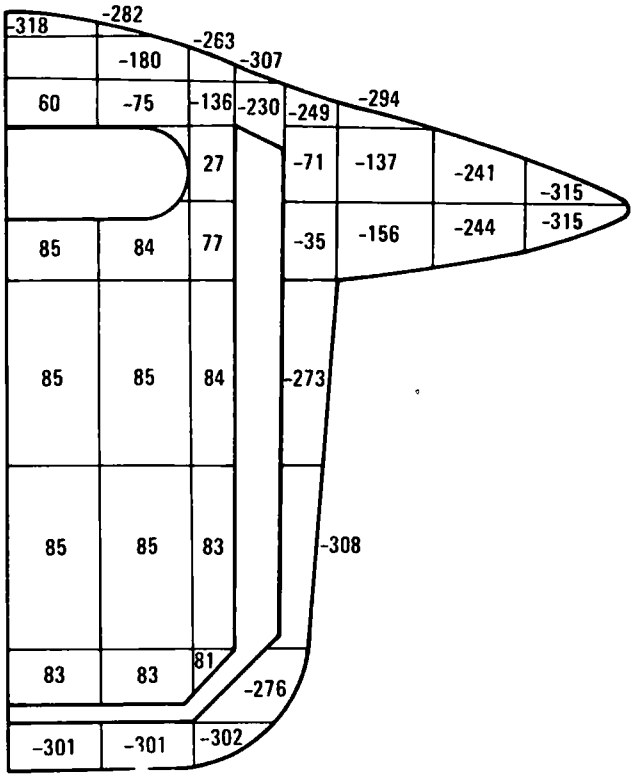

266 635 55

Figure 10-15. Predicted Temperatures (F) 10 Seconds after Chilldown Start at F-111 TACT Sta 19.00

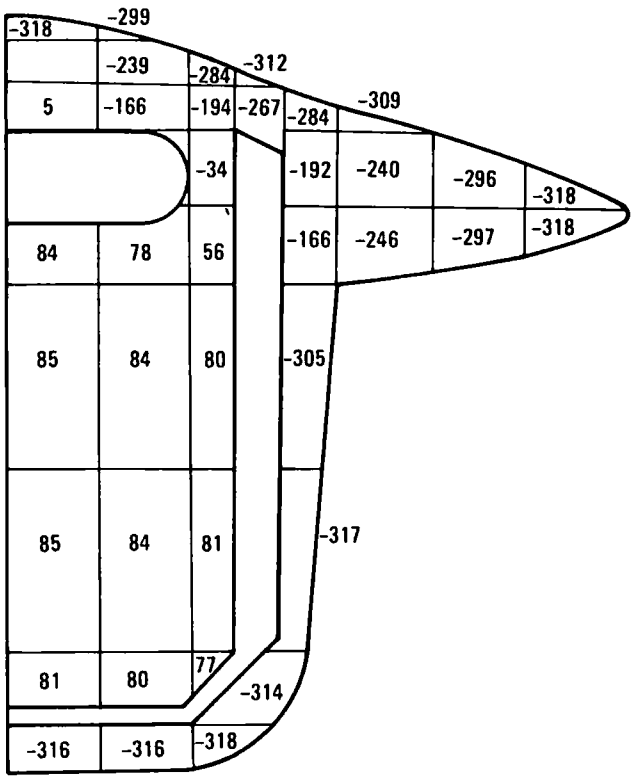

266 635 56

Figure 10-16. Predicted Temperatures (F) 20 Seconds after Chilldown Start at F-111 TACT Sta 19.00

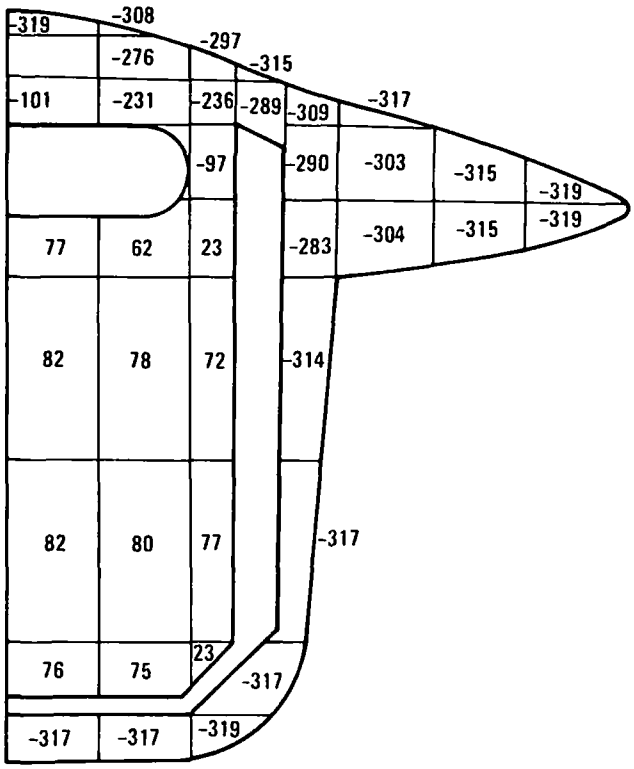

Figure 10-17. Predicted Temperatures (F) 40 Seconds after Chilldown Start at F-111 TACT Sta 19.00

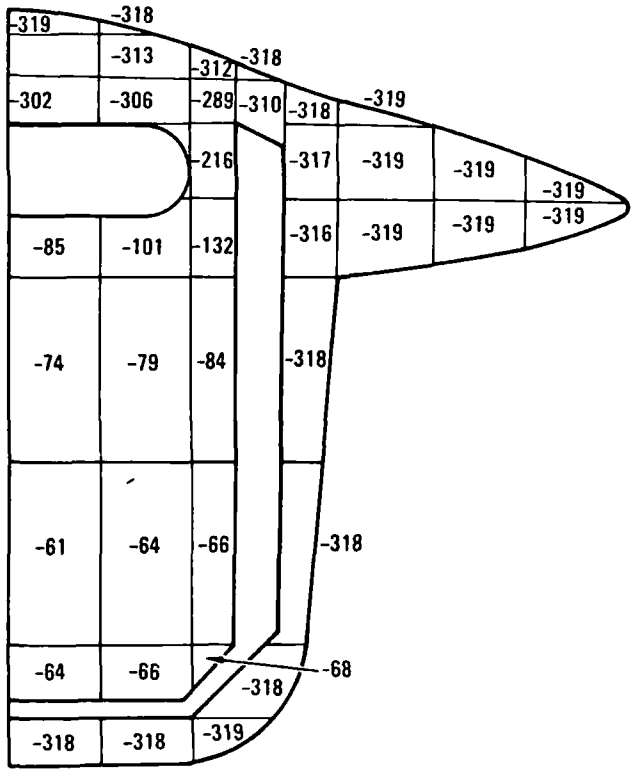

Figure 10-18. Predicted Temperatures (F) 600 Seconds after Chilldown Start at F-111 TACT Sta 19.00

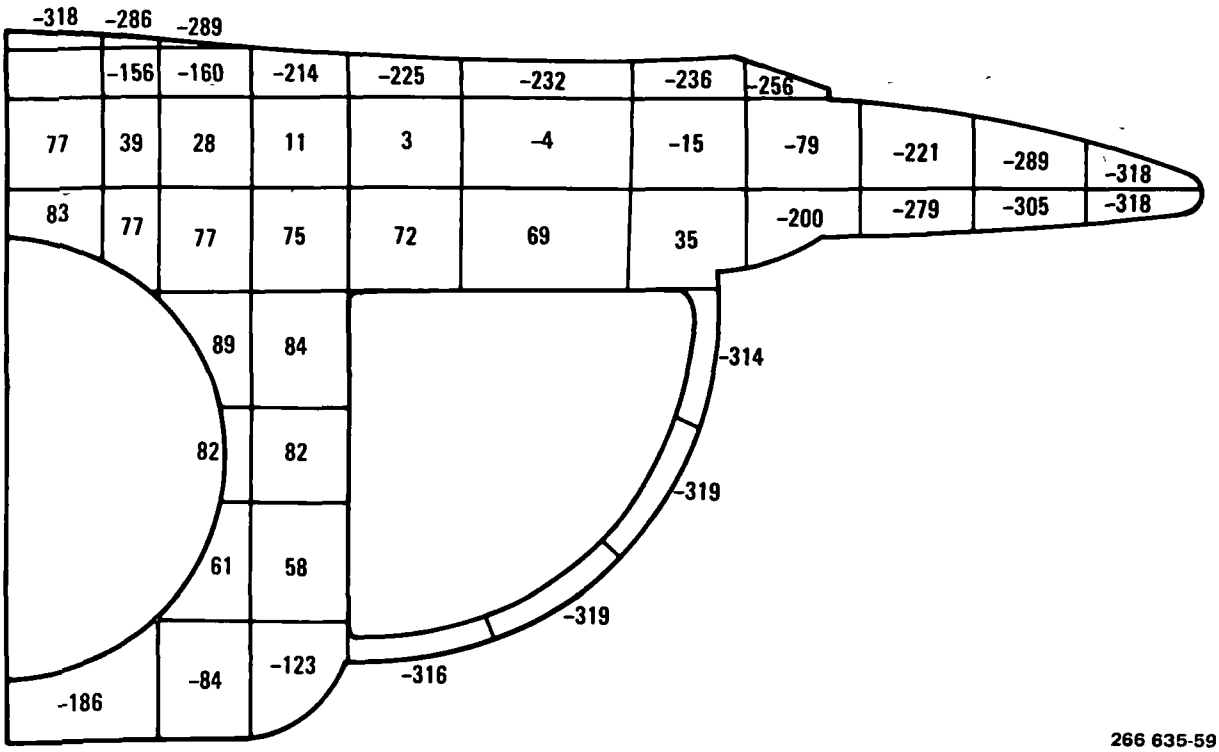

Figure 10-19. Predicted Temperature (F) 10 Seconds after Chilldown Start at F-111 TACT Sta 24.38

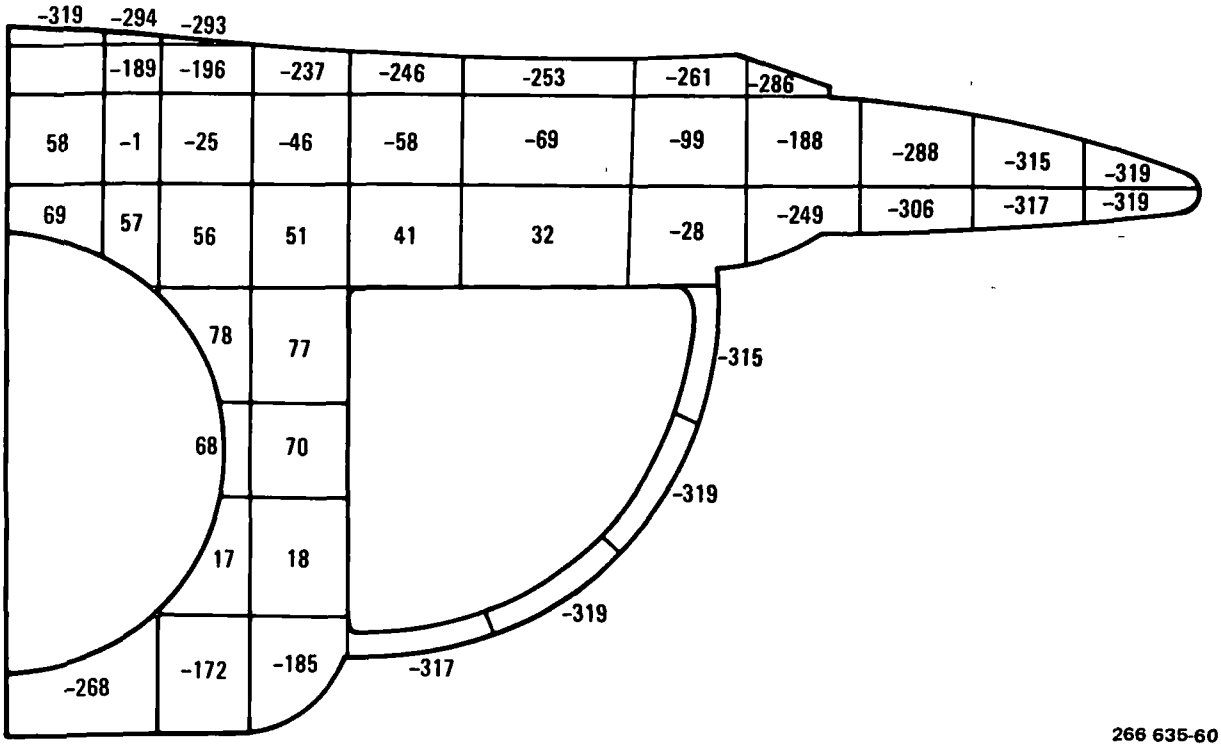

Figure 10-20. Predicted Temperature (F) 20 Seconds after Chilldown Start at F-111 TACT Sta 24.38

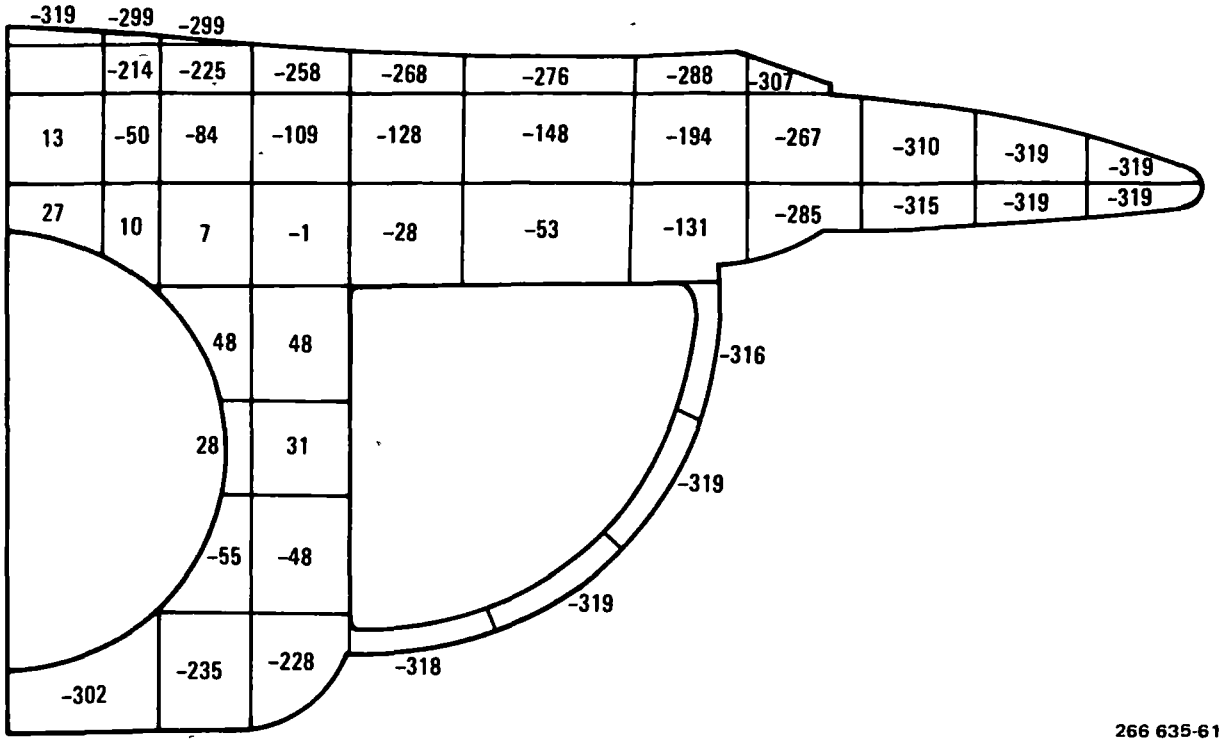

Figure 10-21. Predicted Temperature (F) 40 Seconds after Chilldown Start at F-111 TACT Sta 24.38

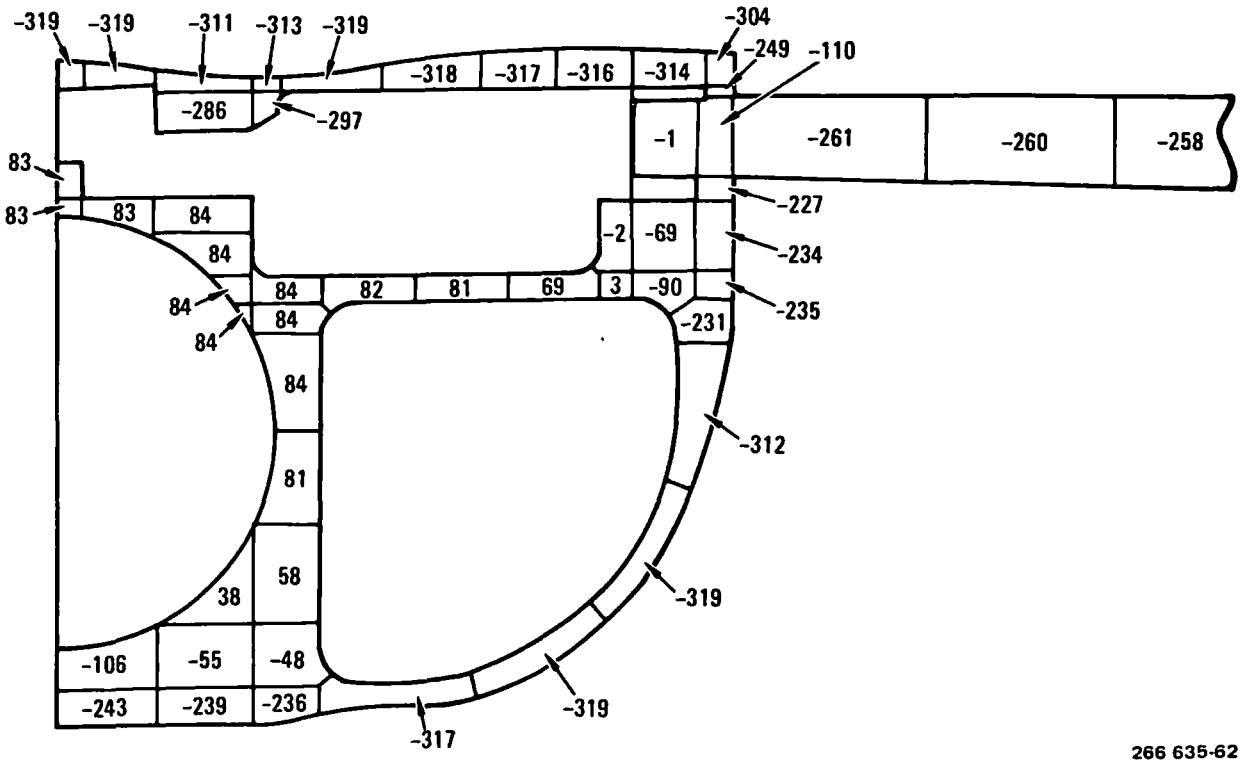

Figure 10-22. Predicted Temperature (F) 10 Seconds after Chilldown Start at F-111 TACT Sta 27.00

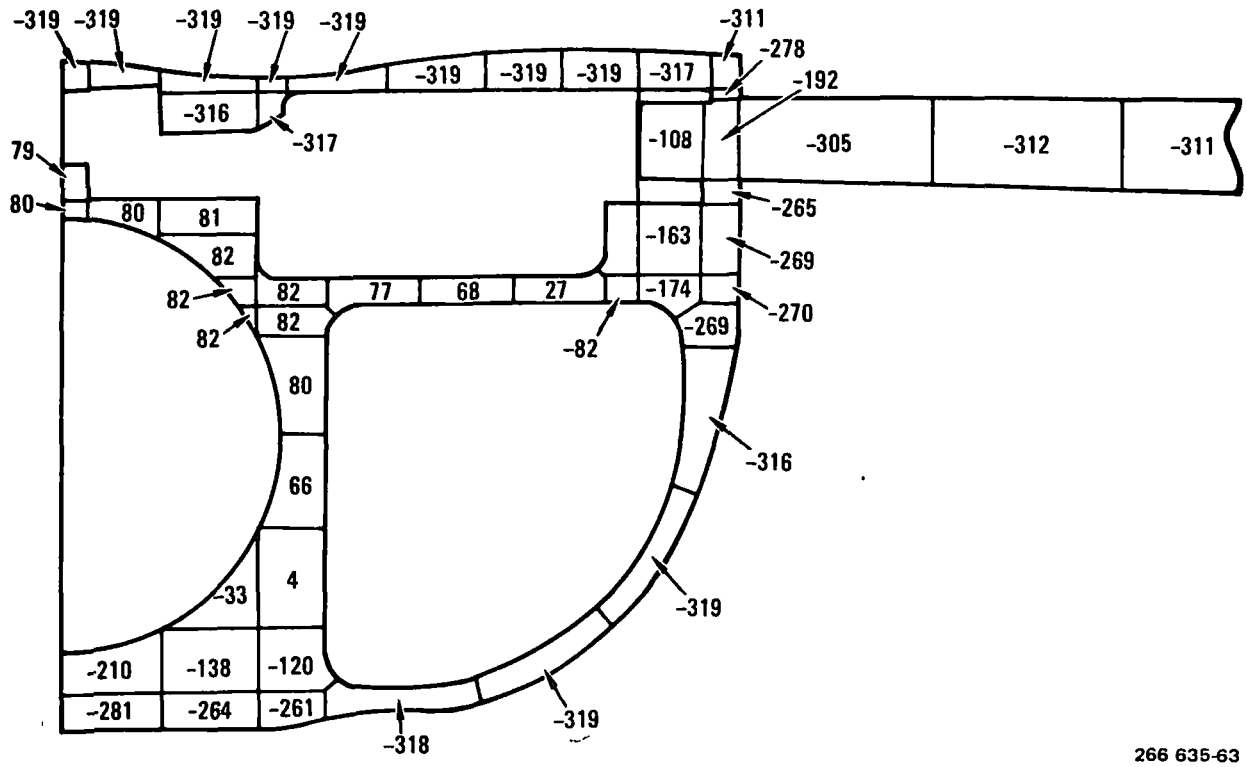

Figure 10-23. Predicted Temperature (F) 20 Seconds after Chilldown Start at F-111 TACT Sta 27.00

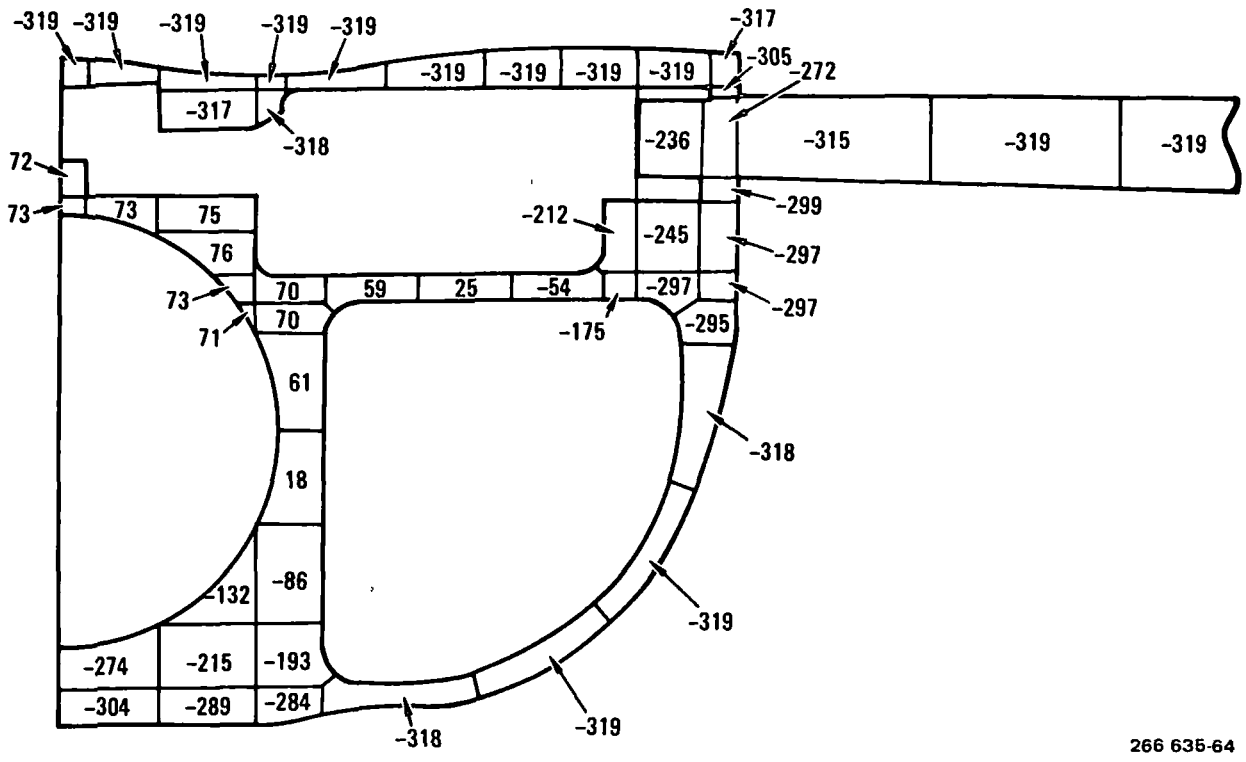

Figure 10-24. Predicted Temperature (F) 40 Seconds after Chilldown Start at F-111 TACT Sta 27.00

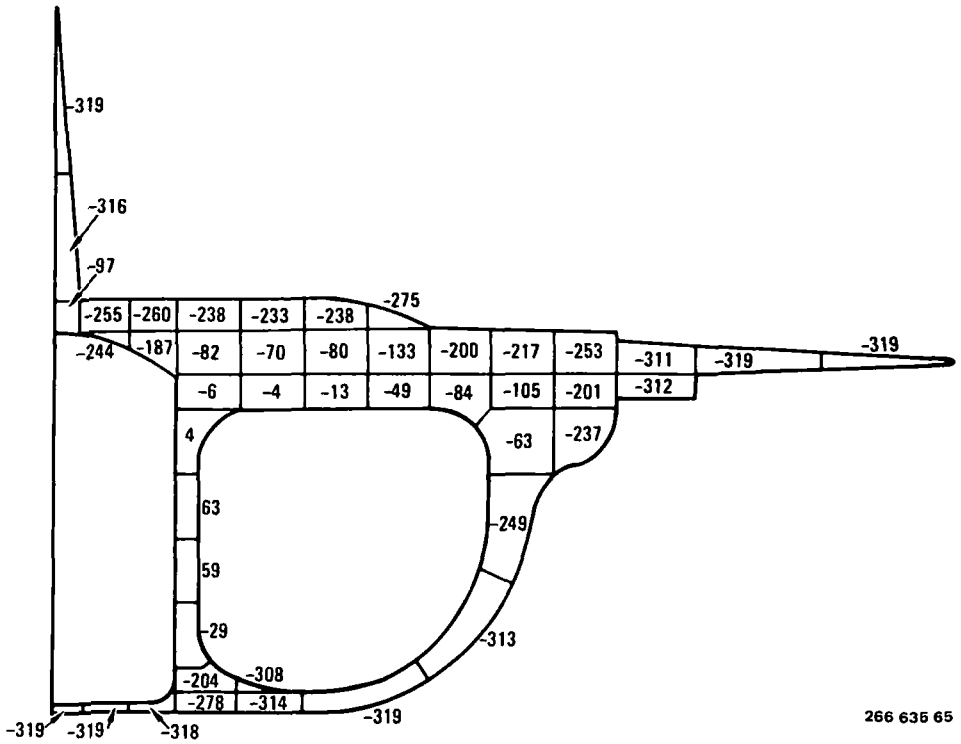

Figure 10-25. Predicted Temperature (F) 10 Seconds after Chilldown Start at F-111 TACT Sta 38.51

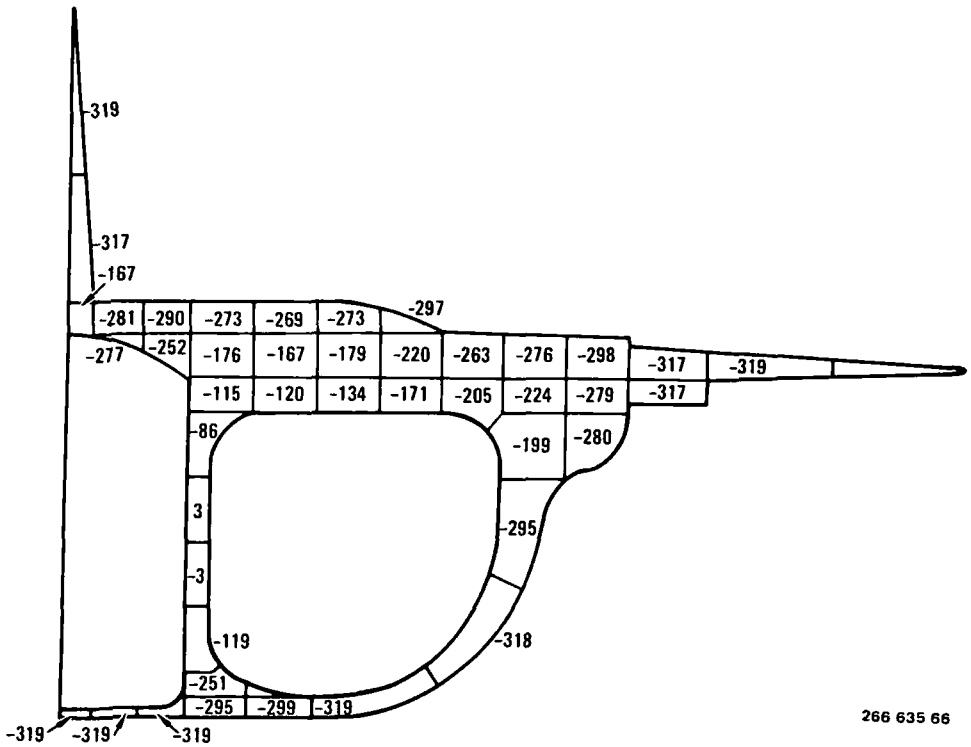

Figure 10-26. Predicted Temperature (F) 20 Seconds after Chilldown Start at F-111 TACT Sta 38.51

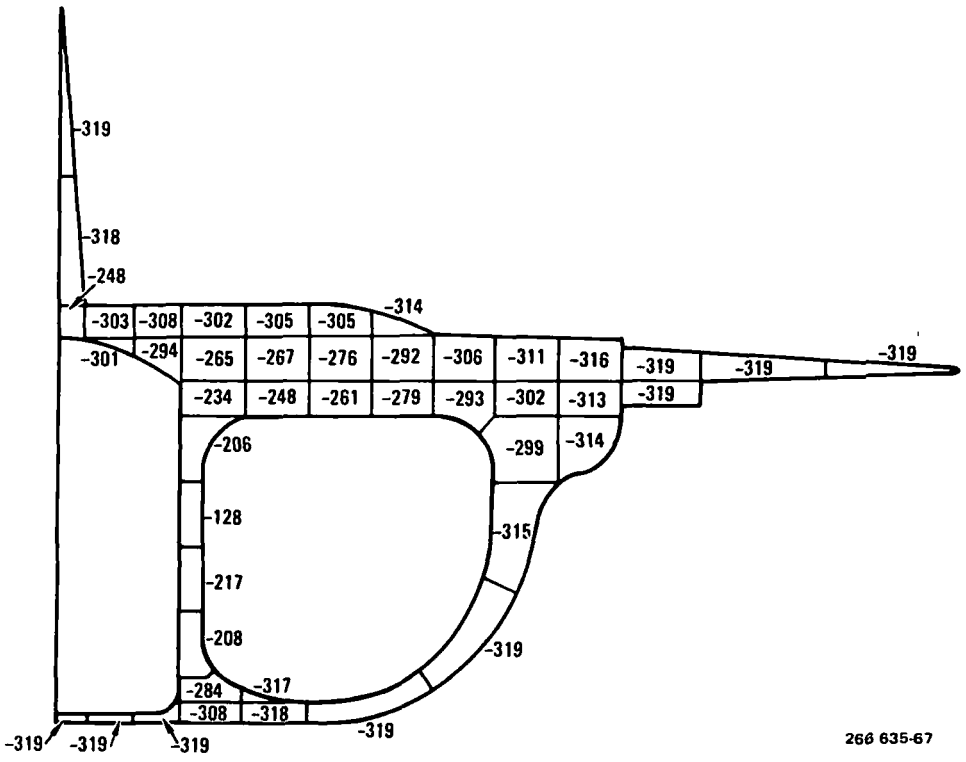

Figure 10-27. Predicted Temperature (F) 40 Seconds after Chilldown Start at F-111 TACT Sta 38.51

The instrumentation packages are insulated from the external surface temperatures by the forward body (Kevlar 49®) shell and an insulation foam surrounding the packages as shown in Figure 10-28.

The heater watt-density requirements were calculated as follows (see Figure 10-2):

x_1 = 0.25 in.

A = 1 ft^2

k_1 = 0.30 Btu-ft/hr-ft^2-deg F

x_2 = 0.125 in.

k_2 = 0.2 Btu-ft/hr-ft^2-deg F

$$R_1 = \frac{x_1}{k_1 A} = 0.69 \text{ hr-deg F/Btu}$$

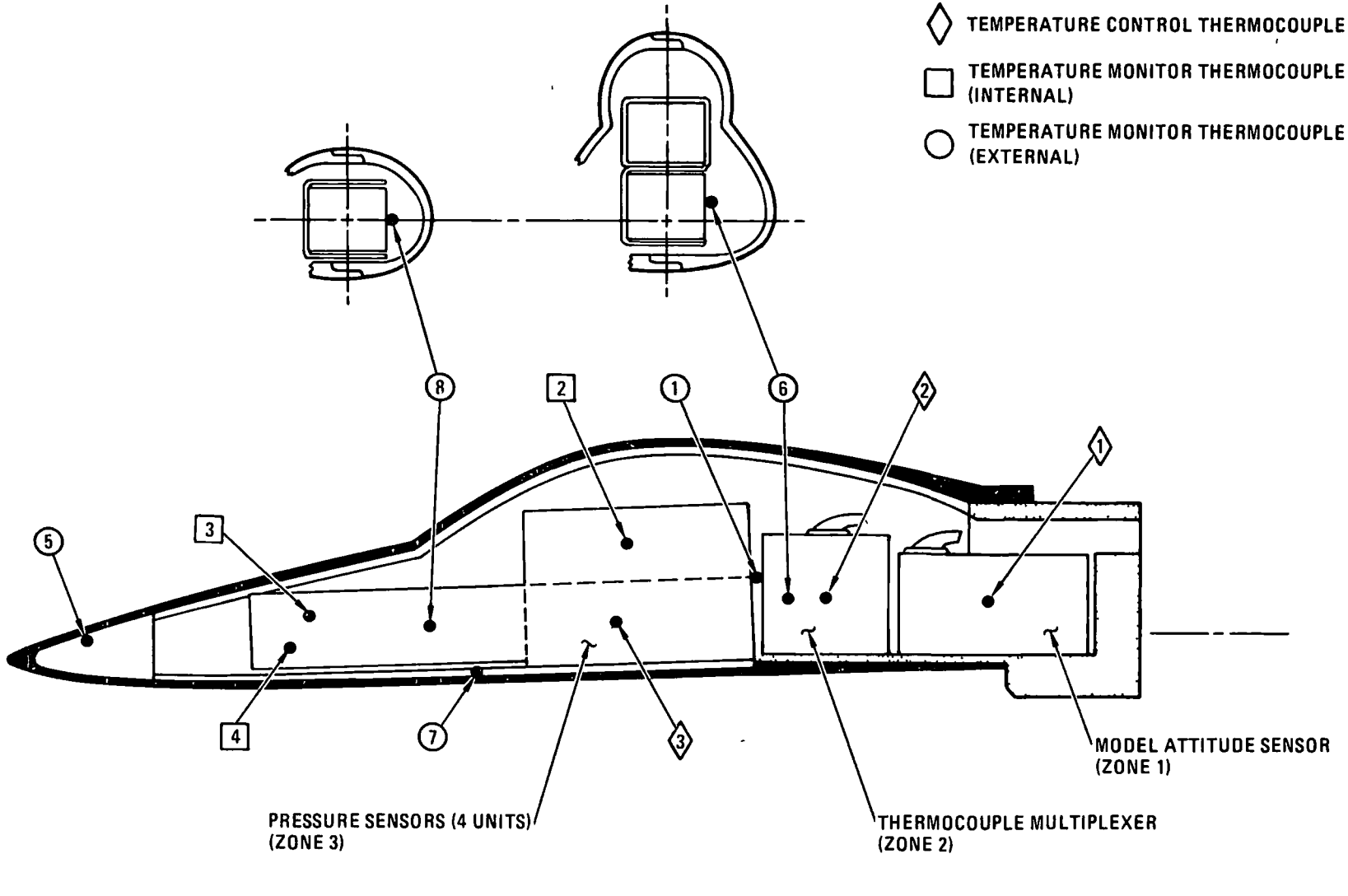

Figure 10-28. Forward Body Specimen Thermocouple Locations

R_2 = 0.05 hr-deg F/Btu

R_T = 0.74 hr-deg F/Btu

$$Q = \frac{\Delta T}{R_T} = \frac{492 - 140}{0.74} = 476 \text{ Btu/hr-ft}^2$$

Q = 138 watts/ft^2

Q = 0.96 watt/in^2 (heater watt-density)

Electric resistance heaters are commercially available at watt-densities well suited to meet these requirements.

Appendix A1 for description and results of the instrumentation bay proof-of-concept test.

10.1.4 MODEL TEMPERATURE DISTRIBUTION DURING A TEST RUN. The model temperature distribution was estimated based upon tunnel static, recovery, and total temperatures for Mach values of 0.8 and 1.2.

Figure 10-29 depicts the model temperature gradients or the CWC. Analysis indicates similar results for the F-111 TACT.

10.2 STRUCTURAL ANALYSIS – CWC

The wing panels, wing attachment, wing movable surfaces, fuselage, and sting support systems are analyzed in this section.

CWC WING PANEL (See Figure 10-30.)

The wing panels are fabricated from 18Ni-200 maraging steel. The panel is basically a two-piece construction consisting of an upper wing and lower cover plate. The cover plate is attached by pins along the ribs and by laser welding the periphery of the cover plate – obtaining, in effect, a single panel (see Section 9.1.5).

Sections taken through the wing tang, wing station 9.140, and diagonal to the span (see Figure 10-30) were analyzed. The results, using the wing section properties, are shown in Table 10-1.

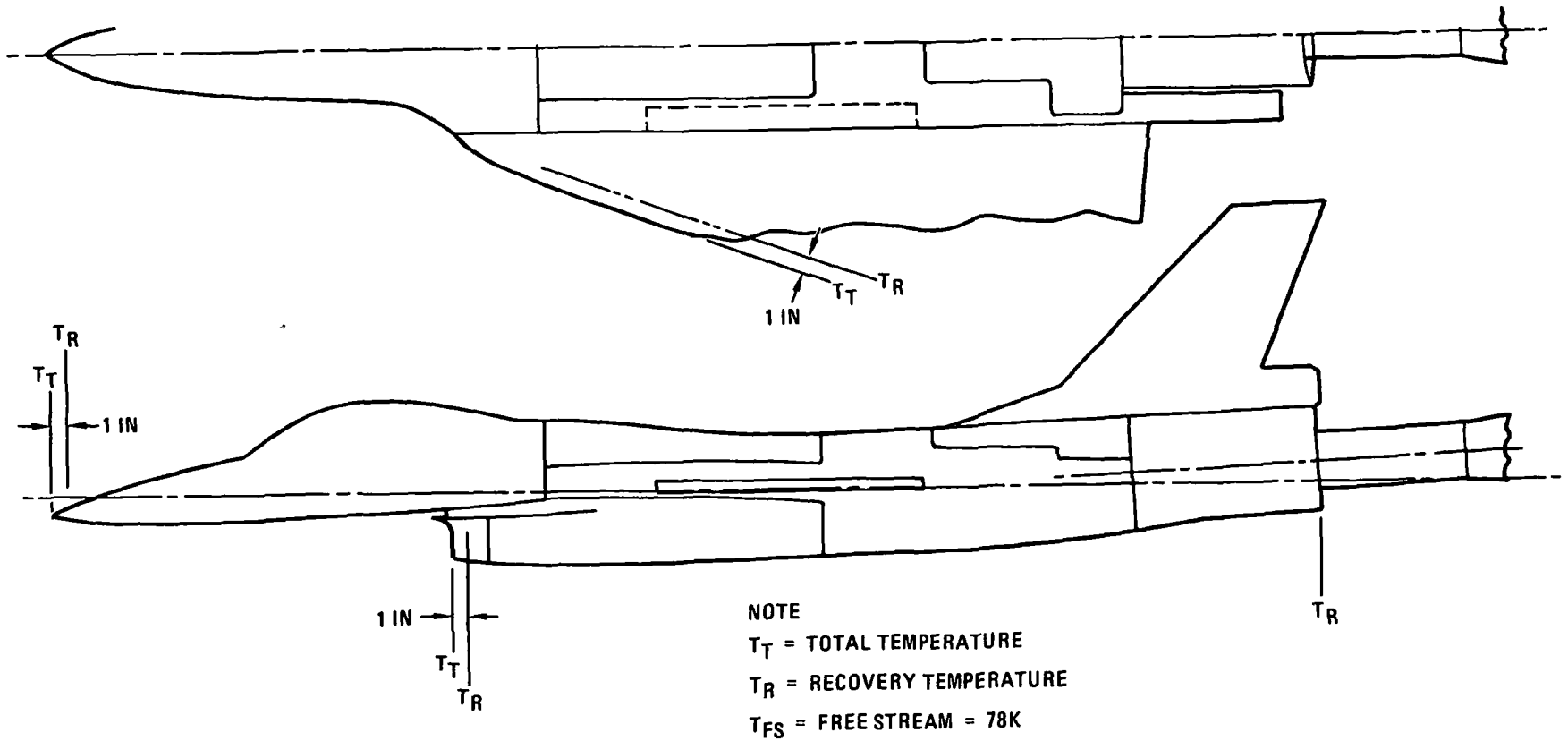

MACH NO	α (DEG)	T_T	T_R	CIRCUMFERENTIAL TEMPERATURE GRADIENT		LONGITUDINAL TEMPERATURE GRADIENT			
				UPPER	LOWER	FORWARD UPPER	AFT UPPER	FORWARD LOWER	AFT LOWER
1 2	0	100K	97K	97K	97K	97K	97K	97K	97K
1 2	20			97K	78K				
0 8	0	87K	86K	86K	86K	86K	86K	86K	86K
0 8	20	87K	86K	86K	78K				

266 635 69

Figure 10-29. Model Temperature Gradients

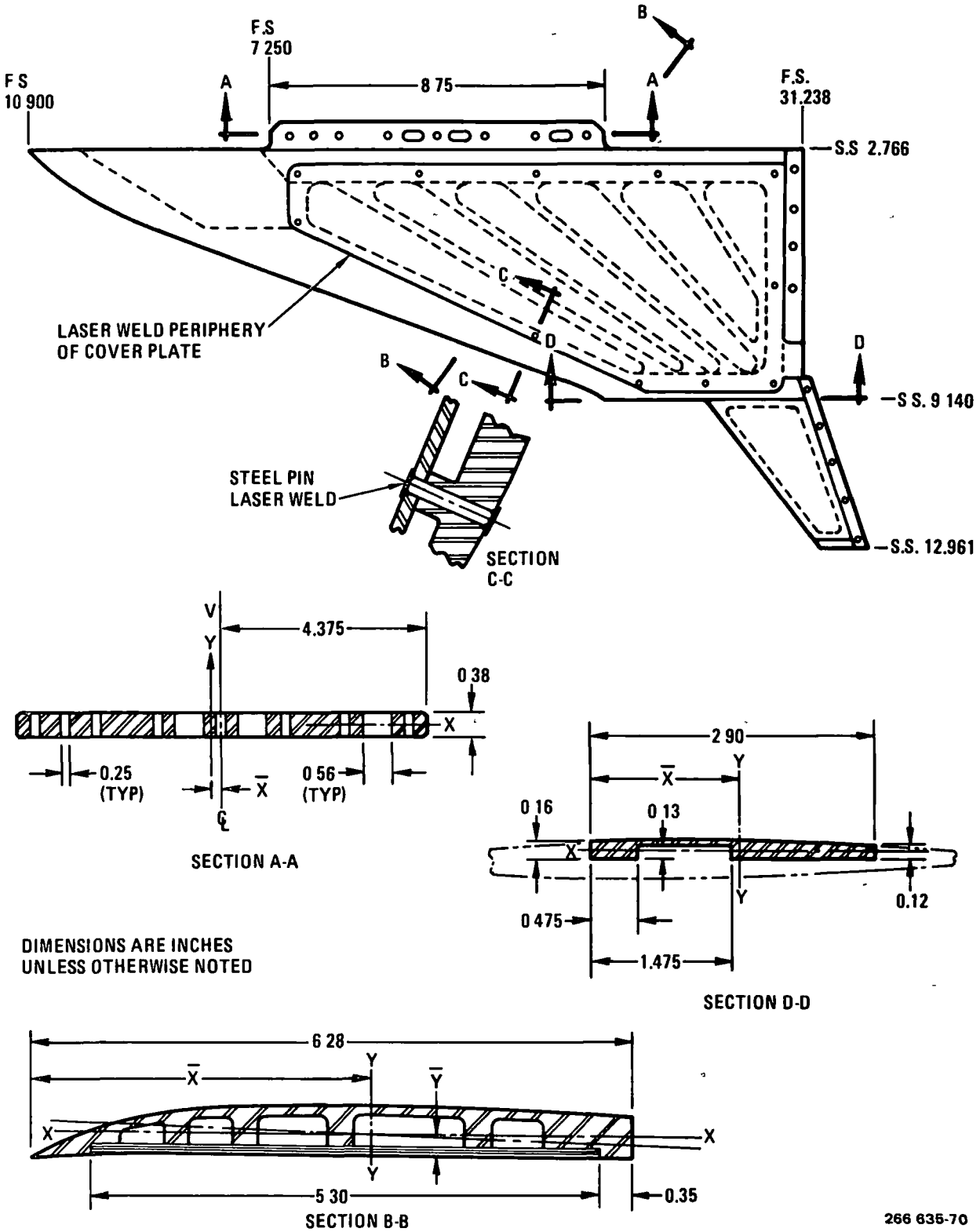

Figure 10-30. CWC Wing Panel

Table 10-1. Wing Analysis Results

Section Properties – CWC

Section	$\bar{x}$	$\bar{y}$	A	C_t	K	I_{max}	I_{max}
	in.	in.	in^2	in.	in^4	in^4	in^4
A-A	0.198	0.190	1.93	---	---	0.02318	13.1912
9.140	1.526	0.097	0.345	0.179	0.00329	0.000823	0.275
B-B	3.515	0.220	1.779	---	---	0.04301	5.7678

Loads and Stresses

Section	Loads (see Figure 5-11)			Calculated Stresses		Safety Factors④	
	V	M	T	f_b	f_s	SF_y	
	lb	in-lb	in-lb	(ksi)	(ksi)	78K	300K
A-A	1640	5500	3700	45.00①	9.02②	5.7	4.3
9.140	250	450	150	49.21①	8.12③	5.5	4.0

Section	Loads (see Figure 5-11)			Calculated Shear Flow⑤			Safety Factors
	V	M	T	q_1	q_2	q	
	lb	in-lb	in-lb	lb/in	lb/in	lb/in	78K
B-B	660	2000	1500	1380	652	1526	3.0

Notes:

Calculated Stresses

① $f_b = \dfrac{Mc}{I_{min}}$

② $f_s = \dfrac{[3 + 1.8(\frac{h}{b})]}{bh^2} T$

③ $f_s = \frac{T_{ct}}{K}$

④ Safety Factors – Combined Loading

$$SF_y = \frac{1}{\left[\left(\frac{f_b}{F_{ty}}\right)^2 + \left(\frac{f_s}{F_{sy}}\right)^2\right]^{1/2}}$$

⑤ Calculated Shear Flow

Shear along surfaces is:

$$q_1 = \frac{VA_1y}{I_{min}}, \quad A_1y = bt\,(y - 1/2t)$$

Shear due to torsion for an assumed single cell section is shown below.

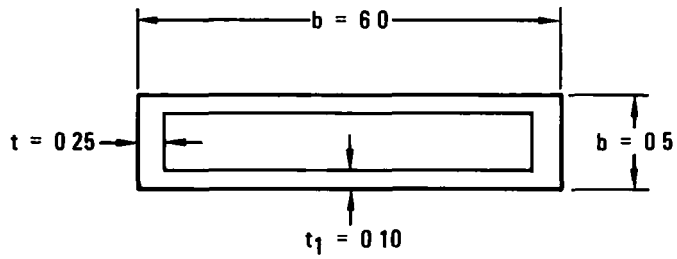

DIMENSIONS IN INCHES

266 635 71

$$q_2 = \frac{T}{2(b-t)(h-t_1)}$$

$$q = \sqrt{q_1^2 + q_2^2}$$

Basing computations on a safety factor (SF) of 3.0 on yield at 300K

$$f_s = \frac{F_{tu}}{SF_y} = \frac{126,000}{3} = 42,000 \text{ psi}$$

Pins having a diameter of 0.25 inch are used. The shear area of each pin is.

$$A_p = 0.049 \text{ in}^2$$

Pin spacing is then;

$$d = \frac{f_s A_p}{2} = \frac{(42,000)\ (0.049)}{1526} = 1.35 \text{ in.}$$

Another method considered was to laser weld the pins in conjunction with dovetailing, and laser welding the outer edges of the cover plate where it mates with the main wing panel (see sketch below). This would resist the peeling action of the cover plate. On this particular configuration the pins are were found to be sufficiently strong in tension, dovetailing was unnecessary.

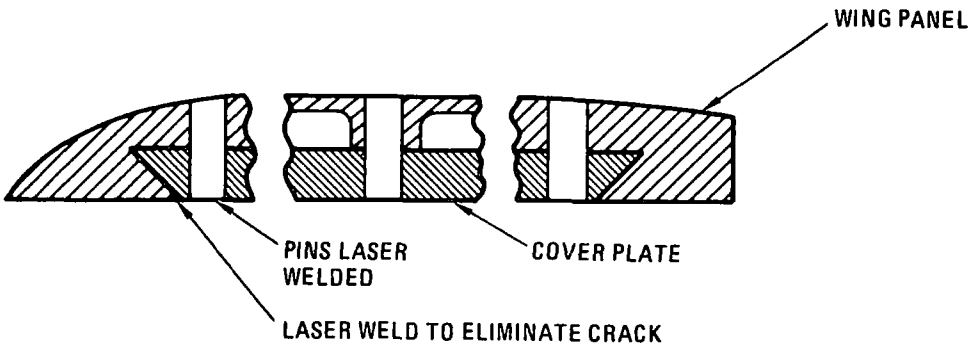

266 635 72

Wing Movable Surfaces

Sections along the screw centerlines and the screws themselves were analyzed. A typical sketch of the surfaces is shown below.

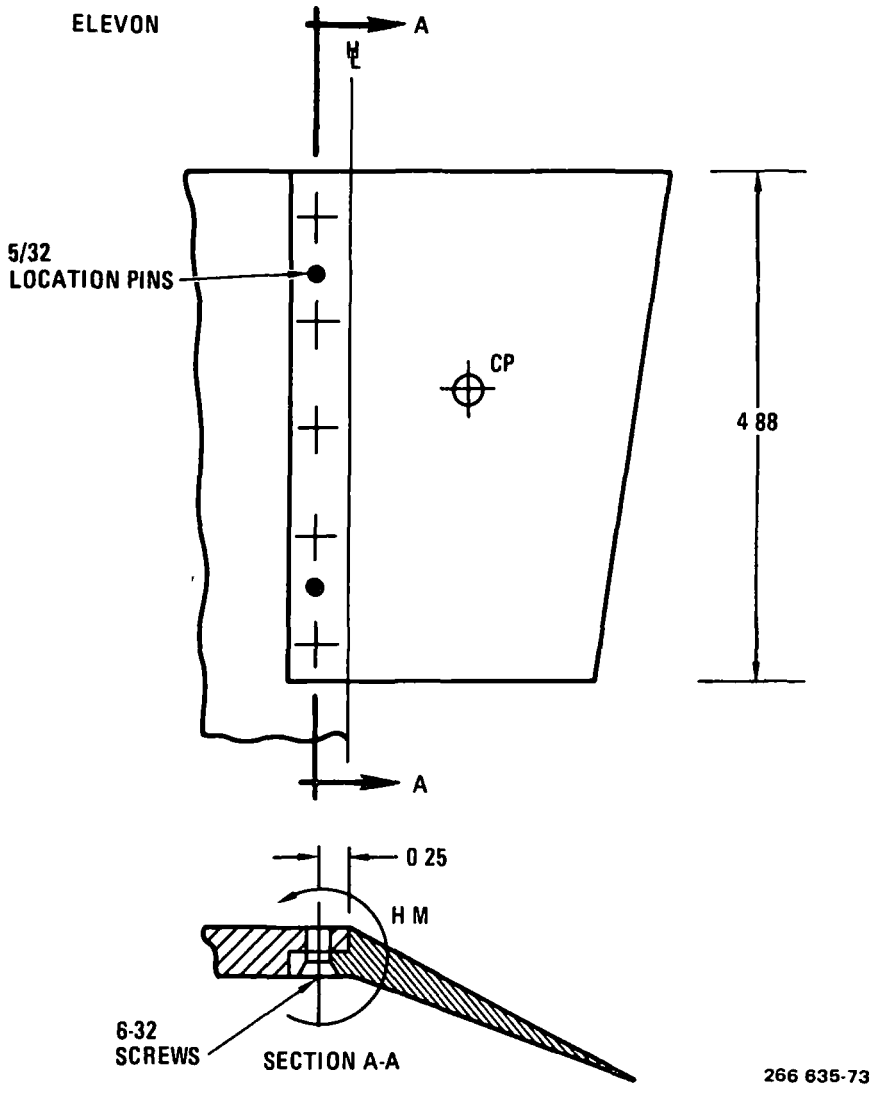

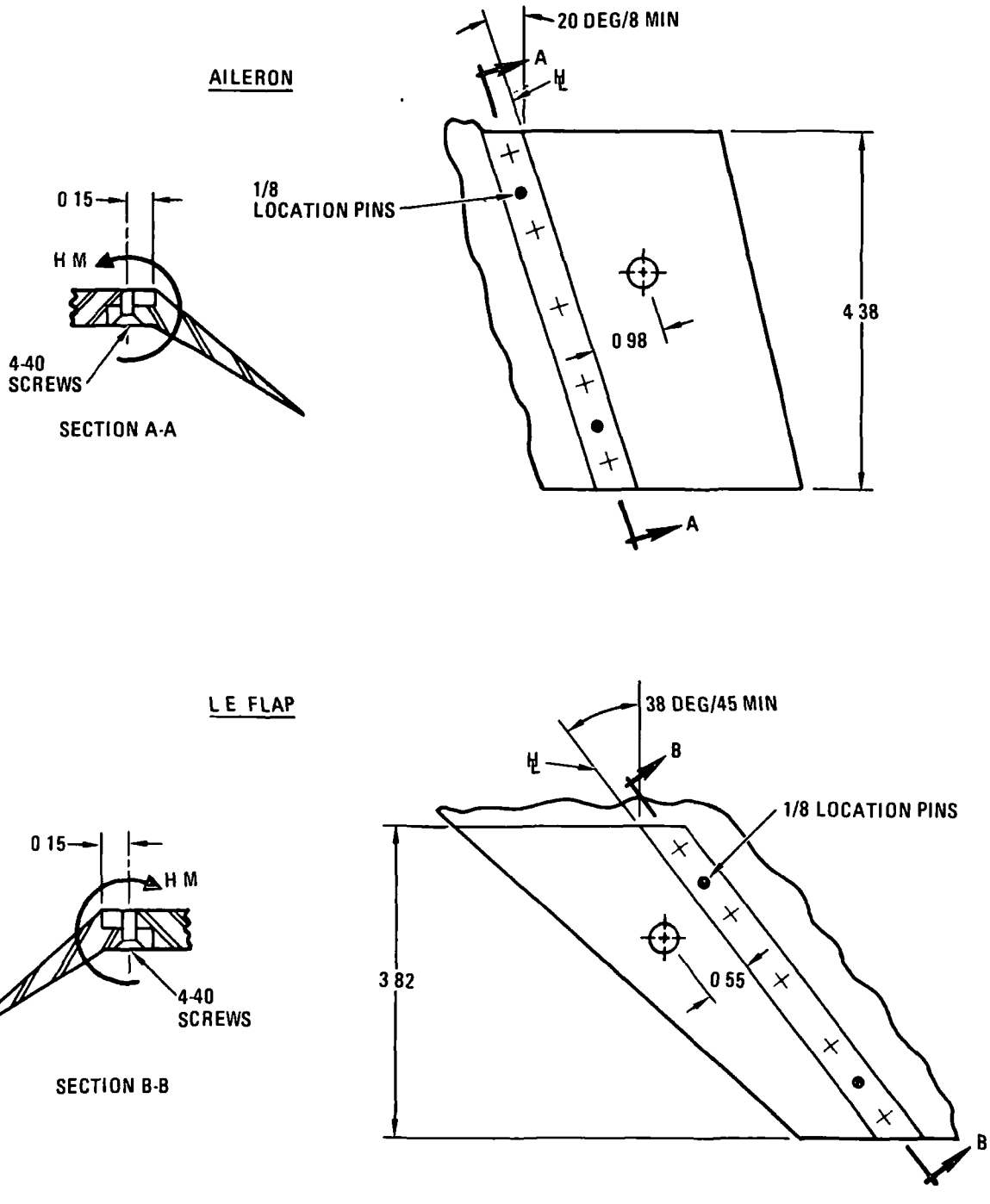
AILERON
20 DEG/8 MIN
A
℄
0 15
H M
1/8
LOCATION PINS
4-40
SCREWS
SECTION A-A
0 98
4 38
A
L E FLAP
38 DEG/45 MIN
B
℄
1/8 LOCATION PINS
0 15
H M
4-40
SCREWS
SECTION B-B
3 82
0 55
B
266 635 74

The allowable loads for screws made from A286 material are given below. Adjustments were made for temperature (Reference 34).

Allowable Loads (F_{tu} = 160 ksi)

Screw Size	300K (R.T.)		78K	
	Yield (lb)	Ult (lb)	Yield (lb)	Ult (lb)
#4-40	521	830	624	1112
#6-32	780	1249	936	1678

The loads on the screws come from two sources: Airloads, and thermal contraction.

Loads on Screws Due to Thermal Contraction of Dissimilar Materials (Table 10-2)

$$\varepsilon = \Delta \ell_{screw} - \Delta \ell_{material} = (\alpha^{t}_{scr} - \alpha^{t}_{mat})(\ell)(\Delta T) \quad (4)$$

$$P_t = \frac{\varepsilon A E}{\ell}$$

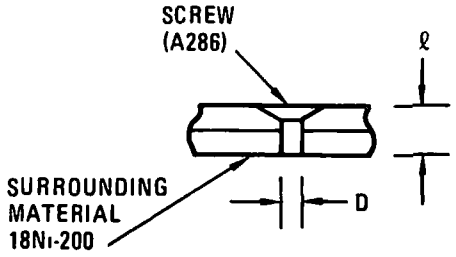

Table 10-2. Tension Load on Screws (78K)

Surface	ℓ (in.)	D (in.)	A (in^2)	ε (in.)	P_t* (lb)
Elevon	0.28	0.0997	0.00781	371.3×10^{-6}	304
Aileron	0.20	0.0813	0.00519	265.2×10^{-6}	202
L.E. Flap	0.20	0.0813	0.00519	265.2×10^{-6}	202

*These loads occur at 78K and are additive to the dynamic loads generated by airflow.

Screw Loads and Safety Factors

Surface	H.M.* V (lb)	H.M.* Max Allow (in-lb)	$P_{t_{crit}}$ (lb)	Safety Factors ③ 300K Yield	300K Ult	78K Yield	78K Ult
Elevon	225	345	390 ①	2.0	3.2	1.3	2.4
			694 ②				
Aileron	120	118	260 ①	2.0	3.2	1.3	2.4
			462 ②				
L.E. Flap	200	110	260 ①	2.0	3.2	1.3	2.4
			462 ②				

① Load on screw at room temperature (300K)

② Load on screw at cryogenic conditions (78K)

③ Though the safety factors at room temperature (300K) are below what is required, proof-of-concept tests performed at our facilities indicate the problem is not as severe as theory shows. Additional proof tests need to be conducted in this area.

The maximum allowable hinge moment (H.M.*) shown above is based upon a safety factor of 2.0 on yield at room temperature for the attachment screws holding the control surfaces. It may be necessary to restrict the model α to ensure that the control surface H.M. is not exceeded. See Section 5.1.3 for model loads data.

An alternative design, shown in Figure 10-31, gives higher safety factors but increases model costs.

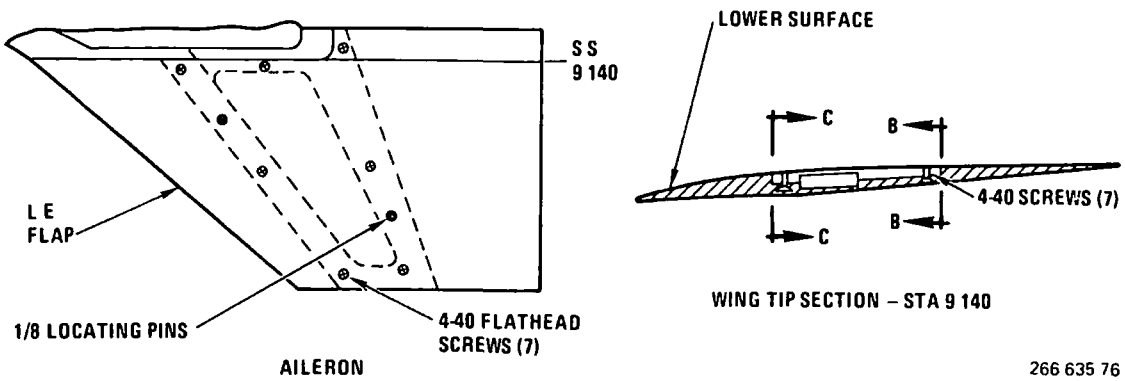

Figure 10-31. CWC Wing Tip Panel

SECTION THRU SCREW HOLES

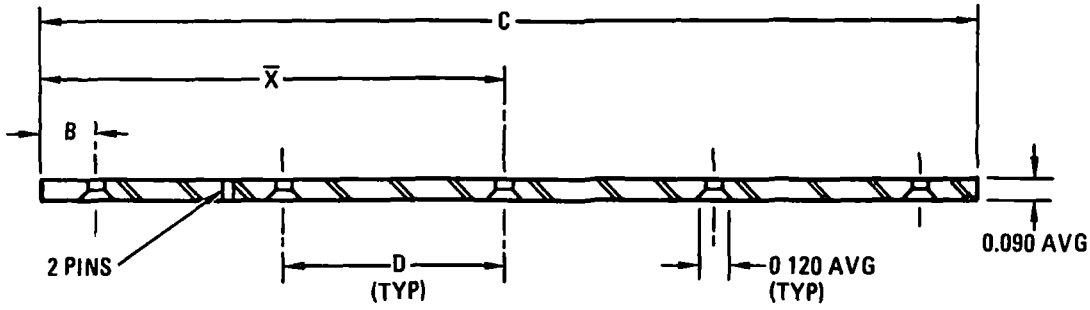

SECTION A-A

266 635-77

Section Properties

Section A-A	C (in.)	B (in.)	d (in.)	A (in^2)	$\bar{x}$ (in.)	I_{min} (in^4)	I_{max} (in^4)
Elevon	4.88	0.44	1.0	0.385	2.44	0.00026	0.73542
Aileron	4.66	0.33	1.0	0.361	2.12	0.00024	0.63152
L.E. Flap	4.90	0.25	1.1	0.387	2.45	0.00026	0.75162

Bending Stress and Safety Factors

Section A-A	H.M. (in-lb)	$f_{b(max)}$ (psi)	Safety Factor (300K) Yield	(300K) Ult	(78K) Yield	(78K) Ult
Elevon	345	59.710	3.3	3.5	4.5	4.6
Aileron	118	22,130	9.2	9.4	12.1	12.6
L.E. Flap	110	19.040	10.7	10.9	14.1	14.7

One Piece Wing Tip Panel

If the Aileron and L.E. flap are designed as a one-piece construction as shown in Figure 10-31, it eliminates the problem of transferring the moments from the moveable surfaces to the main spar or structure. The hinge moments are now taken out by the movable surfaces and the screws are in tension primarily due to the load.

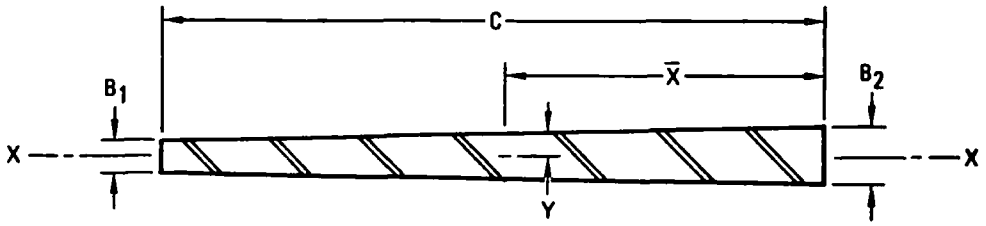

SECTION B B, C-C

266 635-78

Section Properties

Section	C (in.)	B_1 (in.)	B_2 (in.)	A (in^2)	$\bar{x}$ (in.)	y (in.)	I_{min} (in^4)	I_{max} (in^4)
B-B	4.66	0.075	0.112	0.436	2.17	0.094	0.00033	0.77818
C-C	4.90	0.065	0.160	0.551	2.10	0.112	0.00068	1.03741

$HM_{Aileron} = 118$ in-lb

$$f_b = \frac{My}{I_{min}} = \frac{(118)\ (0.044)}{0.000333} = 33{,}610 \text{ psi}$$

$$SF_y = \frac{205}{36.61} = 5.5 \text{ (300K)}$$

$$SF_y = \frac{270}{36.61} = 7.3 \text{ (78K)}$$

$HM_{L.E.\ Flap} = 110$ in-lb

$$f_b = \frac{My}{I_{min}} = \frac{(110)\ (0.112)}{0.00068} = 18{,}120 \text{ psi}$$

$$SF_y = \frac{205}{18.12} = 11.3 \text{ (300K)}$$

$$SF_y = \frac{270}{18.12} = 14.9 \text{ (78K)}$$

Wing Tip Panel Attachment

There are seven #4-40 screws holding the wing tip panel to the main structure (see Figure 10-31).

A download will put the screws in tension. Figure 5-10 shows the maximum down loads to be:

$$H.M._{L.E.\ Flap} = H.M._{Aileron} = 190 \text{ in-lb}$$

$$V_{L.E.\ Flap} = \frac{HM}{d} = \frac{190}{0.55} = 345 \text{ lb}$$

$$V_{Aileron} = \frac{190}{0.85} = 223 \text{ lb}$$

Assume the L.E. flap loads are taken out by only the three forward screws and the aileron loads are taken out by the three aft screws.

Then:

$$P_{t_{(78K)}} = \frac{V}{3}$$

At 78K the load due to thermal contraction is,

$$P_{L.E.\ Flap} = P_{Aileron} = 202 \text{ lb (See Table 10-2).}$$

Then the total screw loads at 300K is;

$$P_{t(300K)} = P_{(300K)} + P_{t(78K)}$$

Screw Loads and Safety Factors

Surface	$P_{t(78K)}$ (lb)	$P_{t(300K)}$ (lb)	Safety Factors 300K Yield	300K Ult	78K Yield	78K Ult
L.E. Flap	115	317	4.5	7.2	2.0	3.5
Aileron	74	276	7.0	11.2	2.2	4.0

Forward Fuselage Section (See Figure FO-5).

The critical area of the forward fuselage section is the attachment to the mid-section. There are three 1/4-20 screws used for the attachment as shown in the sketch below. The analysis is based on a load of 396 lb as shown.

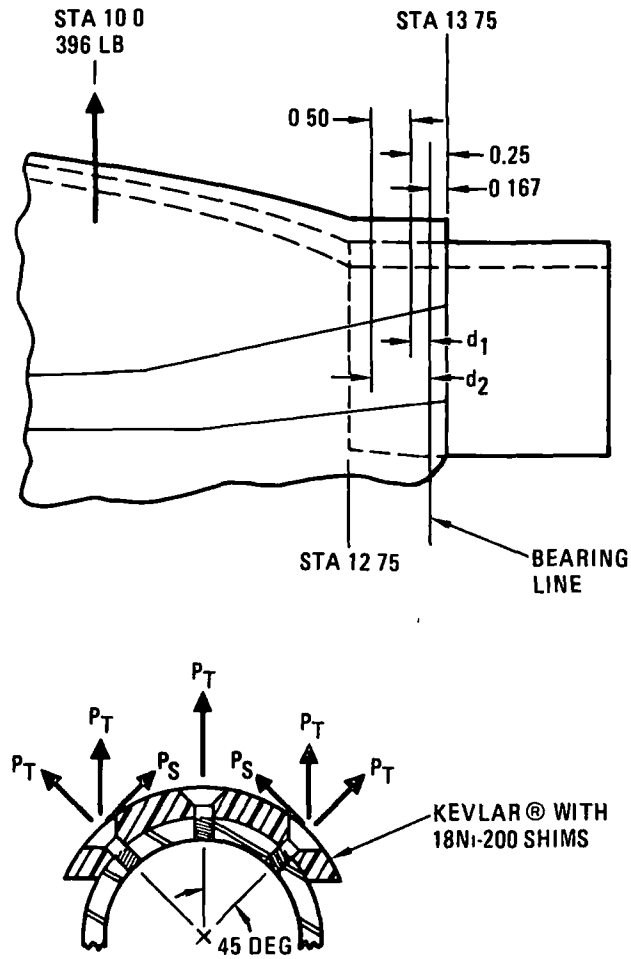

266 635 79

This is the only joint in the model where dissimilar materials were used, and the effect of material contraction differences was considered in the joint analysis.

Assume a bearing line as shown in the previous sketch. The critical tension load at 300K is then:

$$P_{t_{c(300K)}} = \frac{M\,d^2}{\Sigma\, n\, d^2} = \frac{(396)\ (3.75)\ (0.667)}{3\ [(0.167)^2 + (0.667)^2]} = \frac{990}{1.418}$$

$$P_{t_{c(300K)}} = 698 \text{ lb}$$

The shear and tension loads on the side screws are:

$$P^1_{t_{c(300K)}} = P_{t_{c(300K)}} \ (\cos 45) = 493 \text{ lb}$$

$$P_{s_{c(300K)}} = P_{t_{c(300K)}} \ (\sin 45) = 493 \text{ lb}$$

Load Due to Thermal Contraction

There are three different types of materials:

The fuselage shell, made of Kevlar 49 fiberglass with 18Ni-200 shims;

The attachment ring, made of 18Ni-200 steel; and

The fasteners, made of A286 steel.

Considering the shell and screws only:

$$\varepsilon = \Delta\, \ell_{screw} - \Delta\, \ell_{Kevlar}$$

$$\varepsilon = (\alpha^t_{SCR} - \alpha^t_{KEV})\ (\Delta\, \ell)\ (\Delta\, T)$$

$$\varepsilon = (6.4 \times 10^{-6} - 5 \times 10^{-6})\ (0.3)\ (390 \text{ deg F}) = 163.8 \times 10^{-6} \text{ in.}$$

$$P_{t_{(78K)}} = \frac{\varepsilon\, A\, E}{\ell} = \frac{(163.8 \times 10^{-6})\ (0.028)\ (29.43 \times 10^6)}{0.3}$$

$$P_{t_{(78K)}} = 450 \text{ lb}$$

$$\therefore P_{t_{c(78K)}} = 450 + 698 = 1140 \text{ lb}$$

Allowable Loads for 1/4-20 Screw

	300K		78K	
	Yield (lb)	Ult (lb)	Yield (lb)	Ult (lb)
P_T	2818	4474	3937	5995
P_S	2938	4663	4103	6248

Safety Factor*

300K		78K	
Yield	Ult	Yield	Ult
4.1	5.4	3.4	5.2

$$*SF = \frac{1}{\left[\left(\frac{P_t}{P_T}\right)^2 + \left(\frac{P_s}{P_S}\right)^3\right]^{1/2}}$$

Station 12.75

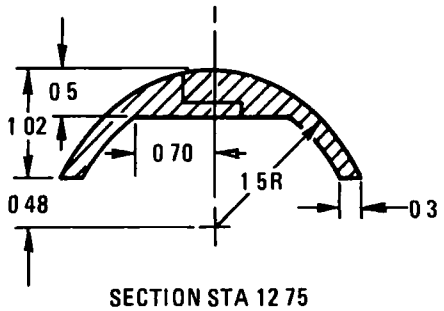

SECTION STA 12 75

266 635-80

Section Properties

Section	$\bar{x}$	$\bar{y}$	A	I_{min}	I_{max}
Sta 12.75	0	0.55	1.323	0.07643	0.71577

Stress

V (lb)	M_D (in-lb)	f_b (psi)	f_c (psi)	Safety Factor Ult (comp) 300K
396	990	7124	6087	2.5

Backbone

The critical section of the backbone is at Model Sta 15.50. The analysis is based on the backbone fabricated from from 18Ni-200 steel.

A sketch of the backbone and the sections analyzed are below.

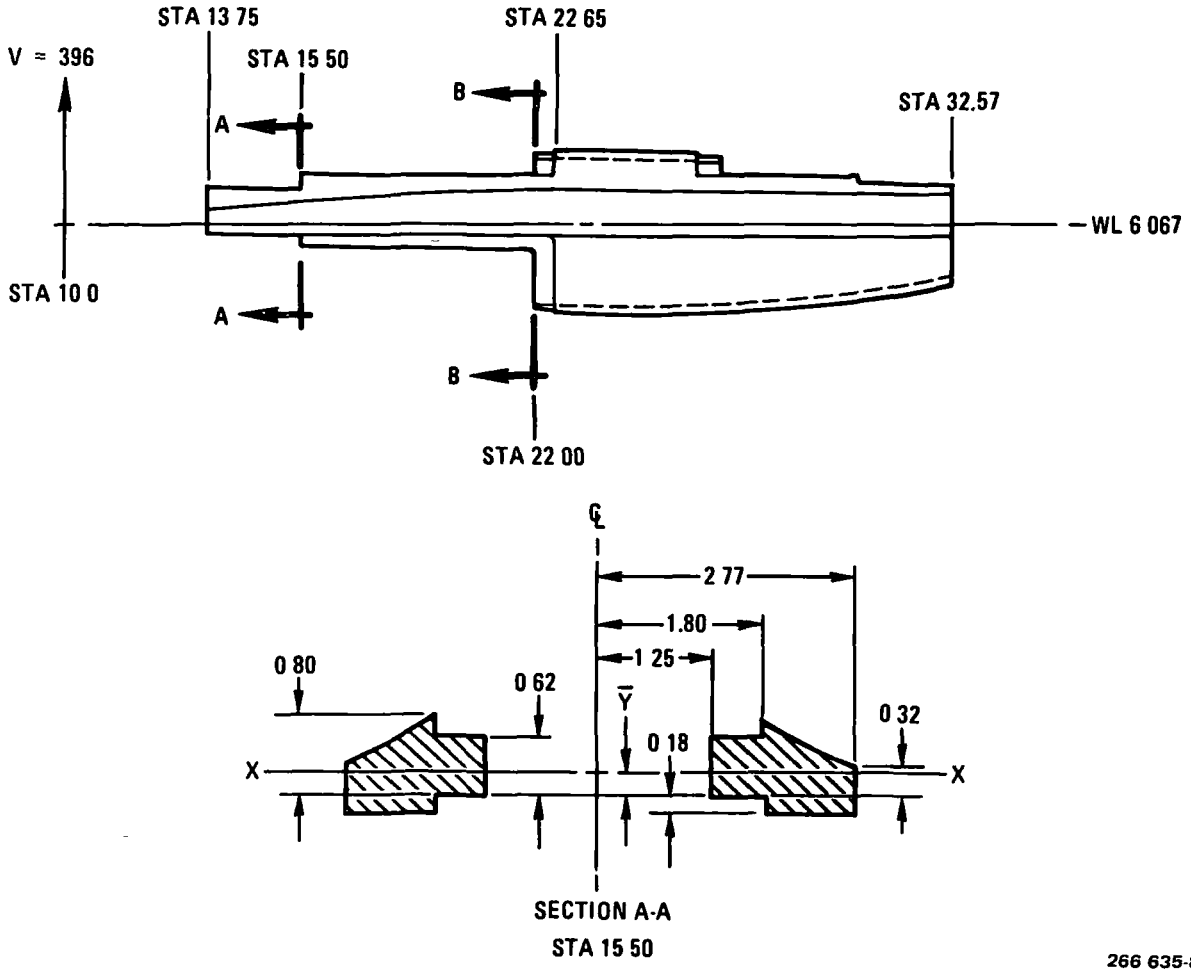

266 635-81

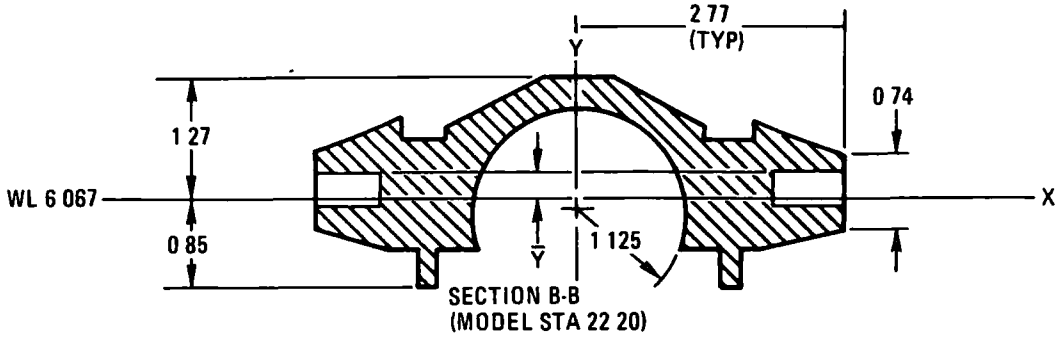

SECTION PROPERTIES

STA	AREA (IN^2)	$\bar{y}$ (IN)	$\bar{x}$ (IN)	I_{MIN} (IN^4)	I_{MAX} (IN^4)
15 50	2 021	0 22	0	0 09466	0 34828
22 20	3 768	0 28	0	0 78284	1 48658

BENDING STRESS

STA	V (LB)	M (IN-LB)	f_{bMAX} (PSI)	SAFETY FACTORS 300K YIELD	SAFETY FACTORS 78K YIELD
15 50	396	2178	9200	22 3	29 3
22 20	396	4752	6880	29 8	39 2

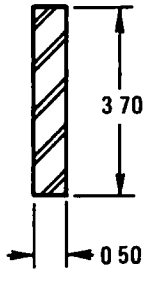

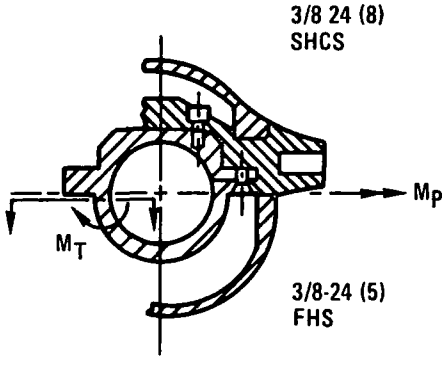

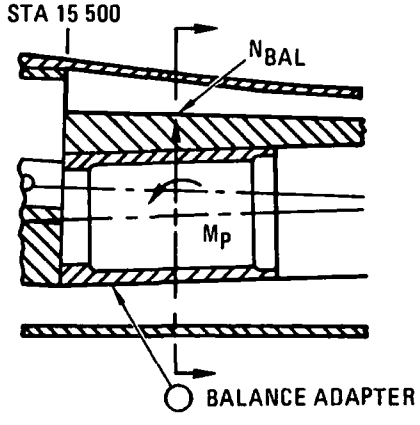

SECTION PROPERTIES

STA	A (IN^2)	$\bar{Y}$ (IN)	$\bar{X}$ (IN)	I (IN^4)	FASTENERS*	P_{ALLOW}(LB)
17 30	1 85	0	0	0 0385	3/8-24 NF	13,400

*NOTE FASTENERS ARE TO BE 18Ni-200 STEEL

LOADS/STRESSES				BAL MTG BLOCK		FASTENERS*	
				FACTOR OF SAFETY		FACTOR OF SAFETY (MIN)	
N_{BAL} (LB)	Mp (IN-LB)	M_T(IN-LB)	$f_{b(M_T)}$(PSI)	300K	78K	300K	78K
4000	10,000	10,726	69,652	2 87	3 87	3 2	4 3

266.635-82

Sting Stresses and Deflection

The sting material is 18Ni-200 maraging steel and is double tapered. The stress and deflection is determined throughout the length of the sting. The loads are applied at the balance moment center (BMC) at Model Sta 23.00.

The following sketch and Table five show the section properties, deflection, and safety factors. The critical section is at sting station 11.4.

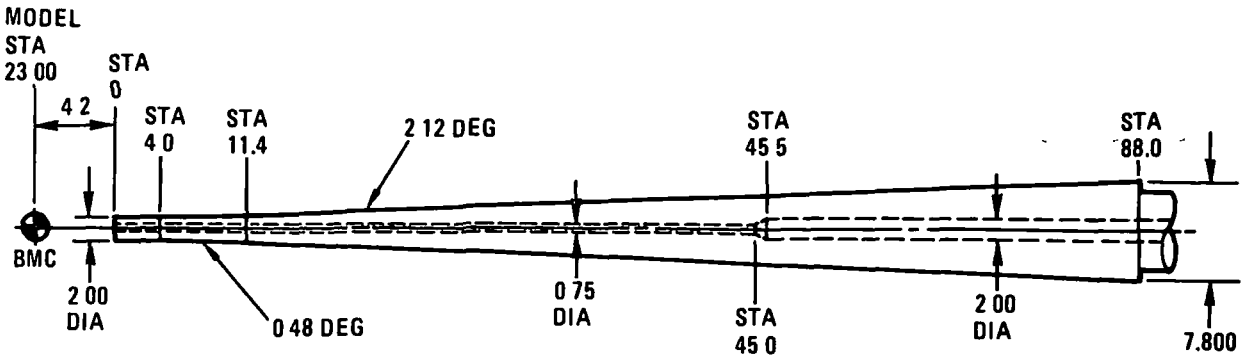

STING DETAIL – CWC

266 636-83

The sting is analyzed using the following combined loads.

Normal Force = 4000 lb

Pitching Moment = 8000 in-lb

Axial Force = 400 lb

Rolling Movement = 5500 in-lb

It is also analyzed in the side force plane using the same combination of loads.

Section Properties and Safety Factors

Sting Station	O.D. (in.)	I.D. (in.)	I (in^4)	M (in-lb)	f_b (psi)	SF_y 300K	SF_y 78K
0.0	2.0	--	--	--	*26,770	4.7	6.2
3.1	2.0	1.31	0.6318	37,200	58,880	3.4	4.5
4.0	2.0	0.75	0.7699	40,800	52,990	3.8	5.0
11.4	2.125	0.75	0.9854	70,400	75,910	2.7	3.5
45.5	4.65	2.00	22.184	206,800	21,670	9.4	12.4
85.8	7.64	2.00	166.70	368,300	8,450	24.2	31.9

*Shear out from socket analysis.

Deflection and Angularity

$E = 28.08 \times 10^6$ psi (300K)

$E = 29.43 \times 10^6$ psi (78K)

Sta (in.)	Deflection (in.) 300K	Deflection (in.) 78K	Angular (deg) 300K	Angular (deg) 78K
0.0	1.324	1.263	3.59	3.43
4.0	1.084	1.034	3.24	3.10
11.4	0.723	0.690	2.28	2.18
45.5	0.110	0.109	0.39	0.38
88.0	0.0	0.0	0.0	0.0

Sting Model Clearance

The end of the model is at Model Sta 38.57, which corresponds to Sting Sta 11.37. Considering a 1-degree deflection between Sting Sta 0.0 and the balance moment center, the maximum clearance between the model and the sting at Model Sta 38.57 is 0.318 in. for room temperature conditions and 0.313 in. for cryogenic conditions.

For further information see Reference 4.

Sting Divergence

Sting divergence was determined for a normal load of 4000 lb with a pitching moment of 8000 in-lb. Two balance rotational angles with respect to the sting were investigated. They were 67 minutes and 2 degrees. Since the sting is symmetrical the side plane will give the same results. Equations used for computing the sting divergence parameter were taken from Reference 35.

The flexibility of the stub sting is unknown, and therefore not considered in the sting divergence calculation. With a minor diameter of 7.800 inches, however, it will not influence the sting deflection significantly.

The results of the computation are as follows. Note that a static divergence parameter (SDP) of 3 or greater indicates that there is non-divergence.

CWC (78K)

Force= 4000.0	Moment= 8000.0		
Ds= 3.427000	Dsf= 3.023060	Dsm= .403940	2 Degree Bal. Rotation
Dbf= 1.000000	Dbm= 1.000000		
Kn= .001006	Km= .000175		
Dcna= .019835	Dcnw= .296750		
Dcma= .117062	Dcmw=-.030148		
SDP= 6.762804			

CWC (78K)

Force= 4000.0	Moment= 8000.0		
Ds= 3.427000	Dsf= 3.023060	Dsm= .403940	67 Minute Bal. Rotation
Dbf= .558335	Dbm= .558335		
Kn= .000895	Km= .000120		
Dcna= .019835	Dcnw= .296750		
Dcma= .117062	Dcmw=-.030148		
SDP= 8.201396			

CWC (RT)

Force= 4000.0	Moment= 8000.0		
Ds= 3.592000	Dsf= 3.168611	Dsm= .423389	2 Degree Bal. Rotation
Dbf= 1.000000	Dbm= 1.000000		
Kn= .001042	Km= .000178		
Dcna= .019835	Dcnw= .296750		
Dcma= .117062	Dcmw=-.030148		
SDP= 6.572048			

CWC (RT)

Force= 4000.0	Moment= 8000.0		
Ds= 3.592000	Dsf= 3.168611	Dsm= .423389	67 Minute Bal. Rotation
Dbf= .558335	Dbm= .558335		
Kn= .000932	Km= .000123		
Dcna= .019835	Dcnw= .296750		
Dcma= .117062	Dcmw=-.030148		
SDP= 7.922525			

10.3 STRUCTURAL ANALYSIS – F-111 TACT

The wing panels, wing attachment, vertical and horizontal tails, tail attachment, and sting support system fuselage attachments, are analyzed. 18Ni-200 maraging steel is the primary structural material.

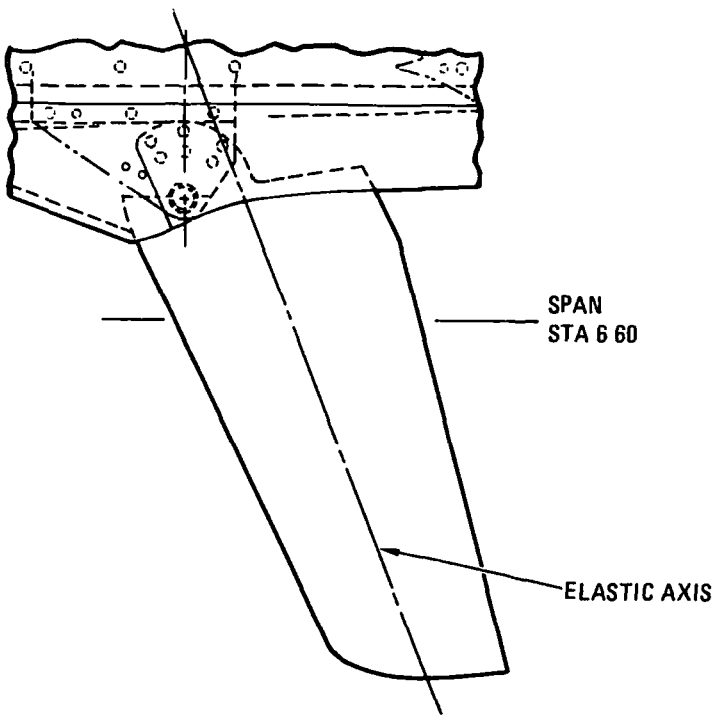

26-DEG WING SWEEP POSITION

266 635-96

Wing Panel

The wings panels are made from 18Ni-200 maraging steel. Each panel is essentially a two piece construction, split at the 60% chord line. The wing section at Sta 6.60 was anlyzed assuming that the first 60% of the panel takes all the loads. No further sections were analyzed as the wing panel appeared to be structurally adequate. Sketches of the wing planform end section follow.

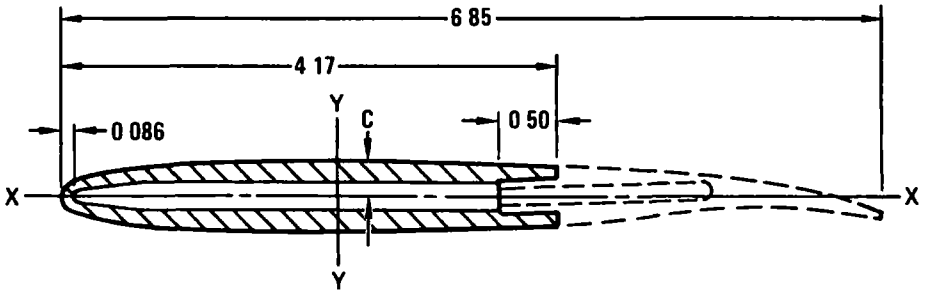

Λ = 16 DEG

WING SECTION STA 6 600

266 635-84

Section Properties

A	= 1.388 in^2	I_{min}	= 0.0578 in^4
C	= 0.320 in.	I_{max}	= 1.3268 in^4
θ	= -0.123 deg	$C_{T/K}$	= 2.58/in^3

Bending and Shear Stresses

V	= 950 lb	f_b	= 23,760 psi
M	= 4300 in-lb	f_s	= 2,580 psi (small)
T	= -1000 lb		

Safety Factor

$$SF_{yield} = \frac{270}{23.76} = 11.3 \text{ (78K)}$$

$$SF_{yield} = \frac{205}{23.76} = 8.6 \text{ (300K)}$$

Wing/Fuselage Attachment

Section through Pivot (S.S.3.515 at 16 deg Λ)

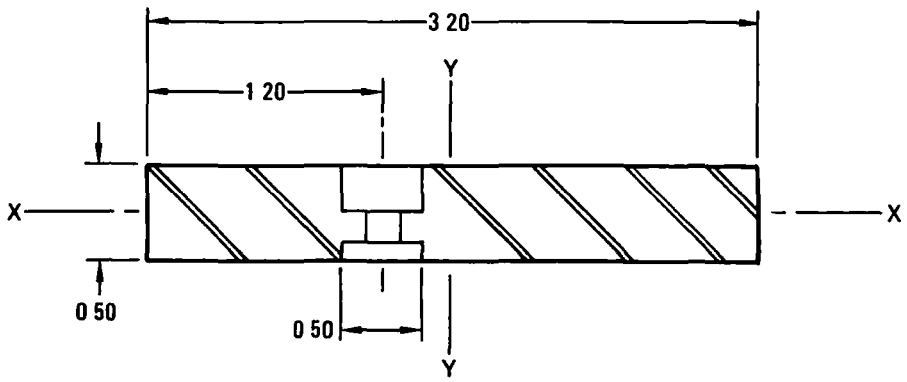

266 635-85

Section Properties

$A = 1.360 \text{ in}^2$ $I_{min} = 0.028251 \text{ in}^4$

$C = 0.25 \text{ in.}$ $I_{max} = 1.37542 \text{ in}^4$

Bending and Shear Stresses

$V = 1100 \text{ lb}$ $f_b = 60,170 \text{ psi}$

$M = 6800 \text{ in-lb}$ $f_s = 5,340 \text{ psi (small)}$

$T = -1300 \text{ lb}$

Safety Factor

$$SF_{yield} = \frac{270}{60.17} = 4.4 \text{ (78K)}$$

$$SF_{yield} = \frac{205}{60.17} = 3.4 \text{ (300K)}$$

Pivot Screw

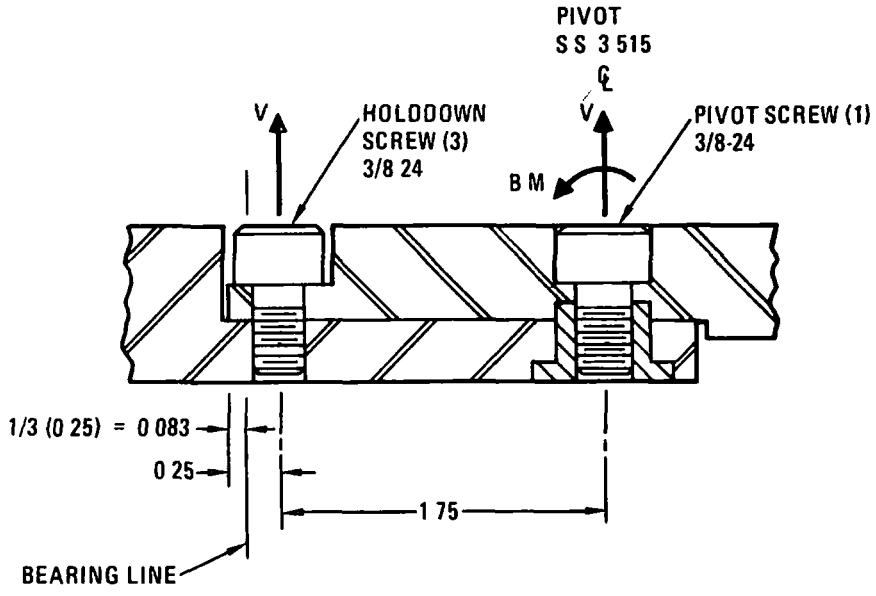

266 635-86

Refer the sketch above, assume bearing line as shown.

$\rho_1 = (2/3)\ (0.25) = 0.167$ in. $\quad n = 3$

$\rho_2 = 0.167 + 1.75 = 1.917$ in. $\quad n = 1$

$V = 1100$ lb

$BM = 6800$ in-lb

$T = -1300$ in-lb

$M = [(6800)^2 + (1300)^2]^{1/2} = 6923$ in-lb

Load on screw (tension):

$$P_t = \frac{V}{n} + \frac{M\rho}{\Sigma n \rho_1^2}$$

$$P_t = \frac{1100}{4} + \frac{(6932)\ (1.917)}{3(0.167)^2 + (1.917)^2} = 275 + 3585$$

$P_t = 3860$ lb

For a 3/8 - 24 screw made from 18Ni-200.

$P_{t_{a_y}}$ = 22,270 lb

$P_{t_{a_u}}$ = 23,095 lb

} 78K

$P_{t_{a_y}}$ = 16,909 lb

$P_{t_{a_u}}$ = 17,321 lb

} 300K

$\therefore SF_y = \frac{23,095}{3860} = 5.9$ (78K)

$\therefore SF_y = \frac{17,321}{3860} = 4.4$ (300K)

Since screws are made from the same material as the wing and body there will be no buildup of stresses due to contraction.

Wing Plate (Sta 24.375)

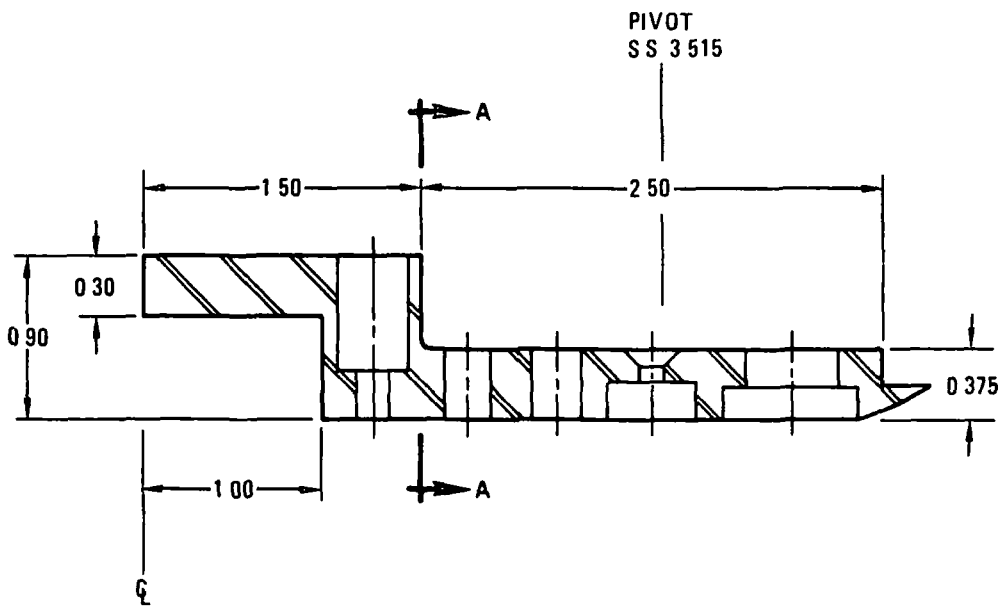

266 635 87

Bending and shear stresses on the section shown above were not critical. Bending about Section A-A is, however, more critical.

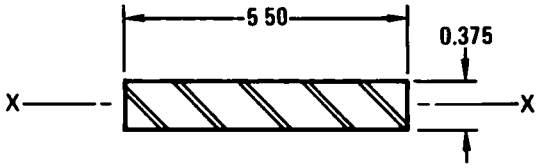

SECTION A-A

266 635-88

$$I_x = \frac{bh^3}{12}$$

$$= \frac{(5.5)\ (0.375)^3}{12} = 0.02417 \text{ in}^2$$

At Pivot

$V = 1100$ lb

$BM = 6800$ in-lb

$T = 1300$ in-lb

$M = 6800 + 1100\ (3.515 - 1.50) = 6800 + 2216$

$= 9016$ in-lb

Stresses

$$f_b = \frac{Mc}{I} = \frac{(9016)\ (0.188)}{0.02417} = 77{,}128 \text{ psi}$$

$$f_s = \frac{[3 + 1.8\ (\frac{h}{b})]}{(5.5)\ (0.375)^2}\ (1300) = 5250 \text{ psi (small)}$$

Safety Factor

$$SF_y = \frac{F_{ty}}{f_b} = \frac{270}{70.13} = 3.8\ (78K)$$

$$SF_y = \frac{F_{ty}}{f_b} = \frac{205}{70.13} = 2.9\ (300K)$$

Vertical Tail

The following sketches show the planform of the vertical tail and the critical section. The analysis is based on the tail being made from 18Ni-200 maraging steel.

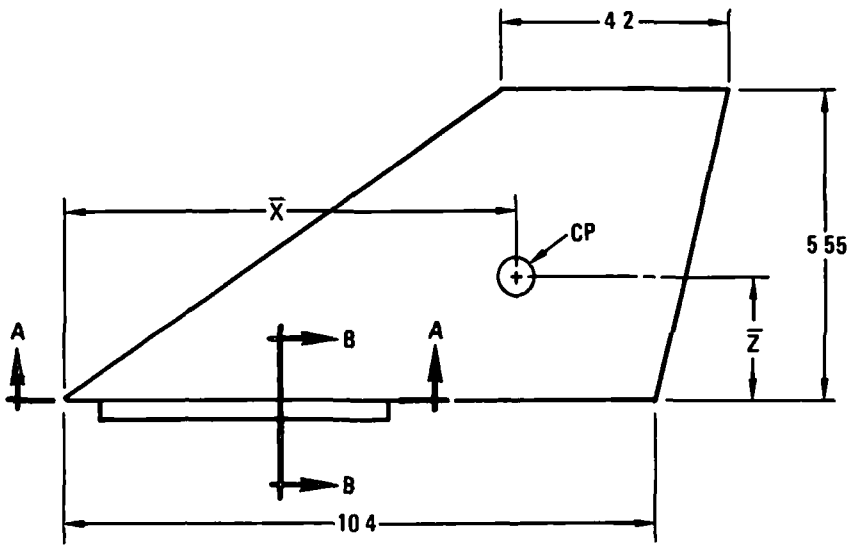

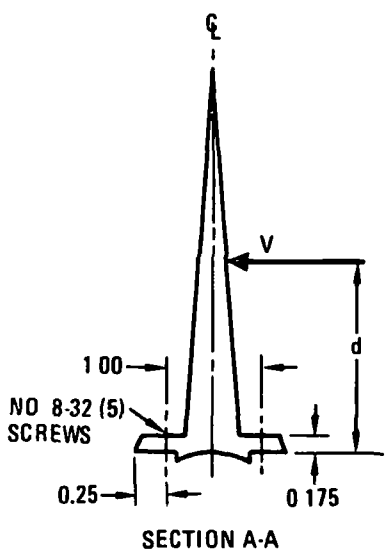

SECTION A-A

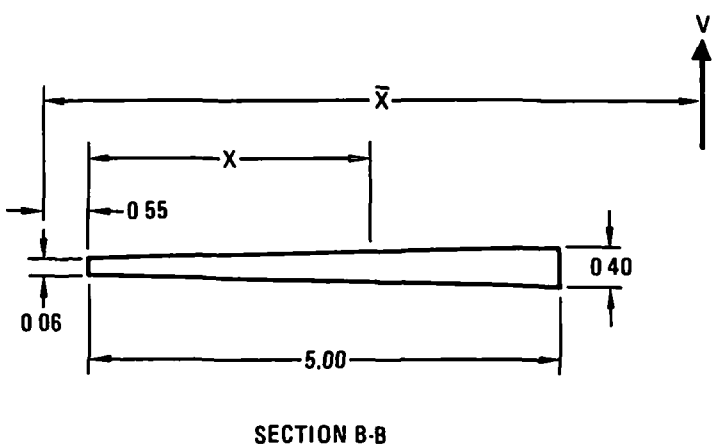

SECTION B-B

266 635-89

$V = 270$ lb $\qquad A = 0.279\ ft^2 = 40.2\ in^2$

$\bar{x} = 718$ in. $\qquad \bar{z} = 2.38$ in.

Section B-B

Properties

$A = 1.15\ in^2 \qquad I_x = 0.007839$

$x = 3.12$ in $\qquad I_y = 1.4595$

$c = 0.2$ in

Loads

$M = \bar{z}\,V = (2.38)\,(270) = 643$ in-lb

$T = [7.18 - (x + 55)]\,V$

$= 3.51\,(270) = 948$ in-lb

Stresses

$$f_b = \frac{Mc}{I} = \frac{(643)\,(.2)}{0.007839} = 16{,}405 \text{ psi}$$

$$f_s = \frac{[3 + 1.8\,(\frac{h}{b})]}{bh^2}\,T = 11{,}067 \text{ psi}$$

$$SF_y = \frac{1}{\left[\left(\frac{f_b}{F_{t_y}}\right)^2 + \left(\frac{f_s}{F_s}\right)^2\right]^{1/2}}$$

$$SF_y = \frac{1}{\left[\left(\frac{16.4}{205}\right)^2 + \left(\frac{11.07}{126}\right)^2\right]^{1/2}} = 9.3\ (78K)$$

$$SF_y = \frac{1}{\left[\left(\frac{16.4}{205}\right)^2 + \left(\frac{11.07}{126}\right)^2\right]^{1/2}} = 8.4\ (300K)$$

Attachment Screws

There are ten #8-32 screws used to attach the vertical stabilizer to the body. They are made from A286 material. Referring to section A-A.

$$P_{t_{(300K)}} = \frac{M \rho}{\Sigma n \rho^2} = \frac{d V \rho}{\Sigma n \rho^2}$$

where

$d = 2.53$

$\rho_1 = 2/3\ (0.25) = 0.167$

$\rho_2 = 1.167$

$n = 5$

$$P_{ta_{(300K)}} = \frac{(2.53)\ (270)\ (1.167)}{(5)\ (0.167^2 + 1.167^2)} = \frac{797}{6.949} = 115 \text{ lb}$$

Load due to thermal contraction:

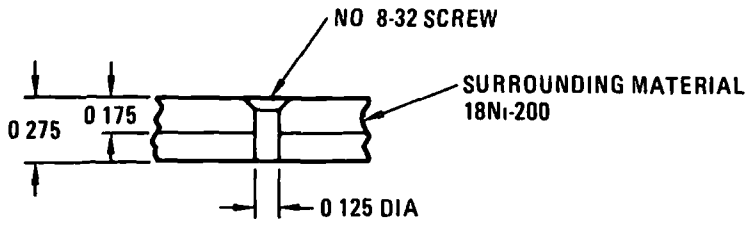

266 635-90

$$\varepsilon = \Delta \ell_{screw} - \Delta \ell_{material} = (\alpha^t_{scr} - \alpha^t_{mat})\ (\ell)\ (\Delta t)^{\dagger}$$

$$\varepsilon = (6.8 \times 10^{-6} - 3.4 \times 10^{-6})\ (0.275)\ (-390 \text{ deg F}) = 364.7 \times 10^{-6} \text{ in}$$

$$P_t = \frac{\varepsilon A E}{L} = \frac{(364 \times 10^{-6})\ (0.0122)\ (29.43 \times 10^{-6})}{0.275}$$

$P_t = 476$ lb Tension in screw due to thermal stresses

†For thermal contraction coefficient values see Figure 7-1.

$$P_{t_{c(78K)}} = 476 + 115 = 591 \text{ lb}$$

$$\therefore SF_y = \frac{P_{TA}}{P_{t_{c78K)}}} = \frac{1488}{591} = 2.5 \text{ (78K)}$$

$$\therefore SF_y = \frac{P_{TA}}{P_{t_{c(300K)}}} = \frac{1240}{115} = 10.7 \text{ (300K)}$$

Horizontal Tail

A planform of the horizontal tail is shown in the sketch below. The tail is made from 18Ni-200 maraging steel with A286 steel screws attaching it to the body. The brackets are also made from 18Ni-200 steel.

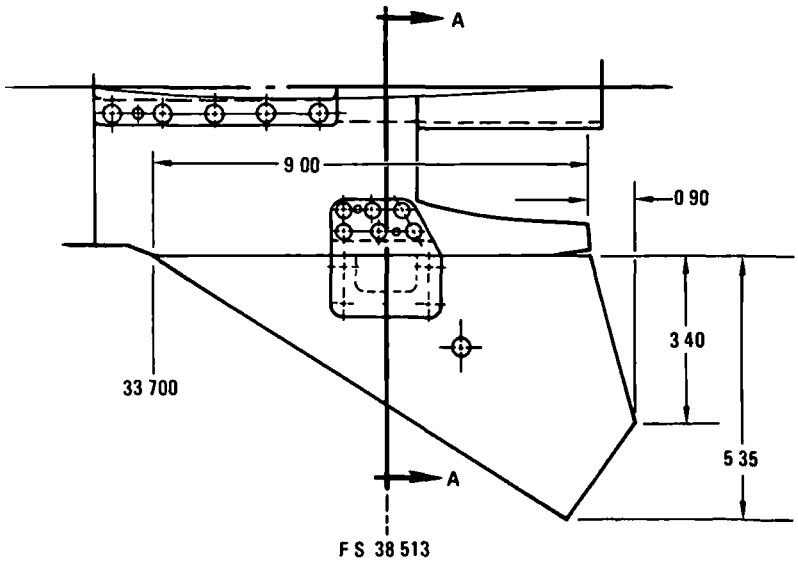

A = 27 3 IN

0 DEG INCIDENCE LOADS

V = 350 LB
M = 750 IN LB } SEE FIG 5 18
T = 580 IN -LB

-10, -20 DEG INCIDENCE LOADS

V = 280 LB
M = 700 IN LB } SEE FIG 5 18
T = 460 IN LB

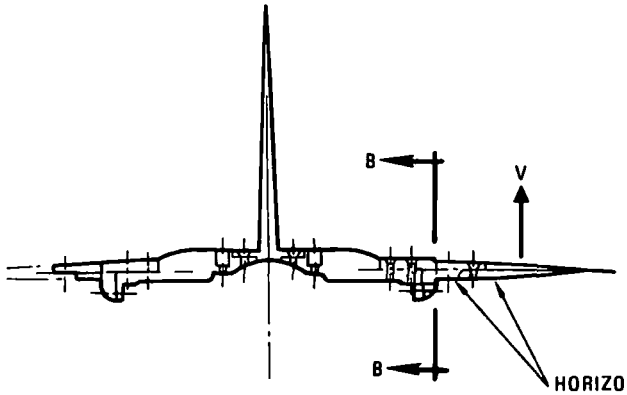

SECTION A A
(ROTATED 90 DEGREES)

HORIZONTAL TAIL & BRKT'S
INCIDENCE ANGLES, ± 5, -10, -20 DEG

266 635 91

Brackets

Brackets for 0, -10, and -20 degrees incidence will be analyzed; 0 and 20 degrees are shown below.

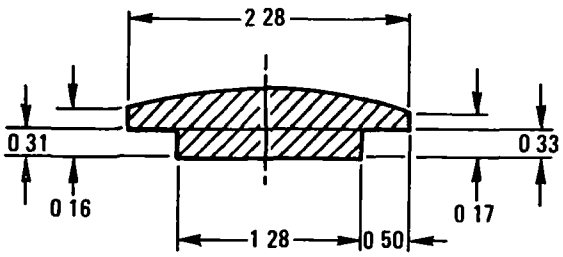

SECTION B-B (0 DEG BRACKET)

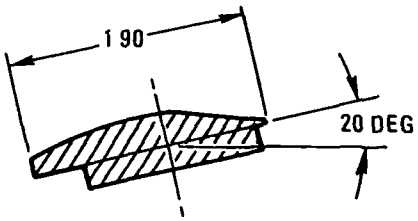

SECTION B-B (20 DEG BRACKET)

266 635-92

Section Properties

Incidence (deg)	Area (in^2)	I_x (in^4)	I_y (in^4)	J (in^4)	C (in.)	C_T (in.)
0	0.603	0.00551	0.1887	0.1942	0.202	1.14
-10	0.504	0.00467	0.1068	0.1115	0.173	0.99
-20	0.406	0.00287	0.0912	0.0401	0.132	0.89

Stresses and Safety Factors

Incidence (deg)	V (lb)	f_b (psi)	f_s (psi)	AF (RT)	AF (78K)
0	350	27,490	3,404	7.4	9.8
-10	280	25,930	4,084	7.9	10.4
-20	280	32,190	10,210	6.3	8.3

Attachment Screws

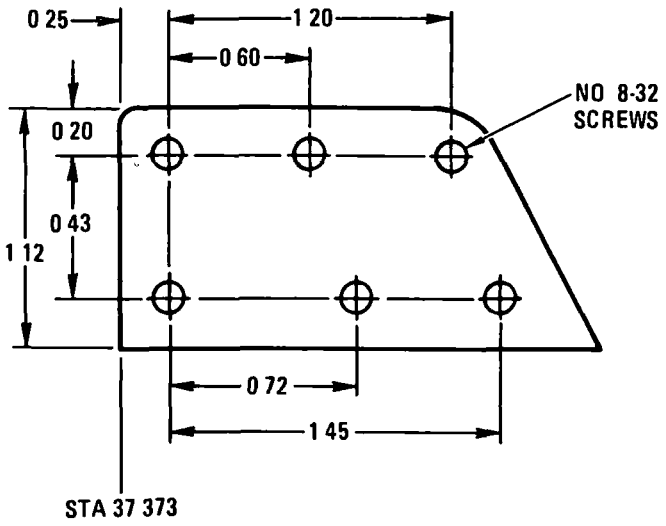

266 635 93

$V = 350$ lb
$M = 750$ in-lb
$T = 580$ in-lb
} See Figure 5-18

$\rho = 2/3\ (0.20) = 0.13$ $\quad n = 6$

$d = 2/3\ (0.25) = 0.16$

$\Sigma n\rho^2 = 1.003$ $\quad \Sigma nd^2 = 5.845$

$$P_{t_{c(300K)}} = \frac{V}{n} + \frac{M\rho_2}{\Sigma n\ell^2} + \frac{Td_5}{\Sigma nd^2} = 58 + 418 + 204 = 682 \text{ lb}$$

A proof test must be performed on the horizontal tail to prove its worthiness.

Screws made from A286 steel show a low safety factor especially under cryogenic conditions where the materials used have different thermal expansion ratios. Use of 18Ni-200 screws provides a higher allowable stress, and also eliminates thermal stresses.

$$\frac{(18Ni)_{yield}}{A286_{yield}} = \frac{205 \text{ ksi}}{100 \text{ ksi}} = 2.05 \text{ (300K)}$$

$$\frac{270}{120} = 2.25 \text{ (78K)}$$

$$P_{T_A} = 1488 \times 2.25 = 3348$$

$$SF_x = \frac{3348}{682} = \underline{4.9} \text{ (78K)}$$

$$P_{T_A} = 1240 \times 2.05 = 2542$$

$$SF_y = \frac{2542}{682} = \underline{3.7} \text{ (300K)}$$

Loads Due to Thermal Contraction:

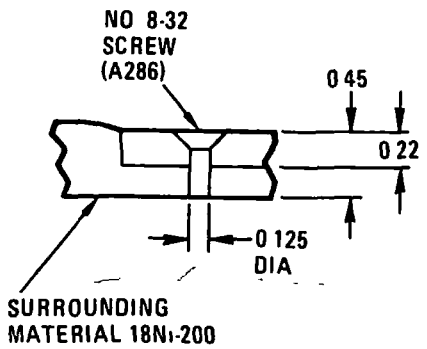

266 635-94

$$\varepsilon = \Delta\ell_{screw} - \Delta\ell_{material} = (\alpha^t_{scr} - \alpha^t_{mat})(\ell)(\Delta T)$$

$$\varepsilon = (6.8 \times 10^{-6} - 3.4 \times 10^{-6})(0.45)(-390 \text{ deg F}) = 596.7 \times 10^{-6} \text{ in.}$$

$$P_t = \frac{\Delta AE}{L} = \frac{(596.7 \times 10^{-6})(0.0122)(29.43 \times 10^6)}{0.45}$$

P_t = 476 lb Tension in screw due to thermal stress

$$P_{t_{c_{(78K)}}} = 682 + 476 = 1158 \text{ lb}$$

$$\therefore \quad SF_y = \frac{P_{T_A}}{P_t(78K)} = \frac{1488}{1158} = 1.2\ (78K)$$

$$SF_y = \frac{P_{T_A}}{P_t(300K)} = \frac{1240}{682} = 1.8\ (300K)$$

These values are conservative for there are additional screws attaching the plate to the side of the body that were not taken into account.

F-111 STING STRESSES AND DEFLECTION

The sting is fabricated from 18Ni-200 maraging steel. The configuration is shown in the sketch below.

The stress and deflection are determined for the entire length of the sting. Loads are applied at the balance moment center (fuselage station 28.54).

Sting deflection, angularity, divergence, and model/sting clearance were determined.

A sketch of the sting is shown below and the following tables show the section properties, deflections, and safety factors. The critical section is at SS 10.4.

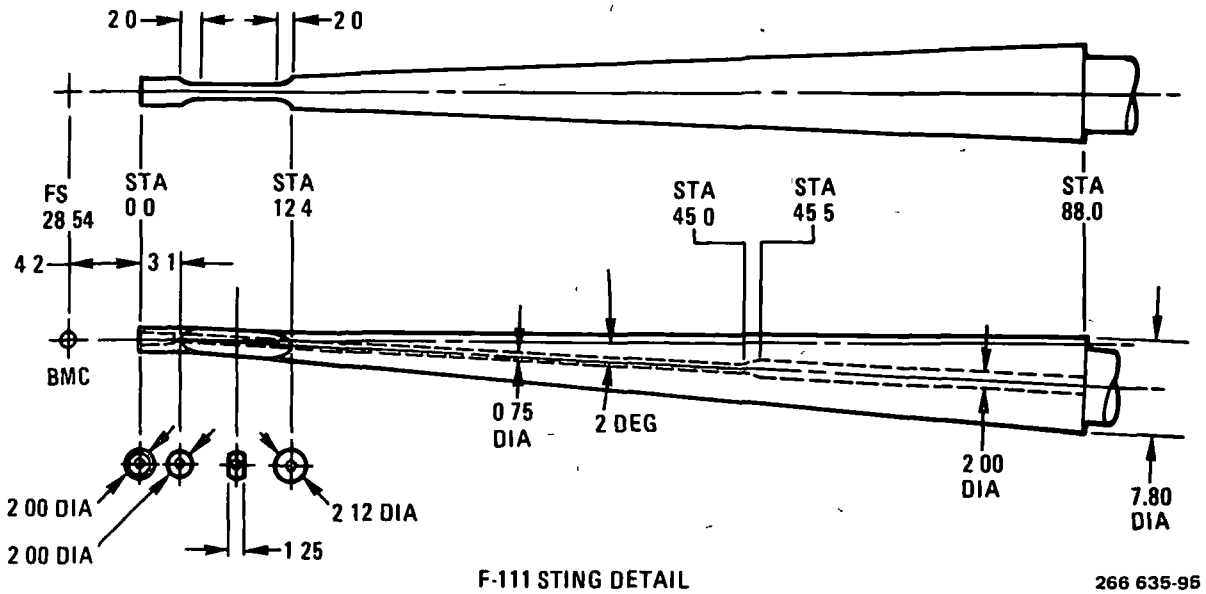

F-111 STING DETAIL

266 635-95

The sting was analyzed for the following load conditions under room temperature and cryogenic temperatures.

Normal Force = 4000 lb
Pitch Moment = 8000 in-lb
Axial Force = 400 lb
Rolling Moment = 5500 in-lb
} In NF Plane

Side Force = 2000 lb
Yawing Moment = 4000 in-lb
Axial Force = 400 lb
Rolling Moment = 5500 in-lb
} In SF Plane

The sting loads are based on a typical 2.00-in. diameter NTF balance envelope.

Normal Force = 4000 lb
Pitching Moment = 8,000 in-lb
Axial Force = 400 lb
Rolling Moment = 5500 in-lb

Side Force = 4000 lb
Yawing Moment = 8,000 in-lb

Section Properties and Safety Factors

Sting Station	OD (in.)	ID (in.)	I_x (in^4)	M (in-lb)	f_b (psi)	SF_y 300K	SF_y 78K
0.0	2.0	—	—	—	26,770*	4.7	6.2
3.1	2.0	1.31	0.6318	37,200	58,880	3.4	4.5
5.1	2.022	0.75	0.6911	45,200	66,122	3.1	4.0
10.4	2.096	0.75	0.7829	66,400	89,190	2.3	3.2
45.5	4.58	2.00	22.184	206,800	21,673	9.4	12.4
86.9	7.72	2.00	173.43	372,500	8,300	24.7	32.5

*Shear out from socket analysis.

Deflection and Angularity

$E = 28.08 \times 10^6$ psi (300K)
$E = 29.40 \times 10^6$ psi (78K)

Sta. (in.)	Deflection (in.) 300K	Deflection (in.) 78K	Angularity (deg) 300K	Angularity (deg) 78K
0.0	1.433	1.367	3.99	3.81
3.1	1.223	1.167	3.73	3.56
5.1	1.097	1.046	3.51	3.34
10.4	0.763	0.771	2.52	2.46
45.5	0.112	0.107	0.40	0.39
88.0	0	0	0	0

Sting-Model Clearance

The end of the model is at fuselage station 43.04, which corresponds to sting station 10.40. Considering a 1-degree deflection between S.S. 0.0 and the balance moment center, the minimum required clearance between the model and the sting at F.S. 43.04 is 0.289 in. (300K), and 0.284 in. (78K).

In the side force plane the required clearance is 0.275 in. (300K), and 0.271 in. (78K). The clearances are based upon the following load condition: side force 2000 lb and yawing moment of 4000 in-lb. For further information see Reference 4.

Sting Divergence

Sting Divergence was determined for a normal force load of 4000 lb and a pitching moment of 8000 in-lb. It was also determined for a side load of 2000 lb with a yawing moment of 4000 in-lb. Two balance rotation angles with respect to the sting were investigated. They were 67 minutes and 2 degrees. Equations used for computing the sting divergence parameter were taken from Reference 35.

The results of the computation are given on the following pages. A static divergence parameter (SDP) of 3 or greater indicates that there is non-divergence.

F-111 (300K)

Force= 4000.0	Moment= 8000.0		
Ds= 3.988000	Dsf= 3.517934	Dsm= .470066	2-degree bal. rotation
Dbf= 1.000000	Dbm= 1.000000		
Kn= .001129	Km= .000184		
Dcna= .019835	Dcnw= .296750		
Dcma= .117062	Dcmw=-.030148		
SDP= 6.155355			

F-111 (300K)

Force= 4000.0	Moment= 8000.0		
Ds= 3.988000	Dsf= 3.517934	Dsm= .470066	68-minute bal. rotation
Dbf= .558335	Dbm= .558335		
Kn= .001019	Km= .000129		
Dcna= .019835	Dcnw= .296750		
Dcma= .117062	Dcmw=-.030148		
SDP= 7.324775			

F-111 (78K)

```
Force= 4000.0        Moment= 3000.0
Ds= 3.305000         Dsf= 3.356505        Dsm= .448495
Dbf= 1.000000        Dbm= 1.000000
Kn= .001089          Km= .000181
Dcna= .019835        Dcnw= .296750
Dcma= .117062        Dcmw=-.030148
SDP= 6.341153
```

2-degree bal. rotation

F-111 (78K)

```
Force= 4000.0        Moment= 8000.0
Ds= 3.805000         Dsf= 3.356505        Dsm= .448495
Dbf= .558335         Dbm= .558335
Kn= .000979          Km= .000126
Dcna= .019835        Dcnw= .296750
Dcma= .117062        Dcmw=-.030148
SDP= 7.589393
```

67-minute bal. rotation

F-111 (300K)

```
Force= 2000.0        Moment= 4000.0
Ds= 2.915000         Dsf= 2.571409        Dsm= .343591
Dbf= 1.000000        Dbm= 1.000000
Kn= .001736          Km= .000336
Dcna= .019835        Dcnw= .296750
Dcma= .058531        Dcmw=-.030148
SDP= 4.807066
```

2-degree bal. rotation

F-111 (300K)

```
Force= 2000.0        Moment= 4000.0
Ds= 2.915000         Dsf= 2.571409        Dsm= .343591
Dbf= .558335         Dbm= .558335
Kn= .001565          Km= .000225
Dcna= .019835        Dcnw= .296750
Dcma= .058531        Dcmw=-.030148
SDP= 5.674454
```

67-minute bal. rotation

F-111 (78K)

Force= 2000.0	Moment= 4000.0		
Ds= 2.781000	Dsf= 2.453204	Dsm= .327796	2-degree bal. rotation
Dbf= 1.000000	Dbm= 1.000000		
Kn= .001727	Km= .000332		
Dcna= .019835	Dcnw= .296750		
Dcma= .058531	Dcmw=-.030148		
SDP= 4.956041			

F-111 (78K)

Force= 2000.0	Moment= 4000.0		
Ds= 2.781000	Dsf= 2.453204	Dsm= .327796	
Dbf= .558335	Dbm= .558335		67-minute bal. rotation
Kn= .001506	Km= .000222		
Dcna= .019835	Dcnw= .296750		
Dcma= .058531	Dcmw=-.030148		
SDP= 5.883209			

10.4 ACHIEVED SAFETY FACTORS

Tables 8-1 and 8-2 summarize the critical safety factors on the F-111 and CWC models. In cases where the safety factor falls below 4.0 on ultimate and 3.0 on yield, a proof test should be conducted.

10.5 PROOF TESTING AND DYNAMIC ANALYSIS

Sections of the model that do not meet the facility safety factor requirements, or in which new processes are used and structural integrity is in question, will be prime candidates for both static and dynamic proof load testing. Such tests will be conducted under conditions that closely simulate the NTF environment.

As indicated in Section 9.6, flutter of the rigid model does not appear to be a problem; fatigue however, in the case of structural joints and/or new processes must be considered. Possible embrittlement of the structure at cryogenic temperatures suggests the need for fatigue testing of critical parts in a vibration laboratory.

Parts identified as requiring proof load/fatigue tests are:

CWC

- Wing panel
- Elevon attachment
- Aileron attachment
- Leading edge flap attachment
- Forward fuselage joint
- Sting

F-111 TACT

- Wing/fuselage attachment (pivot screw)
- Horizontal tail attachment
- Sting

SECTION 11

ESTIMATED MODEL COSTS AND SCHEDULES

In this section, the costs of a conventional force/pressure model is compared with one designed for the National Transonic Facility (NTF). The aeroelastic wing is considered to be nonconventional and is not included in the analysis.

To obtain the most realistic estimates, a complete set of predesign drawings and a work statement were sent to reliable sources having experience in the fabrication of models for NTF. The work statement included pertinent sections of the NASA Handbook (Reference 1). These estimates were then compared with those from the Engineering Department.

The results, shown in Table 11-1, are an average of all the inputs. As can be seen, the conventional model is given a factor of 10, and the equivalent model designed for NTF 21; a ratio of 2.1 to 1. Breaking these numbers down, it can be seen that engineering analysis and design increases by a ratio of 6 to 3.5, and manufacturing by 12 to 5.5.

Further experience with NTF models of this type built primarily of 18Ni-200 is expected to yield a reduction in cost, particularly in the area of manufacturing. We do not expect a reduction in the task of engineering analysis. As for the necessity of proof-of-concept tests, the feasibility of using new materials and processes in a cryogenic environment, under extremely high loads, must be demonstrated satisfactorily. Early models are expected to need extensive testing of this type to ensure the structural integrity of the model. Later models, however, should benefit from this research, and the need for proof-of-concept testing should diminish. Proof loading of critical model parts will continue. In summary, whereas today the ratio of cost for an NTF/conventional model is 2.1 to 1, future models may well decrease to 1.5 to 1 (inflation is not considered). The conventional model at a factor of 1 is estimated at 9000 manhours and a schedule of 6 to 8 months. In comparison, the NTF model will require a minimum of 12 months. The difference can be attributed to increased engineering, planned review periods, quality control, and proof-of-concept tests.

Table 11-1. Cost Comparison of Conventional Pressure Model and NTF Model

	Manufacturing	Engineering	Weighted Cost Ratio		Equivalent Manhours	
			Conventional	NTF	Conventional	NTF
Analysis		X				
Aero/Thermo/Loads			0.75	1	675	900
Stiffness						
Design-stress analysis		X				
Configuration definition/liaison			2.75	5	2,475	4,500
Manufacturing	X					
Raw material						
Machining (milling)			5.50	12	4,950	10,800
Surface finish						
Tolerances						
Pressure tube routing						
Thermal cycling						
Fasteners/filler materials						
Structural testing	X	X				
Environmental testing			0	1	0	900
Instrumentation	X	X				
Pressure measurements			0.50	1	450	900
Buffet-thermocouples						
On-line loads monitoring						
Quality control		X				
Raw material-documentation			0.50	1	450	900
Model inspection						
Raw material			10,000	20,000		
Total			10	21	9,000	18,900

SECTION 12

CONCLUSIONS

Full scale Reynolds number testing in the NTF is an established goal, and in this study we show that goal to be achieved. It must be clearly understood, however, that such an achievement is very configuration sensitive and that each case should be treated separately and no assumption made that full scale Reynolds is always achievable.

Results of this study show that 1/15-scale CWC and 1/20-scale F-111 TACT combined force and pressure models with internal flow can achieve full-scale Reynolds number, with some limiting conditions at sea level combined with high α.

Advantage must be taken of relaxed safety factors recognizing that additional engineering is required. (The standard of 4 × ultimate and 3 × yield can be reduced to 3 × ultimate and 2 × yield.)

The facility drive system should not be endangered by the model, but neither should the model design be so conservative that the full capability of the facility be unusable.

Critical areas of the model must be identified and monitored for strain (see Figure 12-1). When critical strain levels are reached, model altitude should automatically be restricted.

For a given dynamic pressure, testing at 300K is more critical than 78K – material properties increase as temperature decreases.

Models will tend to be sting/balance limited. Control surfaces may also be Reynolds number limited.

Surface finish of 8 to 16 microinches was felt to be needed; for the study configurations, 20 microinches is acceptable. In addition to requiring a good finish, other roughness due to gaps, mismatch, and screw protuberances must be minimized.

Spanwise joints if used must be designed to eliminate unporting. The joint should be checked under load, and pins used for positive relocation.

An environmentally controlled instrumentation bay in the forward fuselage is feasible.

Thermal gradients across the model increase with α and Mach number.

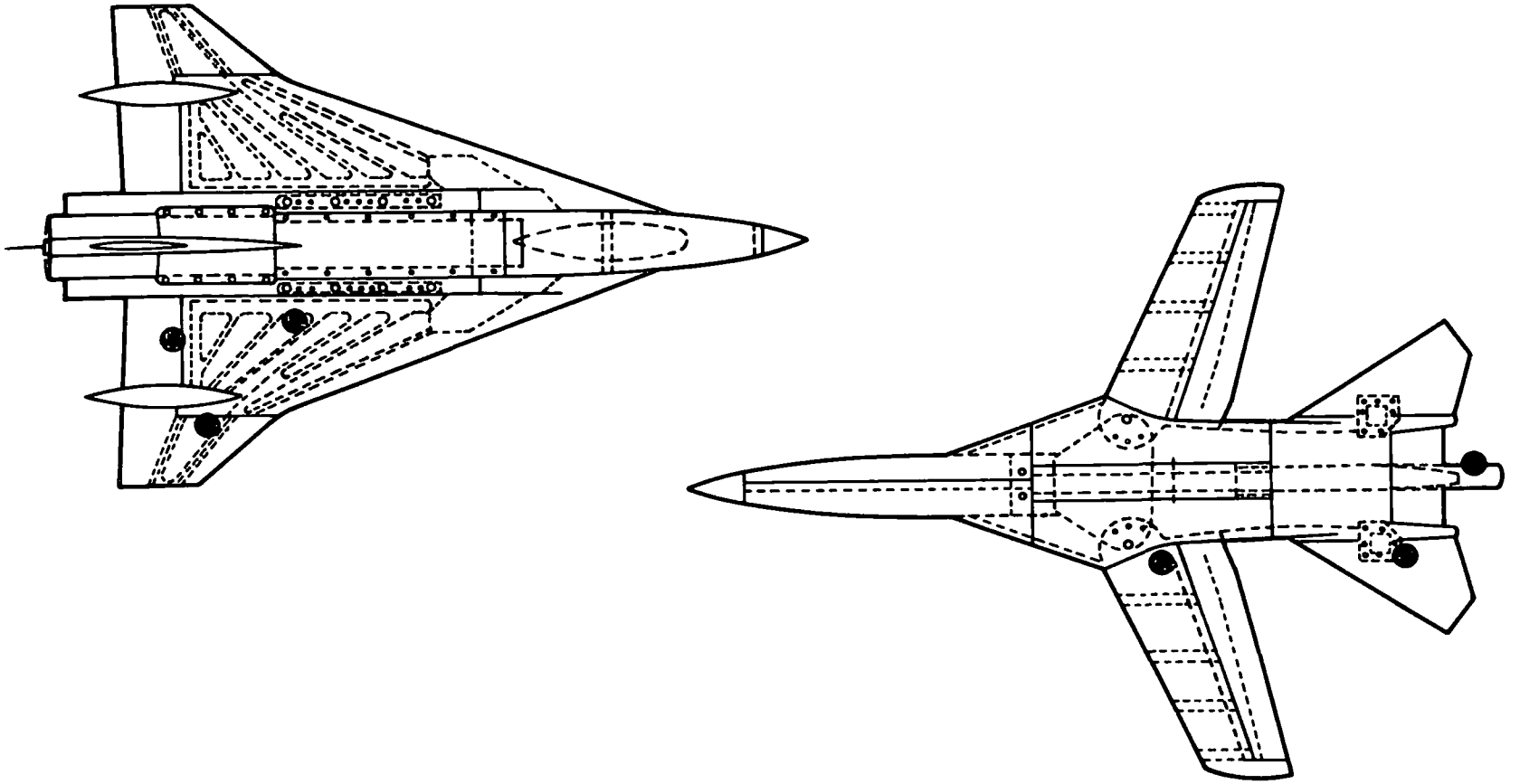

266 635-123

Figure 12-1. Critical Areas of the Model Recommended for Monitoring Strain

The difference in α for A286 screws used in maraging 200 steel results in a significant increase in torque at cryogenic temperatures.

Selected primary structural material is 18Ni-200, for best combination of stability and toughness from 300K to 78K. The higher grade maraging steels 18Ni-250-300-350 might offer the best opportunity for future improvements. Their properties at 78K are at present, however, unacceptable, and stiffness (E) continues to be a problem.

Evaluate new materials and processes under simulated NTF conditions and under load (proof of concept). Do not accept vendor claims without supportive testing. Timely proof-of-concept testing will verify the integrity of the model, thereby safeguarding the facility.

Use of dissimilar materials is desirable from a cost standpoint. Variation in coefficient of contraction (α^t) does, however, present problems. On-going work suggests the potential for varying α^t for some composites (one direction).

NTF force/pressure model costs will be approximately 2 to 1 times higher than current models. This will be reduced by further R&D and experience with early models. The increase can be directly attributed to increased engineering and quality control.

For the static aeroelastic wing (F-111 TACT) it was found that a tailored steel spar was the only solution in satisfying strength requirements, while matching 1/20-scale bending and twisting characteristics of the full scale vehicle. A low-modulus "soft skin" is used for the outside profile and cusp; it remains flexible enough at 78K to contract with the spar minimizing thermal stresses.

The high dynamic pressure ratio at the wind tunnel design conditions eliminated composite "stress skin" approaches. The high internal shear loads in the wing box region exceded allowables for traditional honeycomb structure.

Proof-of-concept coupon test showed that F-16 type graphite-epoxy maintained strength integrity at cryogenic temperatures.

The F-111 TACT rigid wing has considerable aeroelastic effects due to the dynamic pressure. This will be typical for the majority of wings designed for full-scale R_N simulation in the NTF. A rigid (zero deformation) wing cannot be designed for NTF. The alternatives are therefore to design for one aerodynamic condition and correct for the others, or to design static aeroelastically similar wings for each configuration. The latter will yield better data, but is more expensive. In either case, an accurate on-line Deformation Measuring System is mandatory.

SECTION 13

RECOMMENDATIONS

The results of this study show that the National Transonic Facility has a capability that cannot be fully utilized using present day materials and manufacturing techniques. In other words, one can anticipate that some configurations will not achieve full-scale R_N in the NTF because of model/sting/balance limitations. The quality of surface finish is also questionable in a development model where removable parts are required. In addition, there is concern about balance accuracy because of temperature gradients across the model.

The aforementioned potential model system limitations can be directly attributed to the NTF operating environment. It is therefore highly recommended that proof-of-concept tests be initiated in problem areas that are common to many models, and that program managers of new configurations under development for the NTF be advised that proof-of-concept tests in areas of new methods/processes, and possibly reduced safety factors, are mandatory. Such tests must simulate the environmental conditions of the NTF, and where appropriate, the predicted load conditions. They would be carried out early in the design process.

Recommended proof-of-concept tests follow. The results of these tests would be useful in the design of many models.

- Filler materials for development models where removable parts are required.
- Typical joint designs for removable parts, aimed at the elimination of unporting.
- The use of a combination of composites and steels.
- Instrumentation packages designed for use in a cryogenic environment.
- Forced temperature gradient across the balance under cryogenic conditions.

Recommended proof-of-concept tests that would be applicable to specific configurations are:

- New designs where safety factors are lower than 4 on ultimate and/or 3 on yield.
- New materials/processes. An independent evaluation of allowables is mandatory.

- Aeroelastic wing/tail designs.
- Any form of remote control.
- Instrumentation that must be maintained at room temperatures.
- Instrumentation cable crossing the balance.

Further recommendations:

- Approach the steel companies with respect to improving the properties of steels such as maraging 250, 300, 350, for use at cryogenic temperatures. An increase in the value of E is also highly desirable.
- Investigate the potential of matching the coefficient of expansion of a composite material and maraging steel to allow the use of such dissimilar materials. They must match over the entire operating temperature range.
- Provide standard screws made of maraging steel.
- Continue a review of high strength, low temperature/pressure adhesives including the diffusion brazing process. This would be very helpful in the design of thin pressure wings.

SECTION 14

REFERENCES AND BIBLIOGRAPHY

14.1 REFERENCES

1. Wind Tunnel Model Systems Criteria, NASA LHB 1710.15, September 1981.

2. Fuller, D. E., Guide for Users of the National Transonic Facility, NASA TM-83124, 1981.

3. Hadley, S. K., TACT Supercritical Model Scale Effects on Transonic Shocks and Boundary-Layer Separation Characteristics, General Dynamics, Fort Worth Division, Report ERR-FW-1461, December 1973.

6. Young, A. D., and Paterson, J. H., Aircraft Excrescence Drag, AGARD-AG-264, 1981.

7. Schemensky, R. T., Development of an Empirically Based Computer Program to Predict the Aerodynamic Characteristics of Aircraft, AFFDL-TR-73-144, November 1973.

8. Schemensky, R. T., and Howell, G. A., Aerodynamic Accounting Technique for Determining Effects of Nuclear Damage to Aircraft, DNA 4531F-1, February 1978.

9. White, F. M., and Christoph, G. H., A Simple New Analysis of Compressible Turbulent Two-Dimensional Skin Friction Under Arbitrary Conditions, AFFDL-TR-70-133, U.S. Air Force, February 1971.

10. Sevier, J. R., Jr., and Czarnecki, K. R., Investigation of Effects of Distributed Surface Roughness on a Turbulent Boundary Layer Over a Body of Revolution at a Mach Number of 2.01, NACA TN 4183, February 1958.

11. Czarnecki, K. R., Robinson, R. B., and Hilton, J. H., Jr., Investigation of Distributed Surface Roughness on a Body of Revolution at a Mach Number of 1.61, NACA TN 3230, 1954.

12. Eckstein, E. L., A Theoretical Investigation Up to Mach Number 5.0 of the Influence of Sandgrain-Roughness on the Turbulent Skin Friction Drag of an Insulated Flat Plate, General Dynamics Convair Division, Report FZA-080, September 1954.

13. Spalding, D. B., and Chi, S. W., "The Drag of a Compressible Turbulent Boundary Layer on a Smooth Flat Plate with and Without Heat Transfer," Journal of Fluid Mechanics, Volume 18, Part 1, January 1964.

14. The Mean Skin Friction Coefficient for a Rough Flat Plate With a Turbulent Two-Dimensional Boundary Layer in Compressible Adiabatic Flow, With Application to Wedges, Cylinders, and Cones, Royal Aeronautical Society, ESDU 73016 (British Data Sheets), July 1973.

15. Eckert, E. R. G., Survey on Heat Transfer at High Speeds, WADC TR 54-70, April 1954.

16. Braymen, W. W., and Webb, J. W., Lift and Drag Analysis of Aerodynamic Configurations: Aeromodule Version III, General Dynamics Fort Worth Division, Report ERR-FW-1092, December 1970.

17. Winter, K. G., and Gaudet, L., Some Recent Work on Compressible Turbulent Boundary Layers and Excrescence Drag, RAE Technical Memorandum Aero 1115, 1968.

18. Schlichting, H. (J. Kestin, transl.), Boundary-Layer Theory, Sixth Edition. McGraw-Hill Book Co., Inc., c.1968, p.676.

19. Goddard, F. E., Jr., "Effect of Uniformly Distributed Roughness on Turbulent Skin-Friction Drag at Supersonic Speeds," Journal of the Aero/Space Sciences, January 1959.

20. Shutts, W. H., and Fenter, F. W., Turbulent Boundary-Layer and Skin Friction Measurements on an Artificially Roughened, Thermally Insulated Flat-Plate at Supersonic Speeds, University of Texas Defense Research Laboratory, DRL-366, 1955.

21. Transonic Aircraft Technology TACT Program, Volume 2, Aerodynamic Design and Analysis, General Dynamics Fort Worth Division, Report FZM-595-028-2, September 1976.

22. Hoerner, S. F., Fluid-Dynamic Drag. Hoerner Fluid Dynamics (Brick Town, NJ) c.1965.

23. Brady, A. E., Stress Notes for the 1/15 Sc. CWC and the 1/20 Scale F-111 TACT Models for Cryogenic Testing in the NTF, Report 4065, Convair LSWT, 30 March 1983.

24. Tobler, R. L., Materials for Cryogenic Wind Tunnel Testing. NBSIR 79-1624, May 1980. (Available as NASA CR-165716.)

25. Metallic Materials and Elements for Aerospace Vehicle Structures - Volume 2. MIL-HDBK-5C, U.S. Dep. Def., Sept. 15, 1976.

26. Frost, R. C. et al, Transonic Aircraft Technology, TACT Program, Volume 1. Program Summary, AFFDL-TR-78-163, Vol. 1, U.S. Air Force, Sept. 1976.

27. McCullers, L. A., and Lynch, R. W., Dynamic Characteristics of Advanced Filamentary Composite Structures, AFFDL-TR-73-111, Vol. II, U.S. Air Force, Sept. 1974.

28. Lynch, R. W., Rogers, W. A., and Braymen, W. W., Aeroelastic Tailoring of Advanced Composite Structures for Military Aircraft, Volume III: Modifications and User's Guide for Military Aircraft. AFDL-TR-76-100, Vol. III, U.S. Air Force, December 1976.

29. Reed, D. L., Point Stess Laminate Analysis, General Dynamics, Forth Worth Division, Report FZM-5494, 1 April 1970.

30. Smith, B. R., Love, M. H., Lawrence, J. R., Ezeo, J. P., Composite Swept Forward Wing (SFW) Critical Component, General Dynamics Fort Worth Division, Report ERR-FW-2120, 31 December 1979.

31. Irwin, H. M., Kerr, H. C., and Dickey, D. F., F-111 TACT Program Aerodynamic Loads --- Analysis of Wing Pressure Data, General Dynamics Fort Worth Division, Report FZA-449, Addendum 595-02, September 1971.

32. Rogers, W. A., Braymen, W. W., Murphy, A. C., Graham, D. H., and Love, M. H., Validation of Aeroelastic Tailoring by Static Aeroelastic and Flutter Tests, Volumes I-V, AFWAL-TR-81-3160, U.S. Air Force, Sept. 1982.

14.2 BIBLIOGRAPHY

Amuedo, A. R., Jr., A Procedure for Calculating the Static Aeroelastic Divergence and Deflections of a Sting-supported Model/Balance Combination. General Dynamics Fort Worth Division, Data Sheet dated April 14, 1959.

Chiang-Ying M. Tung and Dynes, Paul J., J. of App. Poly. Sci., Vol. 27, p. 569-574, 1982.

Griffin, S. A., Brocard, M., Basin, M., Conveners Report, Model Systems for Pressurized Wind Tunnels, AGARD-AR-105, Appendix 5, August 1977.

McKinney, L. W.; and North, R. J.: Appendix 2 - Report of the Conveners Group on Cryogenic Test Technology. Windtunnel Capability Related to Test Sections, Cryogenics, and Computer-Windtunnel Integration, AGARD-AR-174, Apr. 1982, pp. A2-1 - A2-24.

Supan, E.: Summary of Diffusion Brazing Fabrication Techniques. DWA Incorporated.

Worscheck, G., F-16 Wind Tunnel Model, Predicted Temperature Distribution, Systems Technology Technical Memorandum TM696-82-131, General Dynamics Convair Division, 3 February 1982.

Thermal Analyzer, Systems Technology Technical Memorandum TM696-0-T-80-737, General Dynamics Convair Division, 30 June 1980.

APPENDIX A

RESULTS OF PROOF-OF-CONCEPT TESTS

As stated in Section 7.6, the design of models for use in the NTF is a challenging task. High loads and a severe temperature environment have required, in some cases, a departure from the proven methods of designing and fabricating by conventional methods. The cost of using the facility, and the potential danger to it, make it mandatory that we have a proven model system. To achieve this objective, proof-of-concept tests are recommended for any part of the model system wherein new methods or procedures are used. Such tests should be carried out under simulated cryogenic conditions, and where appropriate, under the load conditions expected in the facility. The tests should be carried out during the design process, as they may well influence or change the design.

In the design study of the 1/15 scale CWC and the 1/20 scale F-111 TACT, the need for proof-of-concept tests became apparent, and the results have caused design changes. Tests were conducted as described in the following sections.

A.1 INSTRUMENTATION BAY - HEATING/VIBRATION TEST

The forward fuselage and instrumentation bay, described in Sections 9.1.1 and 9.2.1, are very similar in design. The purpose of this test was to:

a Determine if the instrumentation packages could be maintained at room temperature in a cryogenic environment.

b. Determine if the vibration of the model would cause a breakdown of the power leads to the instrumentation, when tested under cryogenic conditions.

c. Validate the Kevlar®, fasteners, and metallic inserts in the joint when subjected to cryogenic temperatures and extreme vibration.

The test specimen was the CWC forward fuselage made to the design as described in Section 9.1.1 (see Figure A-1). The actual instrumentation packages were unavailable; therefore, simulated blocks of the same material and mass were used (see Figure A-2). (Instrumentation cables were as per the design.)

Steel pressure tubes were routed to the simulated electronically scanned pressure (ESP) transducers for representative heat loss. Thermocouples were located to monitor temperatures during the test. The model and vibration test stand were installed on a vibration "shaker" table (see Figure A-3). Figure A-4 shows the model in the test chamber. The test equipment included Barber-Colman temperature controllers that regulated temperature through a closed-loop feedback system (Figure A-5). Temperature data was recorded on

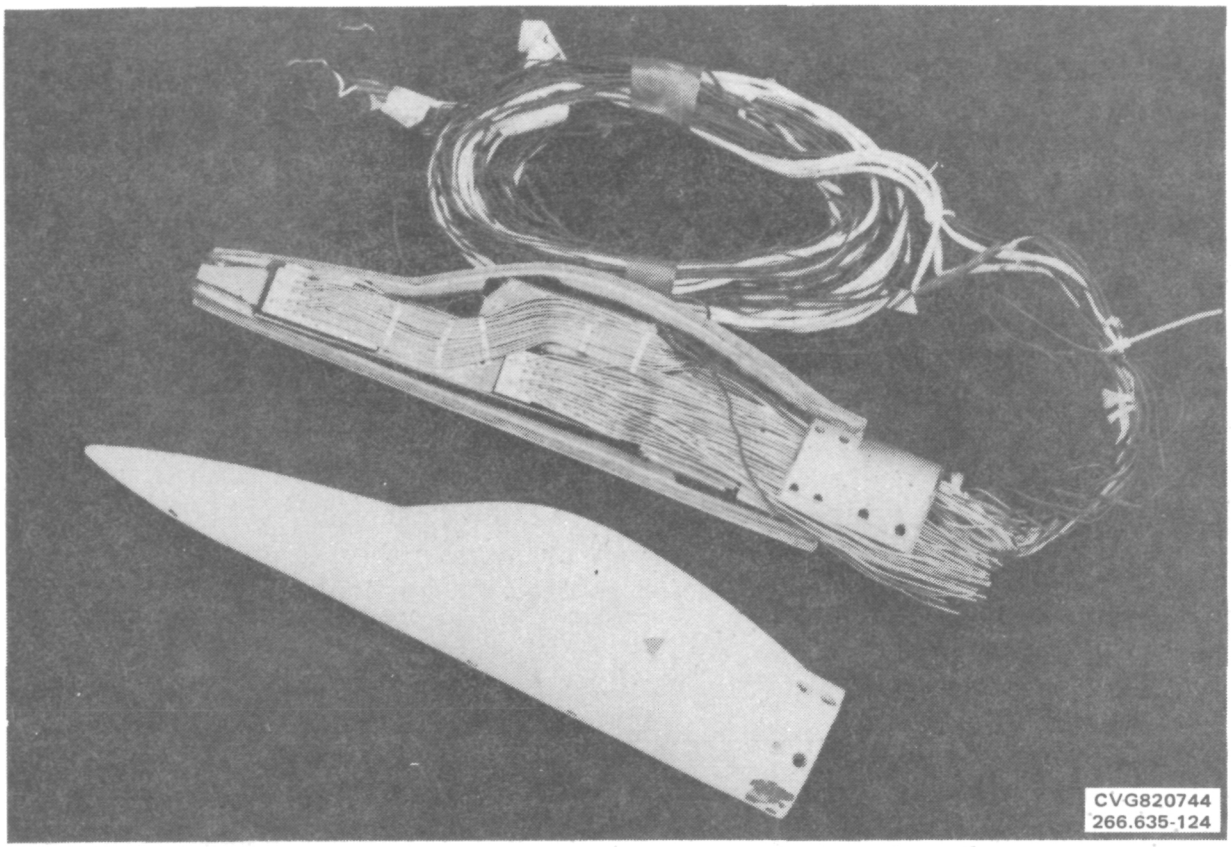

Figure A-1. Instrumentation Bay – Proof-of-Concept Test Specimen

a Fluke data logging system. The model was divided into three heat zones, each separately controlled. A preselected thermocouple served as a control point for each zone (Figure A-6), automatically commanding more or less heat input when the temperature deviated outside the pre-established band width. Figure A-7 shows the thermocouple routing.

With the model subjected to an external temperature of approximately-314F, the internal heating elements were able to keep all but one simulated instrument package at room temperature ±10F. The only area that couldn't be heated to room temperature was the aftmost instrument package, which was exposed directly to the cryogenic atmosphere. An increase in the density of the heating elements or additional insulation in that area of the model should allow the temperature to be stabilized within the safe operating range of the instrument. The test specimen was also subjected to random vibrations at 20 to 2000 hertz frequency levels and up to 5g maximum force for a period of 30 minutes at the low temperature.

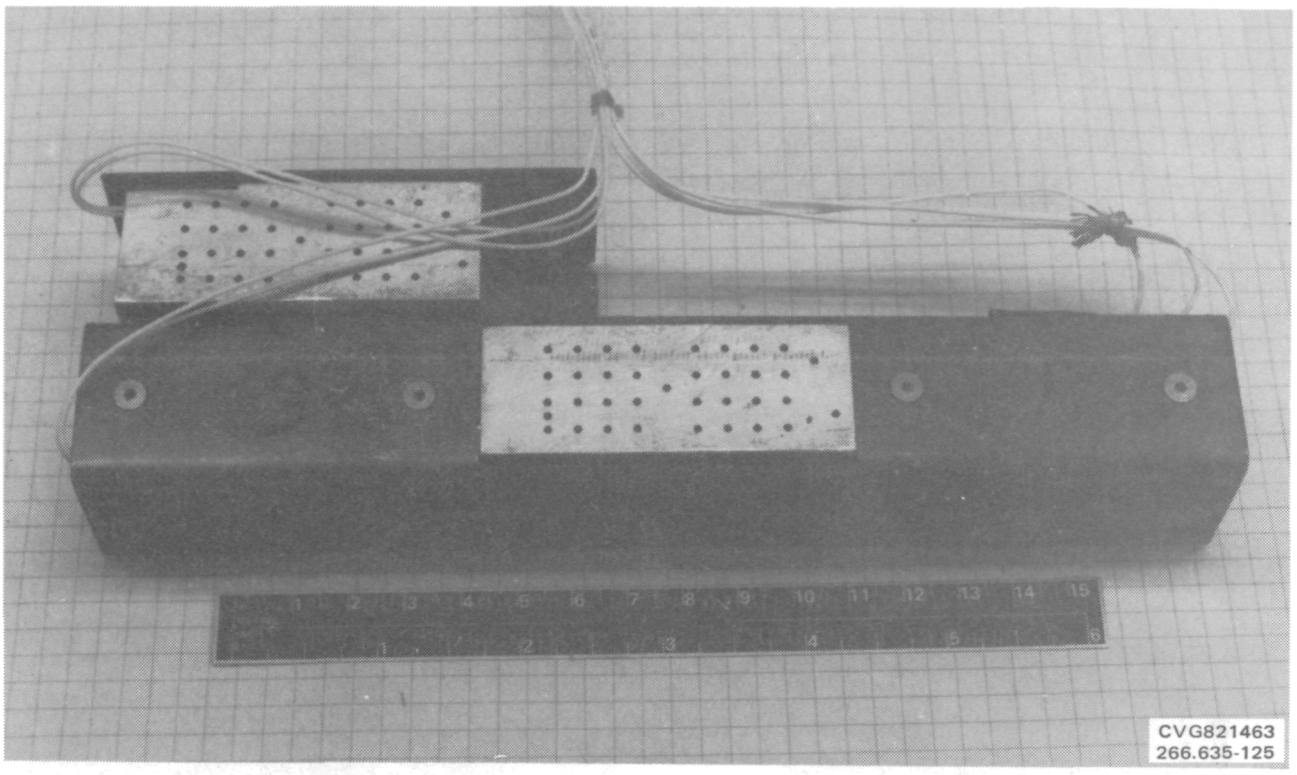

Figure A-2. Simulated Instrumentation Packages

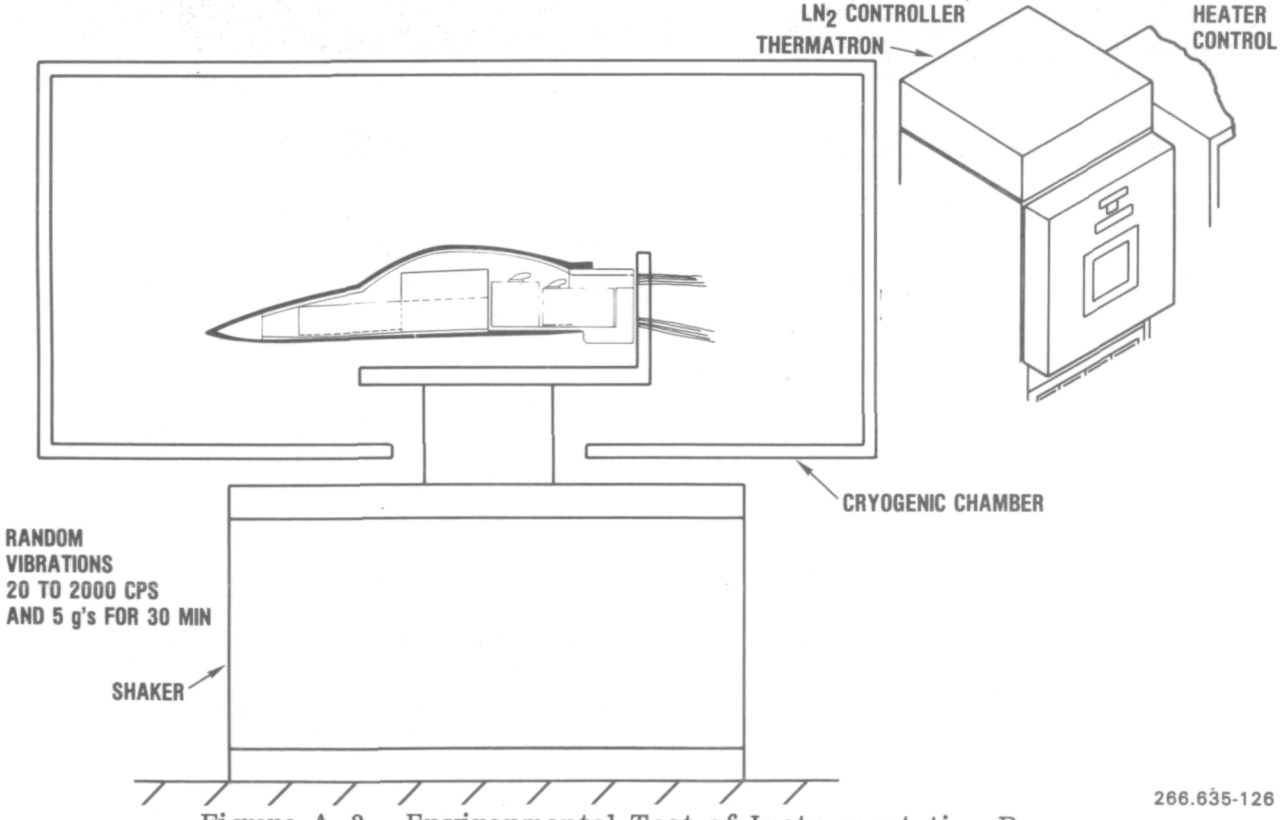

Figure A-3. Environmental Test of Instrumentation Bay

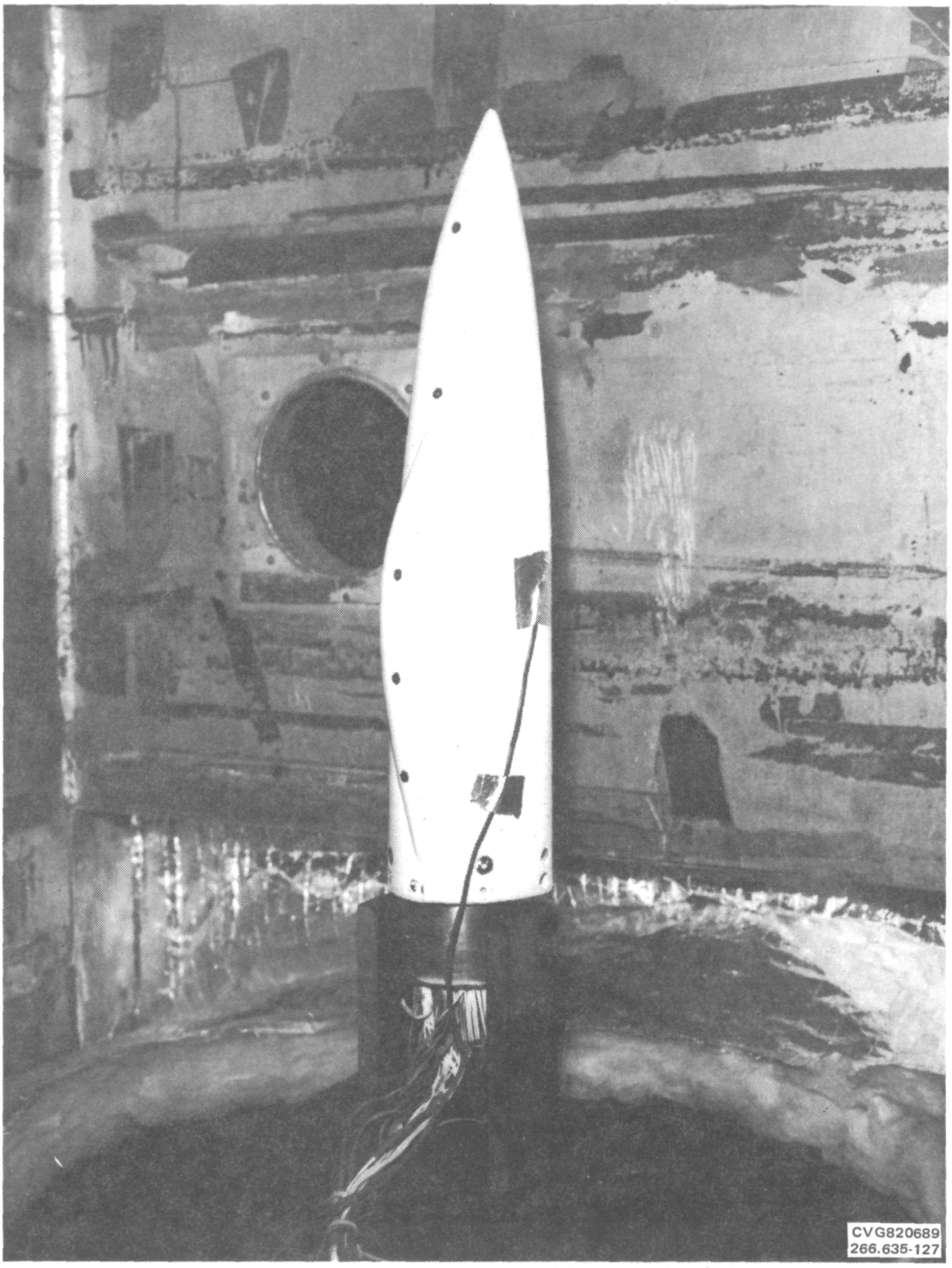

Figure A-4. Model in Test Chamber

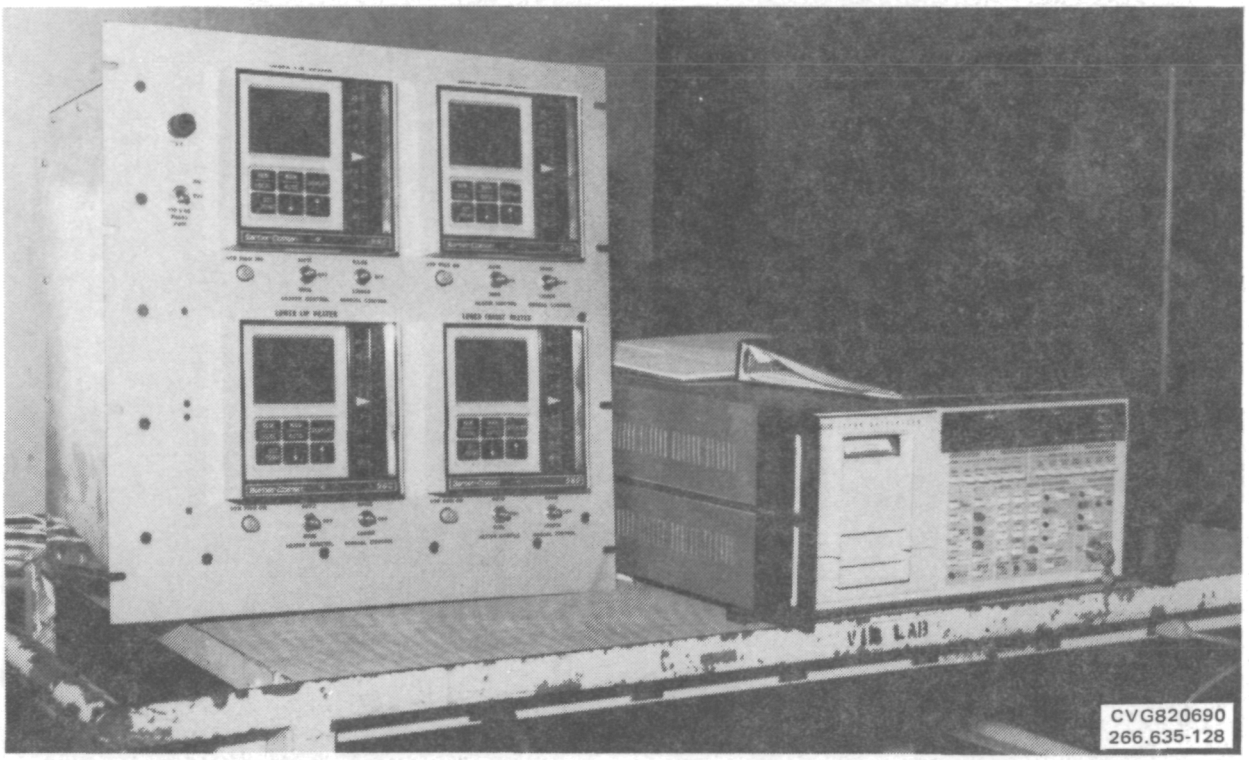

Figure A-5. Barber-Colman Temperature Controllers and Fluke Data Logger

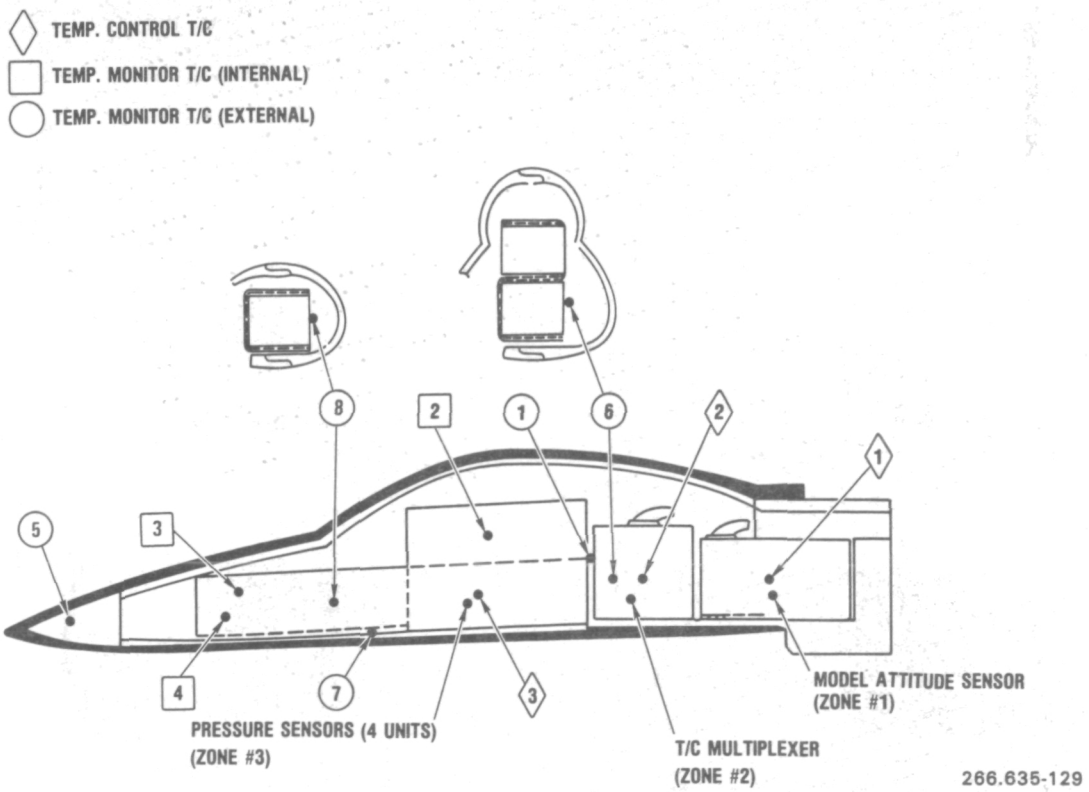

Figure A-6. NTF Cryo/Vibration Test Specimen T/C Locations

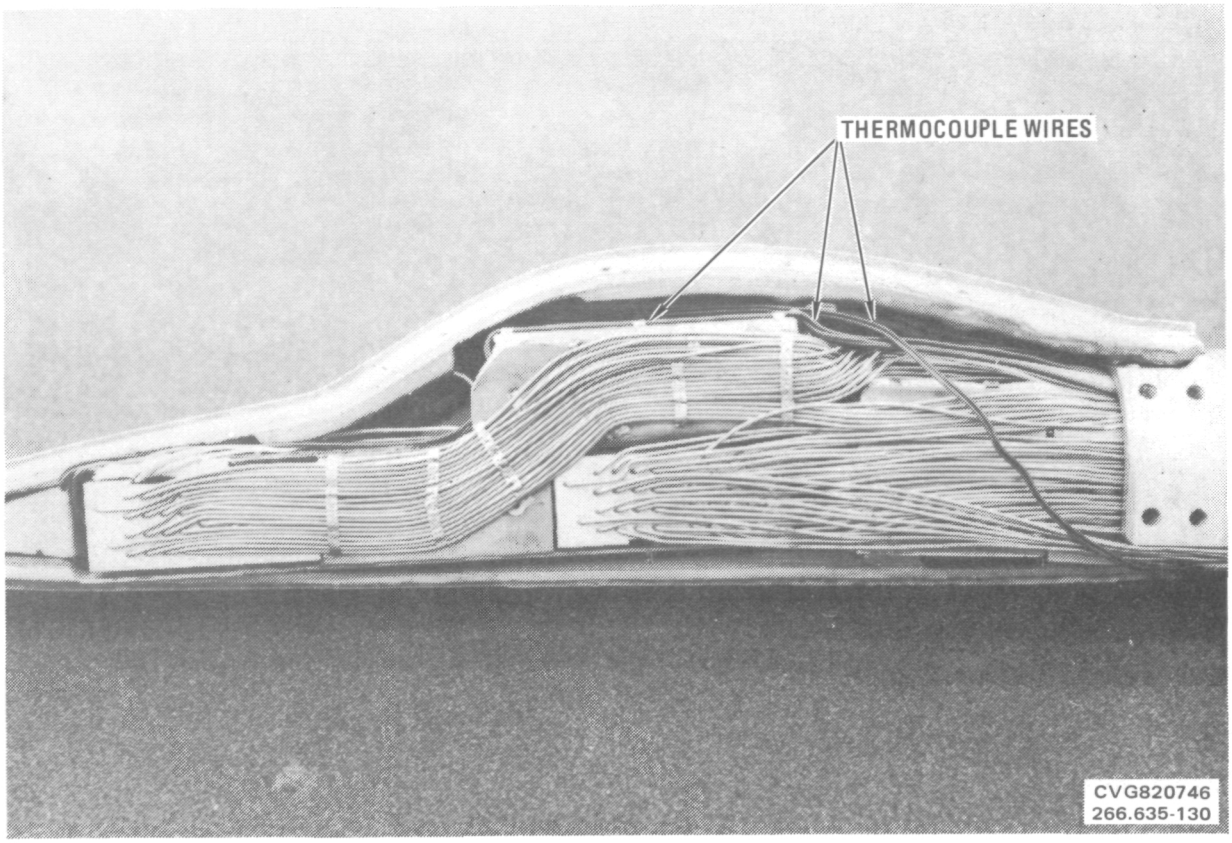

Figure A-7. Test Specimen Thermocouple Routing

Visual examination of the Kevlar®/steel shell that composes the main structure of the specimen shows no damage due to the vibration and temperature conditions to which the model was subjected.

The polyurethane paint used on the model has cracked in some areas. This may be due to the primer used. An earlier test of polyurethane paint with no primer on a piece of Kevlar® immersed in LN_2 showed no visual physical damage (Figure A-8).

The test was conducted in the General Dynamics Vibration Test Laboratory. The results are shown in Figure A-9.

A.2 WING FABRICATION METHODS

The design approach for both the 1/20th scale F-111 TACT and 1/15th scale CWC wings required concepts unique to each configuration. Conventional design and fabrication techniques were combined with nonstandard methods to provide an optimum wing design for each configuration. Early in the design process, it was apparent that there was a need for further research in the area

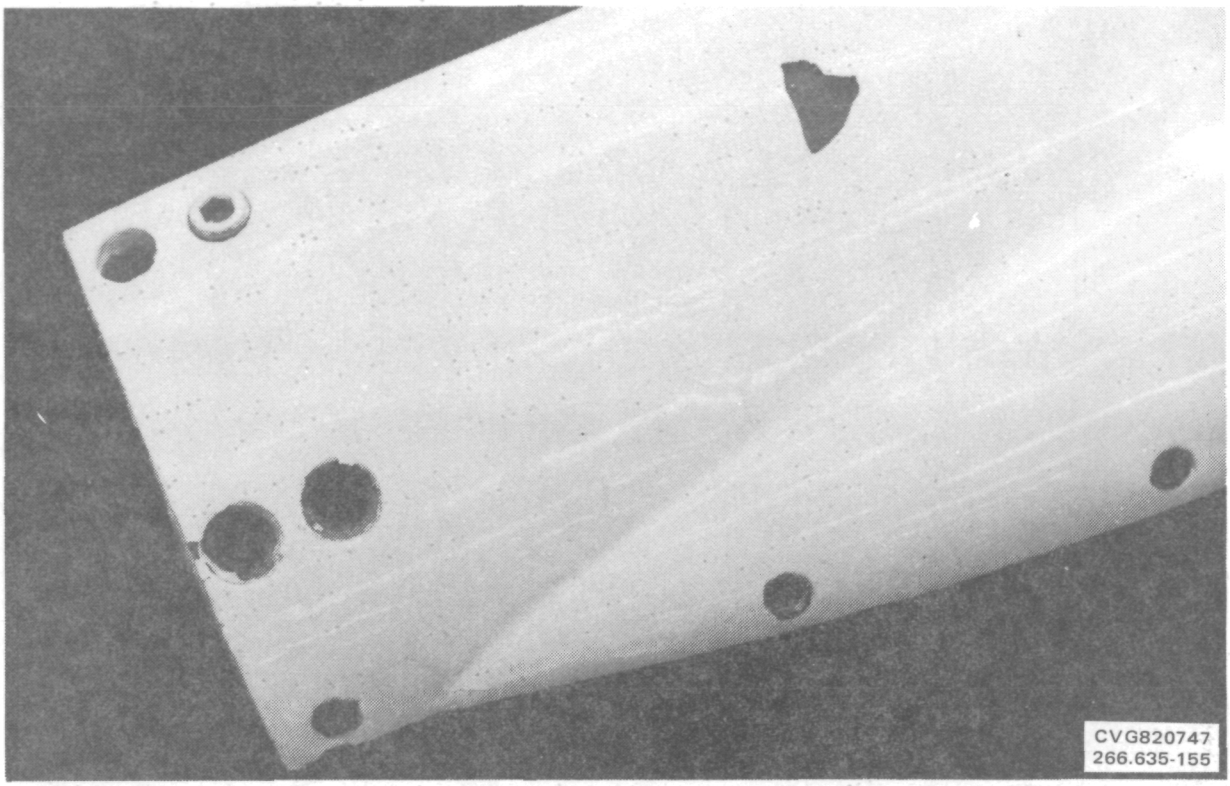

Figure A-8. Close-up View of Model Nose

of joining parts for use in cryogenic applications. A search ensued for an improved bonding agent or process, the desired parameters being: 1) good surface finish, 2) reasonable fabrication cost, 3) temperature application < 900F, and 4) strength 10,000 psi. The optimum process should result in no warpage, allowing each wing part to be fully profiled and aged before joining.

In addition to adhesive bonding, other processes reviewed were diffusion brazing, brazing, diffusion bonding, electron beam welding, laser welding, and spot welding. Diffusion brazing appeared to be the best candidate (see Table A-1).

A.2.1 ADHESIVE BONDING. Initial testing involved lap shear coupons using American Dyanamide's FM-1000® adhesive film, which was recommended for cryogenic applications as the bonding agent.

Test specimens were fabricated of 321 stainless steel sheet stock 0.031 inch thick by 1.10 wide by 13.00 inches overall length. A double shear overlap of 0.50 inch was used for each specimen (see Figure A-10). Test coupons

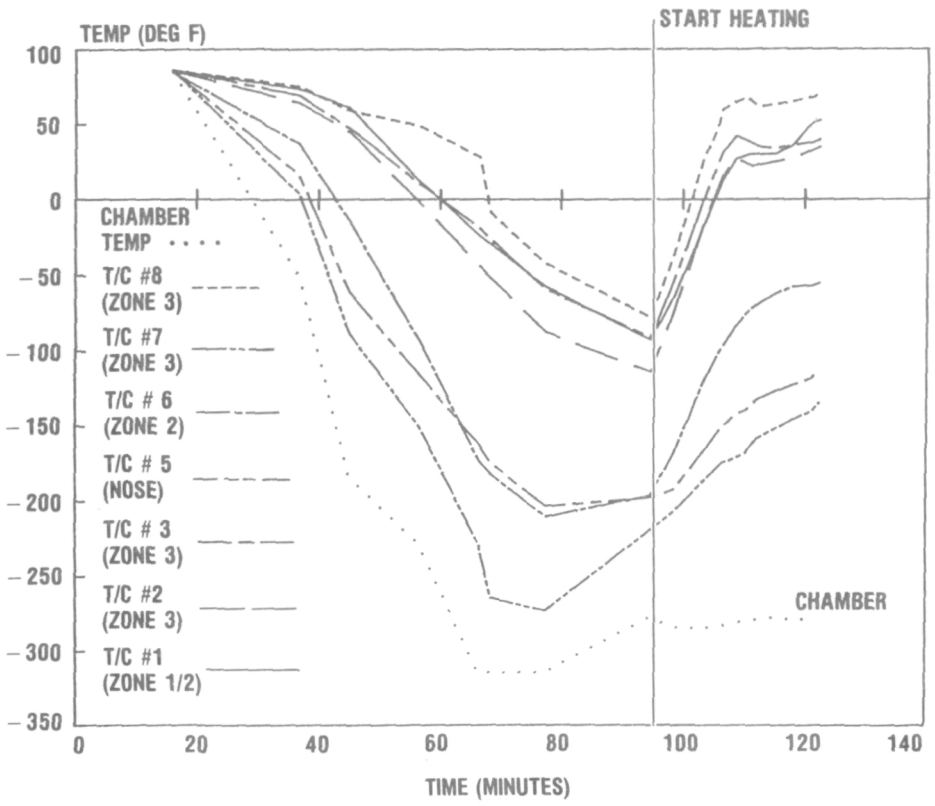

266.635-134

Figure A-9. Environmental Test of Instrumentation Bay - Test Results

were prepared and bonded in accordance with General Dynamics Convair Division process specification 0-00214. The procedure included cleaning and etching the metal, sizing and cutting the FM-1000 film adhesive, and setting up for bonding. Bonding was effected at a temperature of 345F, a pressure of 40 psi, and a time period of 1 hour. Test loads were applied in a Universal test machine (tension only) at two temperature levels (approximately 70F and -320F). A large insulated beaker was used to contain the coolant, LN_2, for maintaining the -320F temperature (see Figure A-11).

The test results were generally unfavorable and inconsistent at both room temperature and -312F (2103 psi). Values attained were well below the expected range of 4200-5000 psi. Table A-2 lists values for all FM-1000 adhesive specimens tested.

Table A-1. Wing Fabrication Methods - Wing 18Ni-200

Fabrication method	Adhesive foil	Fabrication process			Inspection method	Tooling	Estimated strength psi
		Temperature	Pressure	Time			
Adhesive bonding	American Cyanamid FM 1,000	300F	50 psi	1 to 2 hours	Under development GD/FW	Minimum	4,000 to 5,000
Diffusion brazing		<900F	To be determined Approximately 1,000 psi	1 to 3 hours	Ultrasonic or C-scan	Ceramic profiled	10,000
Brazing	Gold alloy	1,800F	Minimum		Ultrasonic or C-scan	Steel flat	50,000
Diffusion bonding	None	1,800F	5,000 psi (example)	3 hours	Ultrasonic or C-scan	Steel profiled	70,000
ELECTRON BEAM/LASER WELDING/SPOTWELDING							

Key parameters:
- Maintain surface finish
- Fabrication cost
- Complete wing profile before joining
- Tooling from wing profile
- Rework incomplete bond without scrappage/warpage
- Strength 6,000 to 10,000 psi
- Curing temperature less than 900F
- Fatigue resistant

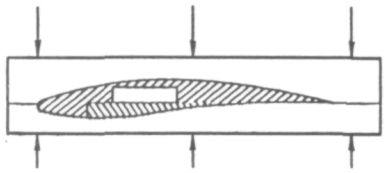

266.635-131

A.2.2 DIFFUSION BRAZING. The process of diffusion brazing involves the application of a bonding agent (e.g., adhesive film, metal foil, or solder) combined with heat and pressure to component parts to effect a permanent joint. A study to determine the feasibility of applying diffusion brazing as a process for joining wing components was undertaken.

A materials research firm (DWA Composites Specialties), which had previous experience in diffusion brazing, was engaged to braze double lap shear coupons made of maraging 200 steel using a variety of aluminum foil materials as the bonding agent. This research was conducted to ascertain the level of load capacity (in psi) at ambient and cryogenic temperatures and the uniformity of the brazed joint.

Machined and ground plate stock (1.65 inches by 2.5 inches by 0.25-inch thick) of maraging 200 steel, heat treated to 200 ksi at 900F was given to DWA for processing. DWA furnished the tooling and bonding foil materials as well as the expertise in developing the initial test specimens (see Figures A-12 and A-13).

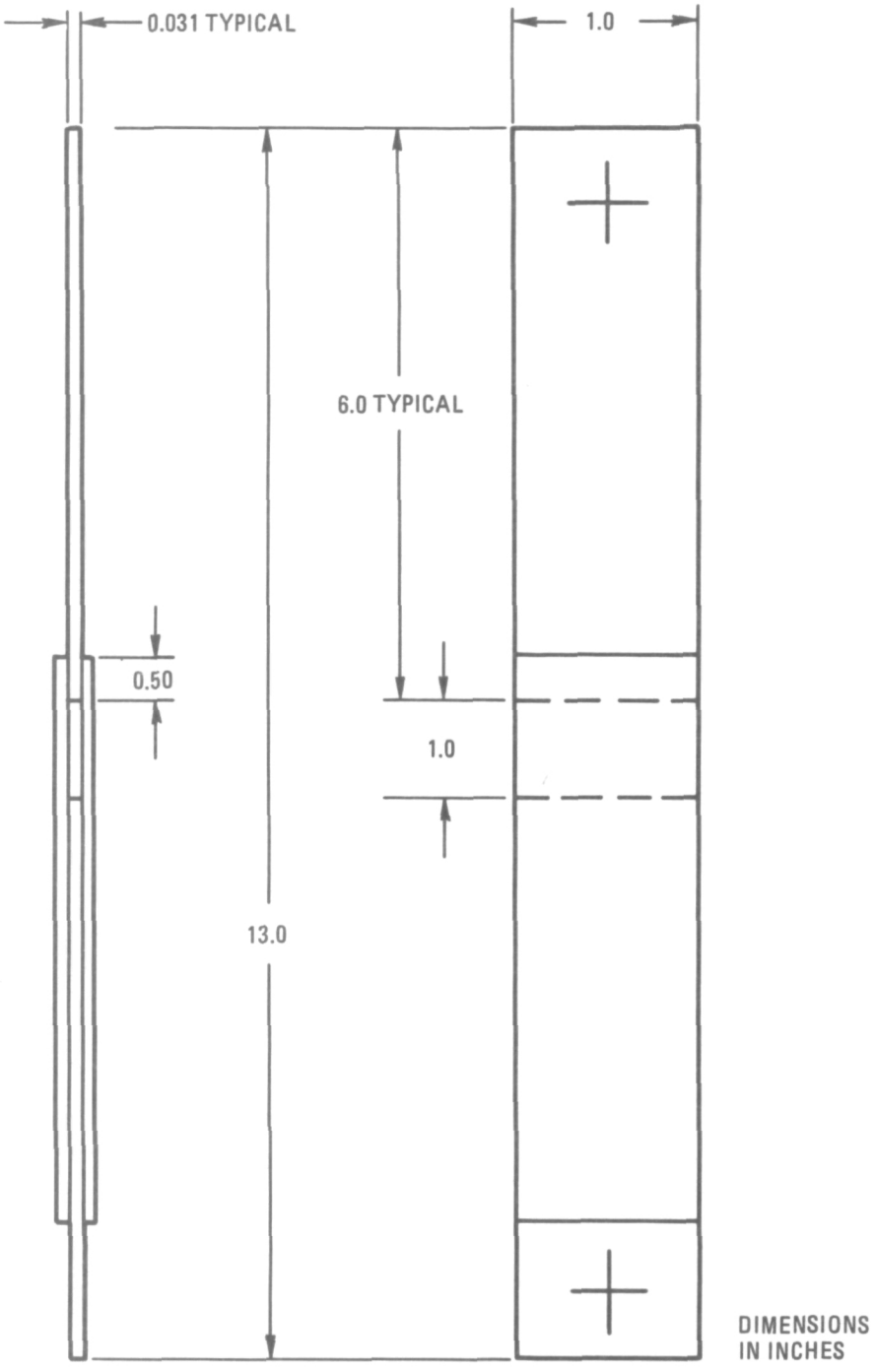

Figure A-10. Lap Shear Tensile Specimen - FM-1000 Adhesive Film

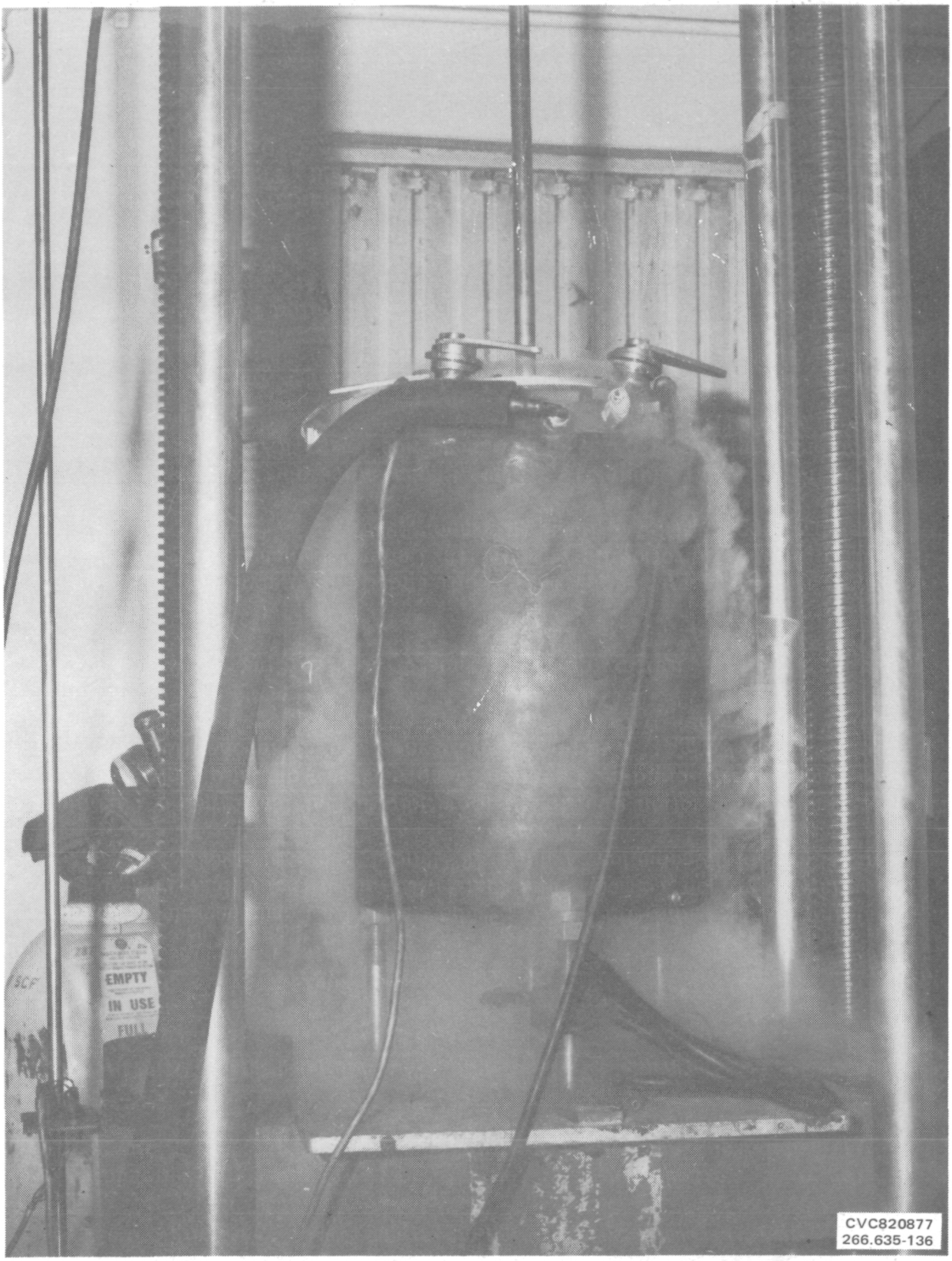

Figure A-11. LN_2 Coolant Beaker

Table A-2. Adhesive Bonding Test Coupon Data

I.D.	Material	Temp/Time	Load (lb)	Ult (psi)
1	FM-1000	-320F	1665	1708
2	FM-1000	-320F	1650	1692
3	FM-1000	-320F	2000	2041
4	FM-1000	-320F	1590	1631
5	FM-1000	-320F	1700	1726
6	FM-1000	-320F	2050	2103
7	FM-1000	RT	2935	2995
8	FM-1000	RT	2350	2350
9	FM-1000	RT	3415	3415

The approach taken in bonding the double lap shear specimens used aluminum foil (2 mils thick) as a bonding agent at the joint interface in a vacuum bag. Since the maraging steel was aged at 900F, it was desirable to limit the bonding temperature to the same level or lower.

Some important variables to the process are surface cleanliness of the specimen components, surface flatness, and bond parameters (temperature, pressure, and time).

Initial bonding trials were made with three specimens made with 2024, 6061, and 4343 aluminum foils 2 mils thick (specimens were identified as 1, 2, 3, respectively). The bond surfaces of the steel were lightly abraded to provide "tooth" to the surface for bonding. Bonding parameters were set at temperature of 875F, pressure of 4000 psi, and a time of 30 minutes.

After brazing, the coupons were visually and dimensionally inspected prior to testing. Specimen 3 was damaged in handling and could not be tested.

The loading test procedure used here was the same as above in the FM-1000 adhesive specimens. A Universal test machine equipped with an insulated beaker containing LN_2 was used to test the parts at a temperature of -320F. The results from the first tests were favorable (although not at the desired

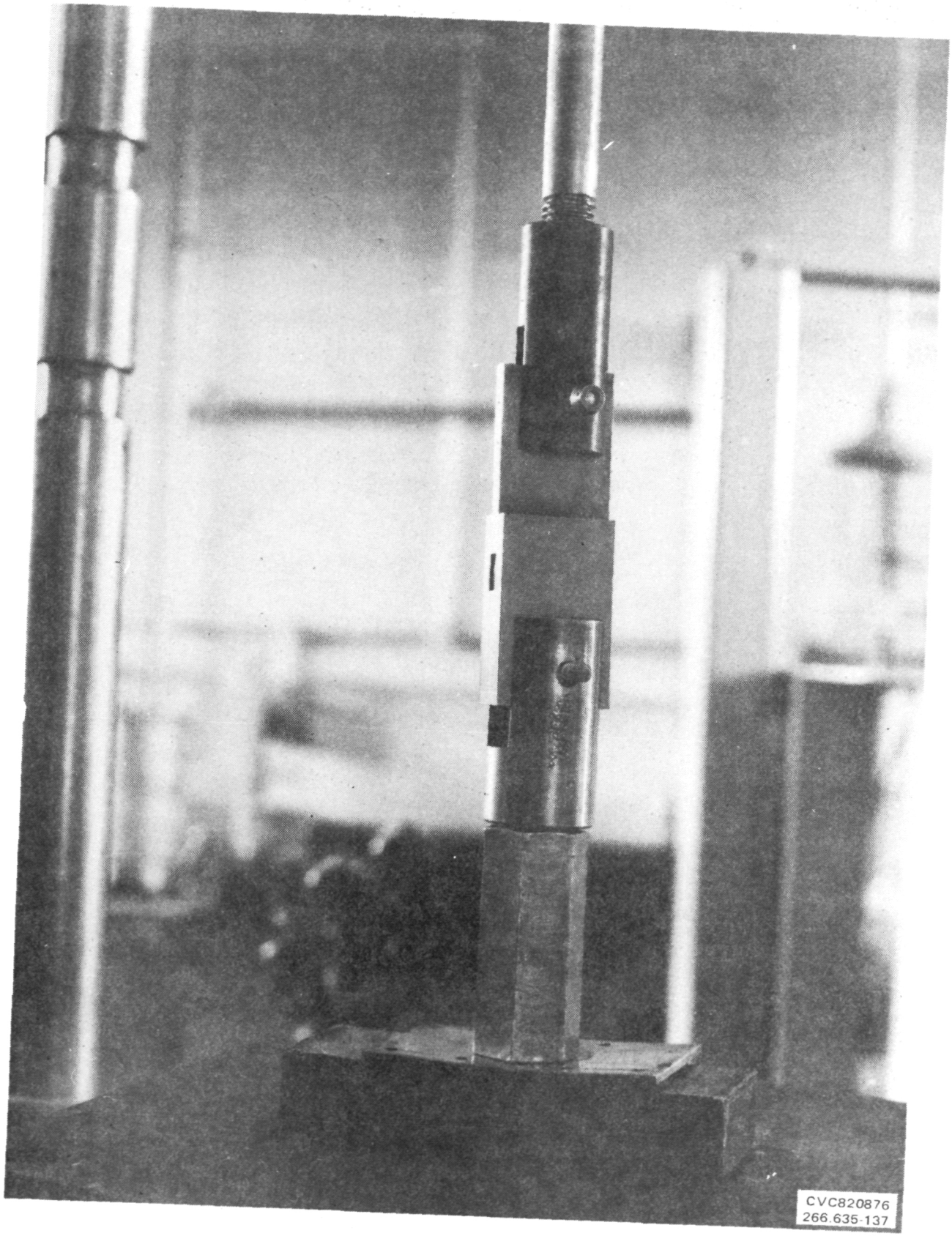

Figure A-12. Diffusion Brazing Specimen

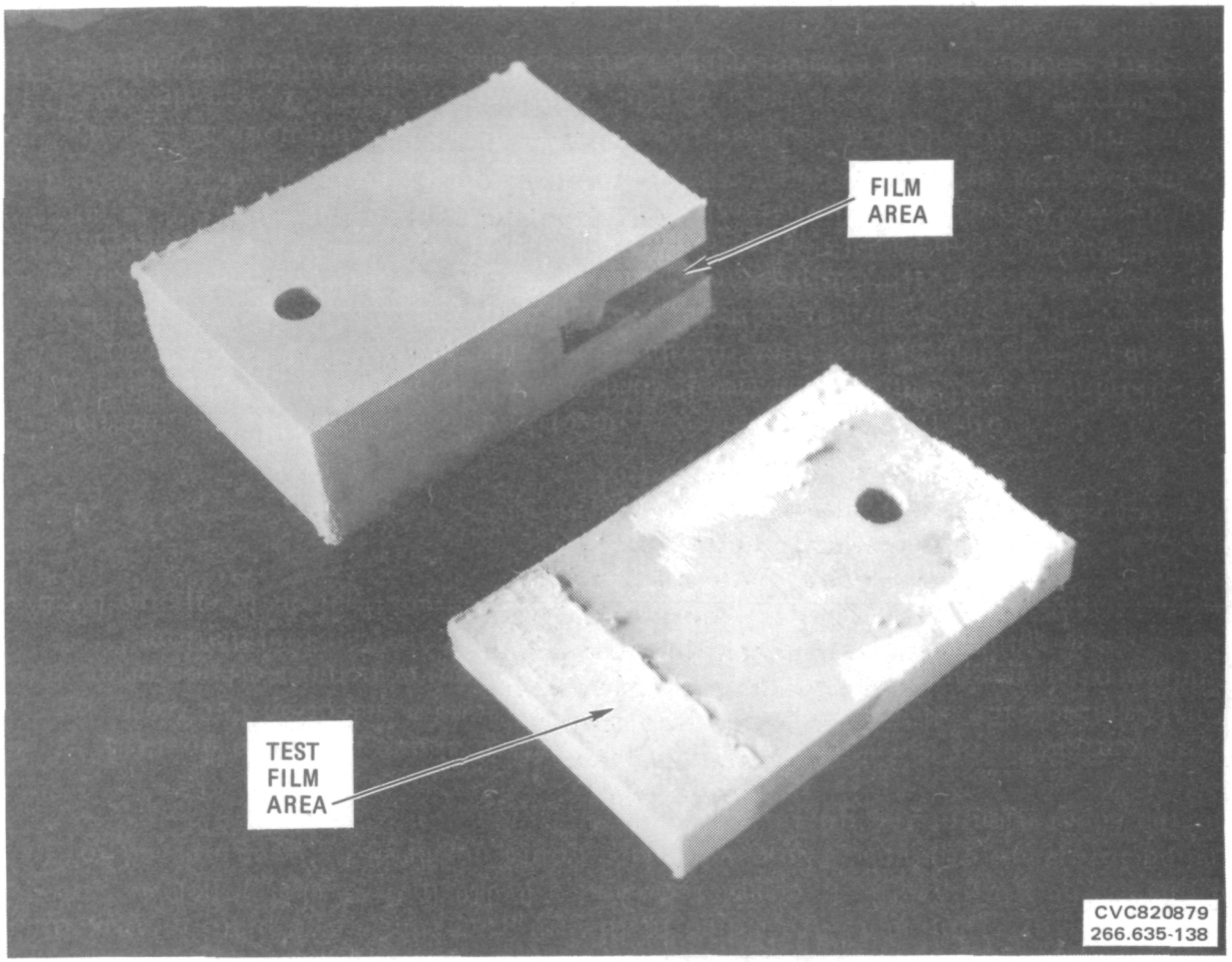

Figure A-13. Diffusion Brazing Specimen after Testing at -320F

level) with the following achieved stress levels: 1) Specimen 1 (2024), 4200 psi; 2) specimen 2 (6061), 4660 psi.

Upon review of the above achievements, it was decided that greater "wetting" action of the foil bonding agent might occur at a slightly higher temperature. The material aging temperature of 900F was selected also as the bond temperature for the next series of specimens. The next series of three specimens (4, 5, 6) were prepared as the first three except that the bonding temperature was increased to 900F. Also, all three were prepared with 6061 aluminum foil as the bonding agent. Specimen 4 exhibited the desired result (5333 psi);

however, specimens 5 and 6 did not (2133 and 2700 psi), which caused new concerns about consistency of the process.

Review and evaluation indicated a greater need for control of surface contamination and increased wetting action of the bond surfaces. A further increase in the bond temperature to 1000F was tried on the next three coupons. Rework of the bonding tooling to eliminate off-gassing contamination was done by changing all carbon steel parts to type 304 stainless steel. The next three specimens tested were made with 2024, 6061, and 4343 aluminum foil. Results were lower in achieved stress levels than previous coupons; however, the trend of the relative levels was similar (6061 foil achieved the highest level) to earlier tests. The higher bonding temperature of 1000F was of no significance and it was decided to revert to the 900F level for future bonding to assure retention of the desired heat treatment.

The following five specimens were entirely new and prepared the same as specimens 4, 5, and 6. All tests were conducted at room temperature and the results were improved.

The achieved levels were 3773 psi (maximum) and 1120 psi (minimum). The results were again evaluated and observations indicated a need to apply differential thicknesses of bonding foil in the specimen overlap area versus the tab (load fixture support) area. Two new specimens were prepared using 6061 bonding foil of 3 mil/3.5 mil thicknesses. These specimens were tested at -320F with improved results both above 4000 psi ultimate strength. These results led to additional testing with increased differential (3.5 mils/5 mils) bonding foil thicknesses. Achieved levels were only moderate (2480-2633 psi), indicating an overstep in the differential increment. Time and availability of materials did not permit making further iterations in this area.

Subsequent testing involved the use of zinc or silver flash coatings in an attempt to reduce contamination and increase ultimate strength properties. This effort was perhaps masked by the other problems of cleanliness, surface flatness, and "wetting action." A clear-cut solution was not obtained.

A final approach taken that showed a degree of promise was the employment of 5056 aluminum screen (30 mesh) as a replacement bonding agent for the aluminum foil previously used. Acid etching of the screen was an added step to enhance the bonding potential. The screen thickness of 5 mils seemed to provide sufficient surface exposure during bonding as the screen crushed and filled in the bond area. Ultimate strength levels achieved were 5039 psi (maximum) and 1358 psi (minimum).

In summary, the process of diffusion brazing exhibits potential as a method of joining components of wings, vertical and horizontal tails, and other parts

where the use of conventional fasteners may be undesirable or impractical. Further research is required to achieve an acceptable and repeatable strength level. This study indicates sufficient evidence to consider further research in this area. Table A-3 tabulates results.

A.2.3 DIFFUSION BONDING. This process was reviewed with respect to its use in the fabrication of thin highly stressed wings. A comparatively new process, it is being used primarily for joining sheet metal. The process achieves a bond by combining high pressure/temperature/time. Steel tooling is required for the high pressure, and for wings this would mean profiled tooling and therefore high cost. Diffusion bonding was not considered further.

A.2.4 LASER WELDING. The process of laser welding does not require a vacuum, can be used with dissimilar materials, can be used in difficult locations, and can be used for spot welding or seam welding. The laser beam can vary the size of the spot/seam weld from 0.001 to 0.100 inch. The heat is concentrated locally at the joint, minimizing the annealed area, and therefore distortion. To achieve a good weld the joint must be a close fit.

The laser weld process was of significant interest in our investigation of wing fabrication processes for the following reasons:

- Good structural characteristics
- Minimum distortion
- The laser beam is relatively narrow (0.010-0.020 inch) resulting in highly localized annealing, minimizing loss of strength.
- Useful for eliminating joint cracks in airfoil surfaces, thereby eliminating the unporting of joints
- Useful in retaining pins

Eliminating joint cracks can be done only where they are permanent (i.e., manu-manufacturing joints). This is significant, however, as our investigations showed that joints tend to unport under load, creating mismatches that are unacceptable in terms of surface finish (see Figure A-14).

The investigation of laser welding for structural purposes involved the use of test specimen panels incorporating the proposed joints employed in the design of the wings. Two panels and shear pins were constructed of maraging 200 steel. One panel incorporated a single overlap joint and the other a tongue and groove arrangement.

Table A-3. Diffusion Braze Test Coupon Data

SPECIMEN I.D.	MATERIAL	PROCESS	TEST TEMP.	TEST DATES/LOAD-ULTIMATE									
				3-18-82		4-2-82		4-9-82		4-23-82		5-13-82	
NO.	TYPE	TEMP / TIME	°F	LOAD (Lbs)	ULT. (PSI)	LOAD (Lbs)	ULT. (PSI)	LOAD (Lbs)	ULT. (PSI)	LOAD (Lbs)	ULT (PSI)	LOAD (Lbs)	ULT. (PSI)
1	2024	875°F / .5 HR	-320	6300	4200								
2	6061	875°F / .5 HR	-320	7000	4660								
3	4343	875°F / .5 HR	–	–	–								
4	6061	900°F / .5 HR	-320			7200	5333						
5	6061	900°F / .5 HR	-320					3200	2133				
6	6061	900°F / .5 HR	-320					4050	2700				
7	2024	1000°F / .5 HR	-320							1875	1250		
8	4343	1000°F / .5 HR	-320							250	167		
9	6061	1000°F / .5 HR	-320							2830	1887		
10	6061	900°F / .5 HR	R.T.									5660	3773
11	6061	900°F / .5 HR	R.T.									4610	3073
12	6061	900°F / .5 HR	R.T.									3870	2580
13	6061	900°F / .5 HR	R.T.									1680	1120
14	6061	900°F / .5 HR	R.T.									2530	1687
				6-3-82		6-28-82		7-14-82		8-30-82		11-23-82	
15	6061	900°F / 1 HR	-320	6060	4040								
16	6061	900°F / 1 HR	-320	6200	4593								
17	6061	900°F / 1 HR	-320			3720	2480						
18	6061	900°F / 1 HR	-320			3950	2633						
19	6061	900°F / 1 HR	R.T.					550	366				
20	6061	900°F / 1 HR	-320					1400	933				
21	6061	900°F / 1 HR	-320					1440	960				
22	6061	900°F / 1 HR	-320							830	553		
23	6061	900°F / 1 HR	-320							470	313		
24	6061	900°F / 1 HR	-320							650	433		
25	6061	900°F / 1 HR	R.T.									1280	5031
26	5143	900°F / 1 HR	-320									500	1965
27	5143	900°F / 1 HR	R.T.									345	1356

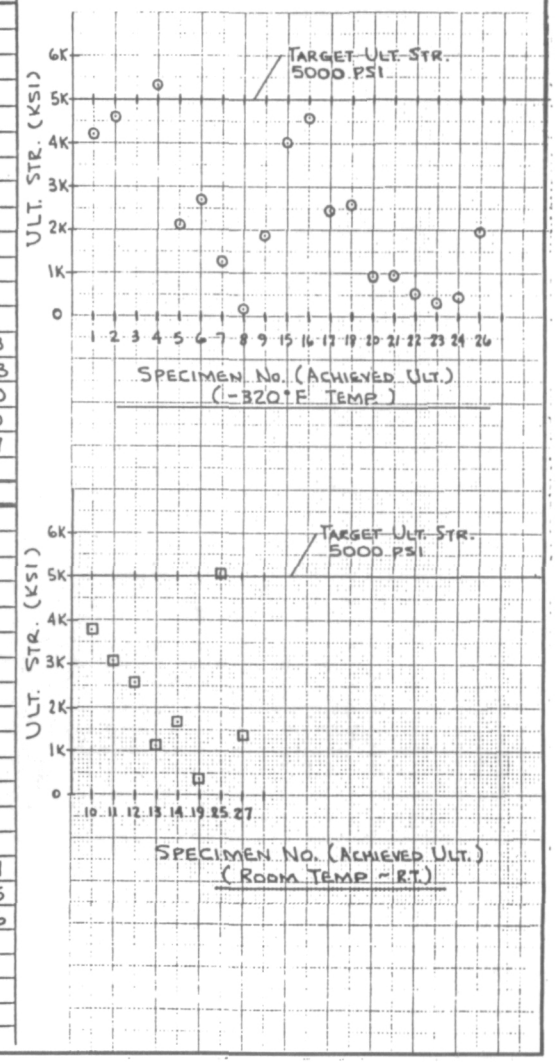

266.635-132

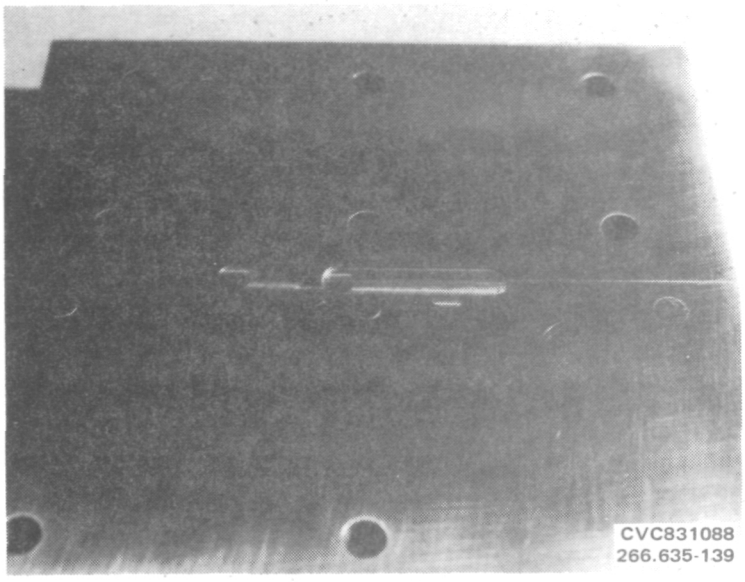

Figure A-14. Laser Welded Joint Specimen

Each joint was designed to maximize strength while minimizing surface imperfections. The joint strength was to be derived from the weld penetration depth achieved. Early studies indicated a maximum depth of 0.025 inch was feasible; however, inspection following the initial tests revealed an average penetration depth of only 0.017 inch.

Testing of the panels included static and cyclical loadings at both ambient and cryogenic (-320F) temperatures. The panels were initially loaded to approximately 50% of the calculated ultimate load at ambient temperature for the purpose of setting up and calibrating the system. Following the above, the panels were subjected to a temperature of -320F and inspected for thermal effects. Cyclical loads were incrementally applied up to the 50% of ultimate level for a total of 1000 cycles. Inspection of the panel for failure or other anomalies followed prior to proceeding to failure loads at the -320F temperature level. Failure of the laser weld occurred along the joint line across the width of the panel at 3600 pounds (of downward load), which produced a moment at the joint of 7200 in-lb. Calculations based upon the above loads and resisting weld area indicated a failure stress level of approximately 85 ksi.

Producing a quality surface at the joint of the welded parts was considered to be as critical to the overall product as the strength properties presented earlier. Laser welding of the parts at the joint created a minor depression along the path of the weld. To produce a quality joint, it was decided to provide a raised (0.010 inch) surface that could be removed by machining after welding. In the panels tested, the raised surface was not produced (for simplicity); however, after welding the joint area surface was machined down until the concavity was removed. An average depth of 0.004 inch was removed

to produce a new "unblemished" surface along the weld joint. This substantiated the design approach taken of using a raised surface for welding purposes to be removed later (see Figure A-15). The weld penetration depth was also checked by machining a pocket into the weld area down to its bottom where the joint line of the parts is visible. The weld penetration depth was clearly defined with this process and verified vendor manufacturing data (see Figure A-14).

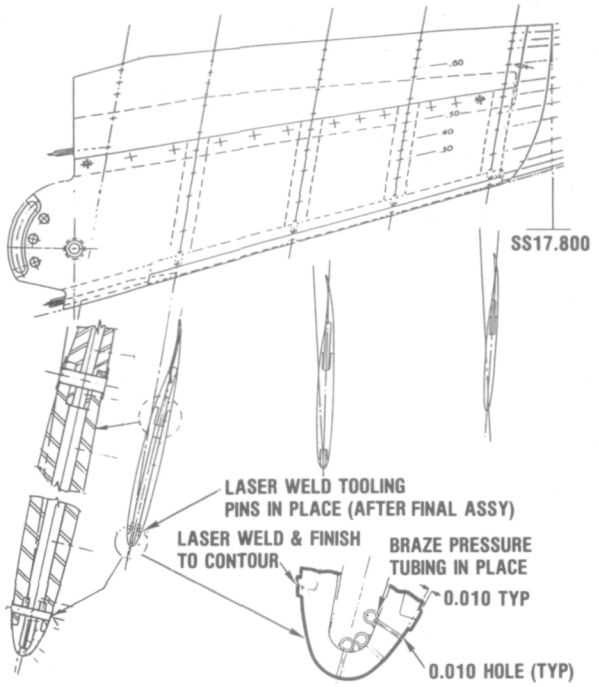

Figure A-15. F-111 TACT Wing - Laser Welding

The failure stress level of 85 ksi is slightly less than the 100-125 ksi level of annealed maraging 200 steel. GDC materials analysis observed that while the laser beam width is relatively narrow (0.010-0.020 inch), the resulting condition of the material adjacent to the weld area is annealed. This condition supports the low ultimate stress level of the failed joint.

The results of the first panel were evaluated and a decision made to continue the research. Subsequent tests were conducted on a panel with an increased weld penetration depth of 0.055 inch. Tests were performed the same as above on the previous panel. The test results indicated failure at 7800 pounds, which produced a moment at the joint of 11,688 in-lb. Calculations again indicated an ultimate stress level of 85 ksi.

The foregoing investigation is not inclusive of all the strength parameters involving laser welding and is therefore not intended to confirm or propose its use without further study. However, the levels achieved would seem to merit additional research and/or proof-of-concept efforts where laser welding may be used in structural applications for NTF cryogenic models.

In considering the use of laser welding for structural purposes in cryogenic models, it is clear that additional effort is required to establish the actual limitations of the process. It should be noted, however, that the process exhibits great potential where permanent joining of parts is necessary. In these cases the joints (crack) can be eliminated, and pins can be retained by laser welding (see Figure A-14). When the depression is removed by machining, the surface finish can be equivalent to the parent metal. In addition the pins are not only retained, but have a tensile strength proportional to the weld area. For a 1/4-inch-diameter pin the tensile value would be 3400 pounds.

A.2.5 ELECTRON BEAM WELDING. Electron beam (EB) welding was investigated briefly as a potential alternative method of joining model components. A simulated wing panel, constructed as an upper and lower section, was machined from maraging 200 steel. The upper and lower panels were seam welded around the perimeter of the plates forming a permanently joined panel.

Excessive heat buildup during EB welding caused warpage and distortion of the upper and lower plates. A discontinuity (surface step) of 0.014 inch resulted due to the excessive heat buildup. Also, the welded area surface finish was irregular and rough with concavities and pit holes.

Although no additional work was accomplished to improve the condition of the wing panel, subsequent discussions with welding engineers indicated that an improvement in the warpage and distortion could be effected by reducing the beam width and input power. It was also felt that a smoothing of the weld surface could be accomplished by rewelding with a "softened" beam and intensity. EB welding has good strength properties and is definitely a suitable candidate for cryogenic models; however, distortion necessitates annealing/aging after welding, and then final profile. For thin pressure wings this would be a costly process, and it was felt that a low temperature/pressure attachment process for a wing cover plate had significant advantages and that further research effort should concentrate in that area.

A.3 SIMULATED WING FATIGUE TESTS

Figure A-16 shows the test fixture used to evaluate simulated wings, filler materials, bolt locking devices, and wing joint specimens. It includes a cryogenic chamber, actuator, load cell, deflection potentiometer, a thermatron for temperature control, and a load system capable of varying frequency and load intensity. Figures A-17 through A-19 show the test setup.

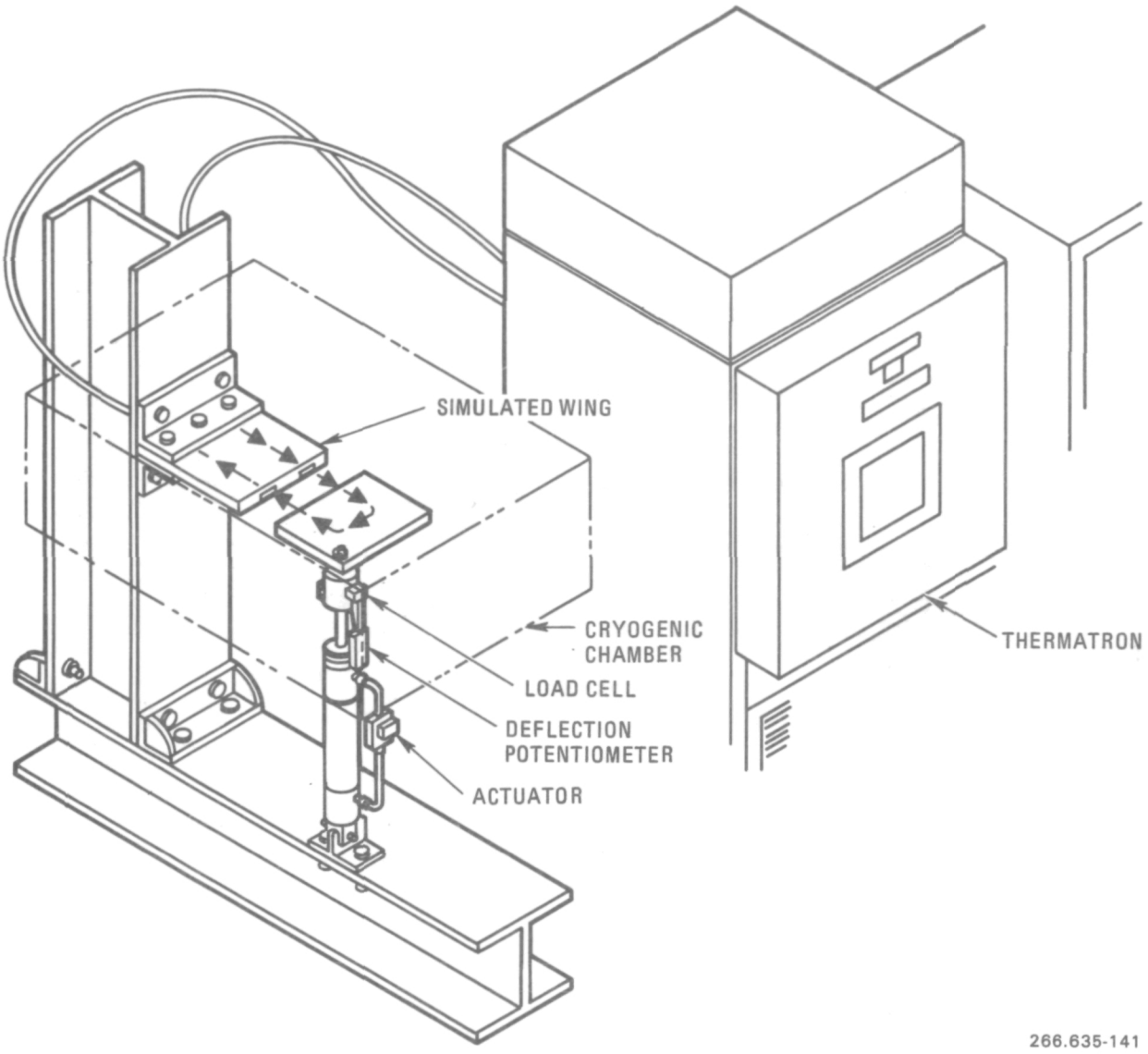

Figure A-16. Simulated Wing Fatigue Test - Cryogenic Temperature

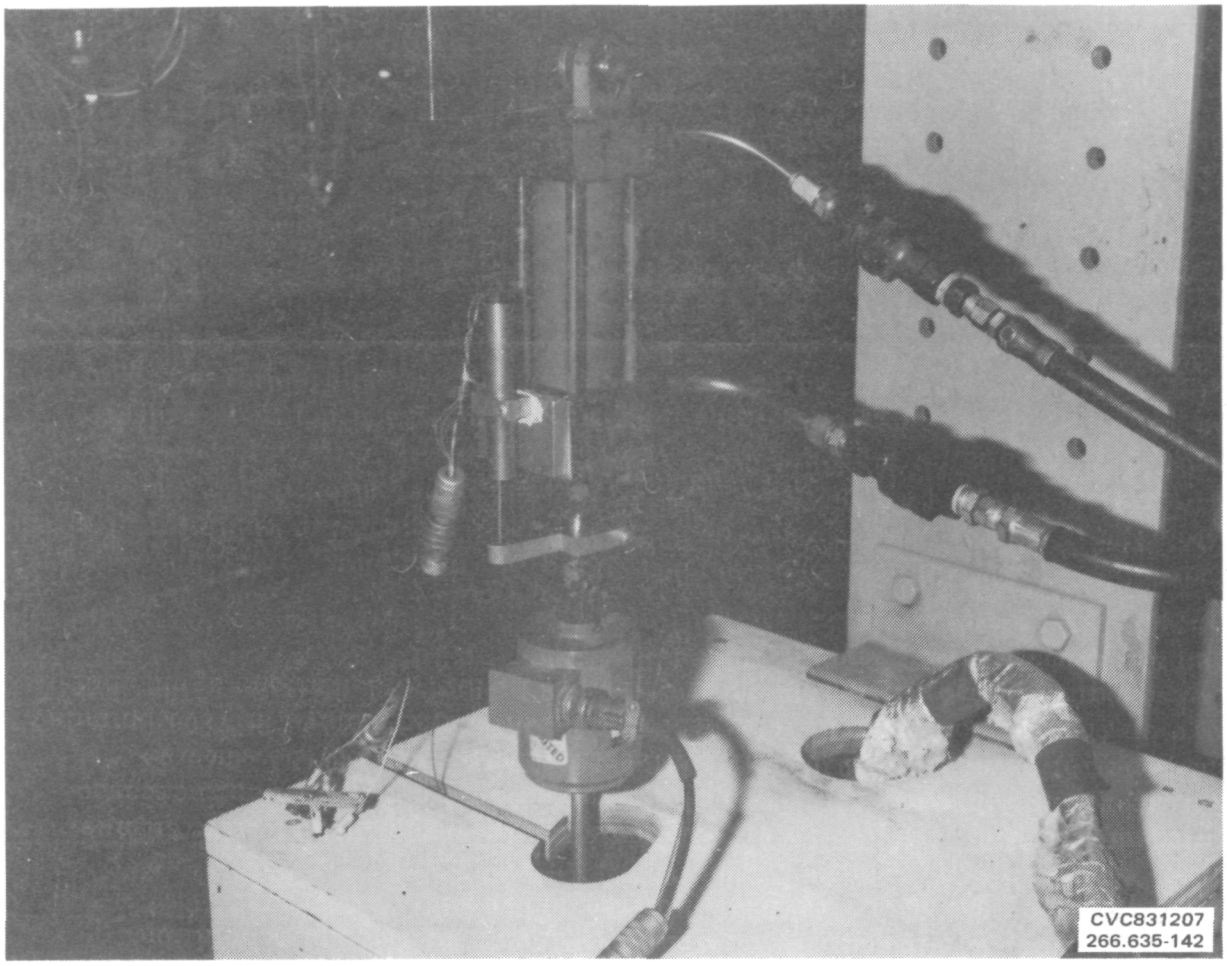

Figure A-17. Fatigue Testing Load Setup

The testing of laser welded wing joint specimens is described in Section A.2.3, filler materials in Section A.4, and screw locking methods in Section A.5. The primary reason for the fixture was fatigue testing of the simulated wing panels. Three panels were constructed of maraging 200 steel with upper and lower panels designed to simulate the structure of the CWC wing. The initial design was based upon the use of diffusion brazing; when this process did not produce the desired results (see Section A.2.1) the panels were modified for electron beam (EB) welding and laser welding. The EB welded panel did warp as indicated in Section A.2.4, and interest centered on the laser welded panel.

The lower panel was recessed into the upper panel similar to the design of the CWC wing, and laser welded around its periphery. It was cantilevered in the fixture, and load was applied at the outer/forward corner to induce twist proportional to that anticipated on the model wing in the NTF. Model stress levels and deflection data were used for that purpose. The wing was subjected to 1000 cycles at 60 cycles per minute. The wing did not fail and visual inspection showed no degradation. The test was conducted at ambient temperature and at -285F.

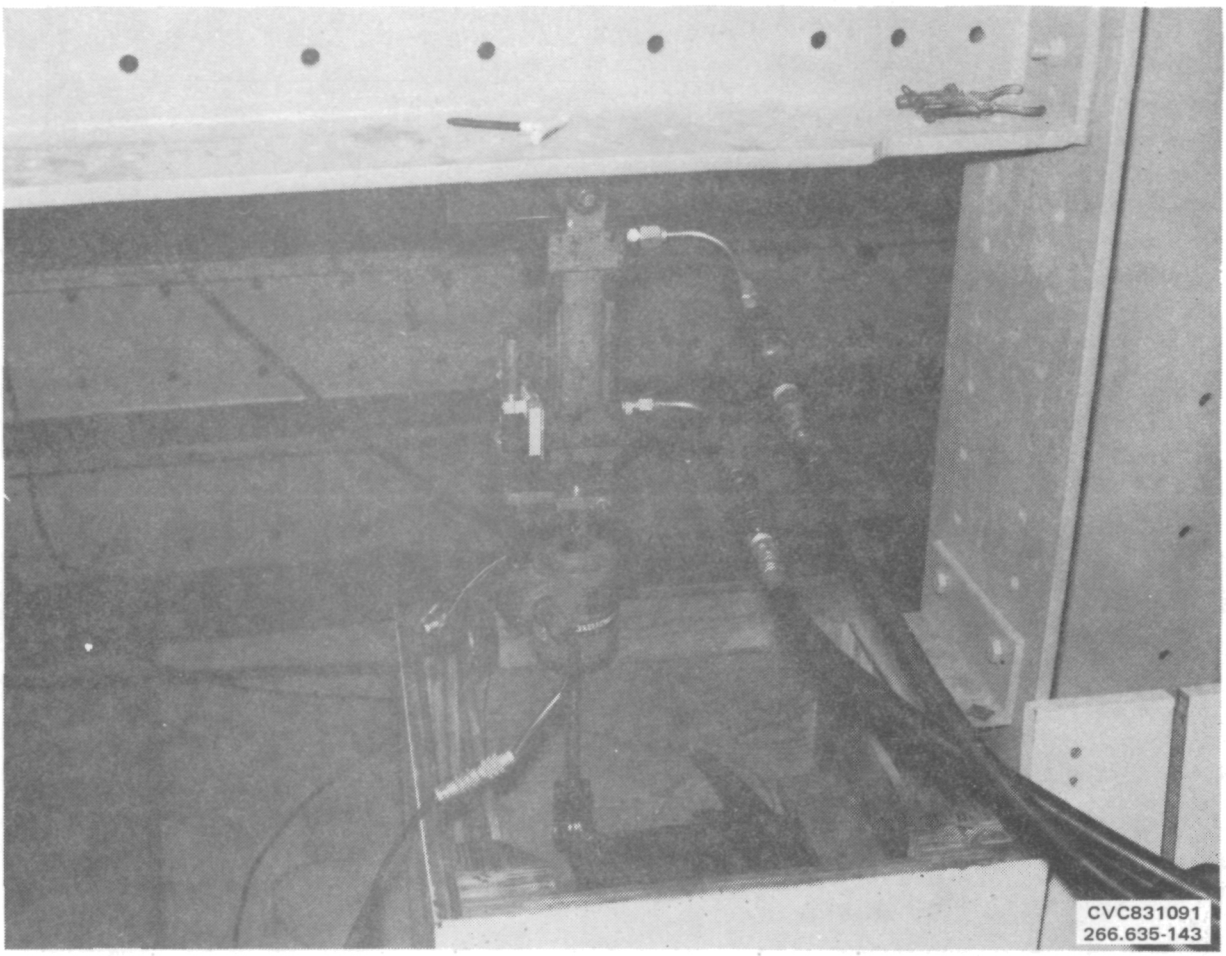

Figure A-18. Fatigue Testing Load Setup

A.4 INSTALLATION OF PRESSURE TUBES

To provide direct correlation with previous models of the same scale/configuration, pressure data requirements and therefore tube locations are required to be identical to those models. A total of 120 wing pressure orifices and 46 fuselage pressure orifices will be installed in the CWC wing and fuselage. Similarly the F-111 TACT configuration will consist of 119 wing pressures and 23 fuselage pressures on the fuselage and over-wing glove surfaces. In both configurations, the upper/lower pressure orifices will be separated with all of the upper surface taps located on the left hand wings and the lower surface taps on the right hand wings. Figures 5-12 and 5-20 and Tables 5-2 and 5-3 of the basic report depict the pressure orifice locations.

During preliminary design several methods of preparing and installing pressure taps were discussed. Many were conventional in application; others were new ideas requiring study and implementation to prove the concepts.

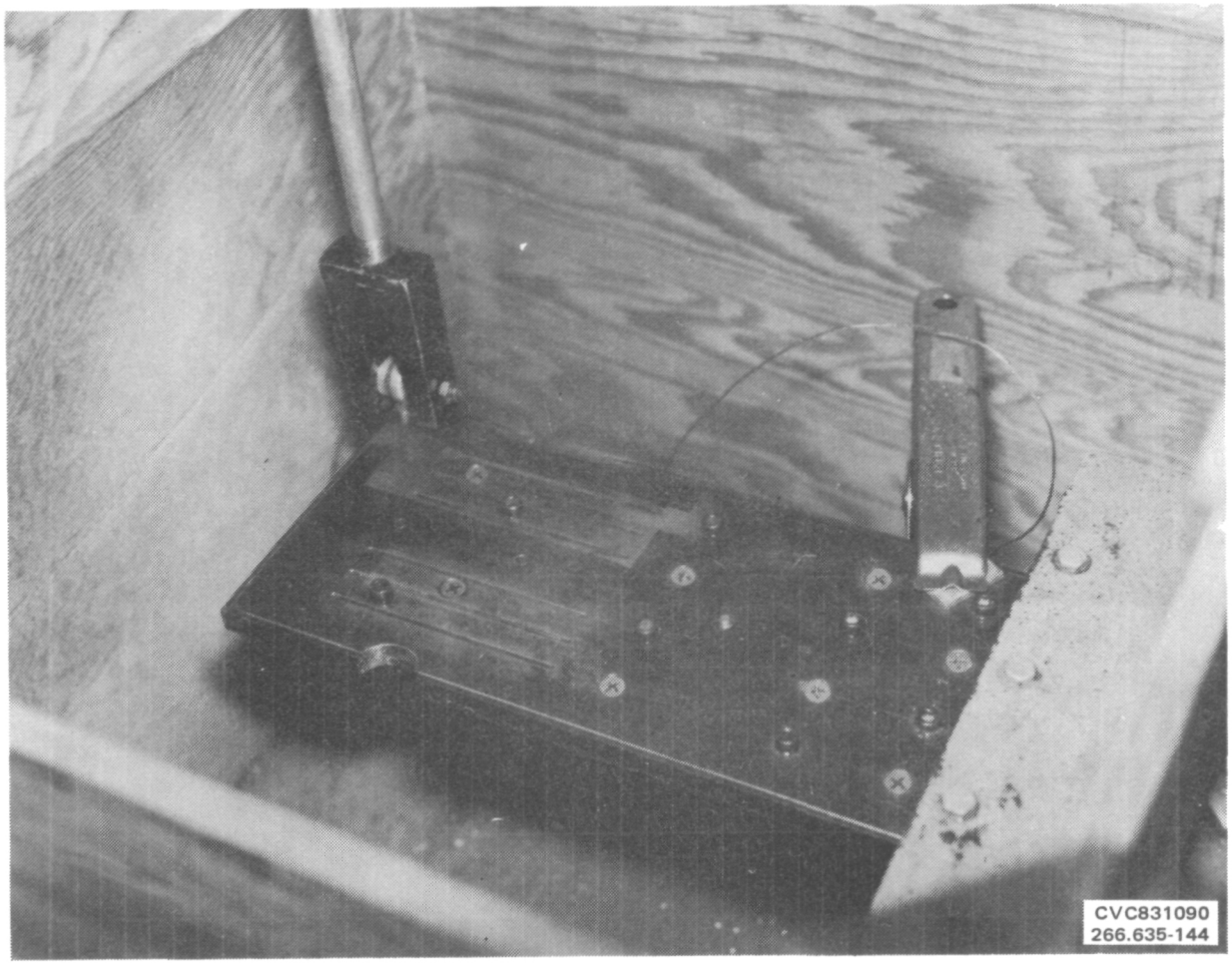

Figure A-19. Fatigue Testing Load Setup

Below is a listing of several pressure tube installation concepts (see Figure A-20).

a. Drill for conventional tube, braze outer diameter in place.

b. Tubes inlaid in surface grooves routed and potted in place.

c. Brazed plugs to tubes that are potted or brazed in place.

d. Laser weld plugs to tubes, and laser weld in place.

e. Braze/weld plugs and tubes, oven braze.

f. Similar to d and e, using porous plugs.

g. For composite wings, molded-in-place tube routing channels with orifices drilled into channel (using lost wax technique).

h. Mill channels in wing surface, attach a cover plate, finish profile, drill orifices.

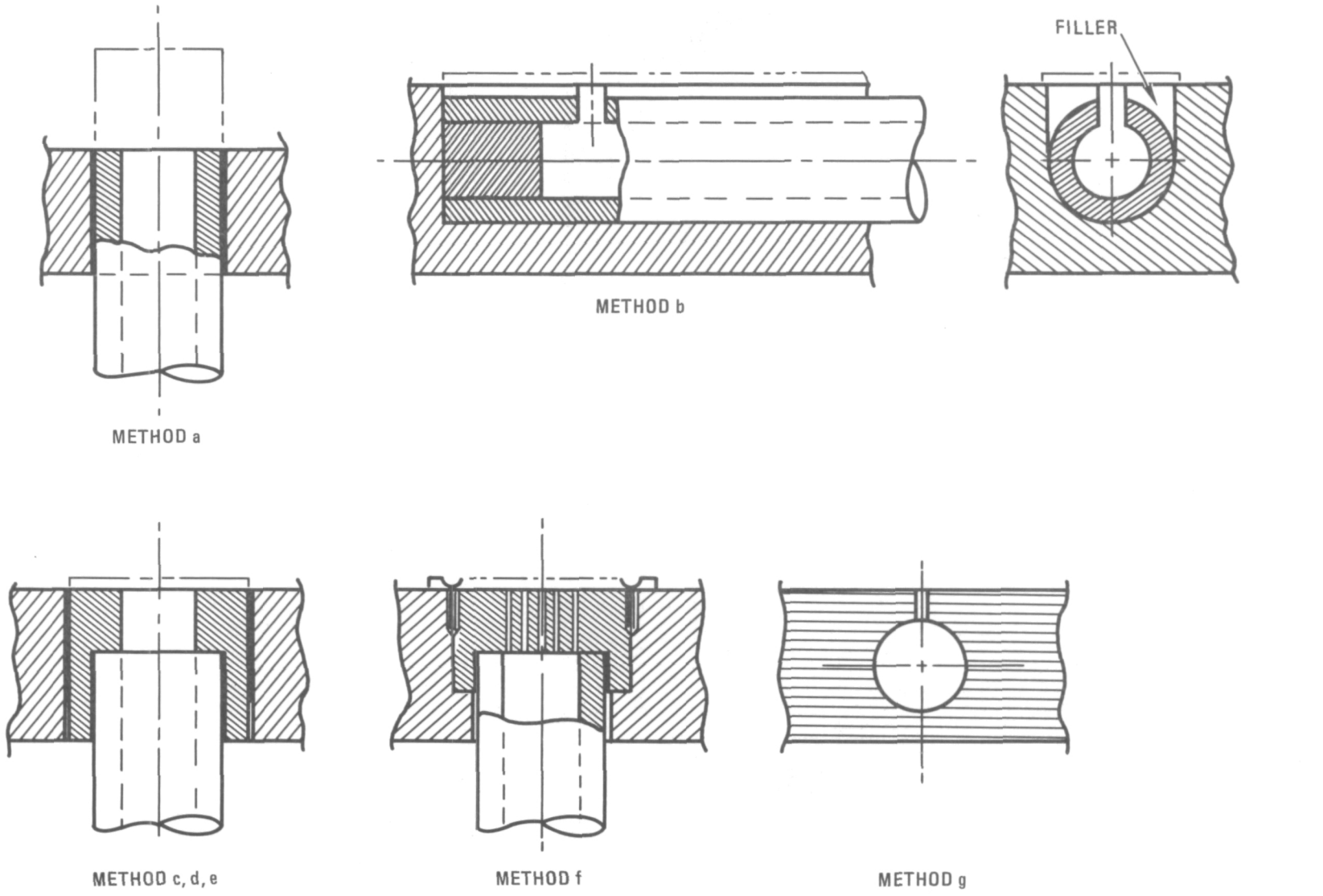

Figure A-20. Pressure Tube Installation Methods

During the proof-of-concept studies conducted on simulated wings (diffusion brazing and laser welding), preliminary work involving methods a, b, c, and f was initiated. The work was largely investigative and included some installation work with methods a and b.

In method a, pressure tubes were installed in the conventional manner where tubes are placed into holes slightly (0.003 inch maximum) oversize and extended above the surface to allow for trimming and finishing to contour after silver brazing in place.

Method b involved machining grooves into the external surface, allowing a minimum of 0.010 inch additional depth to bury the tube completely and surface fill over it. Various filler materials were used including Devcon A and F (steel and aluminum), EA 934, Hysol Epoxy-path, Kwik-Kure, Nickel Flame Spray, and others (see Section A.5).

Method c uses pressure tubes brazed into plugs. A small (0.010 inch) diameter hole is drilled into the plug, creating a small orifice leading into the pressure tube. The assembly is then fitted to the wing, and brazed.

Method d is similar to method c except that laser welding is used for assembly. Here the wing must be left 0.010 inch full to allow for removal of the depression caused by welding. With this process conducton of heat into the wing is well controlled with little effect on the strength of the wings.

Method e is a process that has been used previously in cryogenic applications and presents no significant problems. This process requires the pre-assembly of brazed plugs and tubing combined with oven-vacuum brazing in place.

Method f was an investigative study only; however, the facts gathered support this method as being feasible. In this process, holes are drilled to match the tubing as in method a. A slightly larger diameter counterbore is drilled to create a small plenum at the tube entrance. A shallow spotface (0.020 to 0.050 inch deep) slightly larger in diameter than the plenum is made, into which the porous plug is placed and joined by brazing or laser welding. The porous plug is fabricated using electrodischarge machining (EDM) to create a matrix of holes 0.005 inch in diameter. Approximately 10-15 holes may be EDM drilled per plug.

Method g has been used successfully at General Dynamics Fort Worth Division in non-cryogenic applications. Composite wings are quite suitable for the NTF environment, and the process should be acceptable. This method is very appropriate for thin wings. Individual pressure channels are molded in the wing using the "lost wax" technique. The wax is melted, leaving clean and separate ducts. Each duct becomes a flow channel for the 0.010 inch diameter pressure orifice.

Method h is particularly suitable for thin trailing edges in steel wings. Individual pressure tube slots are milled in the wing, a thin cover plate is brazed in place, the wing profile is completed, and a 0.010-inch-diameter hole is drilled into each groove. The cover plate would normally be oven brazed to ensure separation of the ducts.

An investigation of the various methods presented above provided no clear "best" method for all situations, but rather provided a selection list from which a process could be taken to meet a need. Conventional methods offer very usable solutions to many general purpose pressure tap installations. Special cases will require sufficient review and/or investigation to ensure best results.

A.5 FILLER MATERIALS AND SEALANTS

The need for a quality surface finish is described in Section 5.3. In addition to requiring a good finish, the model component buildup needs special care to minimize additional roughness due to gaps, mismatches, and screw head recesses. In essence a filler material is required, the surface finish of which must be consistent with the primary model material. The development of an acceptable model surface filler material for use in a high pressure/cryogenic wind tunnel is extremely important.

Such a filler material must possess the characteristics of tenacious adhesion, quick removal, and a smooth hard finish. Application should be simple and cure time short. These characteristics must be maintained over a broad temperature range.

As a part of this study, various commercially available materials were reviewed. In many cases the above characteristics were met except for use in a cryogenic environment. An experimental program was needed to verify the integrity of each filler material at cryogenic temperatures.

The following is a list of materials selected for this study:

a. EA 934 two-part adhesive

b. DEVCON A - steel-filled potting compound

c. DEVCON F - aluminum-filled potting compound

d. DEVCON EPOXY - two-part, 5 minute sealant

e. HYSOL EPOXY PATCH - two-part potting compound

f. KWIK KURE EPOXY - two-part potting compound

g. WELCO SR/UNIBRAZE 415 - tin/silver solder

h. BAKING SODA/910 adhesive

i METCO 447 nickel flame spray deposited

The simulated wings described in Section A.2 were modified to include typical slots for burying pressure tubes, and countersinks and counterbores for screw heads. The simulated wings were of maraging 200 steel, aged to 200 ksi (see Figures A-21 and A-22).

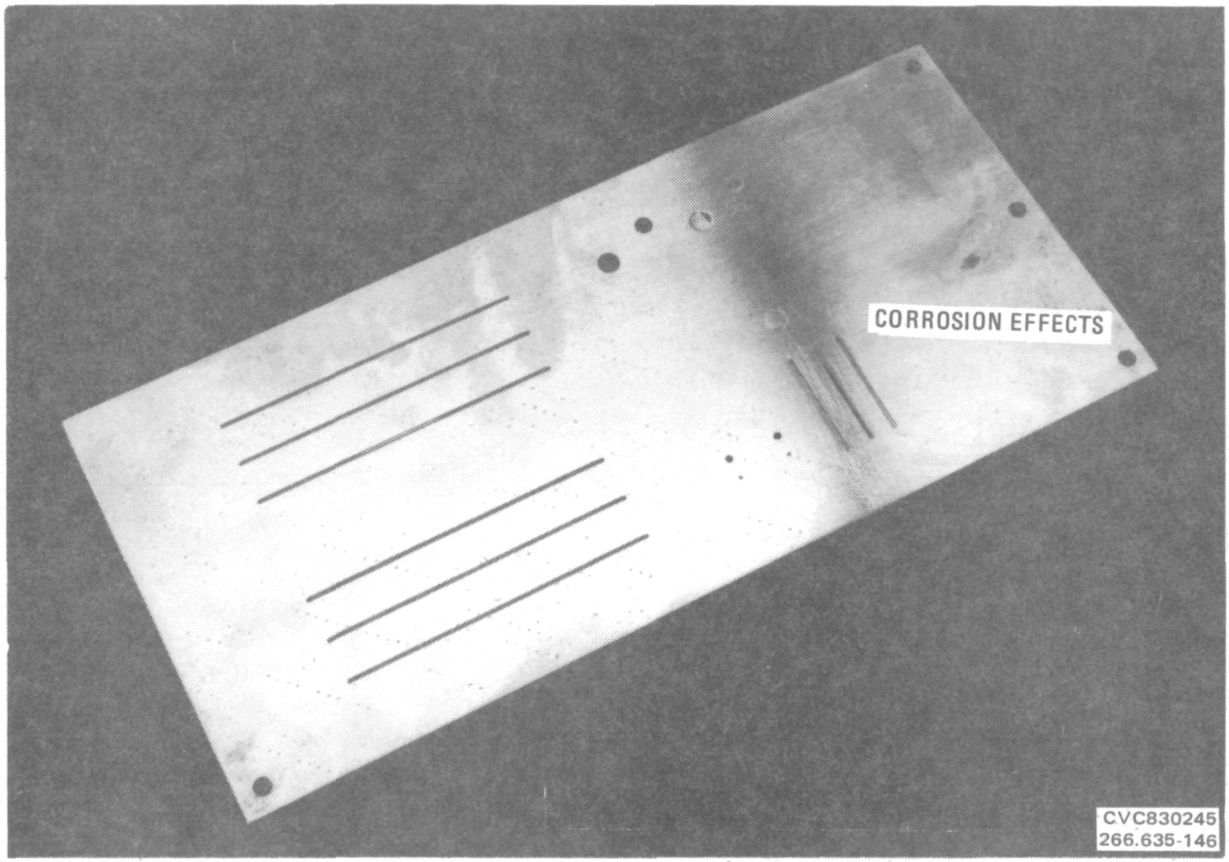

Figure A-21. Filler Materials

Each specimen was subjected to deflections and loads at room temperature and -320F. Cyclical loads were applied at a rate of 60 cycles per minute for 500 cycles at both ambient and -320F temperatures. The wing cover plate was deflected to ±0.25 inch, which required a load of ±50 pounds. The wing main plate was also deflected to ±0.25 inch, requiring a load of 108 pounds due to its greater stiffness.

Each plate was inspected at 250 cycle intervals for damage and/or deterioration of the filler materials.

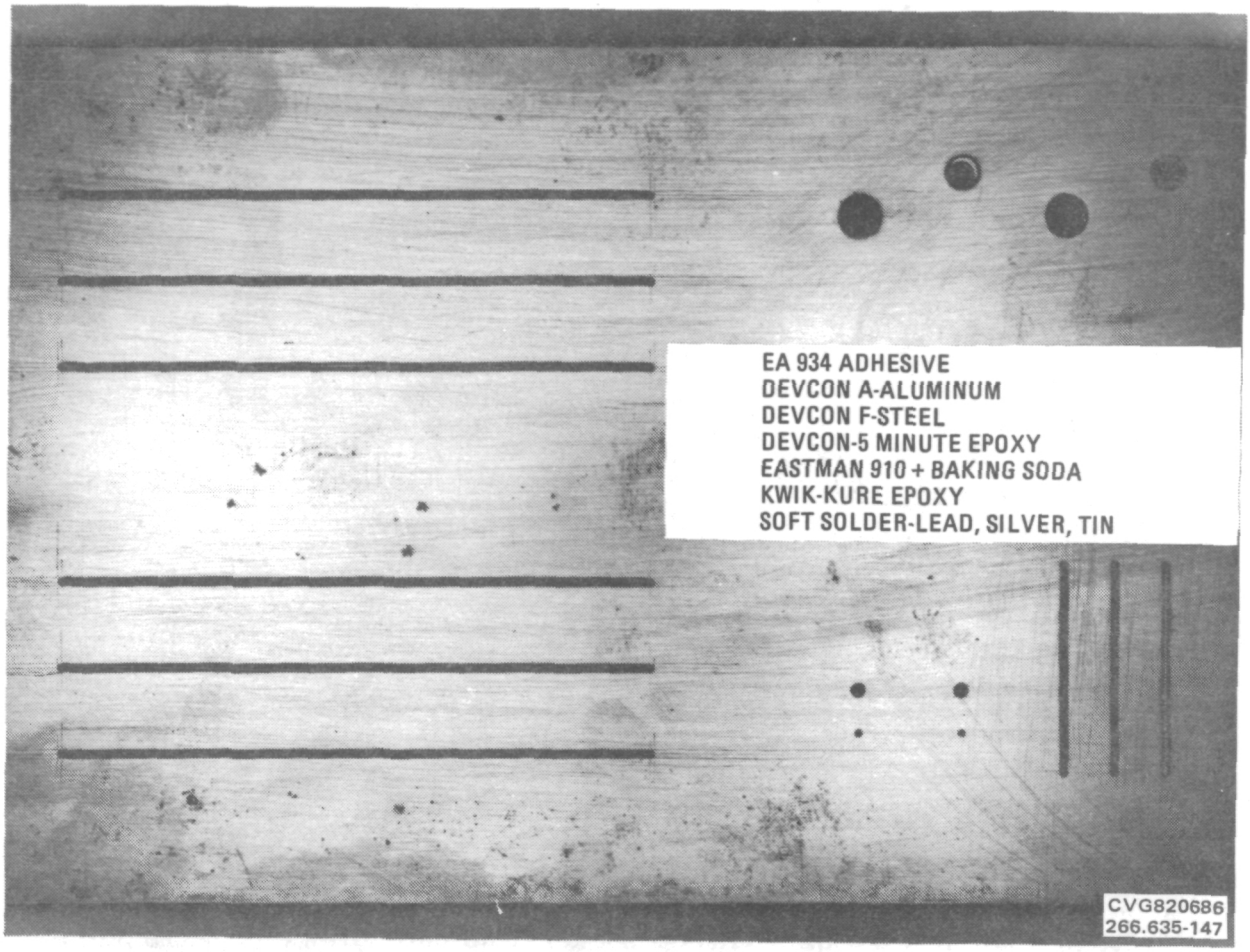

Figure A-22. Filler Materials

Table A-4 depicts the various materials tested and their characteristics as defined by requirements stated earlier. Several materials were found to be acceptable for use with minor negative factors; however, Devcon Epoxy five-minute applicator and Kwik-Kure, also an epoxy-base short-term cure, were rated highest. Several other materials exhibit potential, but require additional testing.

A.6 ATTACHMENT SCREWS - LOCKING METHODS

NTF models will be highly stressed, and the need for retaining attachment screws in development models is critical to the safety of the facility. A study of locking methods was conducted, using simulated wing panels, at ambient and cryogenic temperatures.

The simulated wing panel was a two-piece maraging 200 steel specimen "seam" laser welded around its perimeter. Internally machined areas provided joining surfaces between the upper and lower plates.

Table A-4. Various Filler Materials and Their Characteristics

	EA 934	STEEL DEVCON	ALUM DEVCON	HYSOL EPOXY-PATCH	DEVCON EPOXY (5-MINUTE)	KWIK-KURE	TIN/SILVER SOLDER WELCO SR UNIBRAZE 415	FLAME SPRAY NICKEL METCO 447	BAKING SODA AND 910 ADHESIVE
EASILY REMOVED					✓	✓		✓	
BEST FINISH	✓				✓				
EASE OF INSTALLATION	✓	✓	✓	✓	✓	✓			✓
FURTHER RESEARCH NEEDED					✓			✓	
EASE OF HANDWORK	✓	✓	✓	✓	✓	✓			
POST-TEST DETERIORATION						✓	✓		
CLEAR FINISH					✓				
ADHESION AT 78K	✓	✓	✓		✓	✓			

266.635-148

Size 10-32NC, Flat Heat Torque-Set and socket head cap screws of A-286 and alloy steels, were used to fasten the plates in the above joining areas.

The specimen was prepared by drilling, tapping, and countersinking for the 100-degree angle flat head and socket cap screws. Sixteen fasteners were installed with eight each being flat head torque-set and socket head cap screws (see Figure A-23).

The following methods of retaining screws were planned and provisions made for their implementation:

a. Nyloc inserts (through body)

b. M-bond adhesive under head of screw

c. Lock-tites No. 242, 271, and 290

Fasteners without retainers were initially installed and torqued to 30 in-lb at ambient temperature (Table A-5). The temperature of the specimen was then lowered to -220F and the torque rechecked. It was found to have increased approximately three to four times the 30 in-lb originally set. Also, the torque of several screws could not be checked due to slippage of the wrench.

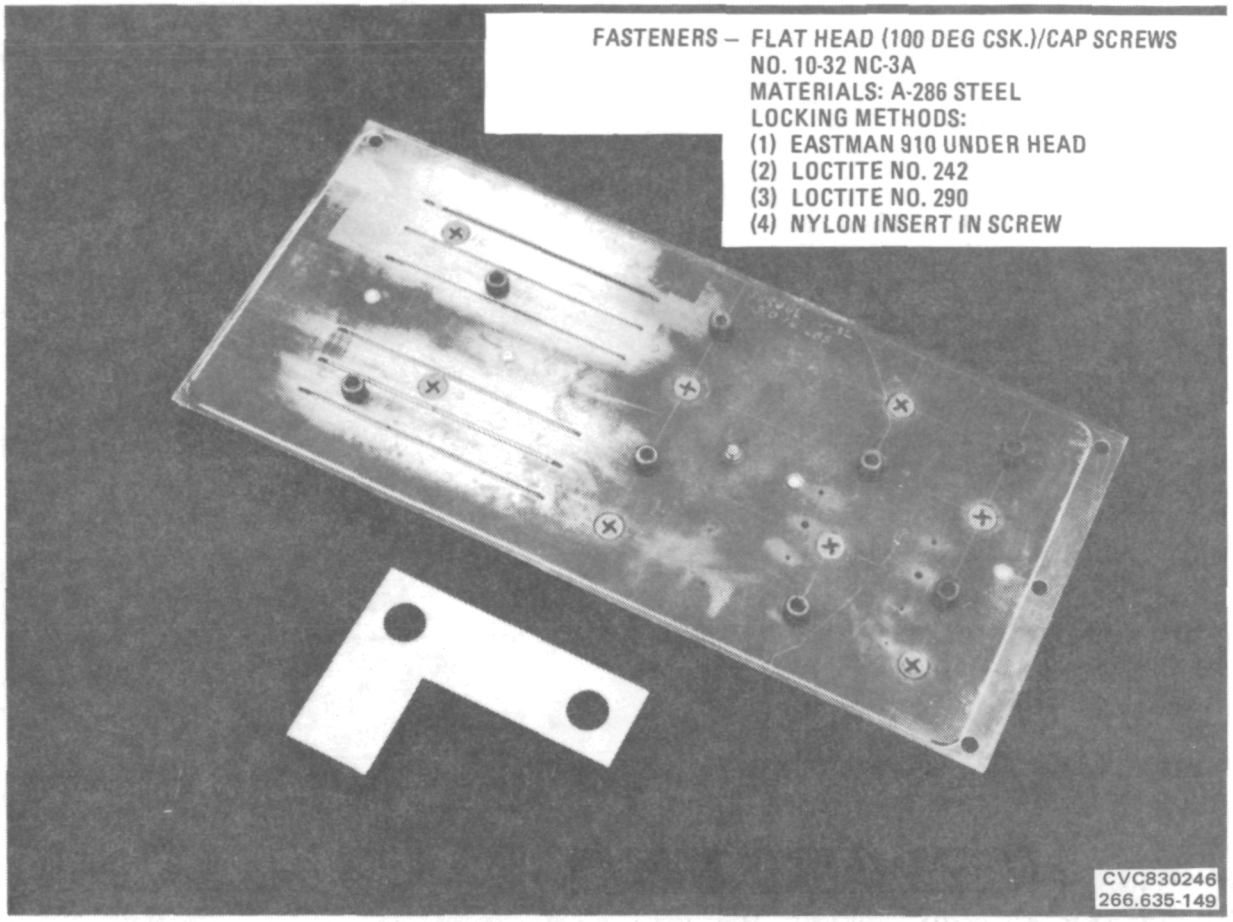

Figure A-23. Screw Locking Methods

The specimen was returned to ambient temperature and the torque rechecked. The values ranged from 30 to 60 in-lb.

Again the panel was subjected to a low temperature of -285F, resulting in increased torque levels up to 125 in-lb. Subsequent runs at -220F and room temperature resulted in similar patterns of increased torque at low temperature and near normal levels at ambient temperatures. During the final low temperature run of -220F the specimen was cyclically loaded through 1000 cycles. Upon completion the torque was again checked at -220F, and the results indicated high torque levels again up to 135 in-lb (see Figures A-17 through A-19).

Analysis of the test data indicates that the shrinkage of a bolt over its length is much more critical than the reduction in diameter. The differential in coefficient of thermal contraction between the bolt material (A-286) and the simulated wing (maraging 200) created a binding effect on the threads at the lower temperature, acting in a similar way to a spring washer under a bolt head (a proven locking method).

Table A-5. Screw Torque Levels at Ambient and Low Temperatures

SCREW NO.	3/23/83				3/25/83							
	TEMP. (F)	TORQUE (in-lb)	TEMP. (F)	TORQUE (in-lb)	TEMP. (F)	TORQUE (in-lb)	TEMP. (F)	TORQUE (in-lb)	TEMP. (F)	(B) TORQUE (in-lb)	TEMP. (F)	TORQUE (in-lb)
1	AMB.	30	−220	(A)	AMB.	30	−285	(A)	−220	(A)	AMB.	35
2	AMB.	30		110	AMB.	55		85		120	AMB.	85
3	AMB.	30		100	AMB.	60		105		120	AMB.	70
4	AMB.	30		(A)	AMB.	35		85		(A)	AMB.	35
5	AMB.	30		(A)	AMB.	30		(A)		(A)	AMB.	25
6	AMB.	30		85	AMB.	50		95		90	AMB.	75
7	AMB.	30		85	AMB.	40		90		80	AMB.	60
8	AMB.	30		(A)	AMB.	40		85		100	AMB.	45
9	AMB.	30		(A)	AMB.	30		70		100	AMB.	35
10	AMB.	30		(A)	AMB.	35		125+		(A)	AMB.	35
11	AMB.	30		85	AMB.	40		95		95	AMB.	60
12	AMB.	30		95	AMB.	45		125		135	AMB.	95
13	AMB.	30		80	AMB.	35		115		120	AMB.	75
14	AMB.	30		85	AMB.	50		100		95	AMB.	65
15	AMB.	30		(A)	AMB.	30		105		(A)	AMB.	30
16	AMB.	30	−150	(A)	AMB.	30	−164	75	−150	80	AMB.	35

(A) NO READING, SLIPPAGE BETWEEN WRENCH AND SCREW HEAD

(B) AFTER 1000 CYCLES

266.635-133

It is apparent that the use of dissimilar materials such as A-286 bolts in a maraging 200 wing can result in a problem of too much torque at low temperature, thereby weakening the bolt. In addition, if the test plan calls for a range of test temperature from ambient to cryogenic, the bolts may need to be tightened at the ambient temperature, and loosened at cryogenic temperature, not a practical solution.

It is recommended that any critical bolts/screws be made of maraging 200 and locked by one of the methods indicated above.

A.7 EFFECT OF CABLE CROSSING THE BALANCE

Calibration and checkout of the model, balance, and support system is a standard requirement, part of which is checking out the effect of the instrumentation cable crossing the balance.

In conventional models the cable remains flexible at ambient temperatures, and a loop or spreading of the cable is often sufficient to eliminate cable effects on the balance. In a cryogenic environment, however, the cable is routed through an unheated model, and becomes very stiff. In this simple test a mockup of the F-111 TACT cable was set up with a sensitive load cell. Model offsets and anticipated cable resistant points were included. Relative movement between the cable clamp (model) and the cable clamp (sting) was provided in three planes: axial, vertical, and side. As shown in Figure A-24, the cable mockup was enclosed in a cryogenic chamber, and the load cell was insulated from the low temperature.

The results of the close coupled clamp arrangement are shown in Figures A-25 through A-27. Data for a longer unsupported cable is shown in Figure A-28. The results for the close coupled clamp are more realistic; the passage for the cable on the F-111 TACT is restricted, and there is no room for looping.

Reviewing the results: 1) a relative axial movement of ±0.06 inch may cause an error of 1-5 pounds of axial load, 2) vertical movement of 0.10 inch an error of 0.70 pound of axial load, 3) side movement of 0.10 inch an error of 0.20 pound of axial load, and 4) change of length of cable due to change from room temperature to cryogenic caused an error of 0.90 pound of axial load. This is not a conclusive test, and of course it is very configuration sensitive. It does show, however, that routing the instrumentation cable is much more critical for an NTF model and if not done correctly will cause unacceptable balance errors.

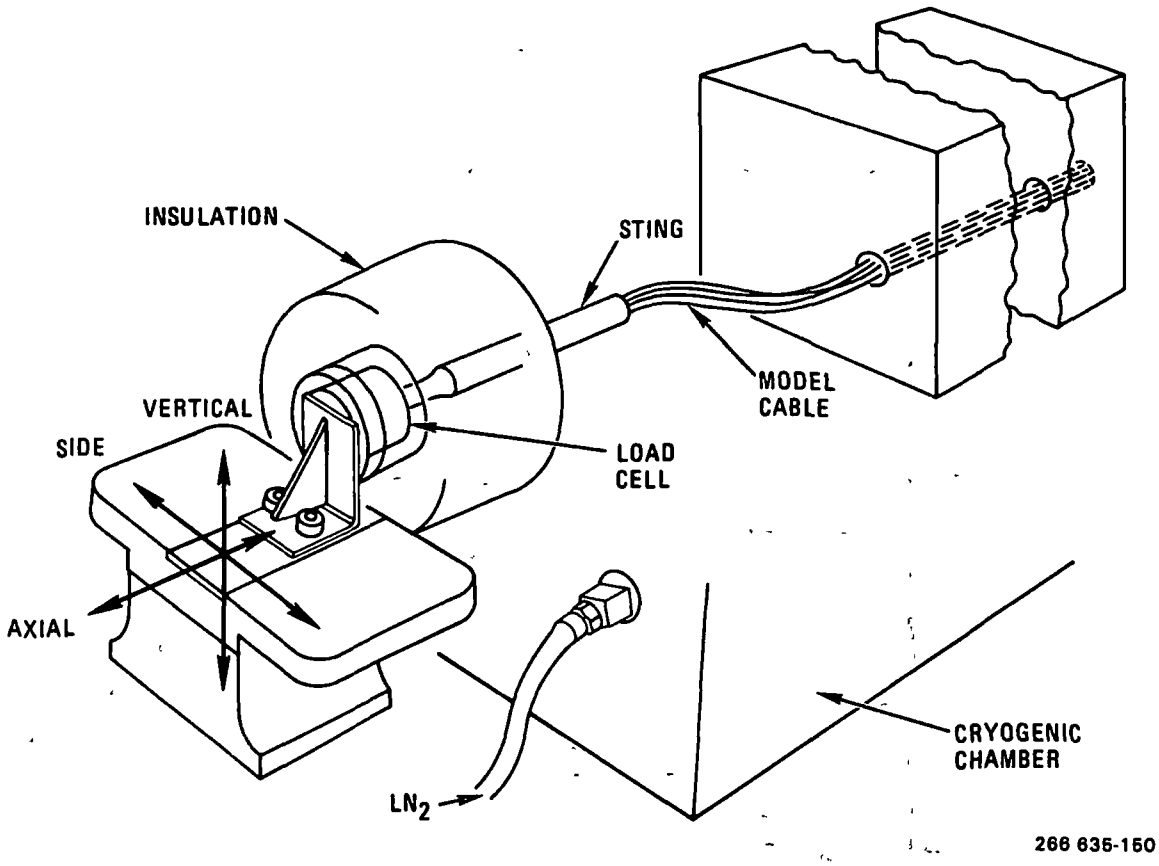

Figure A-24. Model Cable Cryogenic Test

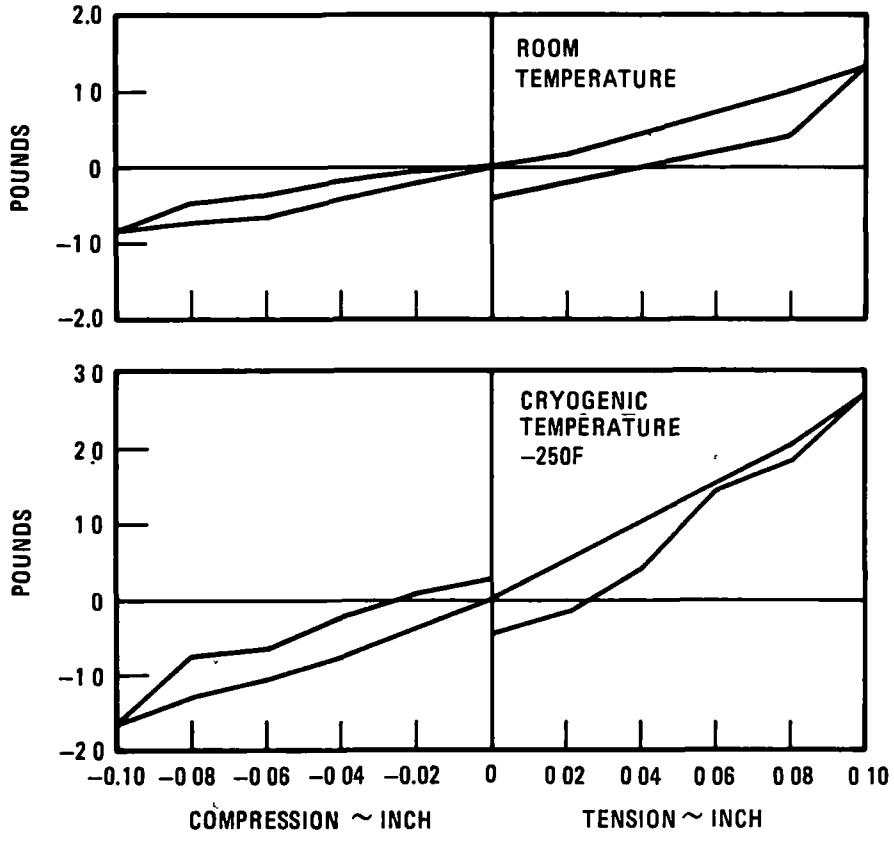

266 635-151

Figure A-25. Effect of Axial Movement

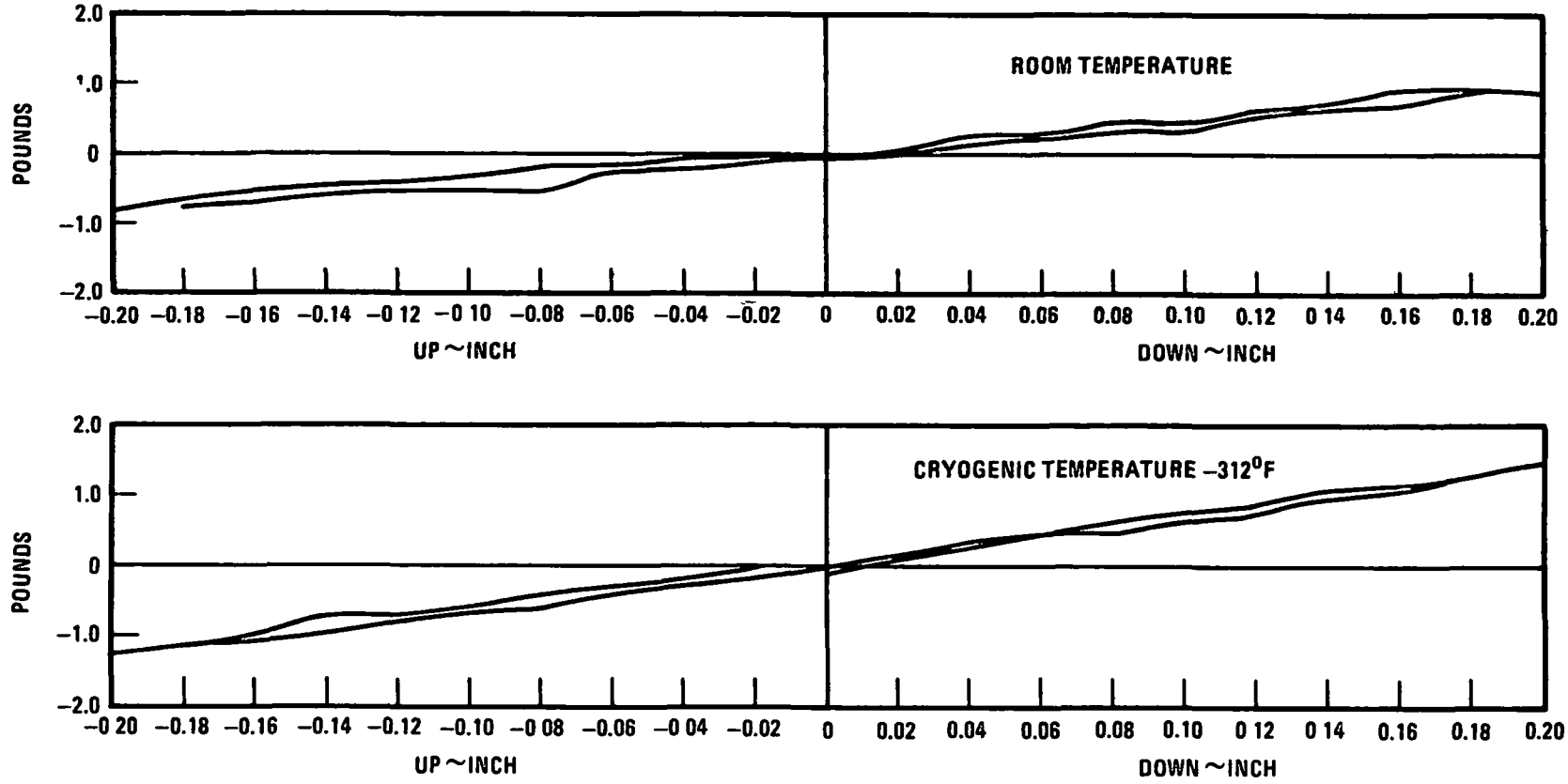

Figure A-26. Effect of Vertical Movement

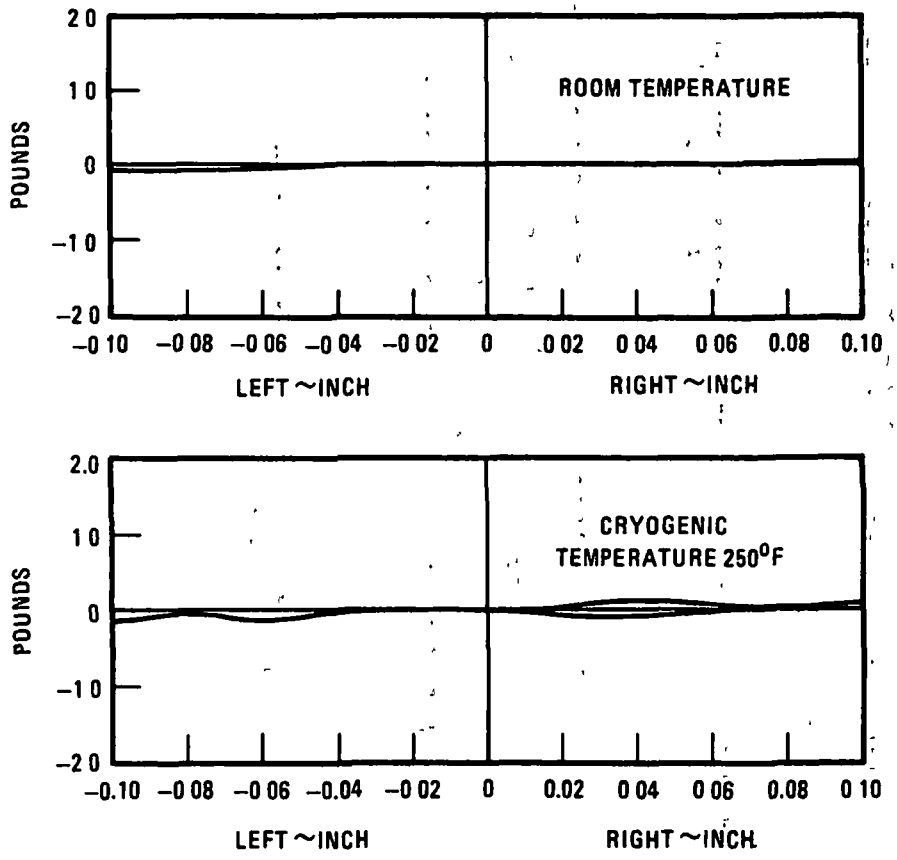

266 635-153

Figure A-27. Effect of Side Movement

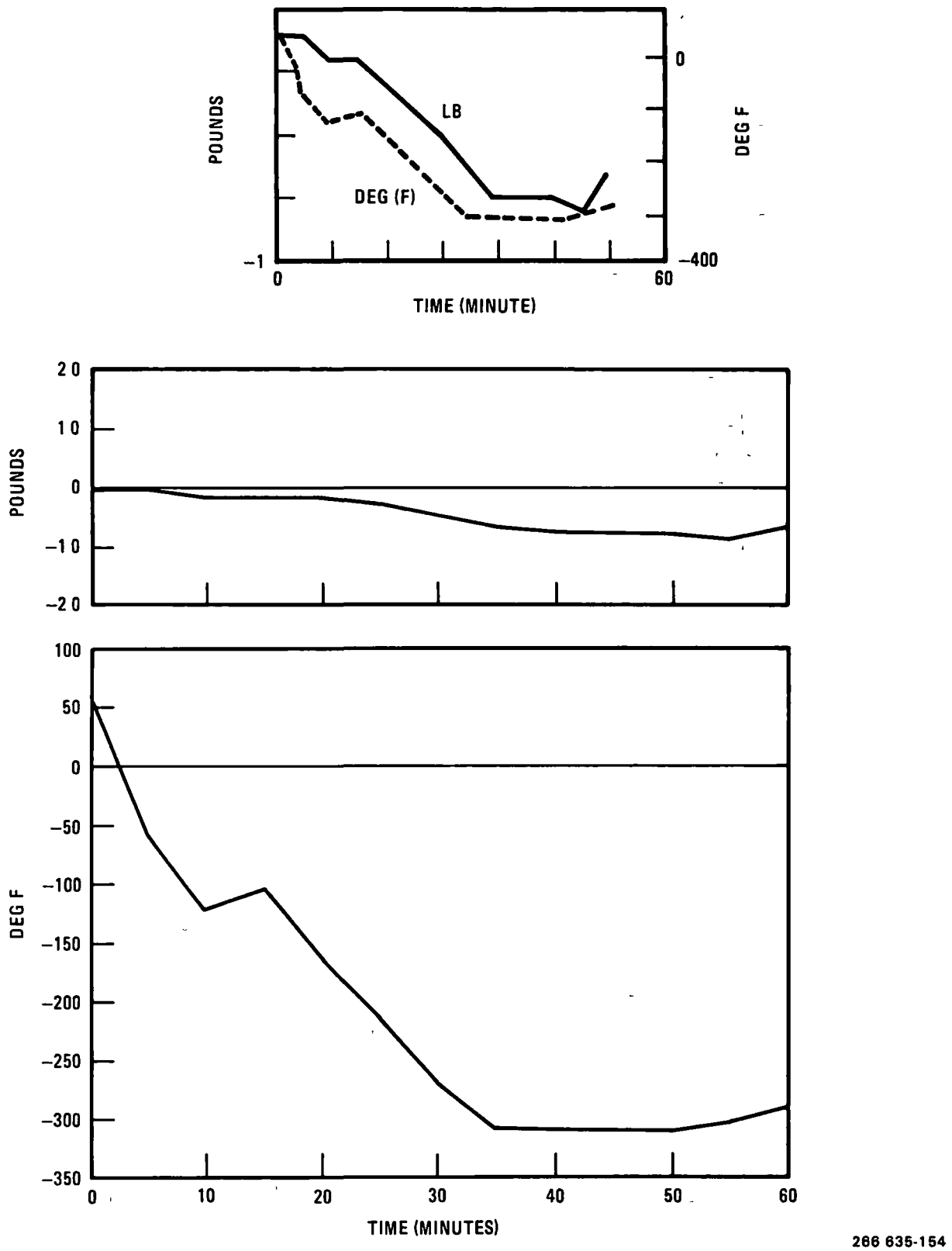

Figure A-28. Error Due to Cable Contraction

APPENDIX B

FEASIBILITY STUDY OF A 1/20 SCALE STATIC AEROELASTICALLY SIMILAR, F-111 TACT WING

Efforts were undertaken at the General Dynamics Fort Worth Division to investigate the design and manufacturability of a 1/20-scale F-111 TACT flexible wing for the NTF. The wing design had to conform to the NASA criteria, Reference 1. The emphasis of the study was designability with efforts broken up into three areas.

- Model design and analyses were accomplished for the 26-degree leading edge sweep configuration.
- Material testing was performed in coordination with the design effort.
- A proof-of-concept phase was planned for a representative component; however, it was not completed due to budgetary and fabrication problems.

B.1 MODEL DESIGN AND ANALYSES

The F-111 TACT flexible wing and wing carrythrough-structure design includes considerations for static aeroelastic similarity, wing instrumentation, and fabrication concept. The focus of the study included the 26-degree leading edge sweep configuration and a critical load design condition at Mach 0.9, 10,000 feet, and 7.33g. However, the results of the study produced a design (Figure B-1) that consists of a "soft-skin" flexible wing-structure in which the wing steel spar is machined to a pivot fitting at the wing root, and is combined with an F-111-type carrythrough structure to provide variable sweep. Instrumentation in the wing is carried in the bondline between low stiffness skins and the spar. Analyses at the design condition show that the spar primarily provides the static aeroelastic similarity of the full scale F-111 TACT wing box while the entire wing structure maintains its integrity in terms of strength and flutter. Fabrication methods were explored throughout the design process by examining the viability of controlling contour tolerances and surface finishes as well as manufacturability. A fabrication concept that includes secondary bonding of pre-cured skins to the steel spar is proposed.

B.1.1 CONCEPTUAL DESIGN. The F-111 TACT flexible wing and wing carrythrough-structure design was selected from four design approaches that were developed and analyzed. These approaches are displayed in Figure B-2. The selected approach, shown in Figure B-1, is viewed at the bottom of Figure B-2. It was the only configuration that could simultaneously meet the strength and static aeroelastic similarity (i.e., stiffness) requirements for the wind tunnel design condition. The upper two design concepts include a stress-skin

SKINS (181-75 GLASS EPOXY)	
PLIES	SURFACE
4	FORWARD OF 60% SPAR
9	CUSP REGION (AFT OF 60% SPAR)

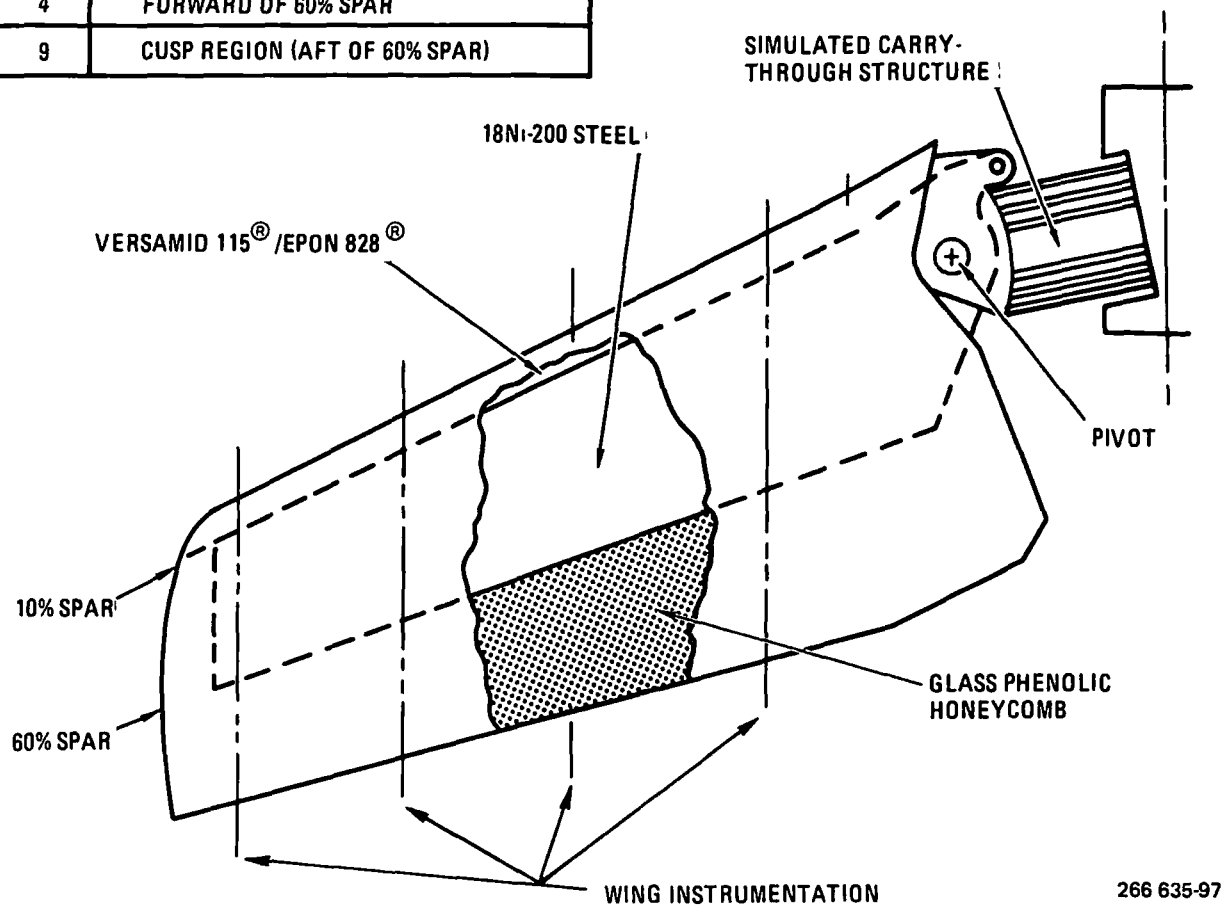

Figure B-1. F-111 TACT Aeroelastically Similar Wing Concept

approach, and although the stiffness requirements were achievable, the load could not be taken internally. These two concepts are similar to those that were employed successfully in previous F-111 TACT flexible models (Reference 1). In the third concept, it was determined that a closed graphite-epoxy torque-tube would take the load internally, but could not meet the stiffness requirements. The driving aspect in this study is the design dynamic pressure ratio of the model to the full scale. This ratio, 4.899, dictates that the model must carry large loads internally while simultaneously maintaining deflections one-twentieth of full scale.

B.1.1.1 Primary Design Tool. Preliminary design concepts were developed primarily for the wing from the pivot area outboard. The TSO procedure (References 27 and 28) was used to generate flexibility influence coefficients, stress analyses for a trimmed airplane configuration, and a matched-point flutter analysis of the wing at the Mach 0.9 flight condition. TSO is an interdisciplinary design program combining aerodynamic, static aeroelastic, flutter, and structural calculations to provide optimum composite and metal wing skin thickness distributions and ply orientations that satisfy specified design constraints.

DESIGN APPROACH	STRENGTH/STIFFNESS ANALYSIS	
BONDED ASSEMBLY, HONEYCOMB CORE, LAMINATED SKINS	• GRAPHITE EPOXY SKINS GOOD FOR TWICE DESIGN LIMIT LOAD • NOMEX®, PHENOLICS, AND ALUMINUM HONEYCOMB CORES CANNOT WITHSTAND LOAD	NOT ACCEPTABLE
BONDED ASSEMBLY, LAMINATED SKINS & SPARS, HONEYCOMB CORE	• SHEAR LOAD TRANSFER FROM SKINS TO SPARS EXCEEDS ADHESIVE BONDING CAPABILITY • ADDITION OF METAL FASTENERS UNSATISFACTORY BECAUSE STRAIN IN SKINS AT ULTIMATE LOAD EXCEEDS BEARING ALLOWABLE FOR GRAPHITE-EPOXY	NOT ACCEPTABLE
CLOSED GRAPHITE-EPOXY TORQUE TUBE, LOW MODULUS GLASS-EPOXY SKINS 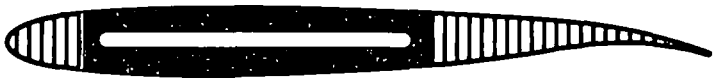	• REDUCED CROSS-SECTION DEPTH TO ALLOW FOR SKINS DICTATES USE OF HIGHER MODULUS MATERIAL FOR NECESSARY STIFFNESS	NOT ACCEPTABLE
STEEL SPAR, LOW-MODULUS GLASS-EPOXY SKINS 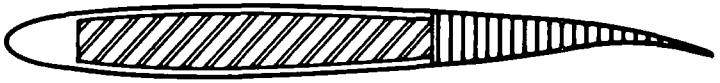	• STEEL SPAR CAN PROVIDE NECESSARY STRENGTH AND STIFFNESS	MERITS FURTHER DEVELOPMENT

266 635-98

Figure B-2. F-111 TACT Aeroelastic Wing Structural Design

The designs can be determined using nonlinear programming techniques. Included within the framework of the procedure are capabilities for considering flexible leading- and trailing-edge control surfaces; inertia relief; a control reversal constraint; design objectives for camber, twist, and roll effectiveness; and calculation of flexible and rigid drag polars.

Steady-state aerodynamics for the method are provided by a modified version of the Carmichael finite-element lifting surface procedure, which provides an output tape that contains the aerodynamic coefficient matrix. Pressure loads are computed using this matrix in combination with corresponding configuration geometry (planform geometry and surface slopes). Lift, drag, and pitching moment characteristics are developed from these pressure loads. Superposition is used to combine the individual effects of angle of attack, camber, twist, aeroelasticity, etc., to determine the aerodynamic characteristics of a given configuration.

Unsteady aerodynamics for the method are provided by a modified version of the Cunningham Kernel-function procedure (Reference 30), which provides an output tape that contains the unsteady aerodynamic coefficient matrices. Generalized forces are computed for each reduced frequency using a combination of the corresponding matrix and the generalized structural mode shapes. A flutter solution is acquired within TSO for the set of reduced frequencies.

A TSO model was derived at the outset of this study. The theory within TSO allows for trapezoidal shaped surfaces, and the planform geometry for this study is shown in Figure B-3. The wing box covered a chord length that extends from the 10% chordline to the 60% chordline. Geometry at the root varied in the design process, depending on whether the carrythrough-structure concept included a pivot attachment or a one-piece structure. Thus boundary conditions also varied. In the design process of the wings the TSO structural model was clamped at the pivot for a variable sweep concept, and clamped along the centerline and the pivot for a one-piece carrythrough concept. Wing ordinate geometry from three span stations (Table B-1) was surface fitted for both root geometry configurations. These ordinates are in terms of full depth of the wing, because they are used in TSO for structural box depth only. Aerodynamic considerations are accounted for through camber and twist slopes for individual Carmichael finite-element panels. Material properties varied with each of the four design concepts (Table B-2).

B.1.1.2 Design Approach. Within the design approach of all four concepts, static aeroelastic similarity to the full scale F-111 TACT wing structure was the primary goal. The most readily available, accurate data base describing the structural character of the full scale wing is a finite element model that was tuned to the results from the full scale wing static proof test of the F-111 TACT program (performed at Wright Patterson Air Force Base). Structural influence coefficients were extracted from TSO at planform locations coinciding with node points from the finite element model (Figure B-4). TSO designs were measured through correlation with the finite element model (Table B-3), which included the boundary condition of the wing clamped at the pivot. TSO models the wing

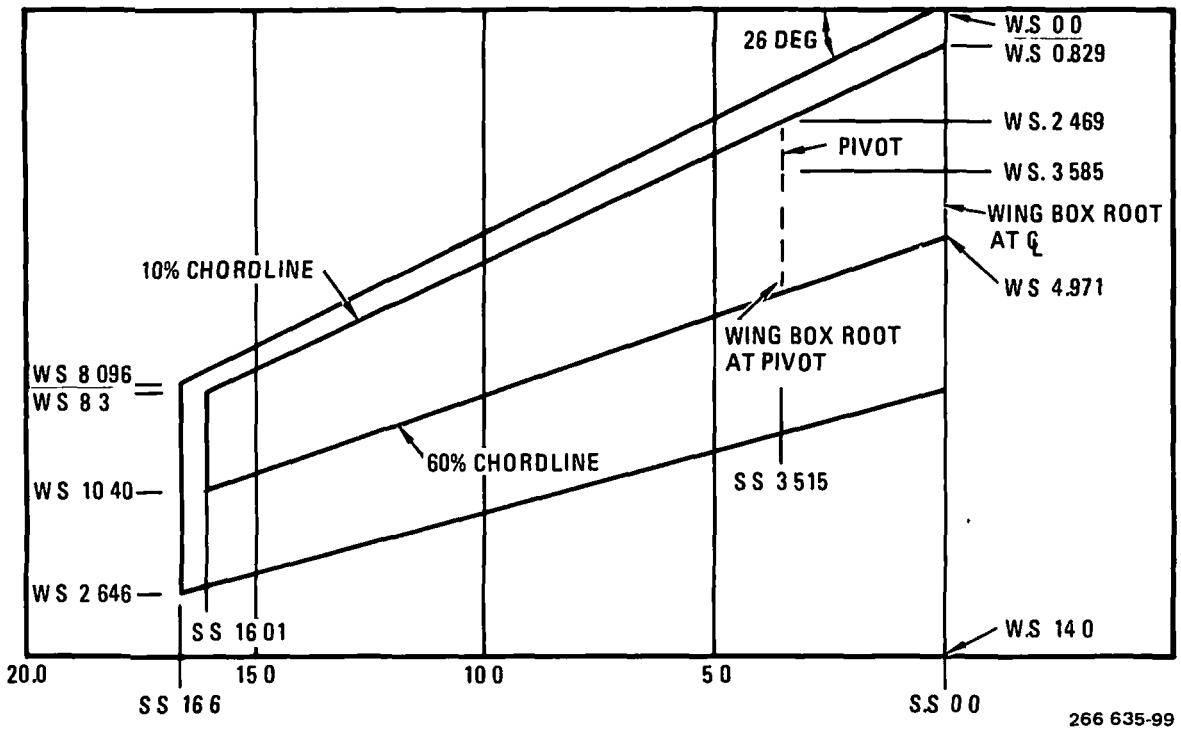

Figure B-3. Planform Used for Aeroelastic Wing Study

skin thickness through continuous polynomial functions similar to those used in the surface fits of the ordinate geometry. Stiffness is formulated using plate theory and these two sets of polynomial functions (Reference 27). Designs were accomplished through iteration of the thickness polynomial functions.

Preliminary stress analyses were performed for the model trimmed aircraft configuration for the Mach = 0.9, 10,000 feet, 7.33g design condition. The final design loads are a result of a combination of Carmichael aerodynamic pressures with wind tunnel loads from the 1/15-scale F-111 TACT flexible wing test program. Static aeroelastic solutions for each design concept were obtained in TSO, and wing surface stresses were obtained simultaneously.

A Carmichael finite element paneling scheme for the full scale F-111 TACT configuration was devised, and an aerodynamic influence coefficient matrix was produced for TSO. The paneling scheme, shown in Figure B-5, has 175 finite-element panels, and this scheme has been used successively in previous F-111 TACT programs. For the design conditions, the F-111 TACT aircraft has a normal force coefficient, $C_N = 1.03$ for a 70,000-pound gross weight. The Carmichael model predicts that the wing contribution is $C_{N_W} = 0.72$. Load comparisons with data from the 1/15-scale flexible wing test program (Reference 31)

Table B-1. F-111 TACT Wing Ordinate Geometry

Reference 16-deg Sweep Configuration	Model Ordinates of 26-deg Sweep Configuration		
Full-Scale Span Station	Wing Station	Span Station	Wing Full Depth
70.3	2.567	3.690	0.555
70.3	3.158	3.586	0.652
70.3	3.699	3.490	0.710
70.3	4.266	3.390	0.731
70.3	4.847	3.288	0.723
70.3	5.413	3.188	0.693
70.3	6.004	3.084	0.632
124.0	3.742	6.209	0.522
124.0	4.397	6.094	0.607
124.0	5.052	5.978	0.635
124.0	5.707	5.863	0.634
124.0	6.367	5.746	0.602
124.0	7.022	5.631	0.529
325.0	8.122	15.642	0.221
325.0	8.575	15.562	0.263
325.0	9.028	15.482	0.279
325.0	9.481	15.402	0.284
325.0	9.939	15.322	0.275
325.0	10.392	15.242	0.253

Table B-2. Aeroelastic Wing Material Properties

Graphite - Epoxy	Room Temperature Properties	
	E_1	20.05 msi
	E_2	1.41 msi
	G_{12}	0.567 msi
	ν_{12}	0.303
	ρ	0.058 lb/in^3
18 Ni - 200 Steel	Estimated Properties at -260F	
	E_1	27.5 msi
	E_2	27.5 msi
	G_{12}	11.0 msi
	ν_{12}	0.30
	ρ	0.290 lb/in^3

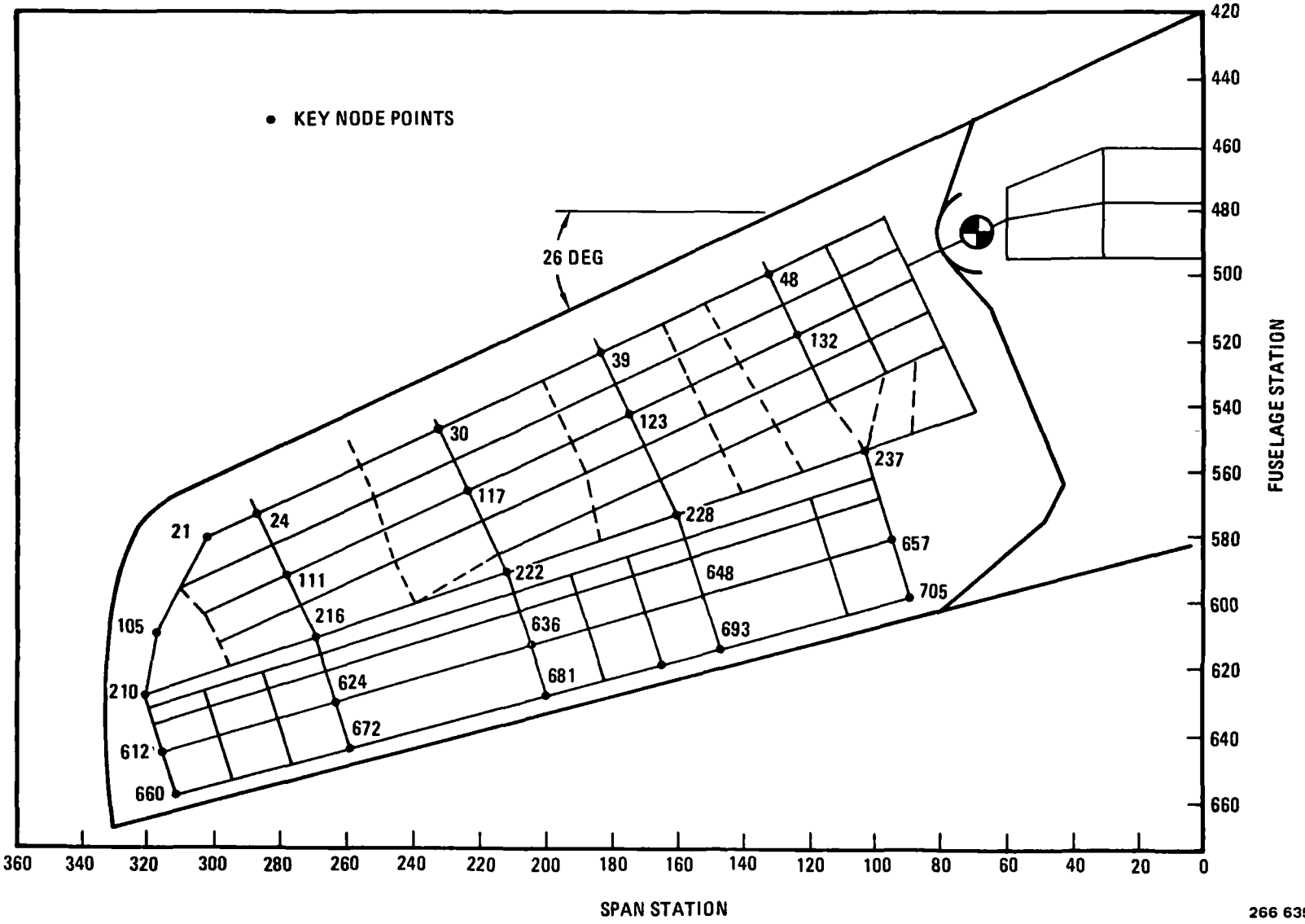

Figure B-4. Influence Coefficient Node Points

Table B-3. Structural Influence Coefficients Diagonal Terms × 10^{-2} (Inches per 100 Pounds)

F_{Spar} Coordinate	SIC_{FS}	SIC 1/20	R_{Spar} Coordinate	SIC_{FS}	SIC 1/20	M_{Spar} Coordinate	SIC_{FS}	SIC 1/20
21	0.0337	0.1376	210	0.0562	0.2362	105	0.0484	0.1976
24	0.0233	0.1033	216	0.0252	0.1029	111	0.0238	0.0972
30	0.0089	0.0363	222	0.0094	0.0324	117	0.0083	0.0339
39	0.0030	0.0122	228	0.0038	0.0155	123	0.0027	0.0110
48	0.0006	0.0021	237	0.0016	0.0065	132	0.0005	0.0020
54	0.0003	0.0012	243	0.0029	0.0118			

$$SIC_{Model} = \frac{\text{Length Ratio}}{\text{Dynamic Pressure Ratio}} \times SIC_{Full\ Scale}$$

$$= \frac{20}{4.899} \times SIC_{Full\ Scale}$$

Nomenclature:
- FS = Full Scale
- 1/20 = Model Scale
- F Spar = Front Spar
- R Spar = Rear Spar
- M Spar = Mid Spar
- SIC = Structural Influence Coefficient

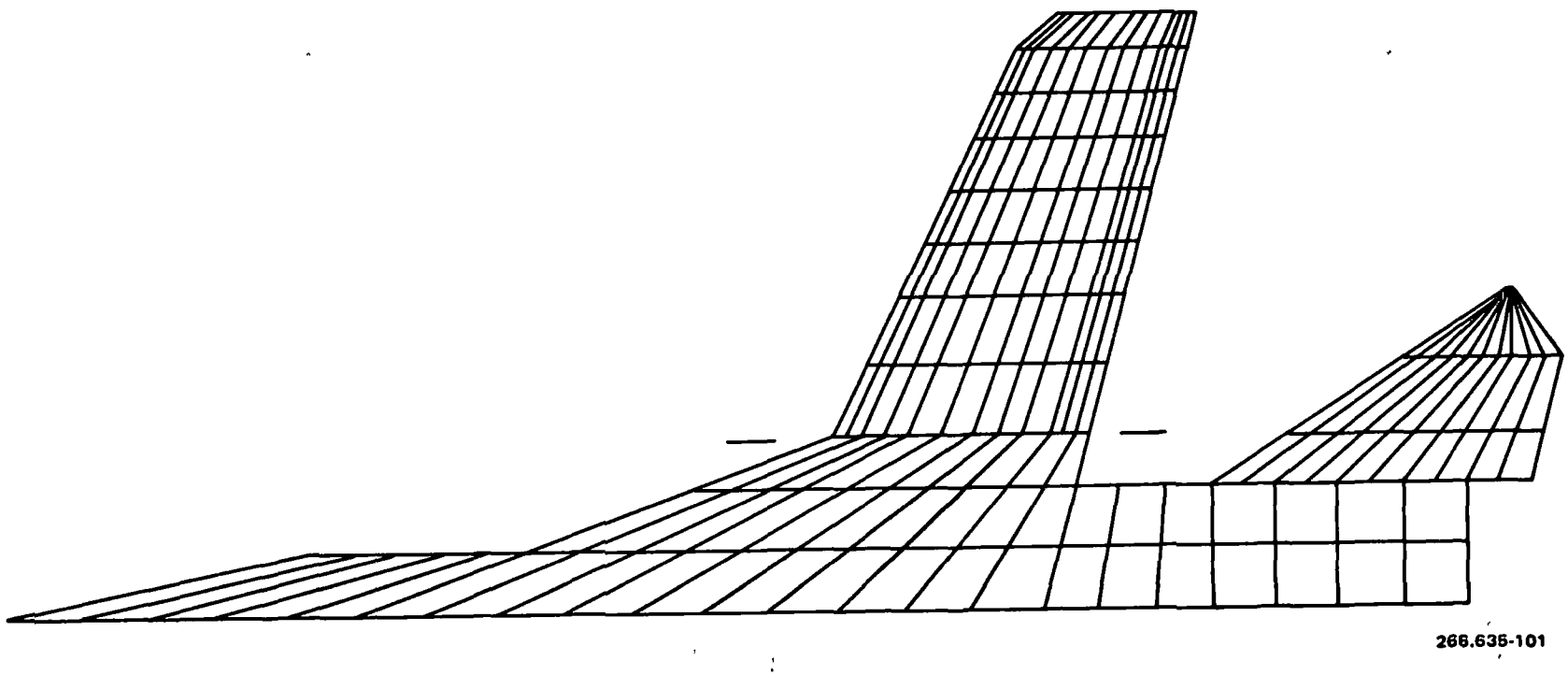

Figure B-5. F-111 TACT Finite Element Paneling Scheme

showed that the wing contribution in Carmichael is conservative, and the difference is probably due to flow separation at high angle of attack and aeroelastic effects.

A summary of these results is provided in Figure B-6. Wing and total airplane normal force are shown at Reynolds numbers (RN) of 2.5×10^6/ft and 6.5×10^6/ft. The higher RN data are assumed to be representative of wing normal force coefficient expected in the NTF and were extrapolated to the required design total CN of 1.03 using the low RN data as a guide. This provides a wing C_{N_W} of 0.58 at the design point. Therefore, the following design paramters were recommended for use in design loads.

- C_{N_W} per side = 0.58/2 = 0.29
- Design load per panel = $C_{N_W} \times q \times S_{\text{Model Ref}}$ = 1770 pounds

where

q = dynamic pressure = 4042 lb/ft

$S_{\text{Model Ref}}$ = 604 ft/400

The total model load for the design condition is 6286 pounds

$$\text{Model Load} = C_N \times S_{\text{Model Ref}} \times q$$

$$= 1.03 \times \frac{604}{400} \times 4042$$

Although the model balance limit is currently 4000 pounds, it was concluded that the flexible wings should be designed to the full design load (6286 pounds) to enable full flight envelope testing in the event of a new high capacity balance.

Consequently, the TSO trimmed aeroelastic solution was performed at a trimmed load that would produce a wing panel load of 1770 pounds. This was achieved using Carmichael distributed pressures and trimming at a load of 4920 pounds at 1g. This load was derived from the ratio of the 1/15-scale panel-test C_{N_W} to the Carmichael panel C_{N_W}, 0.29/0.36. This ratio was multiplied by the total load, and a couple of iterations were made on the final load until the panel load was approximately 1770 pounds. In a detailed design of this model, adjustment to the discrete pressures would be required to ensure accurate distributions.

Wing panel load distributions varied ±3% with each TSO analysis due to aeroelastic effects differing in each design. Typical loads extracted from a TSO analysis and used to design the flexible wings from a strength standpoint are summarized in Figures B-7 through B-9. Hand stress analyses were performed at wing cross sections using these loads.

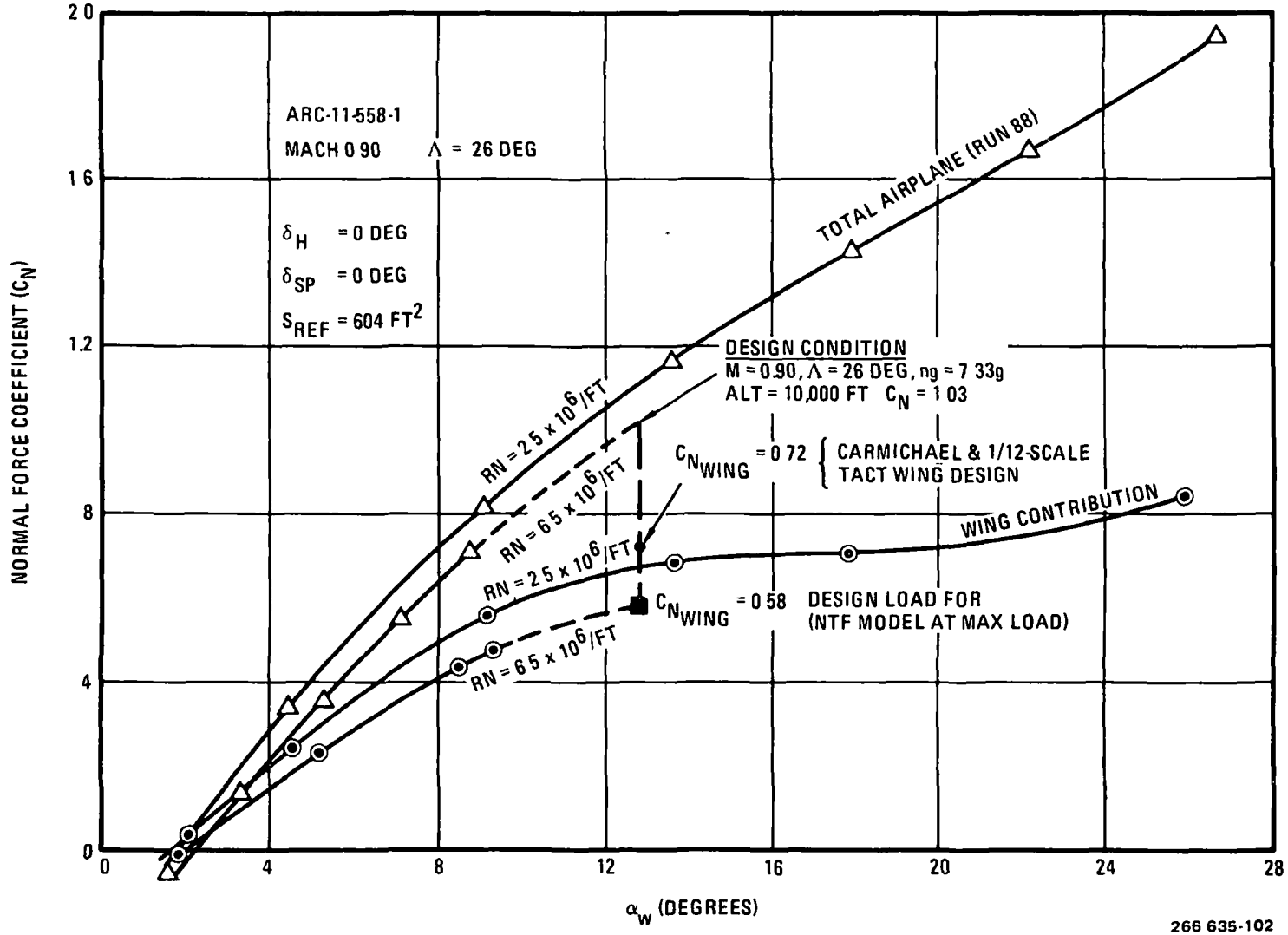

Figure B-6. Wing Normal Force Contribution

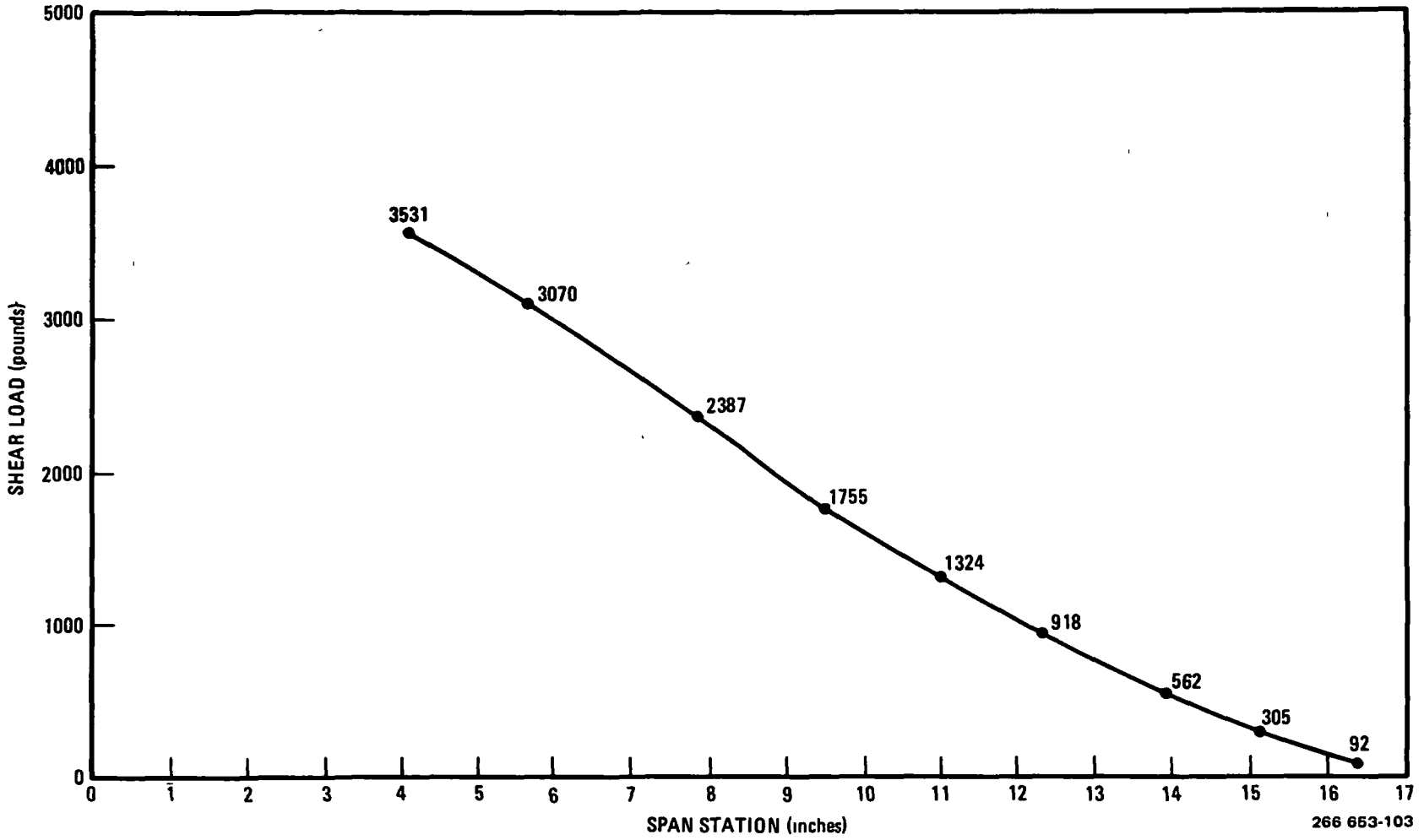

Figure B-7. Shear Load Diagram (Ultimate Load)

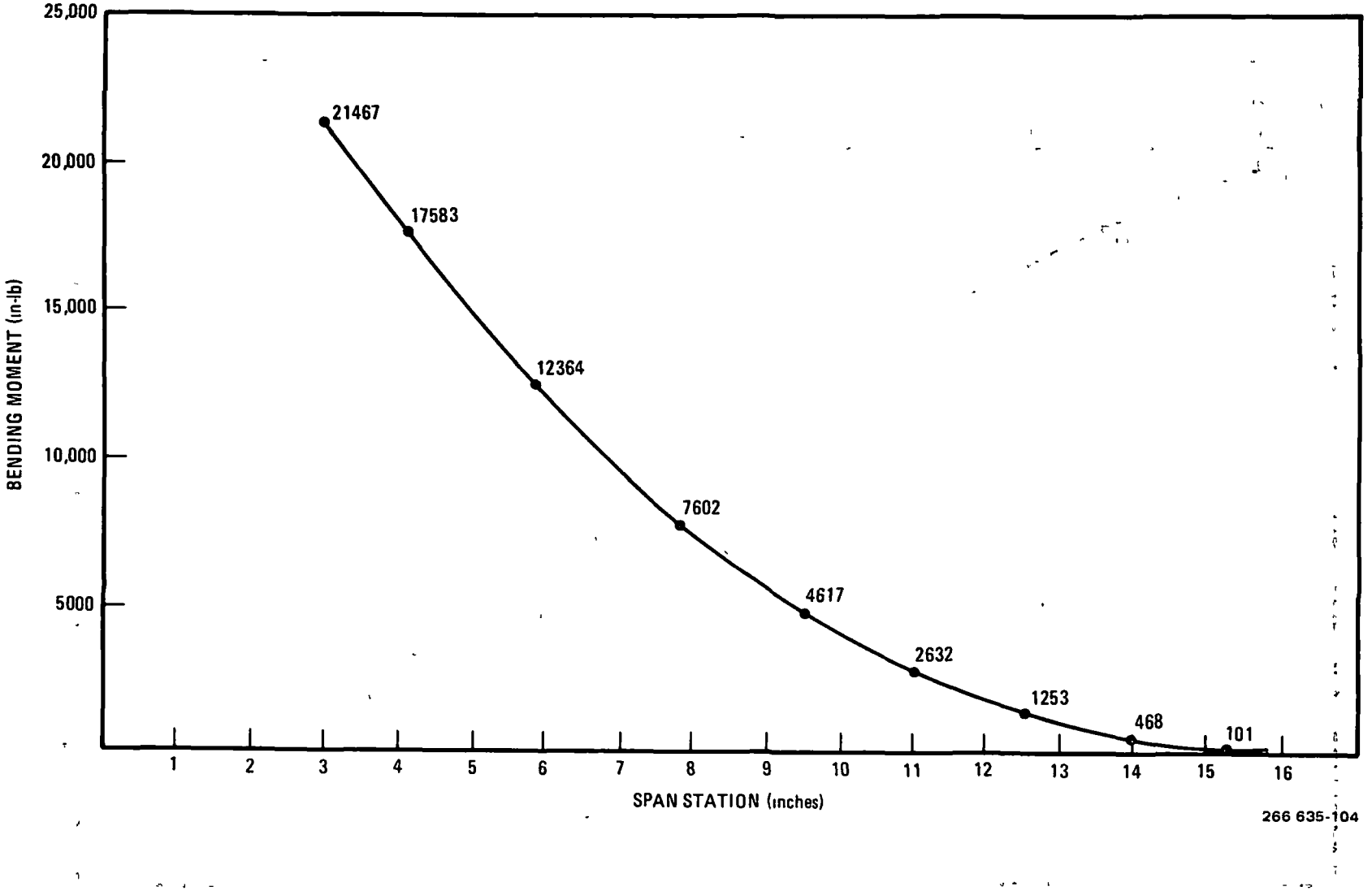

Figure B-8. Bending Moment Diagram (Ultimate Loads)

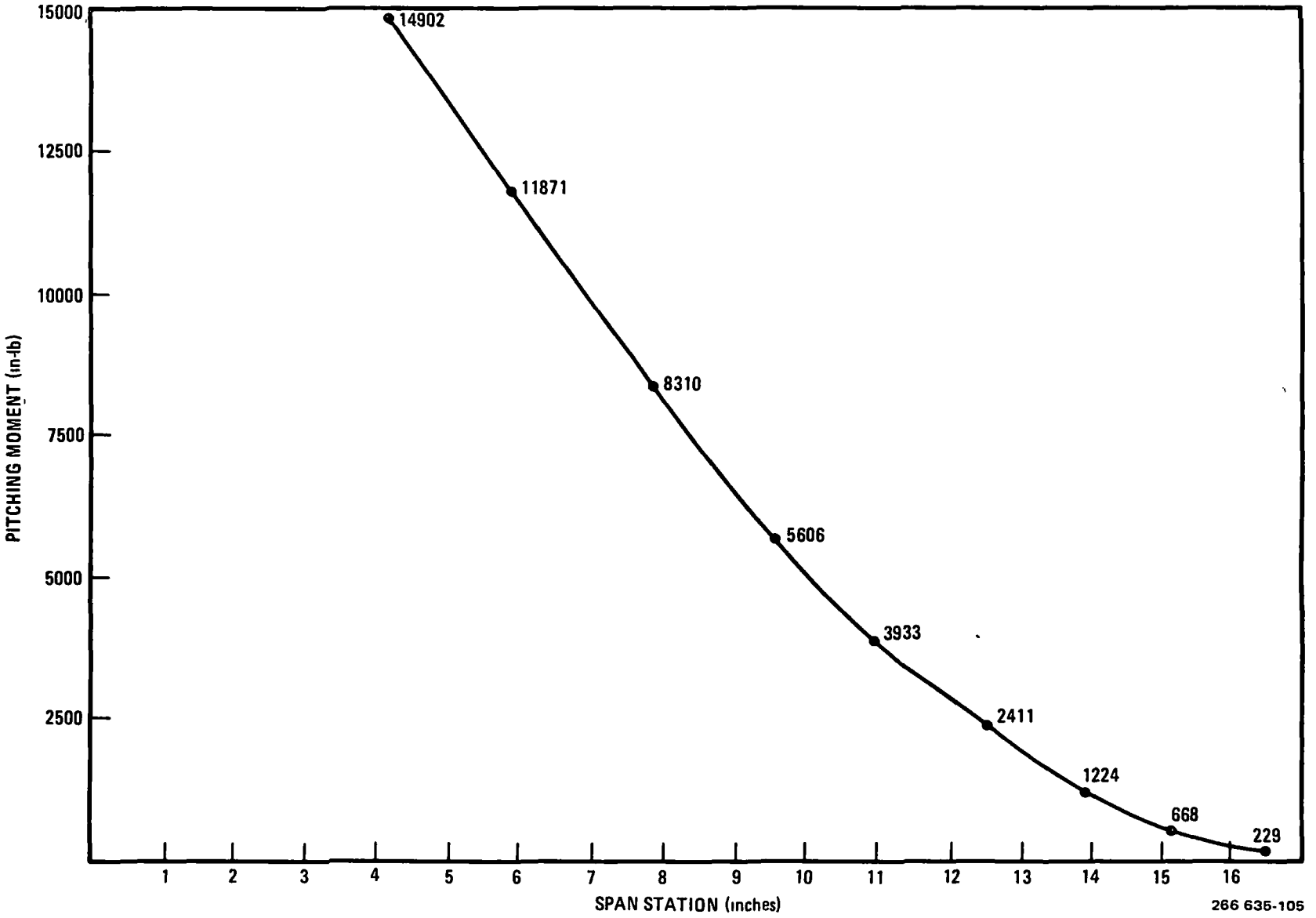

Figure B-9. Pitching Moment Diagram (Ultimate Load About Front Spar)

A matched-point flutter analysis was performed on the selected design concept only. Four solutions were obtained for the Mach 0.9 flight condition, each at different tunnel densities. The results are discussed in Section B.1.1.5, Analyses.

B.1.1.3 Final Design Concept. The selected design approach for the F-111 TACT 1/20-scale flexible wing model is derived from a "soft-skin" concept. In this concept the understructure provides the primary load path and the skins provide the airfoil shape. The wing and wing carrythrough-structure design are depicted in Figure B-1. Static and dynamic analyses were performed to assess the design for static aeroelastic similarity to the full scale and for structural integrity of the design system.

B.1.1.4 Design Description. The wing design is broken into five component areas. The primary structural component is an 18Ni-200 steel spar designed to outer contours that provide the combination of geometry with material properties (bending and torsional stiffness) to approximate the static aeroelastic similarity of the F-111 TACT wing box. "Soft" wing skins are 181-75 glass fabric oriented at ±45 degree bias and provide the F-111 TACT supercritical airfoil contour. The skins are supported in the trailing edge with a glass-phenolic honeycomb core, and the entire structure is bonded together with Versamid 115®/Epon 828® epoxy. The fifth component area of the wing design is the pressure channels, thermocouples, and light emitting diodes (LED).

The severity of the high panel loading produced from the dynamic pressure ratio, 4.899, necessitates a structure that not only has high stiffness but high strength as well. The wing design with a steel spar as the primary load carrying structure has evolved because of this loading. To draw correlation to the 1/12-scale high-strength flexible F-111 TACT model, which was also designed for Mach 0.9, 10,000 feet, 7.33g, it is noted that the total design load for the 1/20-scale is 95% of the 1/12-scale, and for 36% of the 1/12-scale cross-sectional area. The design dynamic pressure ratio for the 1/12-scale model was 1.86, and this combined with the dynamic pressure ratio of the 1/20-scale model 4.899 along with the ratio of surface areas of the two models, produces the 95% figure. The high strength steel spar provides an opportunity to meet the strength and stiffness criteria while simultaneously providing a smooth transition of load into a pivoting carrythrough structure.

The spar depth is described by a polynomial function whose variables are decimal chord and span stations of the planform box. This function is shown in and depicted by Table B-4. The bi-quadratic nature of the spar surface lends itself easily to numerical controlled machining. Details for the pivot area will need to be worked in the final design. The pivot area design will be governed by the stress concentration factors. The 18Ni-200 maraging steel was chosen because of high strength and toughness at cryogenic temperatures.

Table B-4. Spar Depth (inches) as Described by Polynomial Function

Span Station (%)	Chord Station (%) 0	25	50	75	100
0	0.3726	0.4708	0.5119	0.4958	0.4227
25	0.3207	0.4018	0.4361	0.4235	0.3641
50	0.2524	0.3117	0.3492	0.3407	0.2944
75	0.1676	0.2246	0.2512	0.2474	0.2134
100	0.0665	0.1163	0.1421	0.1437	0.1214

$$\text{Spar Depth} = 0.372622 + 0.507106\,x - 0.457016\,x^2 - 0.174752\,y_2 - 0.387824\,xy + 0.350978\,x^2y_2 - 0.131391\,y^2 + 0.128448\,xy^2 - 0.087030\,x^2y^2$$

Where x and y are decimal chord and span locations of the TSO box geometry (i.e., 10% chordline = 0.0, 60% chordline = 1.0)

The spar was designed from a number of iterative TSO computer runs. Although the TSO theory was developed to model and design wing skins, the program was easily applied to model a solid spar instead. The spar was essentially modeled as full depth skins over a box area that included chordlengths from the 10% chordline to the 60% chordline (Figure B-3). Specifically, the polynomial thickness functions and the polynomial wing contour depth functions were input as identically equal functions, and this reduced the TSO wing structure theory to simple plate theory. Designs were iterated by manipulating discrete spar depths over a 5 by 5 grid area of the box planform, surface-fitting the depths to polynomial functions, and inputting the functions into TSO as skin thickness and depth functions. Manipulation of the depth function did not affect the aerodynamics of the TSO model because the aerodynamic modeling and the structural modeling are treated separately in TSO.

Figure B-10 demonstrates the static aeroelastic similarity of the spar design along the 10, 35, and 60% chordlines. Diagonals of the structural influence coefficients are plotted for the spar design, an F-111 TACT full-airfoil-depth spar, and the full scale finite element model ratioed by dynamic pressure and geometry to the NTF configuration. It is noted that a full-airfoil-depth spar for an F-111 TACT model (i.e., rigid) would have considerable aeroelastic effects. It is also noted that although the stiffness of the design spar is more than an order of magnitude larger than the remaining structural contributions of the wing model, a finite element model of the entire structure will be required to tune the spar with the remaining wing stiffness constituents for the final design.

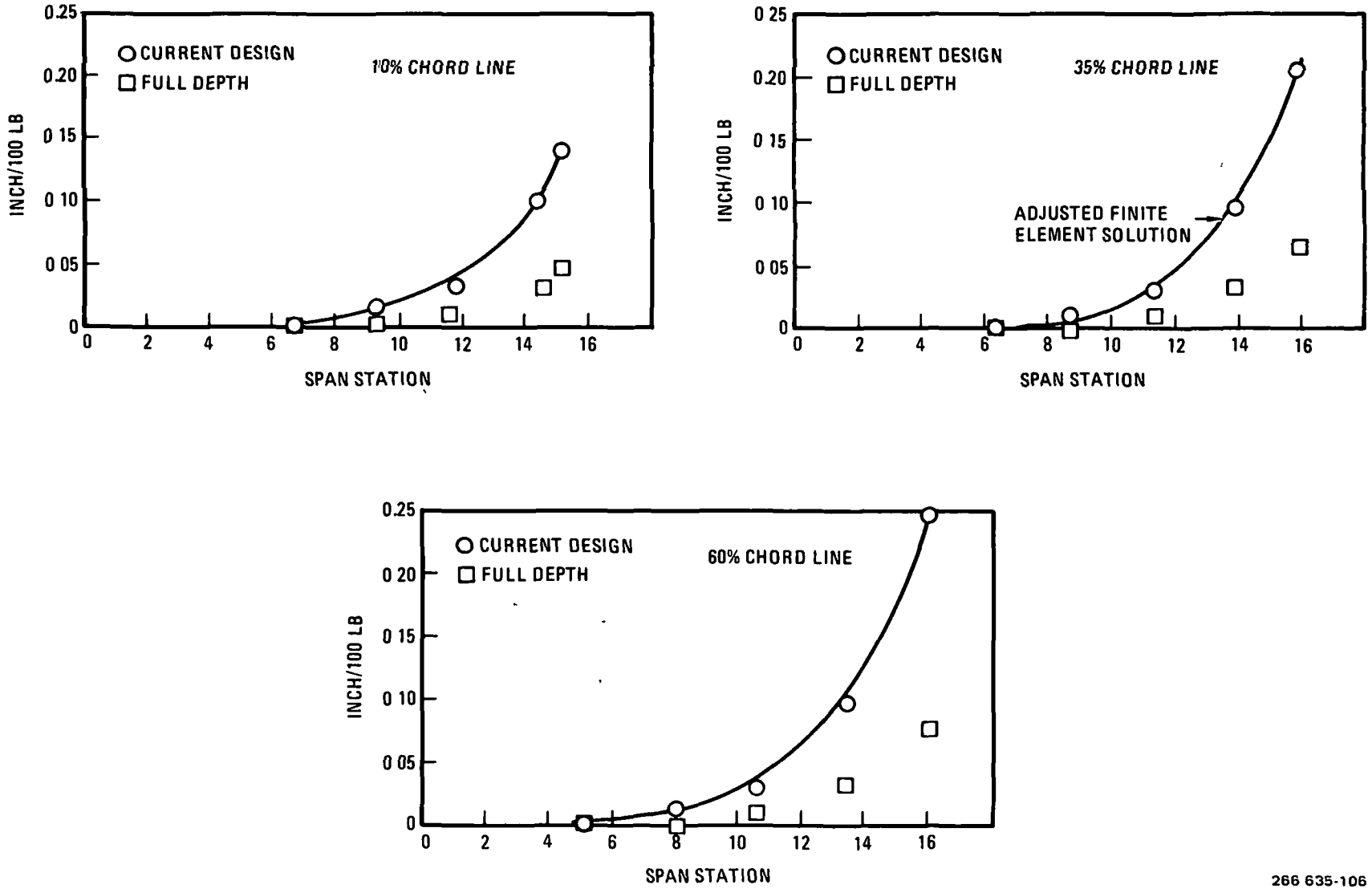

Figure B-10. F-111 TACT Aeroelastic Wing Stiffness Characteristics

Three design requirements governed the selection of 181-75 glass fabric for the wing skins.

a. The skin material had to provide minimum contribution to the overall stiffness of the wing in the spar region.

b. The skin material had to be stiff enough to maintain the supercritical airfoil shape and in particular, chord-bending in the cusp region.

c. The skin material had to be strong enough (i.e., strain capability) to withstand twice the limit load.

By laying the glass on a bias (+/-45 degrees) to the spar, these three requirements are addressed. Four plies of glass fabric (0.008 inch thick/ply) over the spar will provide minimum additional stiffness in the box region, and a build-up to nine plies in the cusp region will provide the necessary stiffness to maintain the supercritical airfoil shape. Finally, glass-epoxy has a strain to failure at cryogenic temperatures that is more than adequate to satisfy a safety factor of 2 at limit load. The room temperature mechanical properties for 181-75 glass fabric are provided in the material specification of General Dynamics - FMS-1023 Class I-7781.

Existing data and tests for graphite-epoxy, which were performed during the investigation of the other design concepts, indicate that the glass-epoxy mechanical properties at -260F will satisfy the strength and stiffness requirements for the design. Tests consisting of glass-epoxy were not completed.

The glass-epoxy skins in the cusp region of the airfoil are reinforced with a glass-phenolic honeycomb core. Preliminary stress analyses performed along the 60% chordline indicate the requirements of core understructure with shear strengths in a range above the capacity of Nomex®. This is discussed further in the analyses. Specific core weight has not yet been chosen for the design.

Secondary bonding of pre-cured skins to the core and spar will be accomplished with Versamid 115®/Epon 828® epoxy. The spar and the core will be floated in between the skins. The bondline will range from 0.030 to 0.070 inch in thickness, thus reinforcing the airfoil shape. To reinforce the epoxy, because this is a thick bondline, glass matting will be mixed with the epoxy. Double-lap shear tests were run at room temperature and -260F for specimens made with two glass-epoxy skins, glass matting, Versamid 115®/Epon 828® epoxy, and a steel tongue. The results showed sufficient bond strength to withstand shear loads between the skins and understructure due to panel loading and thermal effects. This is discussed further in Section B.2. Also in Section B.2 is a discussion of the screening tests that were performed in the selection of the bondline material. Fabrication methods were an additional consideration used in the screening tests.

All wing instrumentation will lie in the bondline between the skins and understructure. Wing instrumentation includes pressure channels, thermocouples, and LED. The details of this phase of the design will be worked out during the planned proof-of-concept tests. However, internal housing of instrumentation in an epoxy bondline is currently being developed at General Dynamics, as well as other industry and government facilities, for such things as fiber optics. Wing pressure channels will be formed using the so called "lost wax" method. This method was used successfully in the 1/12-scale F-111 TACT flexible wing model (Reference 26) where the wax carrier was a plastic as opposed to epoxy. In the "lost wax" method, wax is used in lieu of steel pressure tubes, and after fabrication of the wings, the wax is melted out leaving open passages. The advantage, especially in the "soft skin" concept of wing design, is that no stiffness is added to the structure.

Pressure channels, thermocouple leads, and LED leads in a final design would be gathered into two groupings – one forward and one aft of the spar. These groupings allow for manifold attachment. Figure B-11 shows the desired pressure orifice locations. Table B-5 lists the discrete coordinates. Decisions have not yet been made for the thermocouples. Results from a proof-of-concept component are required to provide the capacity of the bondline to carry all instrumentation.

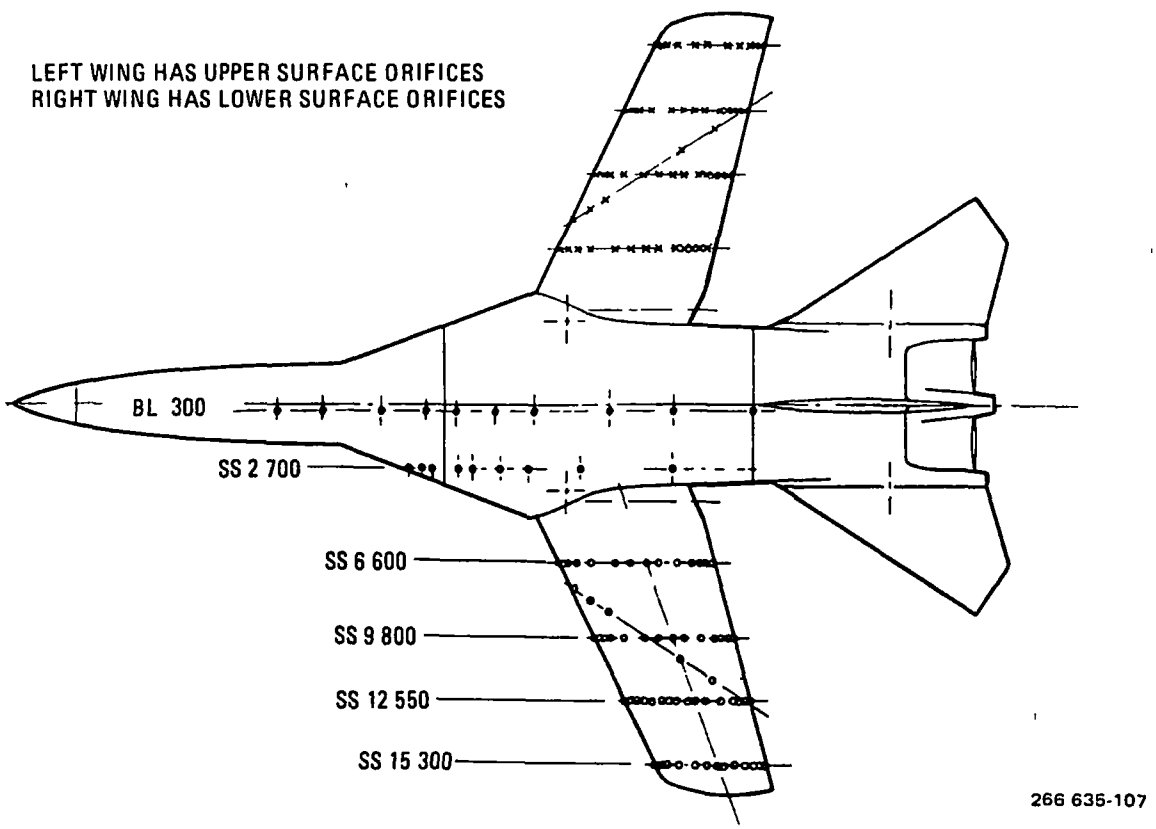

Figure B-11. F-111 TACT Pressure Orifice Array

Table B-5. Dimensional Location of Orifices – F-111 TACT

Span Station	%C		Span Station	%C		Span Station	%C		Span Station	%C		Span* Station	%C	
6.600	LE	o	9.800	LE	o	12.550	LE	o	15.300	LE	o	7.796	2	●
	2	●		2	●		2	●		2	●	8.277	11	●
	5.75	x		6	●		6	●		6	●	8.776	20	x
	6	o		11	●		11	●		11	●	8.797	19.13	o
	10.24	o		20	●		20	●	15.315	18.97	o	10.733	55	●
	11	x		35.83	●		30	o	15.220	19.11	x	11.485	75	●
	19.96	●		45.68	●		35	●	15.300	35	●			
	35	●		55	●		40	o		45	●			
	45	●		63	o		45	●		56.16	o			
	55	●	9.807	63.39	x		50	o		63	●			
	63	●	9.800	75	●		55	●		75	●			
	75	●		79.16	x		63	●		85	●			
	79.33	x		85	●		75	●		90	●			
	85	●	9.764	89.96	●		79.08	x		95	●			
	90	●	9.800	95	●		85.01	●		99.77	o			
	95	●		99.82	o		89.90	●						
	99.85	o					95	●						
							99.80	o						

● Upper and lower surface orifice
o Upper surface orifice only
x Lower surface orifice only
* Λ = 50-degree ray at SS 138.5

A most vital part of the wing design is the surface finish. The discussions in Section 5.3 noted that a maximum surface finish of 20 microinches should be used in the rigid models. This value applies for the flexible model as well.

The carrythrough structure allows for a pivoting wing concept and locks at two wing sweeps. The final design needs to be completed. Experience shows that multiple attempts combining design and fabrication are required for accurate flexibility. The structure is designed to match flexibility at the pivot only. For the 1/20-scale this flexibility is

$$\begin{Bmatrix} w \\ \theta \\ \phi \end{Bmatrix} = \begin{bmatrix} 10.05 & 1.90 & -.104 \\ 1.90 & .657 & .014 \\ -.104 & .014 & 1.417 \end{bmatrix} \times 10^{-6} \begin{Bmatrix} P \\ M_R \\ M_P \end{Bmatrix}$$

where

w = vertical displacement
θ = roll rotation
ϕ = pitch rotation
P = shear load
M_R = bending moment
M_P = pitching moment

B.1.1.5 Analyses. Static and dynamic analyses were performed on the selected flexible wing concept. Deflections were predicted for the wing clamped at the pivot and for the elastic pivot (i.e., flexible carrythrough structure) boundary conditions. Stress analyses showed that positive margins-of-safety with factors of 2 at the design limit load are achieveable with the selected design concept. Finally, a matched-point flutter analyses was performed for the elastic pivot boundary condition, and a large margin-of-safety was determined for the wing.

Aeroelastic deflections were predicted for the steel spar from the TSO model for the Mach 0.9, 10,000 feet, 7.33g flight condition. Figure B-12 displays the deflection of the spar for the clamped pivot boundary condition. The leading and trailing edge (i.e., 10% and 60% chordlines) lines are plotted. The tip twist is -5.4 degrees. Figure B-13 similarly displays the deflection of the spar for the elastic pivot boundary condition. The tip twist is -5.9 degrees. It is noted that the loads used to generate these deflections were formulated as discussed in Section B.1.1.3. For the clamped pivot aeroelastic trimmed aircraft solution, the total wing panel shear load was 1753 pounds. For the elastic pivot aeroelastic trimmed airplane solution, the total wing panel shear load was 1721 pounds.

Stress analyses were performed in the wing in four areas. A surface stress survey for the steel spar was accomplished through the TSO aeroelastic solution. A point stress analysis was performed on the bondline just outboard of

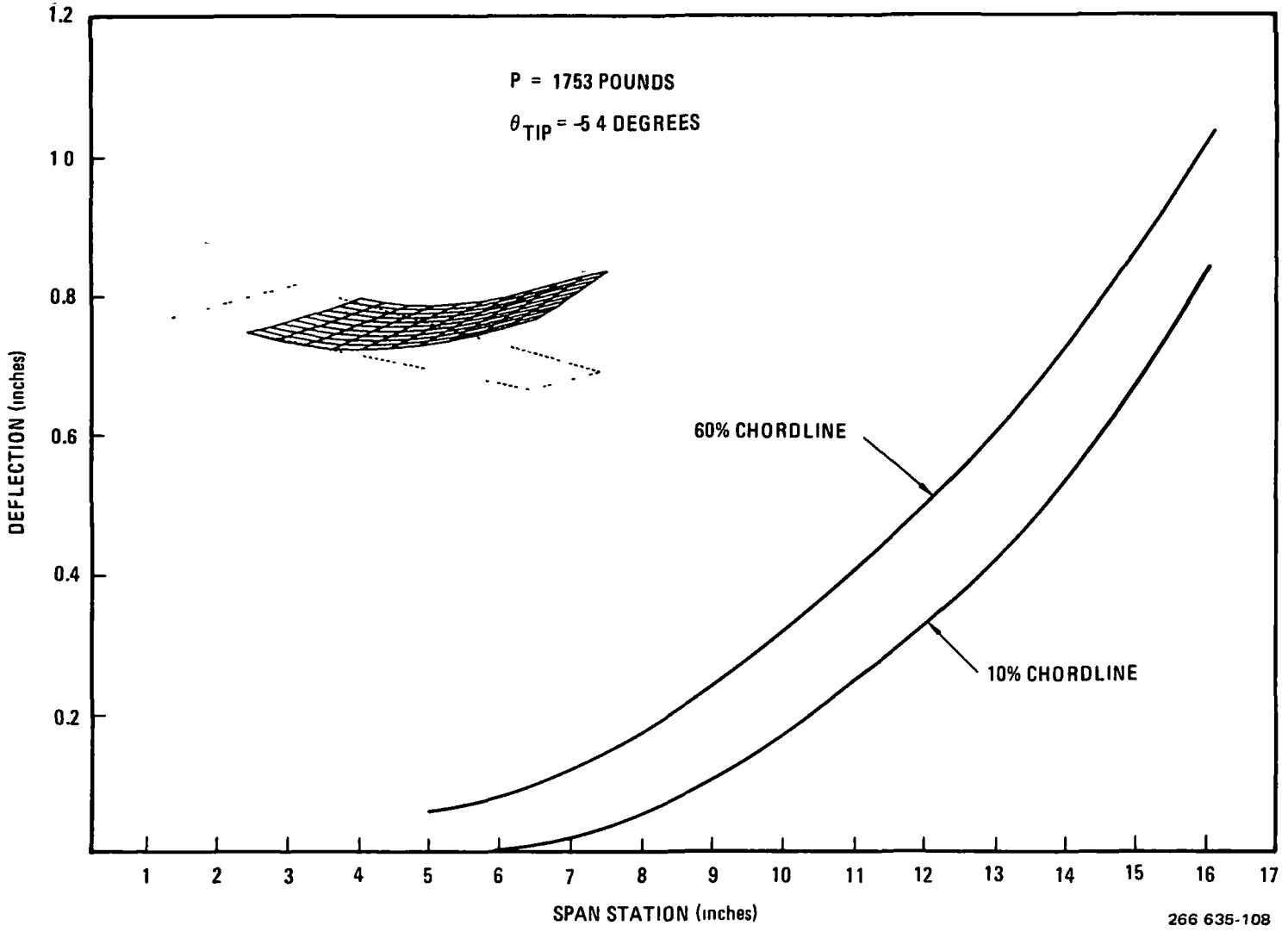

Figure B-12. Steel Spar Aeroelastic Deflection Clamped Pivot

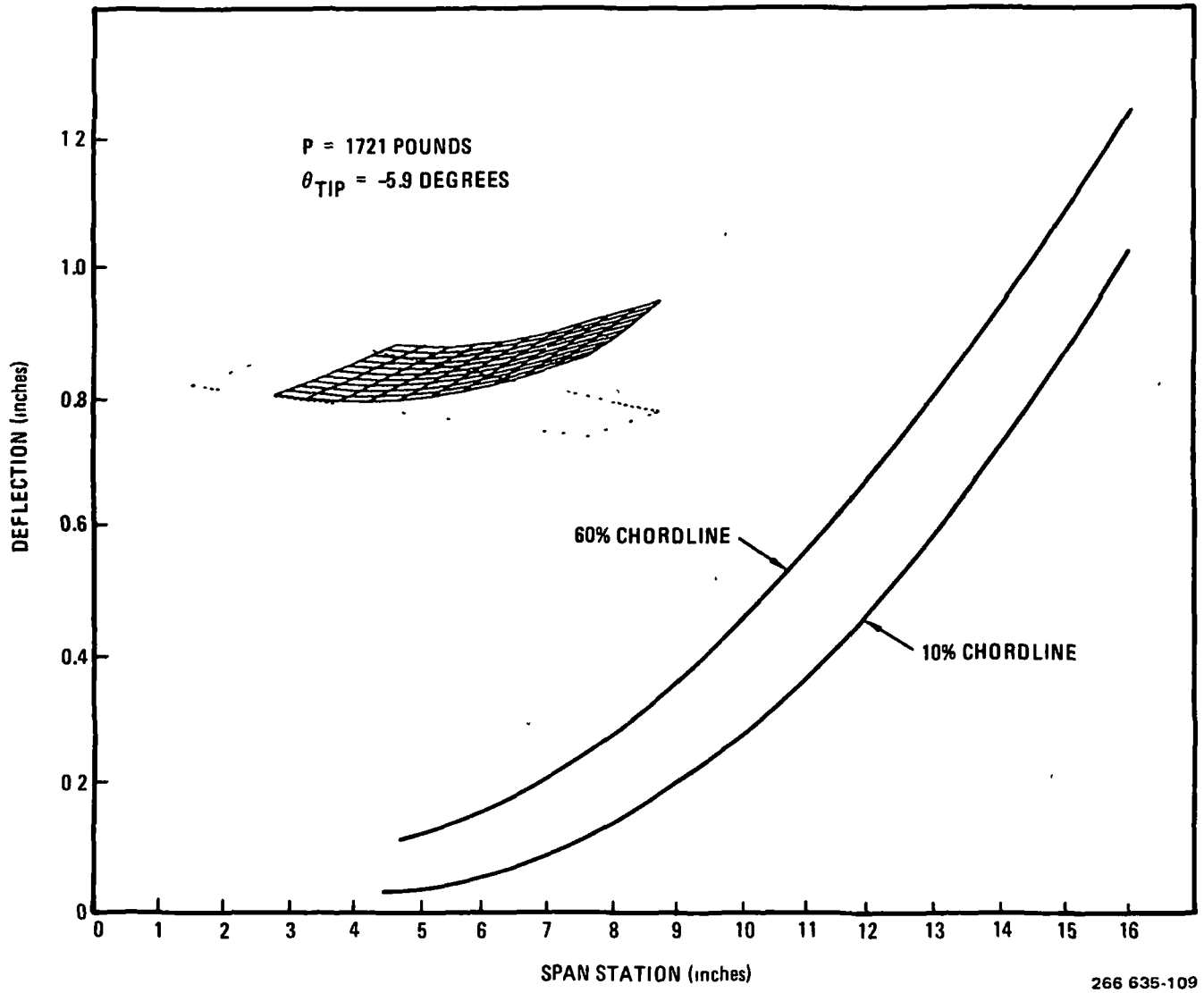

Figure B-13. Steel Spar Aeroelastic Deflection Elastic Pivot

the pivot to evaluate the differential shear load between the skin and the spar. A thermal stress analysis was performed at the same point to evaluate the different coefficients of contraction between glass-epoxy and steel. Finally, sectionwise stress analyses were preformed in the cusp region of the airfoil to evaluate chord bending.

TSO was used to evaluate spar surface stresses for the clamped aeroelastic solution. Figure B-14 shows the stresses at discrete points selected in TSO on an evenly spaced distribution. The stresses are in terms of σ_x, σ_y, and τ_{xy} at limit load. The circled point has the highest spanwise stress and was chosen for further point stress analysis. Using Mohr's Circle, these stresses were resolved into maximum and minimum principal stresses. The maximum principal stress is 85,000 psi at limit load and 170,800 psi at ultimate. This value is well below the yield strength of 18Ni-200 maraging steel at -260F.

For the same area of maximum spanwise stress the bondline shear characteristics were investigated. This stress analysis was performed prior to when the four-ply glass-epoxy design was set. It assumes that 10 plies are in the skin, and thus it is actually a more severe case because of the added stiffness in the skins. In this analysis, the change in running loads (lb/in) in the glass-epoxy were calculated between the circled point and the asterisked point in Figure B-14. The theory of elasticity was used to extract the strains from the stresses, and Mohr's Circle was used to resolve the strains into maximum and minimum principal strains. For the glass-epoxy deformation to be compatible with the spar, the strains at the bondline must be compatible. The in-plane stiffness matrix for glass-epoxy was formulated using the Laminate Point Stress Analysis procedure, SQ5 (Reference 29), for the room temperature values disclosed earlier. The spanwise running loads were determined, and thus the bondline shear stress was calculated to be 96 psi. The analysis is as follows.

STRESS ANALYSIS OF BOND LINE

TSO Geometry and Limit Strains

$\eta = 0.2917$ $\xi = 0.5$ to 1 inch outboard of pivot

$\varepsilon_x = -0.0006174$, $\varepsilon_y = -0.00193967$, $\gamma_{xy} = -0.00146463$

Rotated 56.73 degrees (maximum principal direction)

$\varepsilon_x = -0.002885$, $\varepsilon_y = 0.000328$, $\gamma_{xy} = -0.000023$

$\varepsilon_{x_u} = -0.00577$, $\varepsilon_{y_u} = 0.000656$, $\gamma_{xy_u} = -0.000046$

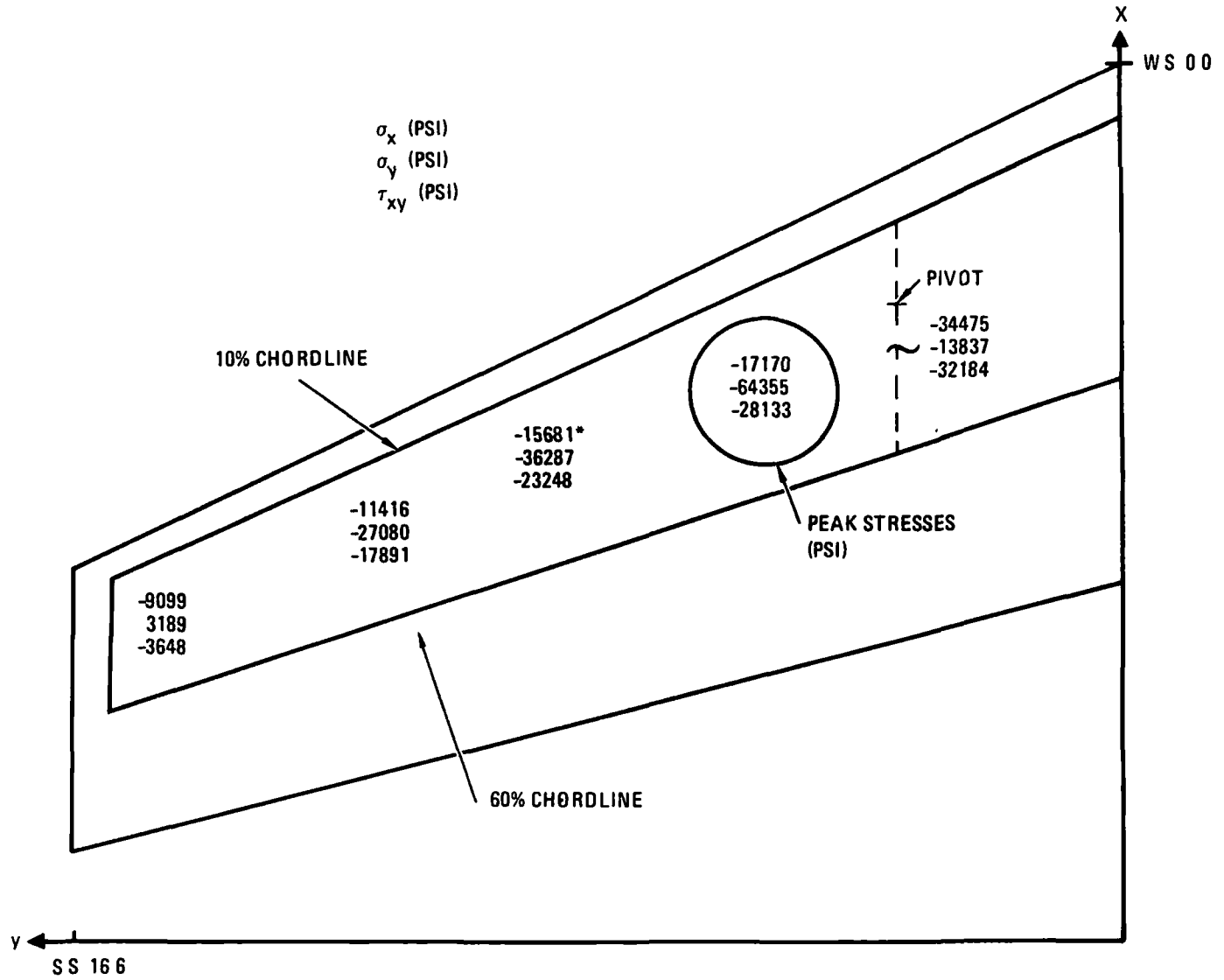

Figure B-14. Upper Surface Stresses Along the Spar Centerline

If glass thickness is 0.082 inch (181 glass-epoxy)

$$A = \begin{bmatrix} 159593 & 54633 & 0 \\ 54633 & 159593 & 0 \\ 0 & 0 & 88578 \end{bmatrix}$$

$N_{x_u} = -885$ lb/in , $N_{y_u} = -211$ lb/in , $N_{xy_u} = -4$ lb/in

$\eta = 0.5$, $\xi = 0.5$

$\varepsilon_x = 0.00011348$, $\varepsilon_y = -0.00142209$, $\gamma_{xy} = -0.00114146$

Rotated 56.73 degrees (coinciding with above)

$\varepsilon_x = 0.002007$, $\varepsilon_y = 0.000698$, $\gamma_{xy} = 0.00025$

$\varepsilon_{x_u} = -0.004014$, $\varepsilon_{y_u} = 0.001396$, $\gamma_{xy_u} = -0.0005$

If glass thickness is 0.082 inch (181 glass-epoxy)

$N_{x_u} = -564$ lb/in , $N_{y_u} = 3.5$ lb/in , $N_{x_y} = -44$ lb/in

$\tau_{xz} = (-885 + 564)/(8.005 - 4.67) = 96$ psi

The lap shear tests performed to evaluate the integrity of the bondline show that the bond strength is 1500 psi at -260F.

This same critical point just outboard of the pivot was examined for thermal effects. SQ5 was used, and the steel and glass-epoxy properties (mechanical and geometric) were assembled in the program - typifying the full depth of the model at this point. A temperature of -260F was input into the problem. The thermal stresses were calculated for the constituents of the assembled structure. The normal stresses (σ_x) in the steel and glass-epoxy ranged from -307 psi to 735 psi respectively. The low modulus of the glass-epoxy (i.e., its expandability) and the compatibility with the steel is demonstrated by the low stress values.

The final area of stress analysis performed was in the cusp region of the supercritical airfoil, which consists of the airfoil from the 60% chordline aft. This analysis is summarized in Table B-6. Transverse shear stresses (V/A) were calculated at eight span stations. Shear loads were determined at each station for the contribution due solely to the cusp. Simultaneously, cusp bending moments about the 60% chordline were determined and used to size the skins (Table B-7). The shear stress calculated at limit load ranges to 666 psi for ultimate load based upon the information in Table B-6. This stress is slightly

Table B-6. Stress Analysis - Cusp Section

Based on Total Panel Shear 1770 Pounds (Limit Load)

S.S. (in.)	Distance Between Stations (in.)	Rear Spar W.S. (in.)	Shear (lb)	ω (lb/in)	Torsion (in -lb)	Average Rear Spar Depth (in.)	τ (V/A) (psi)
	0.40			73			
16.2		10.8	58		56		
	1.10			73		0.262	279
15.1		10.4	102		98		
	1.20			93		0.287	333
13.9		10.0	121		116		
	1.40			100		0.316	316
12.5		9.45	160		170		
	1.50			111		0.349	318
11.0		8.95	173		176		
	1.50			116		0.385	301
9.5		8.4	176		205		
	1.70			124		0.422	294
7.8		7.8	245		302		
	2.0			124		0.467	266
5.8		7.1	252		263		
	1.7			114		0.512	223
4.1		6.45	134		185		

$$q_1 = \frac{58 \text{ lb}}{0.40 \text{ in.}} = 73 \text{ lb/in}$$

$$q_2 = \frac{(102 \text{ lb} + 58 \text{ lb})}{2} \left(\frac{1}{1.10 \text{ in.}}\right) = 73 \text{ lb/in}$$

Table B-7. Requirements of Skin Design at Rear Spar

S.S. (in.)	Mom. at R.S From T.E. Load (in-lb)	h, Depth Less 0.070 Skin Thickness (in.)	M/h	Area ($in.^2$)	σ (psi)
16.2	56	0.109	514	0.053	9698
15.1	98	0.134	731	0.081	9025
13.9	116	0.160	725	0.091	7967
12.5	170	0.192	885	0.102	8676
11.0	176	0.226	779	0.105	7419
9.5	205	0.263	780	0.112	6964
7.8	302	0.301	1003	0.130	7715
5.8	263	0.352	747	0.130	5746
4.1	185	0.391	473	0.060	7883

Glass cloth is probably sufficient for 0.070 inch skins.

beyond the capability of Nomex® honeycomb core but within the reach of glass-phenolic honeycomb cores. In-plane chordwise stresses were calculated for the skins at the 60% chordline and are shown in Table B-7. A cursory look at these stresses shows that skins of approximately 0.070 inch thickness would sufficiently limit the deflections in the cusp region. In the final design, actual aeroelastic effects in this region should be examined.

Table B-8. Point Masses (Cusp Region)

TSO Model Coordinates		Mass (lb)
W.S.	S.S.	(Skins + Core)
7.40	4.80	0.060
8.25	7.40	0.050
9.10	10.0	0.035
10.0	12.6	0.015
10.85	15.2	0.005

Modes and frequencies and a matched-point flutter solution were obtained for the elastic pivot boundary condition and Mach 0.9 flight condition. The flexibility matrix disclosed under the design description of the carrythrough structure was used as the elastic boundary condition. The dynamic analyses included only the wing and carrythrough structure. It is believed that for cryogenic testing, the complete model system should be evaluated for flutter. Such an analysis, however, was beyond the scope of this study.

Modes and frequencies were based on the TSO structural model – the spar and pivot – and the mass properties of the integrated wing structure. Point masses were determined for the core and skins in the cusp region. The spar, adhesive, and skins in the box region were accounted for through distributive weight functions. The total wing weighs 4.018 pounds. The point masses are shown in Table B-8. The spar weighs 3.68 pounds, and the adhesive and skins in the box region weigh 0.173 pound. The modes and frequencies are displayed in Figure B-15.

For the flutter analysis, a Cunningham Kernel-function computer run was made producing unsteady aerodynamic influence coefficient matrices for 20 reduced frequencies (4.5, 3.375, 2.7, 2.25, 1.9286, 1.6872, 1.5, 1.35, 1.125, 0.9643, 0.84375, 0.75, 0.675, 0.60, 0.54, 0.4909, 0.45, 0.4145, 0.3857, 0.36). TSO flutter solutions were obtained at four NTF tunnel densities (0.015, 0.020, 0.026, 0.031 slug/ft^3). The density 0.020 slug/ft^3 corresponds to the Mach 0.9, 10,000 feet flight condition. The density 0.031 slug/ft^3 corresponds to the NTF tunnel limit. The other densities are representative of the tunnel. Velocity-damping plots show the four solutions in Figures B-16 through B-19. The matched-point solution is shown in Figure B-20, where the flutter solutions are plotted on their corresponding constant density line at the equivalent velocity for a density of air at sea level. Theoretically, the curve drawn through the flutter solutions, when extrapolated to the Mach 0.9 line, determines the matched-point flutter velocity. Here it is clearly seen that the wings and carrythrough structure mounted on a "rigid" platform would have a huge flutter safety margin.

B.1.1.6 Other Design Concepts. Two "stress-skin" design concepts and one "soft skin" design concept were investigated prior to the final design concept. Figure B-2 desplays these three concepts in the top three shown. These concepts were abandoned for reasons of stiffness, strength, or manufacturability.

The two "stress skin" approaches were similar to those used successfully throughout the F-111 TACT program (Reference 26) and the Validation of Aeroelastic Tailoring by Static Aeroelastic and Flutter Tests program (Reference 32). Both designs were pursued with graphite-epoxy skins for stiffness. TSO was used to design skin thicknesses and orientations through an iterative process correlating structural influence coefficients to the full-scale finite element model. The initial concern in the design study was whether strength and stiffness in the skins could be satisfied for the high loads and cryogenic environment. The answer was yes for bonded structures such as these. Design of the skins was progressing when initial stress analyses showed that the internal loads in the core exceeded even aluminum honeycomb core at the design limit loads. Shear stresses for these designs are on the order of 1500 psi at the wing root. In the second version of the "stress skin" concept, two spars were incorporated to pick up some of the shear load. Stress analyses showed that the bond strength required to transfer load from the skins to a

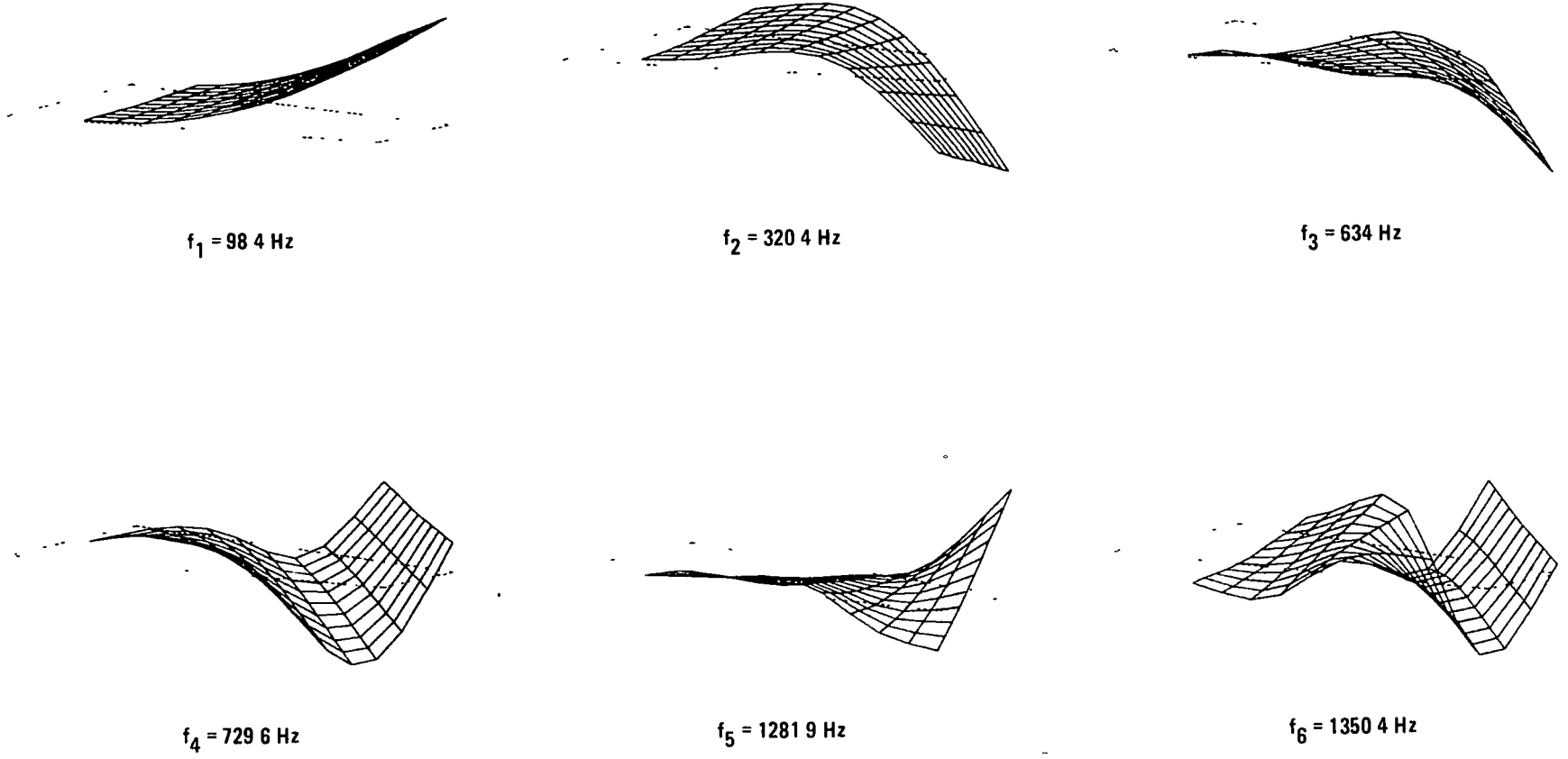

Figure B-15. Modes and Frequencies

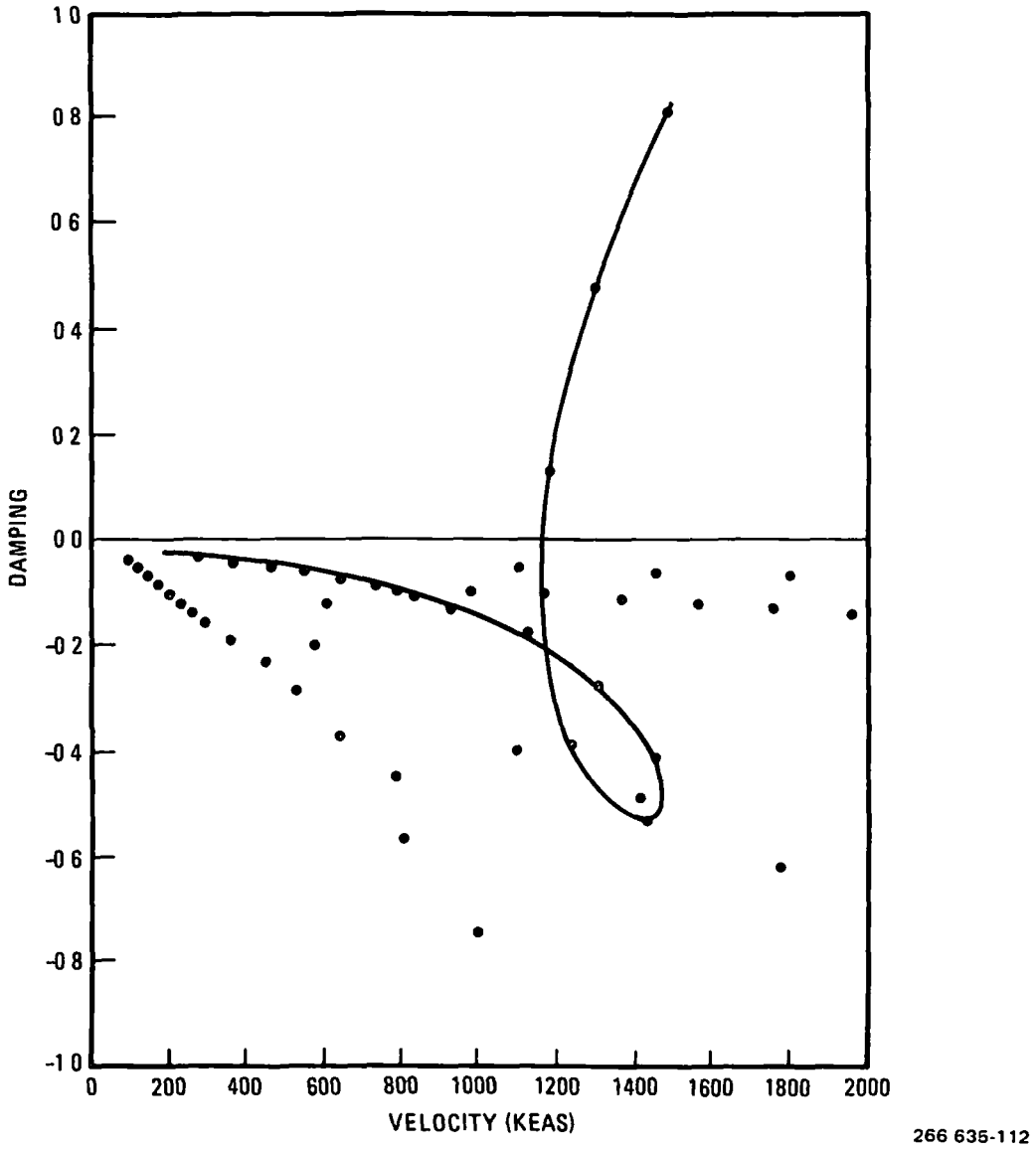

Figure B-16. Velocity-Damping, $\rho = 0.015$ slug/ft^3

spar at the 60% chordline far exceeded existing capabilities. At this point, a cursory look was made at a solid graphite-epoxy laminated structure in the wing box region (10% chordline to the 60% chordline). The maximum transverse shear stress for such a structure under the design torsion load exceeded the interlaminar shear strength of graphite-epoxy. Finally, mechanical fasteners could not be used because the stress concentration factor in the graphite-epoxy limits the strain capacity to 4500 microinches, and 8000 microinches is required for a safety factor of 2.

It was concluded that the severity of the high panel shear loads were dictating a "soft skin" design approach. The first attempt was with a wrapped closed cell graphite-epoxy tube-spar. TSO designs were generated modeling only

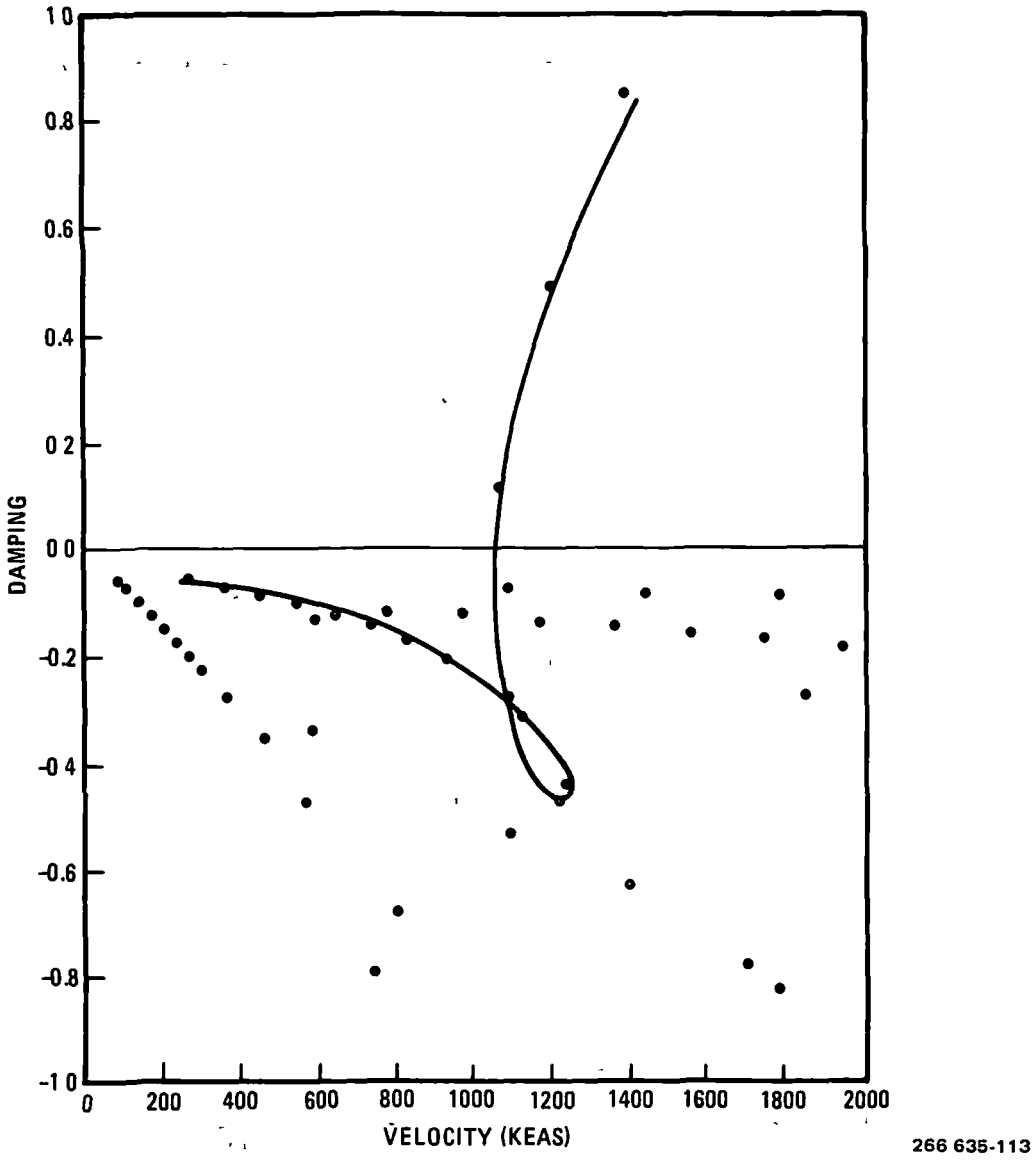

Figure B-17. Velocity-Damping, $\rho = 0.020$ slug/ft^3

the tube. Coinciding with the TSO runs, manufacturability was examined; it was concluded that the geometric cross sections allowed for the tube were insufficient for minimum radii for wrapping and insufficient to generate enough stiffness for the wing structure.

At this point, two conclusions were drawn from the design study.

a. Strength and stiffness requirements dictate a "soft skin" approach with an understructure of high stiffness (i.e., steel).

b. For some configurations in the NTF, there is obviously no such thing as a "rigid" aerodynamics model.

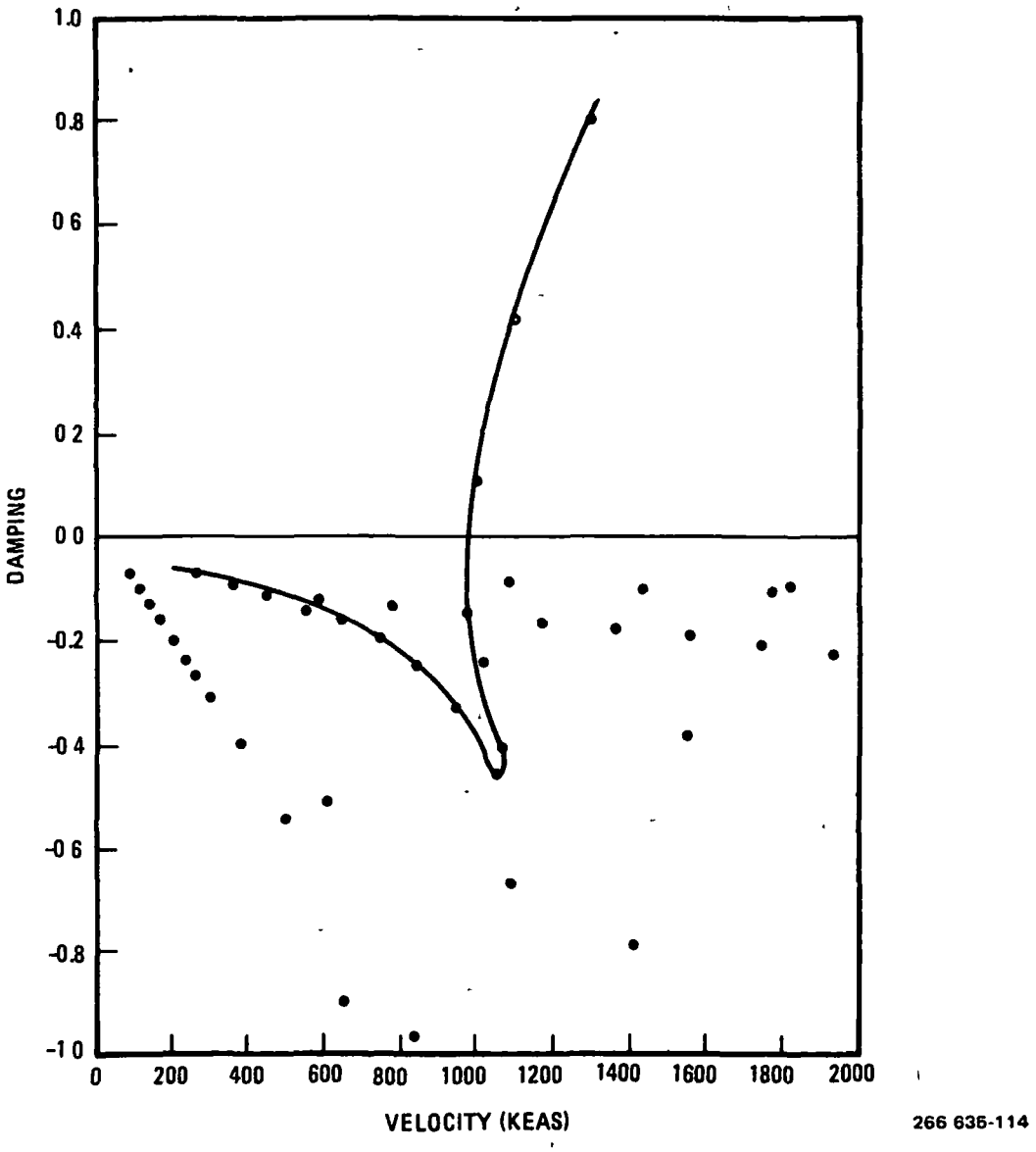

Figure B-18. Velocity-Damping, $\rho = 0.026$ slug/ft^3

B.1.2 FABRICATION CONCEPT. The fabrication concept was derived with the goals of controlling contour tolerances and surface finishes, while producing an integrated model system that includes the required wing instrumentation. The performance of aeroelastic wings often focuses on the fabrication process. The design load criteria for the wings in the NTF tunnel have dictated new design concepts and thus a state-of-the-art manufacturing concept. A baseline method called resin transfer molding (RTM) is proposed. In this process, two female molds enclose the basic structure (spar, instrumentation, and precured glass-epoxy skins). Resin is injected through side ports to fill the cavity, floating the spar between the skins. The outer contour tolerances are

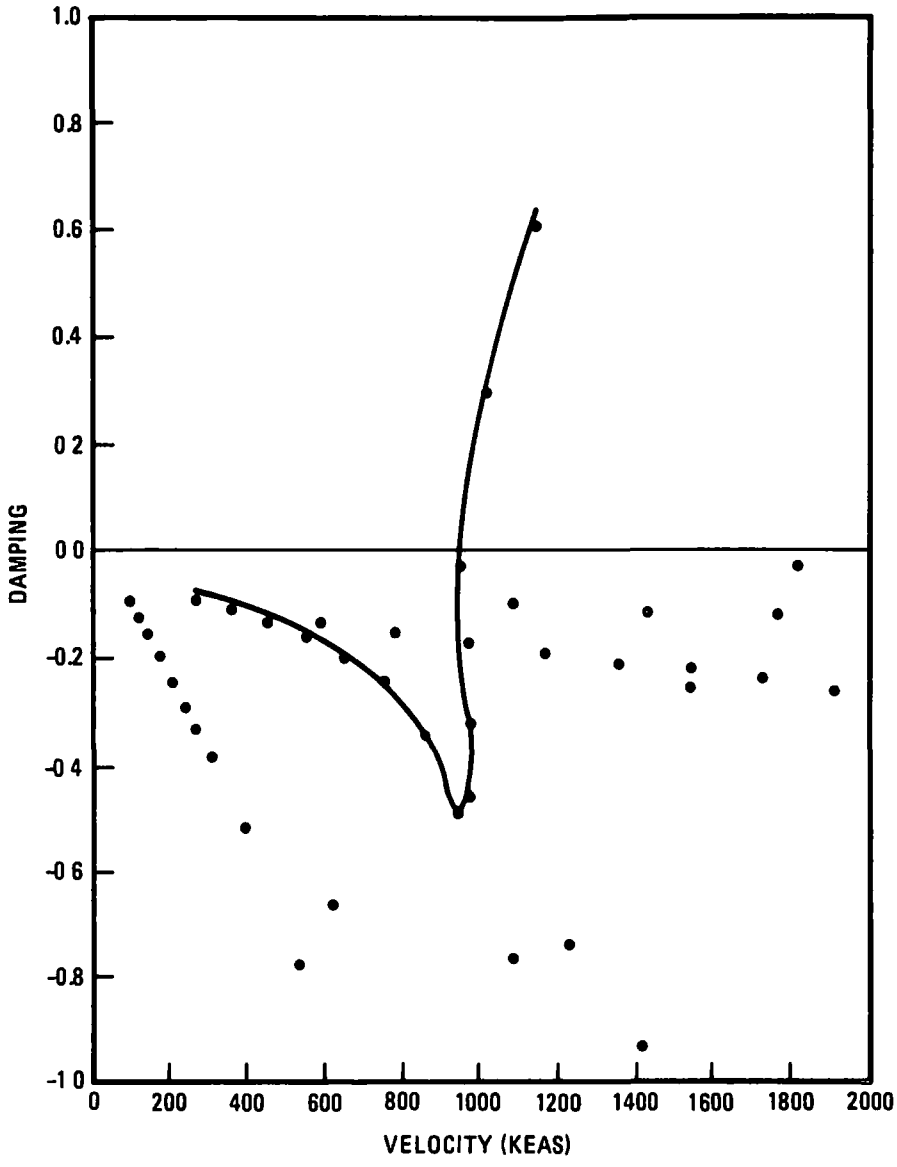

Figure B-19. Velocity-Damping, $\rho = 0.031$ slug/ft^3

as good as the molds because the skins are pushed flush against the molds by the internal pressure of the resin. The skin surface finish is as good as the surface finish of the molds because the skins are pre-cured in the molds before the RTM process.

The RTM process is illustrated in Figure B-21. Two match-die steel molds are machined to outer wing contour. The molds are made for semi-span wings. After the molds are machined, 0.010 inch diameter holes are drilled perpendicularly to the contour at pressure orifice locations. The molds should be inspected for contour tolerance. Next, glass - epoxy skins are cured in the molds with the pressure orifices being formed simultaneously from drill pins

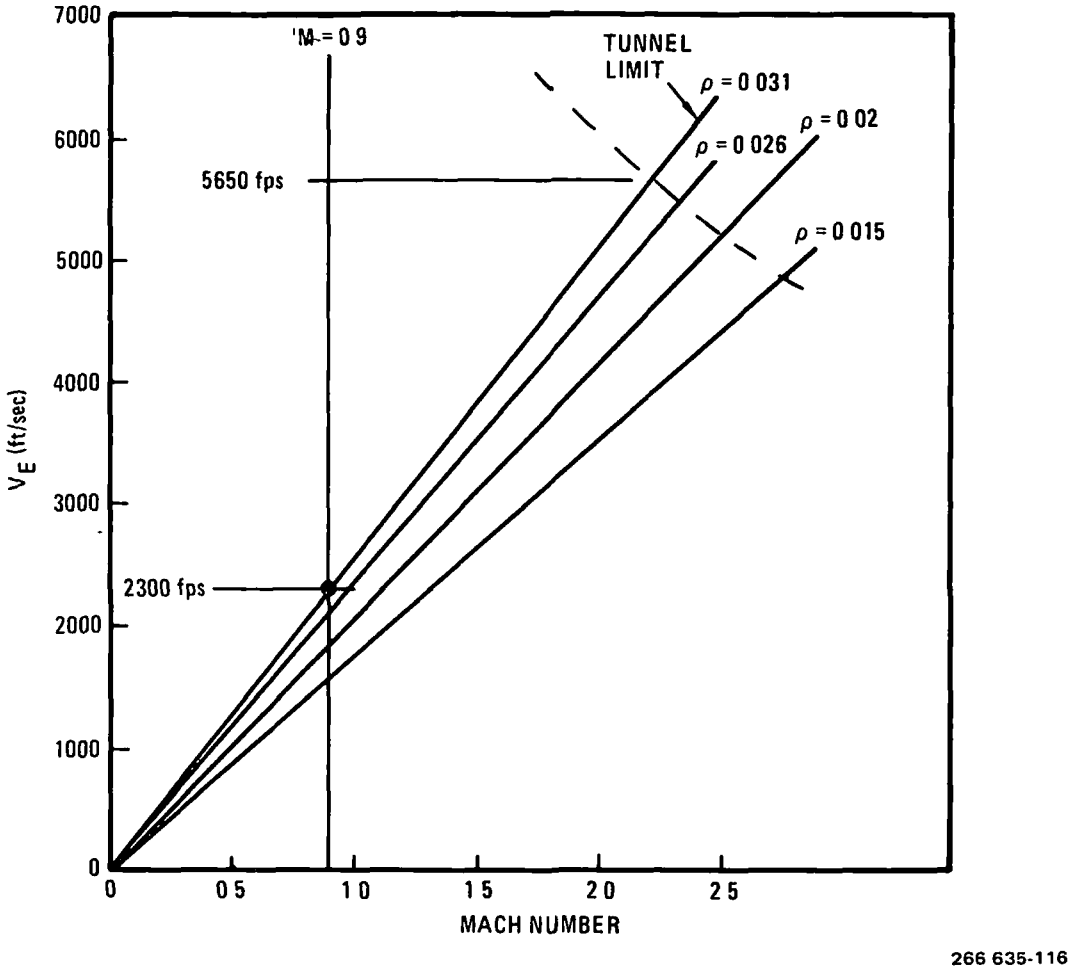

Figure B-20. Match Point Flutter Analysis at M = 0.9

placed in the holes in the molds. After the skins are cured, wax filaments, thermocouples, LED and a honeycomb core are bonded in place to the skins with a room-setting epoxy. This can be done with the skins setting in the molds. Simultaneously with machining the molds, the spar is machined to a tolerance to be specified to ensure matching the desired flexibility. In the RTM process, the two molds are placed together with the spar clamped at the pivot fitting in such a way to enable it to float between the skins. Finally, a room-setting epoxy resin is injected into the molds to bond the system together. After curing, the wings are heated to 150F to melt out the wax, thus providing internal pressure tubes that do not contribute to stiffness.

A key driver in this fabrication process is finding a resin system that, when slightly heated, allows the resin viscosity to drop sufficiently to flow smoothly during the RTM and while pot life is maintained until the mold cavity is filled. In addition, the resin system must hold its integrity at -260F. Such considerations were involved in resin screening tests, and Versamid 115®/Epon 828® was

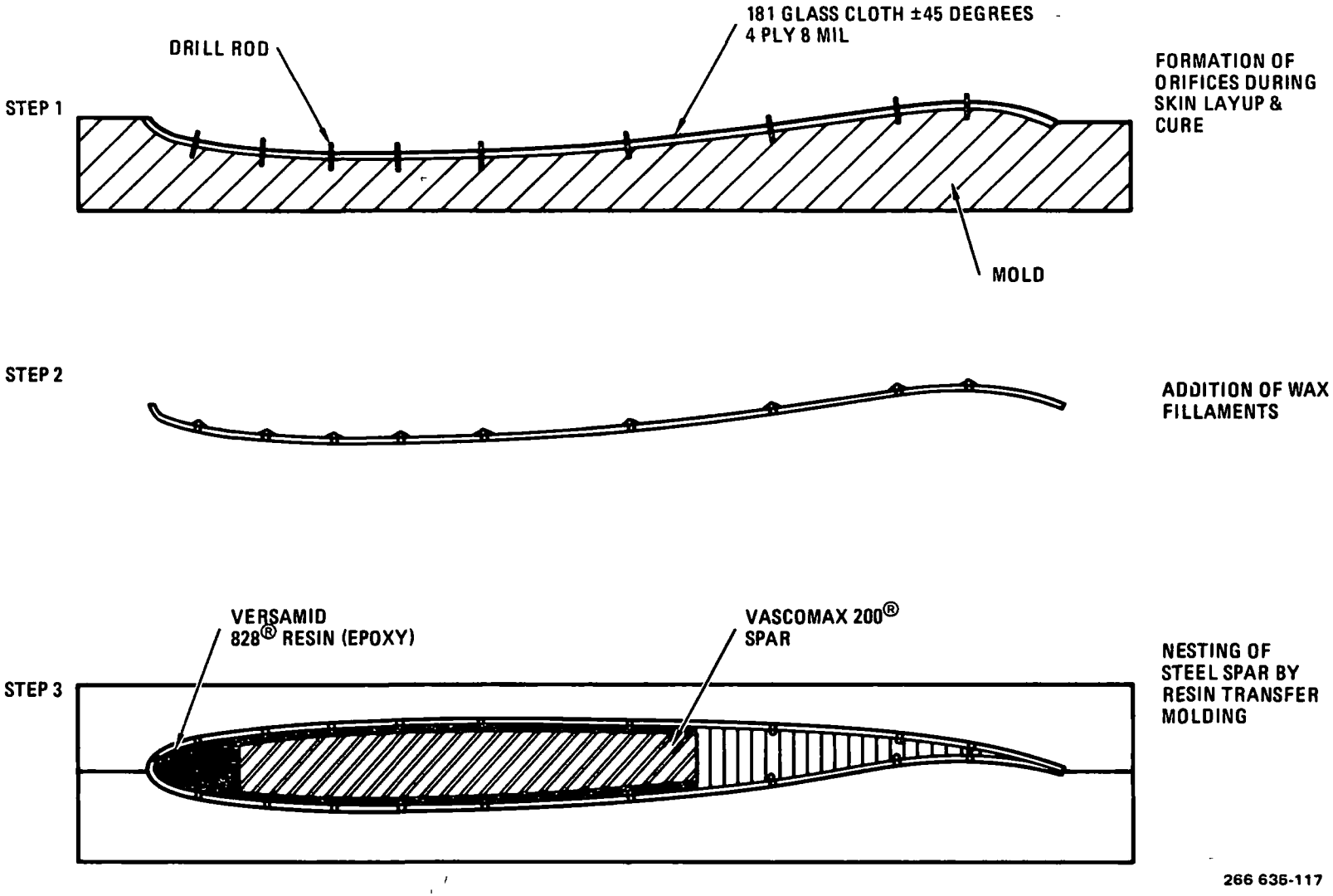

Figure B-21. F-111 TACT Aeroelastic Wing – Proposed Method of Fabrication

selected. Further discussion of these tests and other resin systems investigated is found in Section B.2.

Manufacture of the carrythrough structure can be accomplished using conventional machining techniques. It is estimated, based on experience with F-111 TACT flexible models (Reference 26), that multiple attempts in the carrythrough structure are required for accurate duplication of structural flexibility.

The RTM concept needs further development prior to final fabrication, and other concepts should also be investigated. General Dynamics is currently developing capability and experience with the RTM process. Another promising concept under consideration is elastic reservoir molding (ERM). This procedure consists of a resin carrier, specifically a foam, which is soaked in resin, placed between the two constituents being bonded, and compressed to a desired contour depth.

B.2 MATERIALS STUDY

Considerable effort was expended during the program to develop materials that would be compatible with the design concept, the environment, and the chosen manufacturing method. The environment represented a substantial challenge when coupled with the design loads and manufacturing method requirements.

The initial design approaches included graphite/epoxy skins bonded to nonmetallic honeycomb core, later replaced by a graphite/epoxy spar. Therefore, material screening/selection plans were designed to evaluate graphite/epoxy materials (FMS-2023 type) currently used at General Dynamics and adhesives that were known to have good low temperature properties. While preliminary testing (flexural, horizontal shear, tension, and compression, Table B-9) at room temperature and -300F on the graphite/epoxy material was being conducted, refinement in the analysis indicated that a design approach including a steel spar bonded to fiberglass/epoxy laminates would be a better structural choice. A new material evaluation study was undertaken using a current fiberglass/epoxy material, FMS-1025 Class I. The preliminary results of this evaluation are presented in Table B-10.

Candidate adhesives were originally screened for strength at low temperatures with the requirement of the recommended manufacturing method, resin transfer molding (RTM). Tables B-11 and B-12 show the results of the adhesive screening and evaluation effort while Figures B-23 and B-24 show the results of rheological work performed to evaluate the viscosity of the chosen two-part adhesive (Epon 828® and Versamide 115®).

Table B-9. Graphite/Epoxy (FMS-2023) Test Results

Material	Job	Test Temperation	Test Condition	Fiber Orientation 0 ksi(1)	0 msi(1)	90 ksi(1)	90 msi(1)	HS(1) ksi
Fiberite® T300-6K/976 B C3-483	C2012	RT	Dry	268	19.3	14.4	1.47	17.7
				288	18.2	19.1	1.49	17.6
				282	19.6	17.9	1.66	17.8
			Avg	279	19.0	17.1	1.54	17.7
			S.D.	(9.93)	(0.719)	(2.46)	(0.103)	(0.089)
		-300F	Dry	216	19.4	20.8	2.41	-
				181	19.4	24.0	2.53	27.8
				234	20.2	17.4	2.18	26.7
				249	20.2	20.9	2.39	25.8
				214	18.6	14.9	2.19	23.7
			Avg	219	19.6	19.6	2.34	26.0
			S.D.	(25.2)	(0.645)	(3.51)	(0.152)	(1.72)
B C3-491		RT	Dry	307	19.8	14.6	1.65	17.6
				267	19.2	15.7	1.66	18.1
				311	20.5	14.8	1.62	18.8
			Avg	295	19.8	15.0	1.64	18.8
			S.D.	(24.1)	(0.653)	(0.560)	(0.021)	(0.602)
		-300F	Dry	252	20.7	18.4	2.47	21.8
				194	20.1	17.4	2.46	22.0
				211	21.1	21.1	2.40	-
				250	29.8	32.6	2.47	21.4
				230	20.7	18.0	2.40	25.9
			Avg	227	20.7	19.3	2.44	22.7
			S.D.	(25.0)	(0.351)	(1.91)	(0.035)	(2.10)

Table B-9. Graphite/Epoxy (FMS-2023) Test Results, Contd

Material	Job	Test Temperature	Test Condition	Load: Tension[2] (lb)	Load: Compression[2] (lb)
Fiberite T300-6K/976 Mixed Batches	C2012	RT	Dry	283	325
				287	325
				292	342
			Avg	287	331
			S.D.	(4.51)	(9.81)
		-300F		260	362
				262	360
				264	350
				240	370
				268	392
			Avg	259	367
			S.D.	(10.9)	(15.8)

NOTES:

(1) Test specimens were cut from 15-ply all 0 degree laminates fabricated per GD/FW FPS-2021 (acceptance panels) and tested per FPS-2003.

(2) Test specimen was a pseudo beam with plies 1-4 as the test skin. (See Figure B-22 for test specimen drawing and fabrication in a four-point load fixture with the test skin down for tension and up for compression. The load was applied using a table-top Instron Model TM-L test machine.

(3) S.D. = Standard Deviation

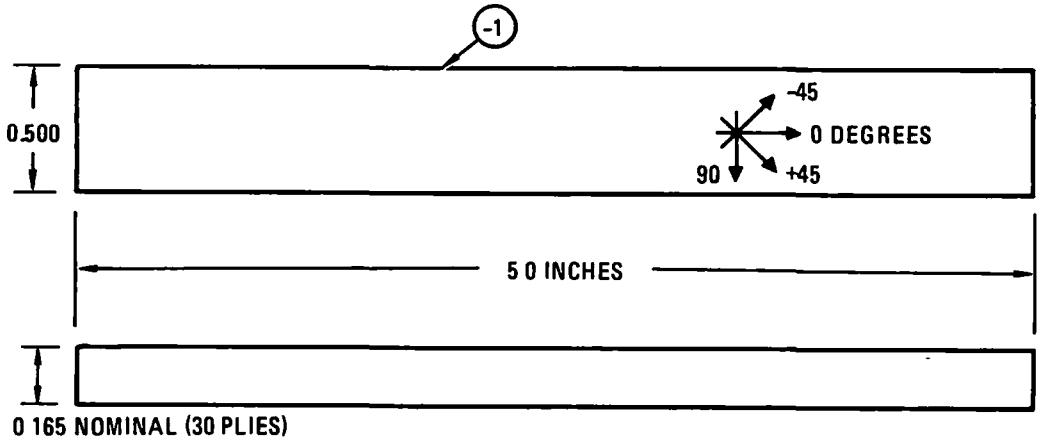

PLY NO	ANGLE
30	0
29	0
28	0
27	0
26	+45
25	-45
24	+45
23	-45
22	+45
21	-45
20	+45
19	-45
18	+45
17	-45
16	-45
15	+45
14	-45
13	+45
12	-45
11	+45
10	-45
9	+45
8	-45
7	+45
6	-45
5	+45
4	-45
3	0
2	90
1	+45

266 635-120

NOTES

1. PROCESS PER FPS-4509 WITH 2 PLIES OF 4819 BLEEDER AND INCLUDING NDI, UNCURED RC, AND CURED RC/FV GRADIENT
2. CUT IN 5.0 IN DIRECTION TO BE MADE WITH MICROMATIC WAFER SAW
3. PLY NO 1 GOES NEXT TO TOOL SURFACE
4. NUMBER PARTS SEQUENTIALLY BEGINNING WITH "1" AND INCLUDING BATCH NO
5. APPROXIMATE MATERIAL REQUIREMENTS
   -1 436 FT OF 3.0 IN TAPE FOR EACH 100 SPEC

Figure B-22. Compression Fatigue Sandwich Specimen

Table B-10. Fiberglass-Epoxy Test Results

Material	Job	Test Temperature	Test Condition		Flexural Strength (ksi)	(Warp)[2] Modulus (msi)
FMS-1023 Class I(3)	C2040	RT	Dry		94.7	3.59
					93.5	3.65
				Avg	94.1	3.62
				S.D.	(0.825)	(0.043)
		-300	Dry		163.0	4.58
					165.0	4.47
					166.0	4.45
					145.0	4.50
					167.0	4.34
				Avg	161.0	4.47
				S.D.	(0.34)	(0.084)

NOTES:

(1) Total test plan included tension and compression test at room temperature and -300F.

(2) Flexural specimens were from panel fabricated for batch acceptance per FMS-1023. Test specimens and procedure was conducted per FPS-1028A-053 (Type 1 specimen).

(3) FMS-1023 Class I is an epoxy inpregnated fiberglass cloth (181-style) material that will cure in an oven under vacuum pressure.

Table B-11. Failing Load, Ultimate Strength and Failure Mode on Short Beam Flex Using Three Adhesives

Adhesive	Test Temperature	Spec No.	Failing Load (lb)	Ultimate Strength (psi)	Failure Mode
Hysol LR 100-497®	75F	1	1135	241.9	Core failure
		2	920	196.6	Core failure
	-300F	3	290	61.8	Core and adhesive failure
		4	730	154.4	Core and adhesive failure
		5	675	145.9	Core and adhesive failure
AF-163	75F	1	1000	219.2	Core failure
		2	1020	220.1	Core failure
	-300F	3	840	182.1	Core failure
		4	1250	271.8	Core failure
		5	1090	237.6	Core failure
828/115	75F	1	887	192.0	Core and adhesive failure
		2	820	177.2	Adhesive failure
	-300F	3	1130	244.9	Core and adhesive failure
		4	1170	249.7	Core and adhesive failure
		5	1035	223.8	Core and adhesive failure

The rheological study summarized by Figures B-23 and B-24 was undertaken to provide processing data for use of the adhesive system with the RTM equipment. Figure B-23 indicated the individual components could be liquified to a point they could be moved (pumped) by the RTM equipment. The viscosity versus time of the mixed system (Figure B-23) indicated the molding process had to be completed within 40 minutes after the components were mixed. Figure B-24 is the rheological viscosity versus temperature of the mixed adhesive and indicates that the viscosity of the system, although high for RTM systems, could be managed.

Because of the necessity for including pressure instrumentation, thermocouples, and LEDs through the bondline, and the requirement of the RTM manufacturing method, a glueline thickness in the order of 0.030 to 0.070

Table B-12. Single Overlap Shear Results Using Three Adhesives

Adhesive	Test Temperature	Spec No.	Failing Load (lb)	Ultimate Strength (psi)	Failure Mode
Hysol LR 100-497®	75F	1	940	1728	100% adhesive
		2	1050	2011	100% adhesive
	-300F	3	800	1407	100% adhesive
		4	750	1364	100% adhesive
		5	835	1443	100% adhesive
AF-163	75F	1	1190	2168	100% adhesive
		2	1330	2516	100% adhesive
	-300F	3	1300	2336	100% adhesive
		4	-	-	-
		5	1160	1955	100% adhesive
828/115 60-40	75F	1	1060	2470	100% adhesive
		2	1055	2494	100% adhesive
	-300F	3	490	1218	100% adhesive
		4	530	1236	100% adhesive
		5	585	1321	100% adhesive

NOTE: See Section B.2.1 for test specimen fabrication and testing details.

inch was expected. To evaluate this thick glueline, fiberglass/epoxy-to-D6ac steel double overlap shear specimens were fabricated. Two plies of 0.020 inch continuous filament fiberglass mat were included in the bondline to give the desired thickness and to include a fiberglass mat reinforcement in the final demonstration part bondline. D6ac steel was used as the tongue material because of its availability and "perceived" surface similarity (flash rust) to the maraging steel chosen for the spar. The results of this evaluation are given in Table B-13. The results indicate that the reinforced 0.040 inch thick glueline should be adequate to carry the predicted bondline stresses (200-400 psi).

B.2.1 SCREENING OF ADHESIVE FOR MODEL USE

Materials:

Hysol LR 100-497® Urethane

3M AF-163® Adhesive

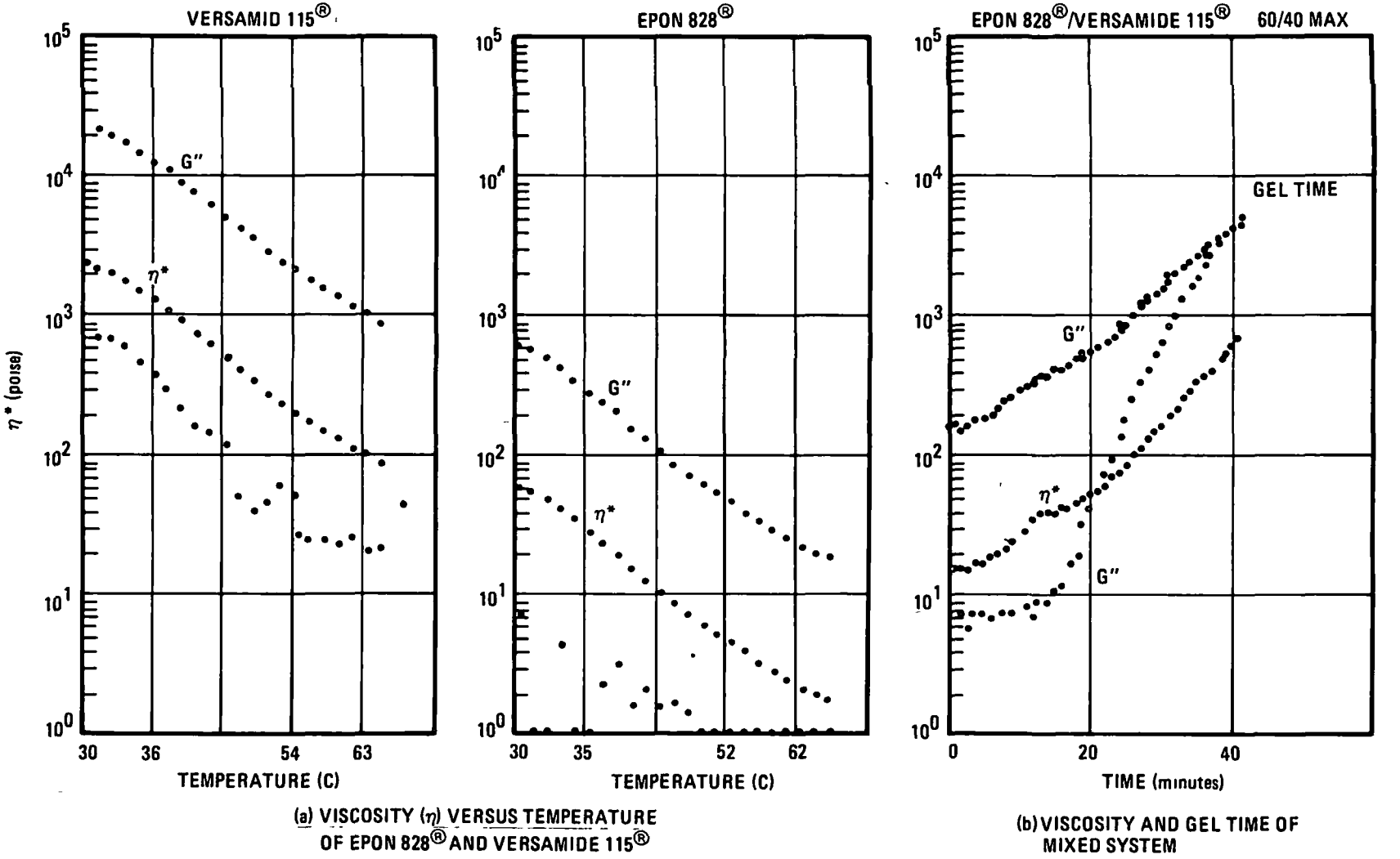

Figure B-23. Rheometric Curves for Adhesive

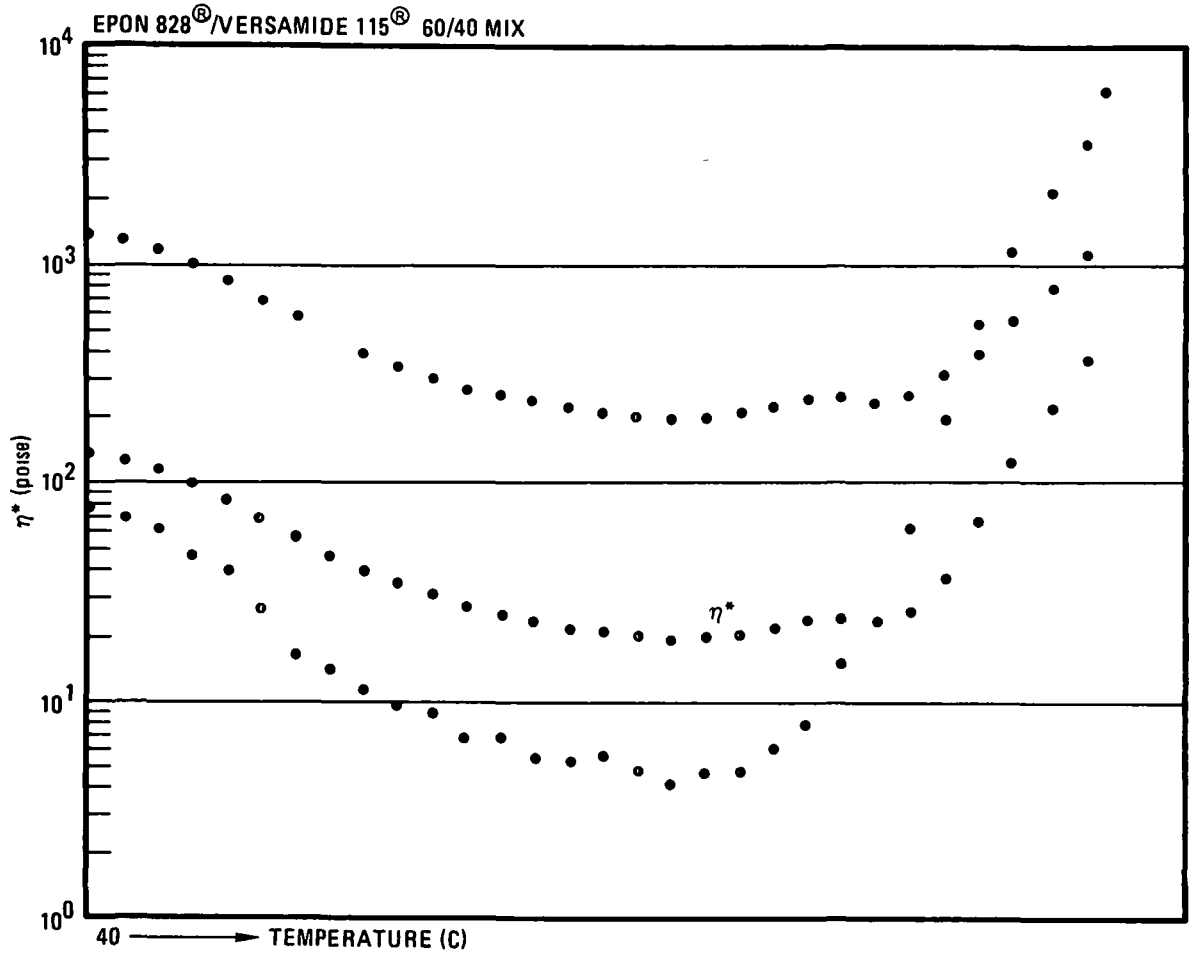

ETA* (POISE)	TIME (MINUTES)	TEMPERATURE (C)
1.358E+02	0.1	40
1 284E+02	1.1	40
1.165E+02	2.1	41
1 005E+02	3.1	42
8 496E+01	4.1	43
7 013E+01	5 1	45
5 763E+01	6 1	47
4.744E+01	7 1	48
4.033E+01	8 1	50
3 527E+01	9.1	52
3 166E+01	10.1	54
2.846E+01	11 1	56
2.610E+01	12 1	57
2 414E+01	13 1	60
2 253E+01	14 1	61
2.153E+01	15 1	63
2.074E+01	16 1	65
2 022E+01	17 1	67
2 042E+01	18 1	69
2 131E+01	19 1	71
2 266E+01	20 1	73
2 467E+01	21 1	75
2 547E+01	22 1	77
2.399E+01	23 1	79
2 699E+01	24 1	81
3.819E+01	25 1	83
7 046E+01	26 1	85
1 313E+02	27 1	87
2 332E+02	28 1	89
3 841E+02	29 1	91

266 635-119

Figure B-24. Rheometric Viscosity of Adhesive with Constant 2-degree (C) Heating Rate

Table B-13. Results of The Double Overlap Specimen Testing[1]

Specimen No.	Test Temperature (F)	Load (lb)	Bonded Area (sq in)	Shear Strength (psi)
P2[2]	-300	1210	0.7082	1709
P4	-300	1200	0.7953	1509
UP2[3]	-300	1890	0.8299	2278
UP4	-300	1560	0.8733	1787
P1	75	1510	0.7521	2008
P3	75	1680	0.7463	2251
UP1	75	1700	0.7591	2240
UP3	75	1960	0.8028	2442

NOTES:

(1) Specimens were FMS-1023 Class I fiberglass/epoxy skin (12 plies) bonded to 0.100 inch thick D6ac steel coupons with approximately 0.5 inch overlap. See Section B.2.2 for additional details.

(2) P = D6ac primed with FMS-3018 primer before bonding.

(3) UP = no prime on metal before bonding.

P6019-12 Epon 828®/Versamid 115® Adhesive

Two ply FMS-1023 Class I Glass/Epoxy Skin

Nomex® core, P653-65

Methyl-ethyl-ketone

240 Grit Sandpaper

Procedure:

1. Shear beams measuring 3.0 × 8.0 inches were fabricated using two plies precured FMS-1023 Class I Glass/Epoxy as skins, Nomex® core (P653-65, -1/8 in. cells, 4 lb cu ft), and three candidate adhesives.

2. For all of the shear beams, 3.0 × 8.0 inch pieces of the glass epoxy were cut from the larger skin with the warp in the 8 inch direction. Prior to bonding, the bag side of each piece was prepared per FPS-3016C 5.3 part C. This involved lightly sanding the part with 240 grit.

3. Pieces of Nomex® core (P653-65) 3.0 × 8.0 inches in dimension were then cut and blown clean with compressed air.

4. Five shear beams were made using each of the three candidate adhesives:

   (1) Hysol LR 100-497® Urethane

   (2) 3M AF-163® Adhesive

   (3) Epon 828/Versamid 115® Adhesive

   a. The Hysol LR 100-497® Urethane adhesive was mixed in a ratio of 100 parts A to 13 parts B, by weight. Small amounts of this adhesive were mixed sufficient only to assemble one shear beam because the work life was not long enough to assemble all of the beams at once. The adhesive was spread on the faying surfaces and the panels were assembled. The panels were cured under contact pressure for 3 days at room temperature.

   b. The AF-163 adhesive was thawed and one layer was cut to the dimensions of each faying surface and assembled. The assemblies were then cured in a steam press with a ramp from 80F to 250F in approximately 35 minutes and then a hold at 250F for 1 hour.

   c. The Epon 828®/Versamid 115® adhesive was mixed in a ratio of 60 parts 828 to 40 parts 115, by weight. Since this adhesive had a rather long work life, enough adhesive could be mixed to assemble all of the beams at one time. The adhesive was applied to the faying surfaces and the beams were assembled. They were then cured under contact pressure at room temperature for 36 hours.

5. Panels measuring 4 × 7 inches to be used in fabricating single lap shear specimens were fabricated using eight plies of FMS-1023 Class I glass/epoxy material. A panel 16 × 16 inches was cured in the cavity press at 75 psi. The cure was a ramp from room temperature to 250F in approximately 35 minutes and then a hold for 1 hour at 250F. After cure, six 4 × 7 sections were cut from the large panel. These 4 × 7 inch pieces were matched in a 1/2 inch overlap, and rivet holes were drilled at each end to ensure a proper overlap.

6. The faying surfaces for each of the assemblies was prepared by removing one layer of glass (the peel ply). The three adhesives were applied to the faying surfaces of the single overlap assemblies in the same manner as was previously described in the procedure for the shear beams, except that the Epon®/Versamid® 828/115 was mixed in a 50/50 ratio and the cure time was 24 hours at room temperature. The single overlap shear coupons were

initially assembled using a 60/40 mixture of Epon®/Versamid®. However, for some reason the coupons did not cure properly. A decision was made to assemble another set of coupons using a 50/50 mixture of the Epon®/ Versamid® did cure properly. Following cure, five 1.0 × 7.5 inch single overlap shear specimens were cut from each assembly.

Testing:

The testing of the shear beams was done on the table-top Instron. Because the chamber of the Instron was smaller than 8 inches, 1/2 inch was cut from each end of the shear beams prior to test. The beams were tested per FPS-1028D, Method B-053, with a 6 inch span, three point loading, and 1 inch wide load pad and 1/2 inch wide support pads.

The single overlap shear coupons were tested on the Instron Model TTDL machine, serial number 1493. The head rate was 0.05 inch per minute and the chart rate was 1 inch per minute. Testing personnel noted that at the extreme negative temperatures, the glass epoxy specimens were by hard to grip in the test fixture.

Results:

The results derived from this exercise were shown in Tables B-11 and B-12.

Conclusions:

The shear beam results at room temperature were relatively consistent except that the results for the Epon®/Versamid® 828/115 were slightly lower than the results for the other two adhesives. The shear beams tested at -300F showed some interesting results. The ultimate strength of the Hysol® Urethane were slightly lower than the results for the other two adhesives. The Hysol® urethane specimens, when tested at -300F, again showed a decreased strength of approximately 25% over those tested at room temperature. The ultimate strength of the AF-163 adhesive at -300F decreased approximately 8% over the room temperature results. Finally, the Epon®/Versamid® 828/115 adhesive ultimate strength at room temperature was 51% higher than the ultimate strength at -300F.

These results show that for specimens exposed to extremely low temperatures the AF-163 adhesive shows the least change in results as compared to those at room temperature. However, if a room temperature curing adhesive is needed, the Hysol® urethane gives higher ultimate strength results at -300F than the Epon®/Versamid® 828/115 adhesive. Therefore, further testing may be necessary to find the optimum adhesive with the appropriate cure cycle needed to perform these procedures in the environments for which they are necessary.

B.2.2. RHEOLOGICAL MEASUREMENTS

All rheological measurements were performed on the Rheometrics, Inc. Dynamic Spectrometer (RDS Model 7700) utilizing the parallel plate fixtures. In typical operation, the resin sample is placed between the two parallel plates. The upper plate (attached to a dc torque motor) applies a sinusoidal strain to the resin. The lower plate is attached to a transducer that measures the resultant torque. The central processor utilizes actual strain, torque, and sample geometry to calculate rheological data. The settings used to test the Epon 828®/Versamid 115® mixture are given in Table B-14. Gel times are for the G = G modulus crossover as suggested by Tung and Dynes (Reference 33).

Table B-14. Spectrometer Settings

Mode: Time Sweep, Cure
Test: Parallel Plates
Plates: 50 mm diameter
Gap: r 0.6 mm
Strain: 50%
Rate: 10 rad/sec
Temperature: 149F or 2C/min ramp
Transducer: 200 gm/cm
Gas: Air

B.2.3 CLEANING AND BONDING OF LAPSHEAR SPECIMENS, P563-809

a. Cleaning of Steel

Material: Lapshears - D6ac

1. Clean all dirt and chips from surface.
2. Wipe surfaces with clean cheesecloth moistened in 1,1,1-trichloroethan. Remove all foreign material.
3. Air dry for 20 minutes.
4. Grit blast with No. 120 aluminum oxide until uniformly gray surface is obtained.
5. Wipe surfaces with previously degreased cheesecloth moistened with 1,1,1-trichloroethane. If local discolored areas appear, remove with No. 320 grit aluminum oxide paper and repeate the wipe operation.
6. Air dry for 20 minutes.

7. Apply one thin coat of FMS-3018 primer within 30 minutes after completion of grit blast. Dry primer at RT for 30 minutes and at 250 +20/-10F for 30 minutes.

   NOTE: Only one-half of specimens are to be coated with primer.

8. Wrap in brown paper after drying of prime.

b. Bonding

Materials: Epon 828® (60 parts by weight)
Versamid 115® (40 parts by weight)
D6ac steel (cleaned) (0.100 in thick)
FMS-1023 Class II Precured Skins
Glass Mat (0.020 in thick)

1. Remove peel ply from one surface of glass laminates (P653-55).
2. Locate laminates on tool to maintain a 0.1 inch gap.
3. Mix adhesive per above ratios.
4. Apply an even coat of adhesive to glass surfaces.
5. Apply one ply of glass mat.
6. Apply an even coat of adhesive.
7. Apply second layer of glass mat.
8. Apply another coat of adhesive evenly over glass mat.
9. Locate D6ac steel on adhesive/glass so as to maintain 0.5 inch overlap.
10. Repeat procedures for applying adhesive, glass mat, and fiberglass laminates.
11. Allow assembly to stand at room temperature with uniformly applied pressure for 24 hours.
12. Heat assembly to 140-150F for 1 hour.
13. Cut and trim specimens to dimension.

B.3 PROOF-OF-CONCEPT PROGRAM

A proof-of-concept program was initiated to verify and develop design concepts, develop the fabrication process of the wing alone, and gain experience for testing at cryogenic temperatures. When the "soft skin" final concept was developed sufficiently to demonstrate the viability of the design, a proof-of-concept component was designed. An attempt was made to build the component, and a test program was devised to investigate wing instrumentation concepts and the structural integrity of the wing concept.

B.3.1 DESIGN OF THE COMPONENT. The component was designed with three goals. The stress level at the critical point analysis discussed in Section B.1.1.5, Analyses, was to be duplicated in the component. The "lost wax" pressure instrumentation method would be tested under loading at cryogenic temperatures to provide ensurance of pressure channel integrity. The component was designed to be built using the RTM process.

Figure B-25 is a sketch of the component. The primary structure is an 18Ni-200 maraging steel spar. The spar was designed for the purpose of reproducing stresses of 170,000 psi (ultimate) at the location of the pressure orifices. The skins of the component are four plies of 181-75 glass-epoxy fabric. The bondline is to be Versamid 115®/Epon 828® reinforced with glass matting as in the final design concept. Blue wire wax, 0.020 inch diameter, was to be used from the orifices to a common manifold per wing side to form the pressure channels.

B.3.2 FABRICATION OF THE COMPONENT. Fabrication of the component was never completed. The fabrication process included resin transfer molding as discussed in Section B.1.2. The tooling consisted of match-die fiberglass reinforced plastic molds. The plastic gel coat used for the molds is new on the market, while the tooling concept is a well-established procedure at General Dynamics. During the process in which the skins were cured for the component, the molds were destroyed when the skins/molds could not be separated. An investigation revealed possible explanations, however, it was clearly determined that the gel coat used came from a bad batch of material. A recovery plan was devised that incorporated returning to the usage of the old standard gel coat.

The manufacturing process steps were:

1. A bass wood replica (i.e., plug) was made of the component, sanded, and a release agent applied.
2. An aluminum holding fixture was prepared for the wood. A reservoir was machined into the aluminum, then an inset for the plug was machined into the reservoir.
3. A gel coat (REN) was applied across the surface of the aluminum reservoir and the exposed side of the plug in the reservoir. (The plug was placed so that the midplane and above was exposed.)
4. One ply of 20 mil matte cloth and six plies of 120 (5 mil) glass cloth (dry) were laid up over the plug to provide structural integrity in the mold.
5. A mixture of 1025 resin and chopped fiber was poured into the reservoir and allowed to cure. Exotherm temperature reached 85F.
6. The mold was removed from the reservoir and flipped over, (with the plug remaining in the mold). Metal strips were built up around the mold, forming a new reservoir. Steps 3, 4, and 5 were repeated.

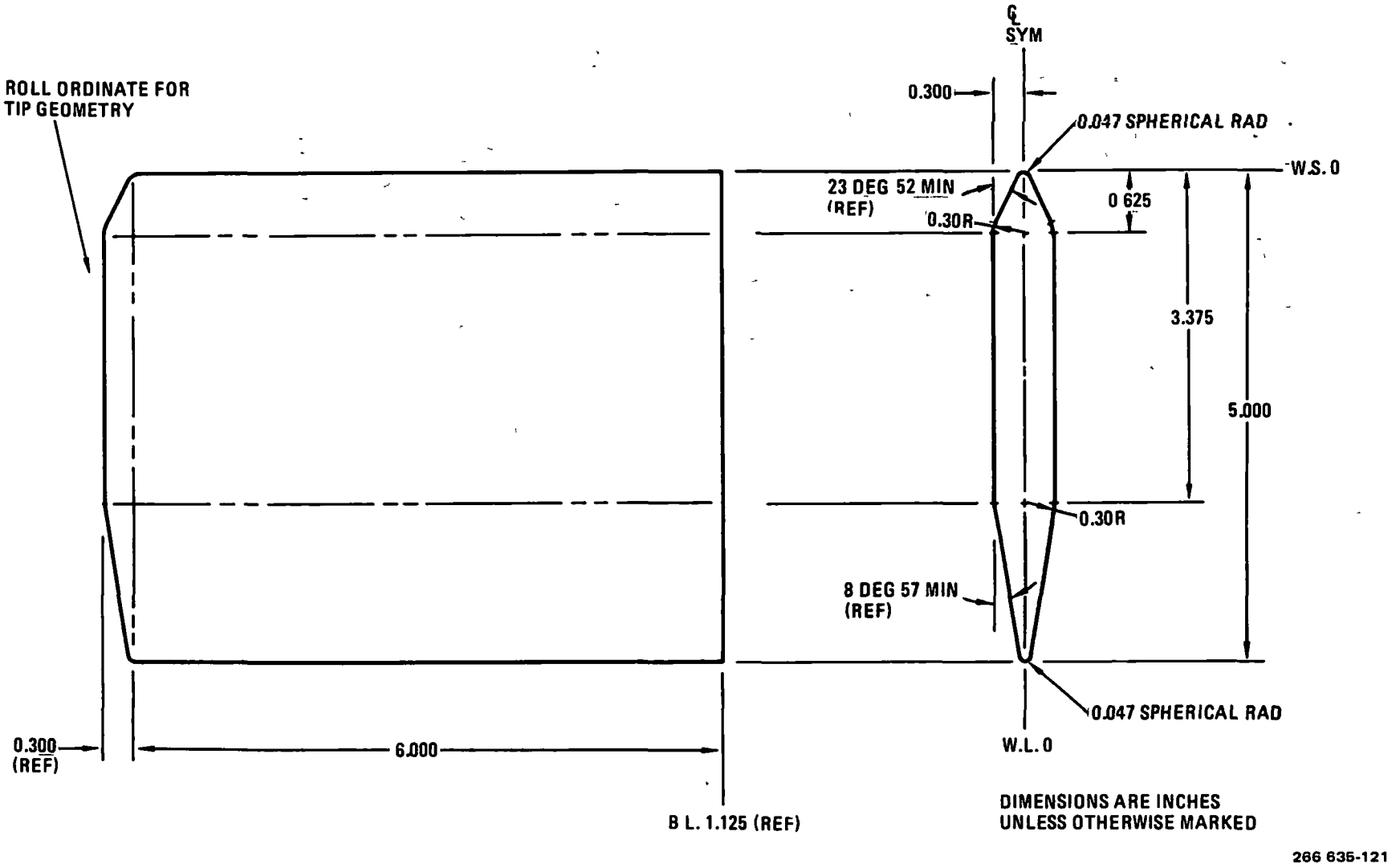

Figure B-25. Wing Geometry and Orifice Location

7. The two mold halves were split apart, the plug removed, and the insets wet sanded.

8. Pin holes (0.14 inch in diameter) were drilled into the insets perpendicular to the contour. Drilling was done with a drill press.

9. At this point it was observed that the molds had warped, and an attempt was made to straighten them.

   - The molds were put together using locating pins drilled at the completion of the mold halves. The plug was enclosed in the molds.
   - Three plies of 181 glass-epoxy pre-preg were laid up on the back surface of each mold half.
   - The glass was cured at 350F and 10-15 psi.
   - The mold half fabricated in the aluminum reservoir was straightened. The other mold half was still warped.
   - In addition, the surfaces of the insets had bubbled and crazed, and voids were detected.
   - The mold halves were repaired by tapping and chipping out the void areas and reapplying the REN gel coat.

10. A release agent (CANT STICK®) was applied to the mold.

11. Drill bits were placed in the mold holes.

12. One ply of 108 glass-epoxy scrim cloth and then four plies of 181-75 glass-epoxy pre-preg were laid up in the mold halves. Layers of Teflon® film, vent cloth, and Teflon® film were put down.

13. A sculptured piece of foam was placed over the drill pins and pushed down on the layup to ensure that the drill bits did not puncture the vacuum bag used for curing. The foam covered the full chord length and a span width of ±1 inch to either side of the pins.

14. The skins were bagged and cured at 275F and 45 psi for about 90 minutes.

The skins could not be separated from the mold. An investigation resulted in two observations:

- The heating rate in the skins varied from the areas under the foam and those not under the foam.
- Other manufacturing groups were having trouble with the same batch of gel coat.

Had the manufacturing process continued, the following steps were planned.

- Machine injection points into the molds, after curing the skins.
- Establish a seal around the edge of the molds and build up shims in the molds to float the spar.
- Place the wax filaments in the skin, and paint with an epoxy.
- Melt out some of the wax filaments before RTM to check pressure channel integrity.
- After RTM, melt out the remaining wax filaments and check both sets for pressure channel continuity.
- Design and build a pressure manifold to hook up to the pressure channel.

B.3.3 PROPOSED TESTING OF THE COMPONENT. Testing of the component is depicted in Figure B-26. An insulating box was built for testing at -260F. The component was to be loaded as shown in the figure for static loads producing stresses in the spar up to 170,000 psi. Using the manifold built in the fabrication process, and by plugging pressure orifices, pressure channel integrity would be checked simultaneous to the loading via a vacuum check.

☆U S GOVERNMENT PRINTING OFFICE 1984 -739 -010/ 19 REGION NO 4

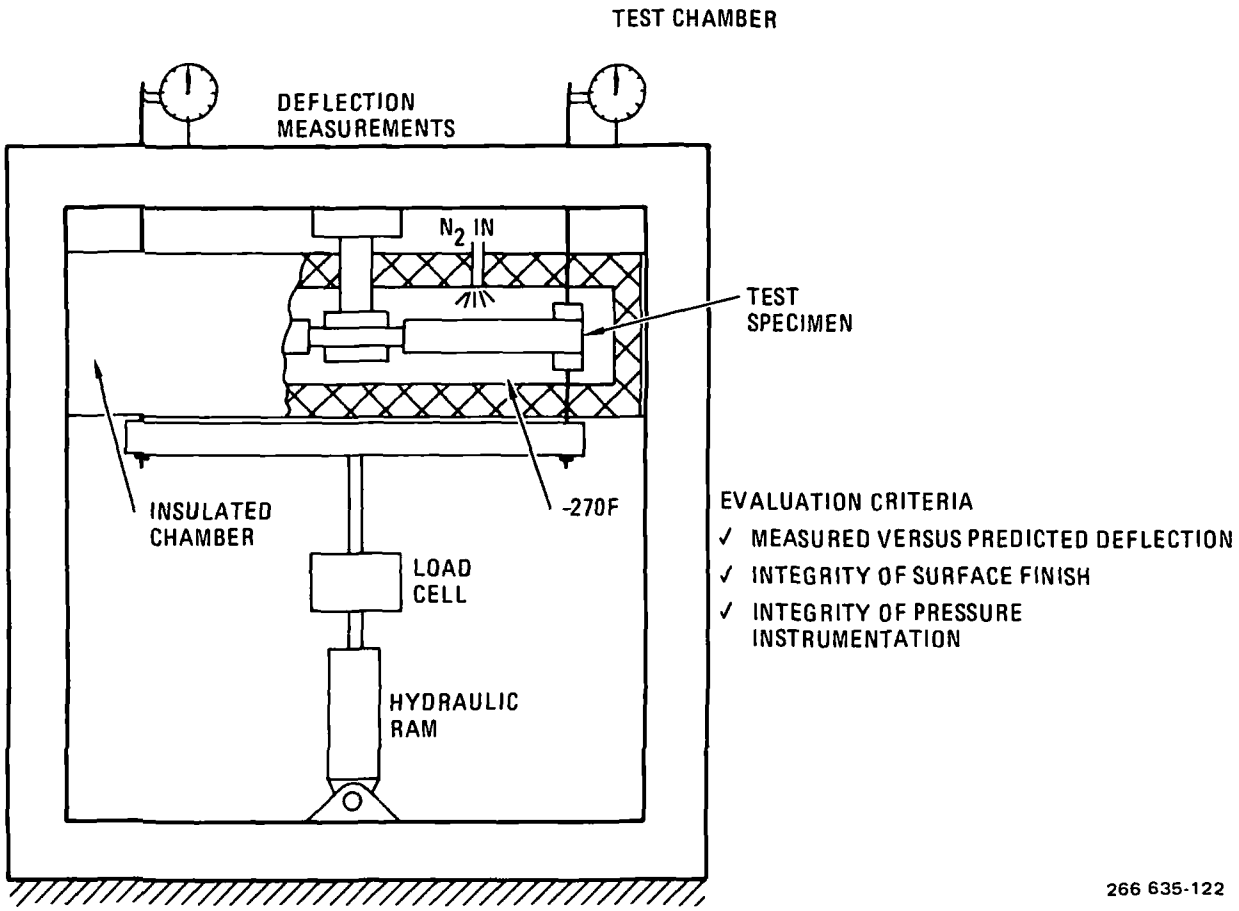

Figure B-26. F-111 TACT Aeroelastic Wing - Proof of Concept Tests

1 Report No	2 Government Accession No	3. Recipient's Catalog No
NASA CR-3827		

4 Title and Subtitle	5 Report Date
DESIGN STUDY OF TEST MODELS OF MANEUVERING AIRCRAFT CONFIGURATIONS FOR THE NATIONAL TRANSONIC FACILITY (NTF)	August 1984
	6 Performing Organization Code
7 Author(s) S. A. Griffin, A. P. Madsen, A. A. McClain, et al.	8 Performing Organization Report No. GDC-CRAD-83-002
9 Performing Organization Name and Address GENERAL DYNAMICS CORPORATION Convair Division, 5001 Kearny Villa Road, San Diego, CA 92123 Fort Worth Division, General Dynamics Blvd, Fort Worth, TX 76108	10 Work Unit No 11 Contract or Grant No NAS1-16848
12. Sponsoring Agency Name and Address National Aeronautics and Space Administration Washington, DC 20546	13 Type of Report and Period Covered Contractor Report Sept 1981 - Dec 1982 14 Sponsoring Agency Code

15. Supplementary Notes
Langley Technical Monitor: Blair B. Gloss
Final Report

16 Abstract The need for a large High Reynolds Number Transonic Wind Tunnel has been widely recognized throughout the industry, both in the USA and Europe for many years. Such a facility will provide a much needed tool for studying phenomena sensitive to Reynolds number. The National Transonic Facility (NTF), located at NASA Langley Research Center, in the USA is now entering the calibration phase and has the desired capability. Its usefulness, however, will be greatly influenced by the ability of industry to develop model systems capable of withstanding the severe operating environment of the facility so necessary to achieve full-scale Reynolds number, without degradation of accuracy, and at reasonable cost.

The basic objective of this engineering study is to determine the feasibility of designing models of advanced aerodynamic technology maneuvering aircraft and to achieve full-scale Reynolds number for each configuration in the NTF. The study concludes that the facility (NTF) does offer the potential for making tunnel to full-scale data correlations for this type of aircraft configuration.

17 Key Words (Suggested by Author(s))	18 Distribution Statement
High Reynolds Number Wind Tunnel Models Cryogenics National Transonic Facility	Unclassified - Unlimited Subject Category 09

19 Security Classif (of this report)	20 Security Classif (of this page)	21 No of Pages	22 Price
Unclassified	Unclassified	310	A14

For sale by the National Technical Information Service, Springfield, Virginia 22161

CONFIGURATION	δ LEF	δe	δa	NO OF RUNS	α	β	MACH NUMBER									$R_{N_{\bar{C}}} \times 10^{-6}$ ($\bar{c}$ = 0.25m = 0.82021 ft)												P_t (ATM)			JUSTIFICATION
							0.6	0.8	0.85	0.9	0.925	0.95	0.975	1.05	1.1 1.2	3	4	6	10	15	25	32	40	50	65	75	SELECT	SELECT	SELECT	SELECT	SELECT	SELECT	
CWC	0	0	0	7	A	0	●									√	X	X	X	√√							√ 21.3			1(RN<15)	2(RN>15)		RN VAR AT CONST Q SELECT RNs CORRESPOND TO ALTITUDE = 30,000 ft & SEA LEVEL
				4	B		●															X				√ 21.3	√ 52.5			3(RN=21.3)	4(RN>21.3)		Q VAR AT CONST RN FOR AEROELASTIC EFFECTS
				8	C					●						√	√	√	√	√√	X	√								1(RN<15)	2(15<RN<32)		RN VAR AT CONST Q SELECT RNs CORRESPOND TO ALTITUDE – 30,000 ft & SEA LEVEL
				6	D					●												√√√		X	X		√ 78.7			3(RN=32)	4.5(RN=32)	6(RN>32)	Q VAR AT CONST RN FOR AEROELASTIC EFFECTS
				10	E										●	√	X	X	X	√√		√√		√			√ 41.8			1(RN<15)	2(15<RN<32)	3(32<RN<50)	RN VAR AT CONST Q AND Q VAR AT CONST RN (WITHIN TUNNEL CAPABILITY)
				3	F										●								√		X	√ 90.2			5(50<RN<75)	6.5(RN=90.2)		SELECT RNs CORRESPOND TO ALTITUDE = 30,000 ft AND 5,400 ft)
				10	F		●	●	●	●	●	●	●	●	●												X 5.0			SEE SCHEDULE H			ESTABLISH DRAG RISE SCALE EFFECTS $RN_{\bar{C}}$ = 5, Q = 880
				27	F		●	●	●	●	●	●	●	●					X	X				X									$RN_{\bar{C}}$ = 10, Q = 880, $RN_{\bar{C}}$ = 15, Q = 880, $RN_{\bar{C}}$ = 50, Q = 2640 lb/ft^2 (Pt=1 @ M=1.2) (Pt=1 @ M=1.2) (Pt=3 @ M=1.2)
	-5			6	+ACE		●			●					●	√											M = 0.6	M = 0.9	M = 1.2	2 (M = 0.6)	2 (M = 0.9)	3 (M = 1.2)	ESTABLISH SCALE EFFECTS ON VARIATIONS IN LEF (i e., CAMBER) (FULL SCALE RN AT ALTITUDE 30,000 ft)
	+10			6			●			●					●	√										√ 21.3	√ 32	√ 41.8				
	+20			6			●			●					●	√																
	+30			6			●			●					●	√																
	0	+10		6			●			●					●	√																SCALE EFFECTS ON δ_e (TRIM) (FULL SCALE RN AT ALTITUDE = 30,000 ft)
		-10		6			●			●					●	√																
		-20		6			●			●					●	√																
		-30		6			●			●					●	√																
		0	10	6			●			●					●	√																SCALE EFFECTS ON δ_a (ROLL CONTROL) (FULL SCALE RN AT ALTITUDE = 30,000 ft)
			-10	6			●			●					●	√																
			20	6			●			●					●	√																
			-20	6			●			●					●	√																
			+10/-10	6			●			●					●	√																
	-5		0	1	F					●																	√ 78.7				6		SCALE EFFECTS ON δ_{LEF}, δ_e, δ_a AT SEA LEVEL
	+10			1						●																						
	0	-10		1						●																						
		0	10	1						●																						
			-10	1						●																						
			0	4	0	G	●			●						√											M = 0.6	M = 0.9		2 (M = 0.6)	2 (M = 0.9)		SCALE EFFECTS ON LATERAL-DIRECTIONAL DATA
				4	10		●			●						√											√ 21.3	√ 32					
				4	20		●			●						√																	

NOTE

α SCHEDULE +A FOR MACH = 0.6, C FOR MACH = 0.9, E FOR MACH = 1.2

√ INDICATES FORCE AND PRESSURE DATA

X INDICATES FORCE DATA ONLY

α SCHEDULE

A 1-10 DEG BY 1 DEG INCR, 10-30 DEG BY 2 DEG

B, 1-10 DEG BY 1 DEG INCR, 10-20 DEG BY 2 DEG

C 1-10 DEG BY 1 DEG INCR, 10-30 DEG BY 2 DEG ($RN_{\bar{C}} \leq 10$)
1-10 DEG BY 1 DEG INCR, 10-22 DEG BY 2 DEG ($RN_{\bar{C}} > 10$)

D 1-10 DEG BY 1 DEG INCR, 10-14 DEG BY 2 DEG (Pt = 3)
1-9 DEG BY 1 DEG INCR (Pt >3)

E 1-12 DEG BY 1 DEG INCR, 12-20 DEG BY 2 DEG INCR (RN <15)
1-12 DEG BY 1 DEG INCR, 15 <RN<32)
1-10 DEG BY 1 DEG INCR, RN>32

F 1-6 DEG BY 1 DEG INCR

β SCHEDULE

G 1-8 DEG BY 1 DEG INCR

SCHEDULE H P_t VALUES FOR M SWEEPS (ATM)

$RN_{\bar{C}} \times 10^{-6}$

M	5.0	10.0	15.0	50.0
0.6	2.10	2.10	2.10	6.31
0.8	1.41	1.41	1.41	4.24
0.85	1.32	1.32	1.32	3.96
0.9	1.24	1.24	1.24	3.72
0.925	1.21	1.21	1.21	3.62
0.95	1.18	1.18	1.18	3.53
0.975	1.15	1.15	1.15	3.45
1.05	1.08	1.08	1.08	3.25
1.1	1.05	1.05	1.05	3.14
1.2	1.0	1.0	1.0	3.0
q(psf) =	880	880	880	2640

266 635-2

Proposed NTF Test Plan for 1/20-Scale F-111 TACT Model

CONFIGURATION	Λ	δH	NO OF RUNS	α	β	MACH NUMBER 0.6	0.7	0.8	0.85	0.875	0.9	0.925	0.95	1.1	1.2	$R_{N_{\bar{c}}} \times 10^{-6}$ ($\bar{c}$ = 25M) 3	4	6	10	15	25	32	40	50	65	75			P_t (atm)
TACT MODEL (FORCE, PRESSURE AND BUFFET)	26	0		A	0		√									√	√	√	√	√									1.0
							√													√	√						32.7		2.0
				B			√																				√		3.5
				E			√																				√		5.0
			14	F			√																	√	√		√	81.5	6.5
				A							√					√	√	√	√	√									1.0
											√									√									2.0
				B							√									√	√	√					42.0		2.5
				D							√																√		3.5
				H							√													√	√	√	√		5.0
				H							√															√		104.8	6.5
			19	H							√															√	90.0		8.0
	58	0		A	0		√									√	√	√	√	√									1.0
							√													√	√						32.7		2.0
							√																				√		3.5
				C			√																				√		5.0
			14	E			√																	√	√		√	81.5	6.5
				A							√					√	√	√	√	√									1.0
											√									√									2.0
											√									√	√	√					42.0		2.5
				C							√																√		3.5
				E							√													√	√	√	√		5.0
				F							√															√			6.5
			19	G							√															√	90.0	104.8	8.0
				A	0										√	√	√	√	√	√									1.0
															√					√	√	√					35.0		2.0
				E											√								√	√			√	56.1	3.5
				E											√													√	4.0
				F											√										√	√		√	5.0
			18	G											√												90.7		6.5
	26	0	32	G	0	√	√	√	√	√	√	√	√							√			√	√	√		5.0		J
	58	0	40	G		√	√	√	√	√	√	√	√	√	√					√			√		√		5.0		J
	26	0		0 DEG	I		√									√													1.0
							√																				32.7		2.0
											√					√													1.0
											√																42.0		2.5
				4 DEG			√									√													1.0
							√																				32.7		2.0
											√					√													1.0
			8								√																42.0		2.5
FORCE AND BUFFET ONLY	26	OFF		B	0		√																				32.7		3.5
		+5					√																				√		
		-5					√																				√		
		-10	4				√																				√		
		OFF		D							√																42.0		
		+5									√																√		
		-5									√																√		
		-10	4								√																√		
	58	OFF		A	0		√																				32.7		3.5
		+5					√																				√		
		-5					√																				√		
		-10	4				√																				√		
		OFF		C							√																42.0		
		+5									√																√		
		-5									√																√		
		-10	4								√																√		
		OFF		E										√													56.1		
		+5												√													√		
		-5												√													√		
		-10												√													√		
		-20	5																										

SCHEDULE		RANGE (DEG)	INCREMENT (DEG)
α	A	1-10 12-20	1 2
	B	1-10 12-16	1 2
	C	1-10 12,14	1
	D	1-10 12	1
	E	1-10	1
	F	1-8	1
	G	1-6	1
	H	1-5	1
β	I	1-8	1

SCHEDULE J P_t VALUES FOR M SWEEPS (atm)
$R_{N_{\bar{c}}} \times 10^{-6}$

m	5.0	15.0	40.0	65.0
0.6	2.10	2.10	5.26	8.80
0.7	1.68	1.68	4.20	7.03
0.8	1.41	1.41	3.54	5.92
0.85	1.31	1.31	3.30	5.52
0.875	1.28	1.28	3.19	5.34
0.9	1.24	1.24	3.10	5.19
0.925	1.21	1.21	3.02	5.05
0.95	1.18	1.18	2.94	4.92
1.1	1.05	1.05	2.62	4.38
1.2	1.00	1.00	2.50	4.18
q(psf) =	880	880	2200	3680

266 635-15

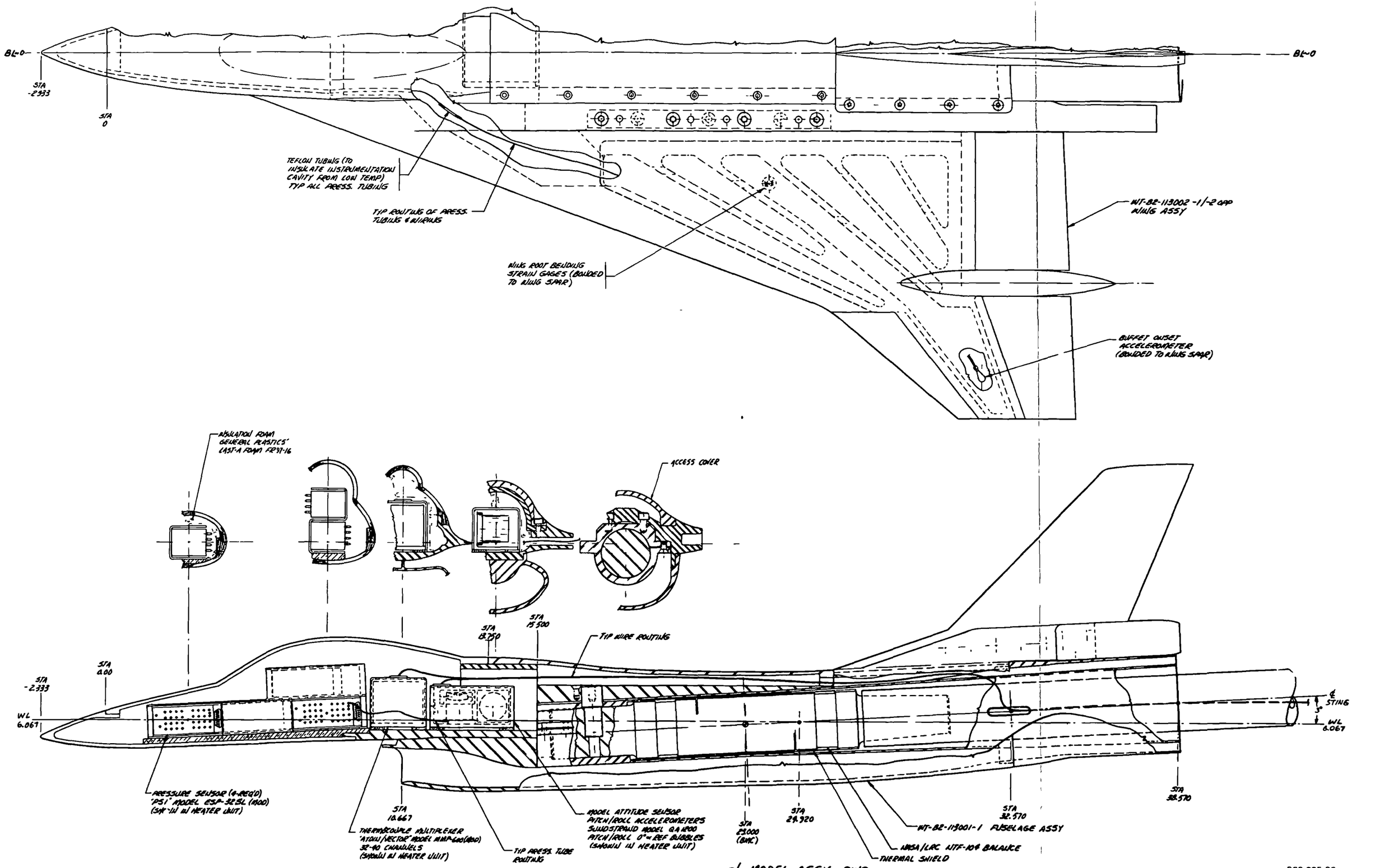

-1 MODEL ASSY~CWC

266 635 26

One-fifteenth-Scale CWC Model Assembly

BL-0

WING ROOT BENDING STRAIN GAGES (BONDED TO WING SPAR)

WT-82-113102 WING PANEL

HORIZ TAIL

PASSAGE FOR ROUTING OF WIRING FROM STING TO NOSE AREA

OVER WING GLOVE PANEL

PASSAGE FOR ROUTING OF PRESSURE TUBING FROM WINGS & BODY TO SCANIVALVES

WT-82-113106 WING MOUNTING PLATE

HORIZ & VERT TAIL SUPPORT BODY PANEL

HORIZ TAIL BRACKET

WIRE CABLES, REF PRESS TUBING, ETC (2) BUNDLES

LOWER BODY PANEL

INSULATION FOAM GENERAL PLASTICS LAST-A-FOAM FR97-16

BUFFET ONSET ACCELEROMETER (BONDED TO WING SPAR)

WT-82-113105 BALANCE BLOCK

LKG FWD

LKG AFT

VERTICAL TAIL

UPPER FUSE COVER PANEL

CABLE ROUTING

AFT FUSE STING FAIRING

NOSE/CANOPY (COMPOSITE KEVLAR)

NOSE

EXIT

BALANCE

2°

WL

BMC

WL 6.500

STA 0.000

STA 9.000

STA 9.0

STA 19.000

STA 24.98

STA 27.000

STA 32.000

STA 38.515

STA 39.312

STA 42.138

STA 43.04

THERMAL SHIELD

NASA/LRC NTF-104 BALANCE

PRESSURE SENSOR (4) PSI MODEL ESP-32SL (MOD) SHOWN IN HEATER UNIT

T/C MULTIPLEXER AYDIN/VECTOR MODEL MMP-600 (MOD) 32-40 CHANNELS SHOWN IN HEATER UNIT

LAMINATED GLASS PHENOLIC INSTRU MTD BLOCK

MODEL ATTITUDE SENSOR PITCH/ROLL ACCELEROMETERS SUNDSTRAND MODEL QA1200 PITCH/ROLL 0° REF BUBBLES SHOWN IN HEATER UNIT

LOWER FUSE PANEL

WT-82-113104 INLET DUCT ASSY

UNDERWING BODY PANEL

266 635 33

One-twentieth-Scale F-111 TACT Model Assembly

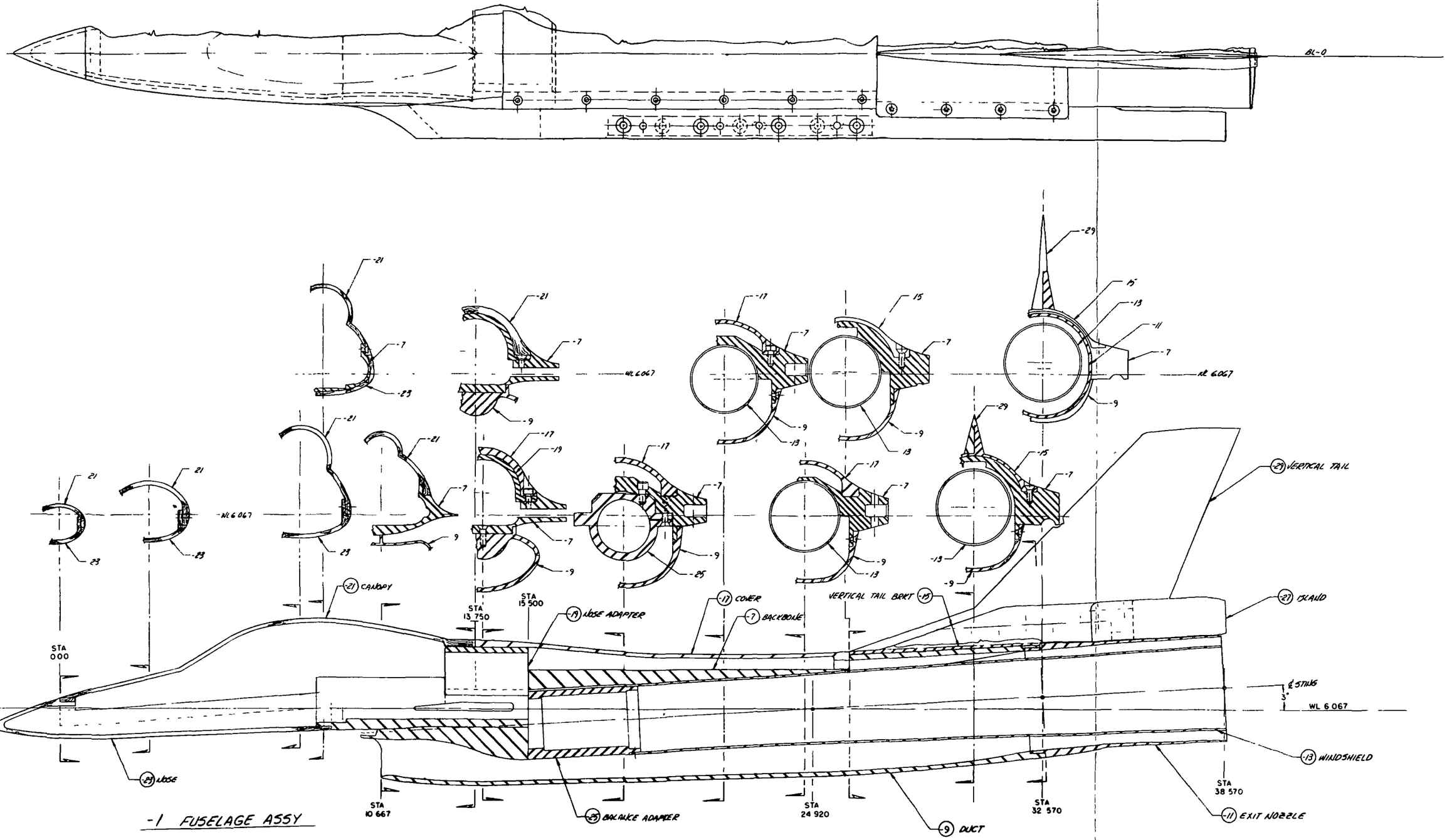

-1 FUSELAGE ASSY

266 635-27

One-fifteenth-Scale CWC Model Fuselage Assembly

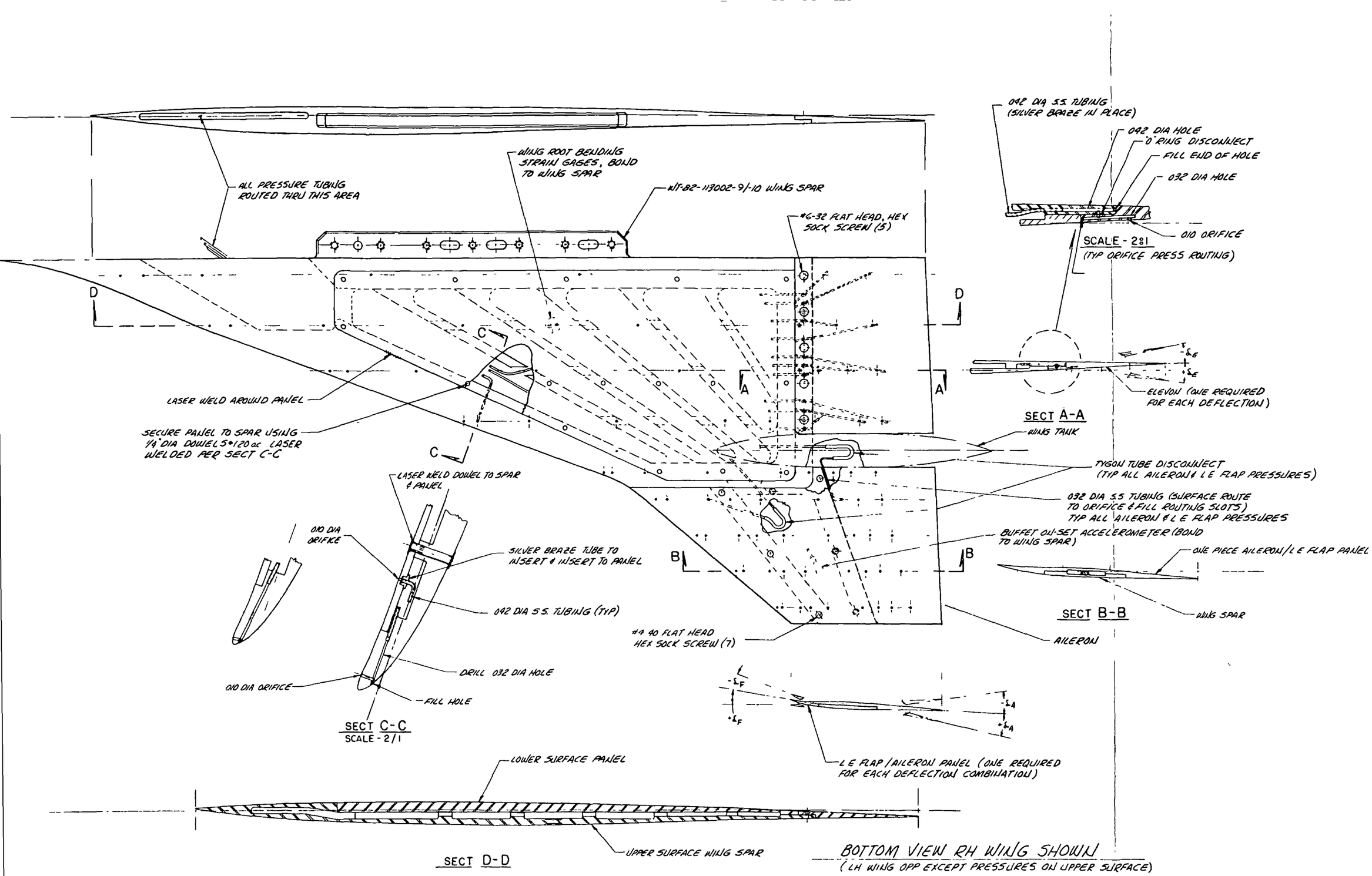

266 635-28

One-fifteenth-Scale CWC Model Wing Assembly and Instrumentation

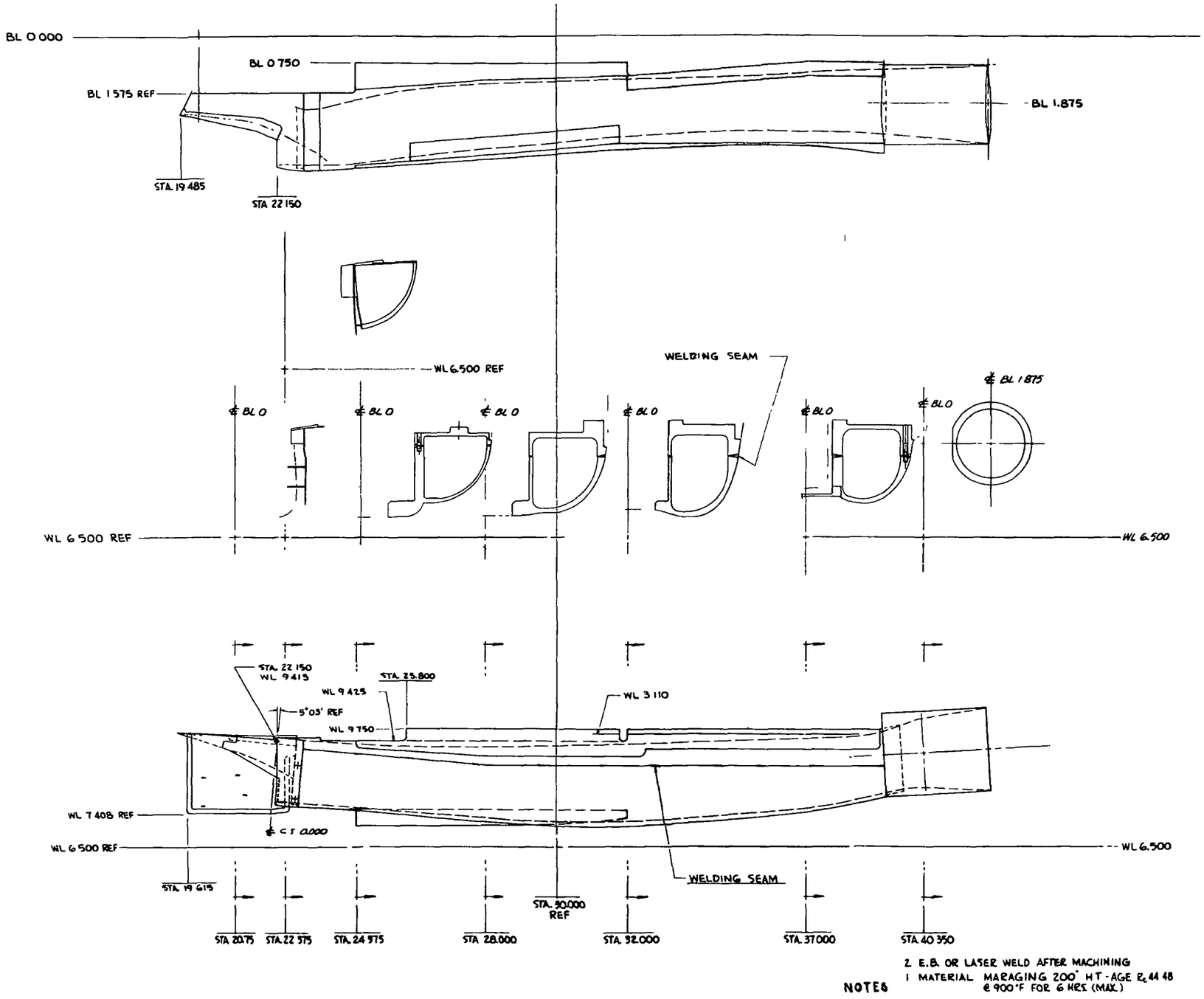

NOTES

1. MATERIAL MARAGING 200° HT-AGE Rc 44 48 @ 900°F FOR 6 HRS. (MAX.)
2. E.B. OR LASER WELD AFTER MACHINING

266 635-34

One-twentieth-Scale F-111 TACT Model Inlet/Ducting Assembly

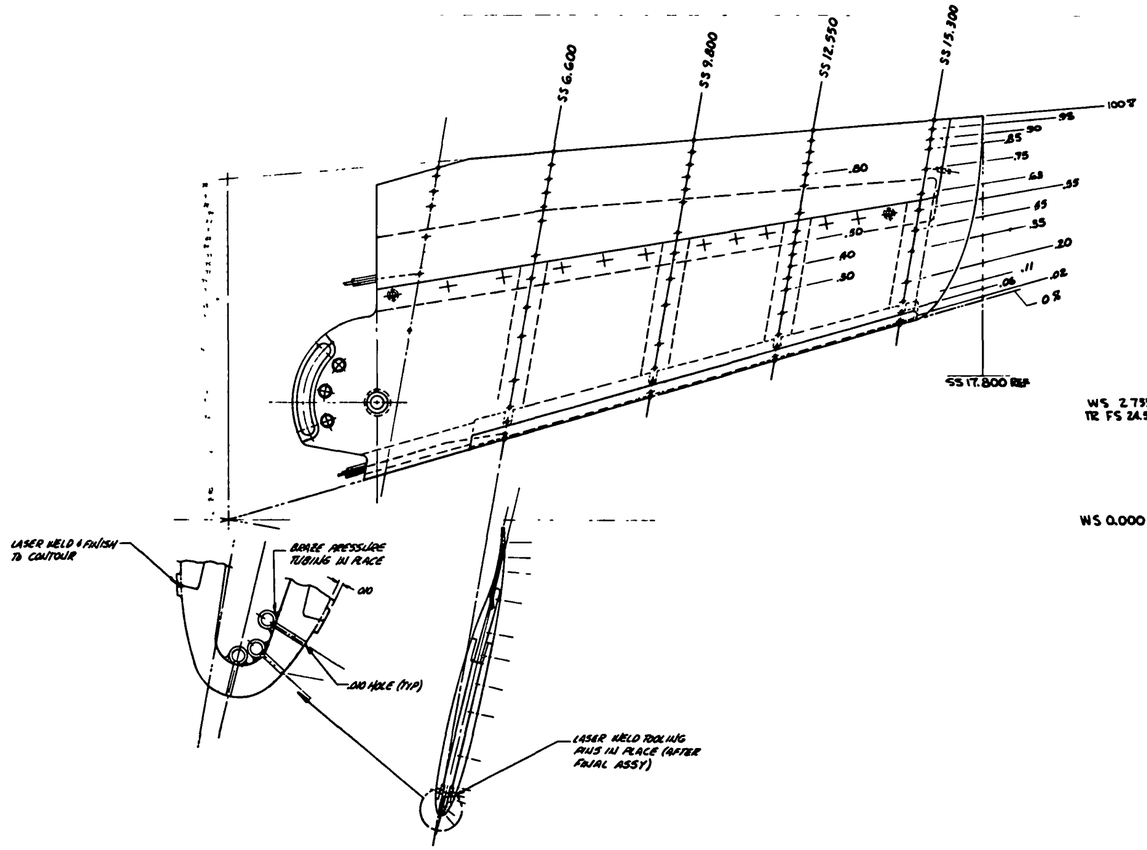

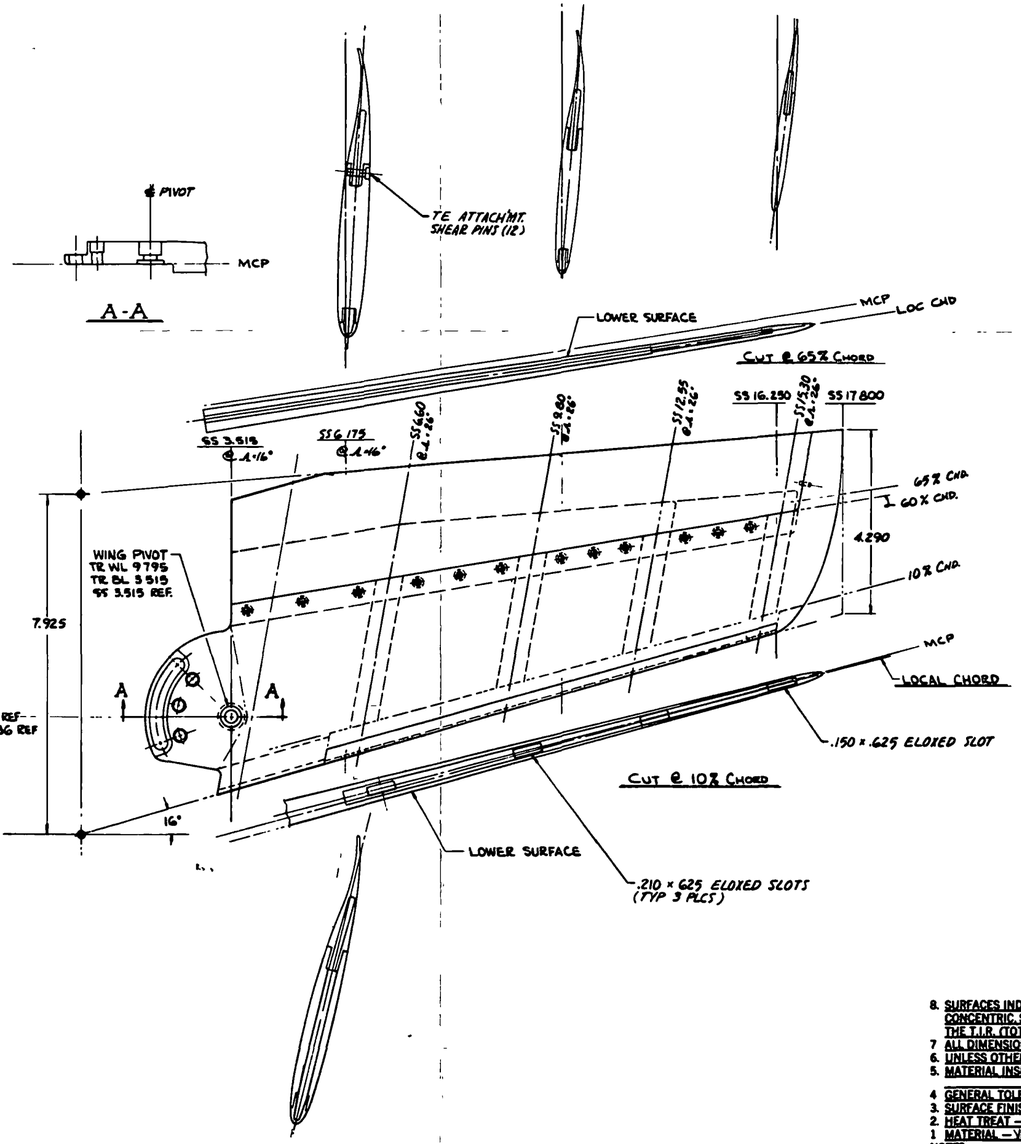

NOTES

1. MATERIAL — VASCOMAX 200 MARAGING STEEL
2. HEAT TREAT — AGE TO 200 KSI
3. SURFACE FINISH — 63 L.E. 16-32 AFT OF L.E.
4. GENERAL TOLERANCES .000 .00 .0
5. MATERIAL INSPECTION SEQUENCE —
6. UNLESS OTHERWISE NOTED ALL TOOL RAD ARE
7. ALL DIMENSIONS MARKED * ARE REF. MATCH ON ASSY
8. SURFACES INDICATED Ⓑ Ⓒ OR Ⓓ MUST BE HELD CONCENTRIC, SQUARE OR PARALLEL RESPECTIVELY WITHIN THE T.I.R. (TOTAL INDICATOR READING) SPECIFIED.

266 635-35

National Aeronautics and
Space Administration

Washington, D C.
20546

Official Business
Penalty for Private Use, $300

SPECIAL FOURTH CLASS MAIL
BOOK

Postage and Fees Paid
National Aeronautics and
Space Administration
NASA-451

NASA

POSTMASTER

If Undeliverable (Section 158
Postal Manual) Do Not Return